Last copy!

REPORT No. 46

SECONDARY FLOW AND LOSSES IN A COMPRESSOR CASCADE

OLOF SODERBERG

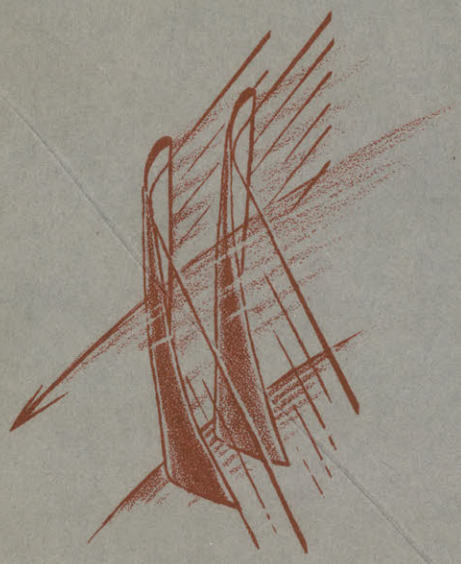

August 1958

GAS TURBINE LABORATORY
MASSACHUSETTS INSTITUTE OF TECHNOLOGY
CAMBRIDGE · 39 · MASSACHUSETTS

SECONDARY FLOW AND LOSSES IN A COMPRESSOR CASCADE

by

OLOF E. SODERBERG

Under the sponsorship of:

General Electric Company
Westinghouse Electric Corporation
Curtiss-Wright Corporation
Allison Division of General Motors Corporation

Gas Turbine Laboratory

Report Number 46

August 1958

Massachusetts Institute of Technology

ABSTRACT

Three ways in which secondary flow can be generated in a straight compressor cascade have been investigated.

1. Wakeflow. The inlet flow is characterized by a constant inlet angle and a varying stagnation pressure over the span.

2. Skewed flow. The inlet flow is characterized by a constant stagnation pressure and a varying inlet angle over the span.

3. Skewed wakeflow. The inlet flow is characterized by a variation of both stagnation pressure and inlet angle over the span.

For a certain combination of inlet angle and stagnation pressure distribution (presented in a formula) in the skewed wakeflow case no secondary flow is generated behind the cascade.

The kinetic energy of the secondary flow was found to be very small in all three cases.

The secondary flow itself did not create any losses but the blades stalled in the skewed flow layer and in the skewed wakeflow layer causing great losses.

The stream pressure and the tangential blade force were lower in the disturbed flow region.

A small perturbation theory (for a non-viscous, incompressible fluid) had been developed to describe analytically the secondary flow.

Formulae readily adaptable for numerical calculations of flow deviation angles, kinetic energy of the secondary flow, and tangential blade force are presented.

Good and satisfactory correlation of theory and experiment was found.

Applied to compressor design the results imply: The secondary flow is very small and may occur as an overturning or an underturning of the flow at the casings depending on the actual design.

The kinetic energy of the secondary flow may be neglected when considering the losses.

The ends of the blades stall in the skewed boundary layer at the casings causing losses. This could be reduced by twisting the blade ends to account for the increased incidence angle.

The stream pressure varies in spanwise direction through the boundary layer on the casings.

ACKNOWLEDGEMENTS

I am grateful to my supervisor, Professor Edward S. Taylor, for his inspiration, interest and advice during the course of this work.

The valuable and constructive criticism and advice given by Professors Ascher Shapiro and Howard Emmons is also very much appreciated.

Professor John Horlock contributed generously his ideas and experience in the initial phase of this investigation.

I also wish to express my sincere gratitute to Mr. John W. McDonald who designed the skewed velocity profile generator, to Mr. Robert Wu, who recorded and processed most of the data, and to all others in the Gas Turbine Laboratory who assisted in building the test apparatus, recording the data or in other ways contributing to this work.

The skillful preparation of the manuscript is due to the efforts of Mr. Philip Mullan and Natalie Appleton.

Dean C. Richard Soderberg arranged my contact with the Gas Turbine Laboratory and was a source of continual encouragement. Financial aid generously supplied by my former employer, the Swedish Turbine Factory, Ljungstrom, Sweden, and by the Swedish-American Foundation made possible my study at M.I.T.

Finally I wish to thank my wife and children for their understanding and encouragement which gave me the greatest support during this work.

TABLE OF CONTENTS

SECONDARY FLOW AND LOSSES IN A COMPRESSOR CASCADE

1. INTRODUCTION

In order to obtain design criteria for a compressor the flow phenomena in it have to be understood. The bulk flow outside the boundary layers (on the inner and outer casing) seems to be closely predicted by using data from two-dimensional cascade tests for turning angles and losses, and assuming axial symmetry when applying the radial equilibrium equation. The flows in the boundary layers on the casings are, however, extremely complicated and the knowledge of these flows and the magnitude and the mechanism of the losses created there is very limited. Due to these boundary layer flows and to the fact that there is a finite number of blades in each blade row secondary flows are created. The secondary flow is here defined as the difference between the actual flow and the axi-symmetric flow.

The losses in an actual compressor cascade have conveniently but arbitrarily been divided into two-dimensional profile loss, wall skin friction loss, and secondary loss (1). Secondary loss is then defined as the difference between the actual loss in a compressor cascade and the two-dimensional profile loss plus the wall skin friction loss. The secondary flow has been made responsible for this loss which includes effects such as interaction between moving blade rows and blade end clearance flows. A more

adequate name for these losses would be complementary losses and the name secondary loss would then be reserved for the loss connected with the secondary flow only.

There has been a great interest in secondary flow in cascades in the past years as indicated by the numerous investigations dealing with this subject. Measurements (2 ÷ 9) and visual studies (10 ÷ 15) of secondary flow in channels and cascade passages have been performed and attempts have been made to describe analytically (16 ÷ 36) the secondary flow. These analytical studies have succeeded in describing the general nature of the secondary flow but have not been successful in showing the mechanism or the nature of the large losses attributed to secondary flow encountered in a real compressor.

An inlet flow to the channel or cascade with constant angle of attack and varying stagnation pressure are assumptions common to all these studies. In a real compressor, however, the boundary layers on casings are skewed i.e. both the inlet angle and the stagnation pressure vary. The variations depend on the actual design from which principally two cases occur as can be seen in Figure 1, where the flow entering the hub of a rotor blade row is shown. In Figure 1a the stator blade row preceding the rotor is equipped with a shroud. The tangential component of the flow entering the rotor at hub has a finite value. The relative velocity in the boundary layer entering the rotor blade row is thus of almost constant magnitude but of varying direction tending to stall the blades at the hub.

In Figure 1b the stator blades preceding the rotor have no shrouds and the rotor extends under the tips of the stator blades. Due to viscosity

the flow adheres to the rotor which, in this case, is the inner casing, and the axial component of the flow entering the rotor is zero at the hub. The magnitude of the relative velocity in the boundary layer entering the rotor blade row increases from zero at the hub up to the free stream velocity outside the boundary layer and at the same time the direction of the flow changes from tangential at the hub to the free stream flow angle. Also in this case the flow tends to stall the rotor blades in the boundary layer. In Figure 1 it was assumed that the flow outlet angle from the stator row was constant in the boundary layer. In reality the flow is also skewed there, however, the general picture of the flow entering the rotor blade rows is similar.

Richardson and Moore (9) experimentally investigated a skewed boundary layer on the end wall between two adjacent blades in a straight stationary compressor cascade. The results were presented as the values of the different terms in the momentum integral equations for a turbulent layer. Only a qualitative description of the flow was given due to the difficulties in solving the pertinent equations for the boundary layer flow.

If these phenomena are to be satisfactorily understood it seems essential to start with simpler cases and then to use the knowledge gained to aid in the attack on the more complex but more realistic problems encountered in a real compressor. The intention of the present investigation was then to study the secondary flow and resulting losses for an incompressible non-viscous flow in a straight compressor cascade for three different cases simulating the skewed flow in the boundary layers at the casings of a compressor. The three cases are as follows:

1) wake flow

2) skewed flow

3) skewed wake flow, which is superposition of the two foregoing cases.

The three cases are illustrated below:

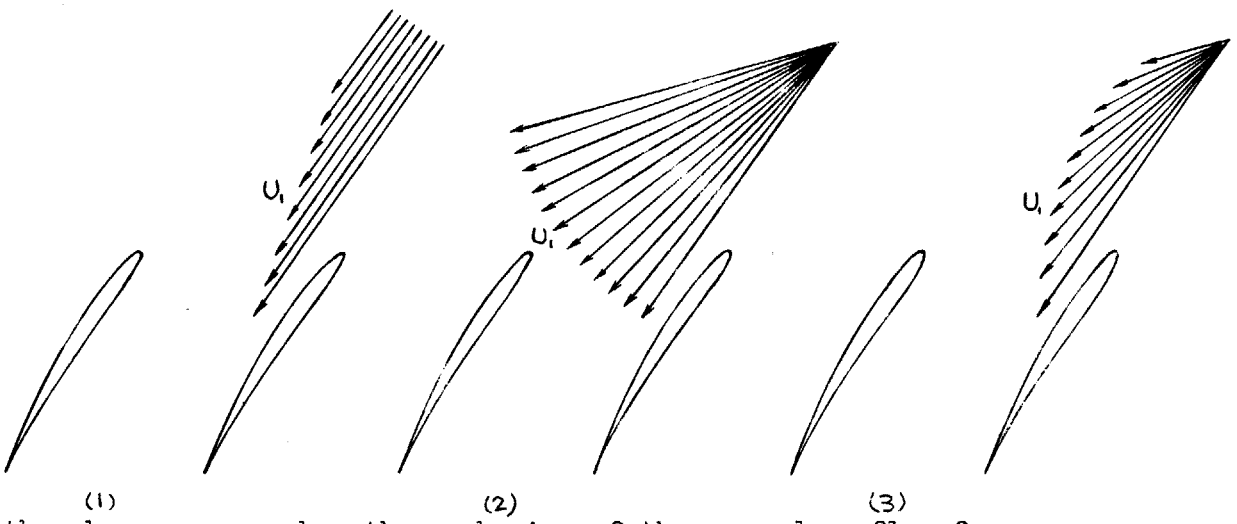

In the above cases, when the mechanism of the secondary flow for a non-viscous flow is understood a better basis for solving the viscous flow problem is established. The case of a wake flow has been studied in many other investigations and the reason for studying it here is only because it was to be used as a basis for the investigation of the skewed wake flow.

The accepted idea in studying the boundary layer flow on the casings of a compressor has been to assume that the static pressure is imposed by the main bulk flow and does not vary in spanwise direction through the boundary layer. This, plus the fact that the boundary layer is energized by the relative motion of the blade rows leads then to the assumption that the flow in general (design point) does not separate at the casings. The validity of these assumptions is examined herein in the case of a non-viscous flow.

The requirement of the skewed flow was therefore that it should

have a flow direction approximately 20° toward the positive stall from the mainstream direction which means that it is well beyond two-dimensional positive stall incidence angle for the cascade configuration that was chosen. The increase in incidence angle is somewhat less than what can be expected in a real compressor. To get a realistic figure of the ratio of the skewed layer and the blade height a skewed layer of about 2 inches was chosen. The flow should of course be uniform in tangential direction, simulating axial symmetry in a compressor.

2 EXPERIMENTAL EQUIPMENT, INSTRUMENTATION, AND MEASURING TECHNIQUE

To perform the desired experimental work an apparatus was built along much the same line as a conventional two-dimensional cascade testing tunnel. The primary departure from work done in the past arose in developing the desired inlet flows.

2.1 Wind Tunnel

Testing was carried out in the Gas Turbine Laboratory low speed cascade wind tunnel which is an open-return tunnel of wooden construction and has a test section of 22 x 16 inches. A description of this tunnel is given in reference (40). Adjustable air bleeds on the plenum chamber made it possible to keep the approach air velocity to the cascade constant (approximately 123 ft/sec) during the tests.

Figure 2 is a diagrammatic sketch of the tunnel. The suction slot at the plenum chamber outlet nozzle removed irregular velocity

distributions formed in the plenum chamber. The suction slots immediately ahead of the cascade were provided for removal of the boundary layers formed on the upper and lower walls. A suction slot on one of the side walls of the tunnel immediately ahead of the cascade had to be installed in order to prevent the corresponding end blade of the cascade from stalling.

2.2 Wake Flow Generator

In order to produce a velocity profile with constant inlet angle and with varying stagnation pressure over a part of the span a splitter-board was inserted upstream of the cascade at midspan. The splitterboard was made of an 1/8 inch thick aluminum sheet with a length of 15 inches in streamwise direction and reaching across the tunnel in tangential direction. It was placed with its trailing edge about 13 inches ahead of the cascade. In order to get a thick turbulent wake very coarse sandpaper was glued to the two sides of the splitterboard.

2.3 Skewed Velocity Profile Generator

The problem of designing a device that would generate a desired skewed velocity profile was made the subject of an S.M. thesis and was excellently solved by John W. Mc Donald. The different methods of creating the desired flow is examined and a detailed description of the device is given in reference (41). Figures 3 and 4 are diagrammatic sketches and Figures 5 and 6 are photographs of the device.

To provide the skewed velocity profile a duct was inserted at midspan upstream of the cascade in the tunnel. The duct was 2 inches

high, extended 17 inches in main-stream direction and was supplied with air by a centrifugal blower rated at 3600 cubic feet per minute at 1.25 psi gauge static pressure. A settling chamber 28.5 inches square by 43.5 inches long, internal dimensions, was placed in the system. The flow was straightened and smoothed by a set of flow straighteners (1 inch diameter x 1/16 inches wall, paper tubes 6 inches long) and a screen (standard 14 x 18 mesh). The flow from the settling chamber was accelerated through a nozzle directly into the ducting crossing the wind tunnel. The outlet of the ducting where the ducted flow met the mainflow was covered with a screen 14 x 18 mesh that turned the air to the proper angle and smoothed out the flow. Control of the skewed flow was provided by a throttling valve at blower exit. The flow was monitored by a wall pressure tap in the ducting connected to an inclined "Meriam" oil manometer. The system gave a skewed flow with most of the desired features. However, it was not possible to get a constant stagnation pressure in spanwise direction because the boundary layer built up on the top and bottom walls of the ducting thus giving rise to two wakes, one above and one below the skewed layer. The deficiencies appear to be a characteristic of the skewed flow that may be diminished but not entirely eliminated. As the flow moves downstream of the duct these wakes smooth out but the thickness of the skewed layer increases and the angle variation reduces at the same time. For this reason the distance between the duct and the leading edge of the cascade was made 10 inches.

2.4 Cascade

A typical compressor cascade configuration was chosen. The characteristics of the cascade are given in the following table:

Blade profile	NACA 6409 with 1% trailing edge thickness
Number of blades	8
Length of blades	16 inches
Chord	4.5 inches
Gap	4.445 inches
Gap-chord ratio	0.988
Aspect ratio	3.556
Stagger angle	60°
Inlet angle	45°
Outlet angle	$\sim 65°$
Turning angle	$\sim 20°$
Reynolds number	2.8×10^5

All angles are measured to the tangential direction of the cascade. A sketch of the cascade configuration is shown in Figure 7. The chosen inlet angle of 45° gives a minimum loss for this cascade configuration (equal to i* according to Howell's (1) definition). A compromise between minimizing end effects and operating at an adequately high Reynolds number to insure turbulent boundary layer on the blades surfaces gave the 4.5 inch chord length.

The cascade discharged into the test cell and the flow was unrestricted downstream of the cascade.

2.5 Instrumentation

The purpose of the tests was to map the flow upstream and downstream of the cascade inorder to get information about the nature of the secondary flow and losses, and to get experimental data against which analytical solutions could be compared.

2.5.1 Reference Pressure

A pitot static tube was used as a reference probe and was located in the mainstream 1 9/16 inches ahead of the cascade and four inches from midspan. All measurements were taken at a constant dynamic pressure (= 3.27 inches of water).

2.5.2 Upstream Measurements

2.5.2.1 Location of Measurements

Since both the skewed flow and the wake flow are subject to diffusion processes tending to change the velocity profiles as the flow moves downstream it is desirable to measure the flow as close to the leading edge of the cascade as possible to get the proper inlet conditions. On the other hand each blade in the cascade is surrounded by a static pressure field that extends upstream of the cascade and measurements too close to the leading edge would then show non-uniformities in tangential direction tending to mask the true inlet conditions. As a compromise the measurements were taken in a plane parallel to the cascade and located 1 5/8 inches in axial direction (2.25 inches in mainstream direction) ahead of the cascade. The flow was investigated over an area 8 inches in spanwise direction by 8.89 inches in tangential direction covering the central portion of the flow through the cascade.

2.5.2.2 Probes and Traversing Rigs

Stagnation pressures and inlet angles were measured simultaneously with a three-hole cobra probe shown in Figure 8. The tubes were .035" OD and .023" ID cut off at the tip to an angle of 60°.

In the skewed flow cases the stream pressure was measured with a stream pressure probe made up of a tube 0.095" OD and shown in Figure 8. The probe was set according to the angles found with the three-hole probe. The traversing mechanism was made up of a probe holder of Pratt and Whitney design fastened to a slide that could be traversed along the cascade by a lead screw connected to a crank. The slide could be positioned with an accuracy of ±0.02 inches. The probe holder was operated by remote control and could traverse the probe in spanwise direction by increments of 0.002". Angles were measured to one tenth of a degree.

2.5.3 Downstream Measurements

2.5.3.1 Location of Measurements

It is difficult to make accurate measurements in the strong wakes which exist immediately after the blades. For this reason, the flow conditions behind a cascade are usually measured about half a chord downstream where the wakes from the blades have been reduced due to viscous action. However, the same viscous action tends also to reduce the secondary flow. To record the whole secondary flow created measurements should be made as close as possible to the trailing edge of the cascade. Measurements have therefore been taken at two positions behind the cascade: namely at 2.25 inches behind the cascade and at 0.1 inches behind the cascade. The data measured further downstream are considered more accurate than those measured

closer to the cascade. With this arrangement it is also possible to measure the decay of the secondary flow downstream. The areas traversed were 8 inches in spanwise direction x 8.89 in tangential direction (two blad spacings) covering the central portion of flow through the cascade. One cross section was covered by a mesh of about 400 measuring points.

2.5.3.2 Probes and Traversing Rigs

Traverses downstream were made with the three-dimensional traversing mechanism described in reference (42). This rig, used with a five-hole probe, allowed nulling for flow directions in horizontal and vertical planes and measurements of stagnation pressure, simultaneously. The positioning of the probe is accurate to $\pm$0.01 inches and the angles are measured to one tenth of a degree. Figure 9 shows the traversing rig. The five-hole probe Figure 8 was of 0.080 inches outside diameter with tubes of 0.016 inches inside diameter. The angle measuring tubes were arranged in pairs with opposite tubes spaced 0.056 inches center-to-center. This spacing introduced errors in measuring angles in steep pressure gradients. The stream pressure was measured with a stream pressure probe made up of a tube of 0.058 inches OD and shown in Figure 8. The probe was set according to the angles measured with the five-hole probe.

2.5.4 Blade Taps

To measure pressure distributions on the blade surfaces, static pressure taps were provided on two blades. Taps of 0.016 inches diameter were drilled in rows normal to the blade span into 0.049 inches diameter tubings recessed into the blade surfaces. Pressures on both surfaces were measured in the same passage by tapping the pressure surface on one blade and the suction surface on the adjacent blade. There were 8 rows of holes

at different spanwise positions and each row had 17 holes on the pressure side and 26 holes on the suction side. The greater number of holes on the suction side was provided to facilitate detection of separation. The pressure tap rows were located in the lower part of the blades and at the following positions measured in inches from midspan -- 1/8, 2/8. 3/8, 5/8, 7/8, 1 1/8, 2 1/8 and 4 1/8.

The tubings recessed into the blades made the surfaces uneven and increased the profile losses on the blade with the pressure taps on the suction surface, and also made it more prone to stall.

2.5.5 Pressure Indicators

All pressure data were taken with differential pressure transducers (manufactured by Statham Laboratories, Los Angeles, California).

Stagnation pressures were measured against stagnation pressure of the reference probe.

Stream pressures were measured against the reference stream pressure in measurements upstream, and against atmospheric pressure in measurements downstream of the cascade.

Flow directions were measured by adjusting the probe until the transducers were balanced.

An original calibration of the system was performed using an NACA manometer (43).

Transducer systems of two different ranges and sensitivities were used.

A transducer with a range of about 5.5 inches of water was used to adjust the inlet mainstream dynamic head (= 3.27 inches of water) and

was also used to measure stagnation pressure differences greater than 1.2 inches of water.

Accuracy of this system was estimated at $\pm$0.01 inches of water which is better than 1% of the measured pressures.

Pressure differences less than 1.2 inches of water were measured with a transducer with a range of about 1.4 inches of water and which had two regions of sensitivity. Pressure differences up to 0.5 inches of water were measured on the high sensitivity scale providing an accuracy of $\pm$0.002 inches of water and pressure differences between 0.5 and 1.2 inches of water were measured on the low sensitivity scale providing an accuracy of $\pm$0.005 inches of water which is better than 1% of the measured pressures.

The transducer system used for measuring angles readily detects angle variations of $\pm$0.1°.

In the tests the measured angles were reproducible within 0.2 of a degree except in regions close to separation.

2.6 Streamline Traces in Carbon Black

The processes taking place in the boundary layers are largely responsible for the losses occuring either because of the friction itself or less directly as a result of separation and vortex formation. To get a qualitative picture of the flow pattern on the blade surfaces and thus of the causes of the losses the streamlines on the blade surfaces were traced in carbon black. It must be emphasized that the information gained from this is only of a qualitative nature when the pictures are interpreted. The absolute velocity of the flow, for instance, plays less part in the production of the pattern than the velocity gradient near the wall, so that the

character of the picture also depends to a large extent on Reynolds number. Since the blades are placed vertically, the force of gravity also tends to influence the pattern. Consequently, these flow patterns cannot be interpreted by rigid rules but can only be satisfactorily judged against the background of qualitative knowledge of the processes taking place in the boundary layers.

A suspension of finely-graded carbon black in kerosene painted on the blade surfaces with a brush was used for this investigation.

3 TWO-DIMENSIONAL CASCADE TESTS

Two-dimensional cascade tests were performed to get basic data for the cascade configuration against which the three-dimensional flow data in the later tests could be compared.

3.1 Upstream Conditions

Inlet angles and stagnation pressure were measured over the test area upstream of the cascade. The flow was steady and fairly uniform. The inlet angle varied between 43° and 46.5° and the stagnation pressure varied less than 0.4%.

3.2 Downstream Conditions

The area integrated mean values of the measured data over the test areas are given on the next page.

	AXIAL POSITIONS			
	0.1"			2.25"
		+0.2		+0.3
Transverse flow angle	64.7°	-0.7	64.4°	-0.7
		+0.1		+0.3
Spanwise flow deviation angle	0.1°	-0.1	0.1°	-0.2
		+0.05		+0.09
Stagnation pressure defect $\frac{\Delta P_o}{q_r} = C_f$	1.84%	-0.20	1.57%	-0.09

Horizontal traverses were made at different spanwise positions and the average values over two blade spacings were calculated for each traverse. These average values were then averaged over the span. The values in the columns to the right of the mean values in the table above are the greatest differences found between the average value over the area and the average values of each traverse. These differences are small indicating that the flow in the cascade is truly two-dimensional and that the accuracy of the measurements is good. Comparison of the values at the two test planes shows good agreement between the angle measurements but indicate greater losses closer to the cascade than further downstream. This apparent violation of the second law of thermodynamics is the result of averaging losses over the area instead of averaging over the mass transported through the area which is the correct but more cumbersome way of calculating losses. The losses were therefore also mass averaged and showed then the same value, 1.31%, for the two traversed positions showing a good accuracy between the two measurements.

3.3 Pressure Distributions Around the Blade

Stream pressure on the blade surfaces was measured at 4 different spanwise positions. The positions were located at 1/8", 1 1/8", 2 1/8" and 4 1/8" from midspan.

The results of the measurements are presented as plots of the tangential component of the pressure distribution on the blade surfaces and as the tangential pressure coefficient C_T. Figure 10 shows the pressure distribution for the measurements at 1/8" from midspan. It is to be noted that pressures on the suction surface are measured on one blade and the pressures on the pressure surface on the adjacent blade. In this investigation however it has been assumed that the flow is uniform in tangential direction and so the pressure distributions have been plotted on the same graph to represent the pressure distribution around one blade. The area between the two curves has been integrated to yield the tangential pressure coefficient C_T.

$$C_T = \frac{1}{S}\left[\int_0^{C_T} \frac{p - p_r}{q_r}\, dx\right]_{\text{pressure side}} - \frac{1}{S}\left[\int_0^{C_T} \frac{p - p_r}{q_r}\, dx\right]_{\text{suction side}}$$

Nomenclature is given in Figure 10.

Measurements gave $C_T = 0.508 \pm 0.008$.

The tangential component of the pressure force on the blade surfaces causes the flow to turn and is therefore a measure of the turning flow. Assuming that the axial velocity is the same upstream and downstream of the cascade, C_T can be related to the flow angles through the following formula;

$$C_T = 2 \sin^2 \alpha_1 \, (\cot \alpha_1 - \cot \alpha_2)$$

The outlet angle calculated by this formula with the measured value of C_T was $\alpha_2 = 63.8°$ which agrees fairly well with the value of direct angle measurements.

The static pressure rise through the cascade was also measured and is presented as the pressure coefficient C_p.

$$C_p = \frac{P_2 - P_r}{q_r}$$

Measured value $C_p = 0.36$.

Combining the energy equation with the continuity equation and assuming no change in axial flow velocity gives

$$C_p = 1 - \left(\frac{\sin\alpha_1}{\sin\alpha_2}\right)^2$$

This formula relates also the outlet angle to the static pressure measurements and gives, using the measured value of C_p

$$\alpha_2 = 62.1°$$

which gives a fair agreement with the values found by measuring the pressure distribution on the blades and by direct angle measurements.

4 WAKE FLOW

4.1 Results of Measurements

4.1.1 Upstream Conditions

Figure 11 shows a vertical traverse of the stagnation pressure at the inlet to the cascade. The flow was uniform in tangential direction over the traversed area and so this stagnation pressure profile may represent the flow over all the measured area. All pressures have been non-dimensionalized by dividing by the reference dynamic pressure. The stagnation pressure profile showed a defect of 47.5% in the center of the wake which had a width of about 2.5 inches at its base. The stagnation pressure defect area averaged over the span (16 inches) was 3.7%.

The stream pressure was not measured but assuming this to be constant in spanwise direction the velocity was calculated. It varied from 123 feet/sec in the mainstream to about 90 feet/sec in the center of the wake.

The inlet angle varied between 43° and 46.5° which was also the case in the two-dimensional tests.

4.1.2 Downstream Conditions

The results of the measurements downstream of the cascade have been presented as contour maps over the areas traversed showing stagnation pressures, stream pressures, transverse flow angles, and spanwise flow deviation angles.

4.1.2.1 Stagnation Pressure

Figures 12 and 13 show contours of constant stagnation pressure, i.e. contours of Bernoulli surfaces, at the two positions.

These pictures show that a fairly strong secondary flow had been created in the cascade and persisted as the flow moved downstream. The Bernoulli surfaces had been turned about 5° at the trailing edge of the cascade and about 10° half a chord downstream. The pictures show that the secondary flow was directed toward the center of the wake on the pressure side and out from the center on the suction side of the blades.

The blade wakes had attenuated half a chord downstream while the stagnation pressure defect in the wake changed only slightly and the shape of the contours at the two positions were essentially the same. The wake had, however, flattened and broadened due to viscous action as it travelled through the cascade and kept on changing, though at a slower rate as it moved downstream of the cascade.

4.1.2.2 Stream Pressure

The stream pressure distribution in a plane 0.35 inches behind the cascade is shown in Figure 14. Except at midspan the blade wakes were at higher than atmospheric pressure. At midspan the pressure in the wake was lower than atmospheric. Low pressure regions were established in the center of the wake between the blades with their centers somewhat closer to the suction surfaces of the blades. Between these low pressure region, in the center of the wake, high pressure regions were located. They were of smaller size and were located close to the suction sides of the blades. These are the locations where the secondary flow has stagnation points. Both the spanwise and the transverse velocity components of the secondary flow are zero at these points. The lower pressure regions then indicate strong secondary flows.

The overall low stream pressure in the horizontal wake indicated

a flow toward the center of this wake tending to smooth it out.

4.1.2.3 Transverse Flow Angles

Contour maps of the transverse flow angles are shown in Figures 15 and 16. Close to the cascade there was a strong overturning of the flow between the blades indicating a strong secondary flow in the wake directed from the pressure sides to the suction sides of the blades with maximum velocity in the centers of the blade passages. This agrees well with the observations made from the study of the stream pressure distributions. At the outer edges of the wake there was a slight underturning of the flow indicating a slight secondary flow in the opposite direction to the secondary flow in the wake.

Further downstream the mainstream had smoothed out as indicated by the disappearance of most of the angle variations in the blade wakes. The transverse flow angles due to the secondary flow, however, had reduced only slightly and the shape of the contours were almost unchanged.

It is of interest to note that the flow angles in the blade wakes remained almost constant in spanwise direction. This justifies the later analysis which assumes that the blade wakes are plane surfaces. The same observations can be made from the contour maps of the stagnation pressures and of the spanwise flow deviation angles.

4.1.2.4 Spanwise Flow Deviation Angles

Figures 17 and 18 show contours of constant spanwise flow deviation angles at the two traversed positions. As can be seen there was no spanwise flow in the center of the wake and in the centers of the blade wakes. Somewhere in the center of the passages bounded by the blade wakes

there was also a region extending over the span where the spanwise flow deviation angles were zero.

4.1.2.5 Streamline Traces in Carbon Black

Streamline traces in carbon black on the blade surfaces are shown in Figure 19 (pressure side) and Figure 20 (suction side).

The dark region extending in spanwise direction and located about 30% from the leading edge on the pressure side indicates transition from laminar to turbulent boundary layer. The long white streaks pointing downwards are caused by gravity which becomes controlling in regions where the skin friction is small. The lighter region at midspan is caused by the wake. The dark transition region is much smaller here and located closer to the leading edge. The higher turbulence level in the wake causes earlier transition to turbulent boundary layer. The lighter colour in the wake region indicates a larger velocity gradient there at the blade surface than outside. The direction of the streaks indicates a spanwise flow towards the center of the wake.

The picture (20) showing the suction side shows only the rear part of the blade. At midspan the streaks indicate a spanwise flow away from the wake. No indication of separation on the blade surface can be detected. The streamline traces thus confirm the general results found by other measurements.

From the interpretation of these contour maps and the streamline traces in carbon black we get the picture of the secondary flow pattern shown on the next page. The fluid flows along the pressure side of the blades toward midspan where it turns into horizontal direction flowing toward the

suction side of the adjacent blade and where it again turns following the suction side away from midspan. When it reaches the outer edge of the wake it gradually deflects toward the pressure side of the adjacent blade forming a closed loop. At the intersection of the center of the wake and the blade wakes the secondary flow has stagnation points.

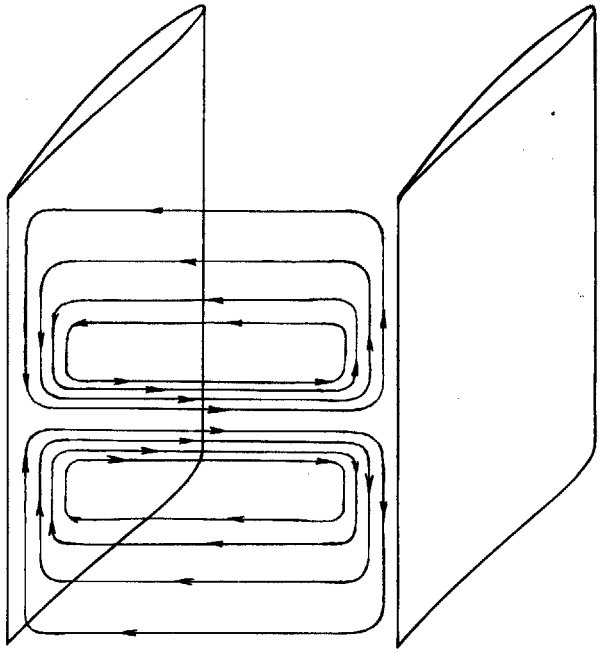

4.2 Analysis of the Secondary Flow

4.2.1 Derivation of the Secondary Vorticity Components Along a Streamline Behind the Cascade

Squire and Winter (17) derived a formula for the secondary vorticity component in streamwise direction behind a cascade when the vorticity was caused by a variation of the approach velocity along the span of the blades.

$$\xi_2 = -2\varepsilon \frac{dU_1}{dz} \qquad 4\text{-}1$$

where the ϵ = cascade turning angle

and $\frac{dU_1}{dz}$ = incoming vorticity strength.

This result is strictly applicable only for an inviscid incompressible flow in an impulse cascade in which the basic motion is a free vortex. The incoming vorticity $\frac{dU_1}{dz}$ has to be small.

Hawthorne (20) developed a general theory for the flow in an inviscid, incompressible rotational fluid and gave the follwoing formula for the vorticity component along a streamline behind a cascade:

$$\left(\frac{\xi}{U}\right)_2 = \left(\frac{\xi}{U}\right)_1 - 2\int_1^2 \left|\frac{\nabla p_0}{\rho}\right| \frac{\sin\phi}{U^2}\, d\theta \qquad 4\text{-}2$$

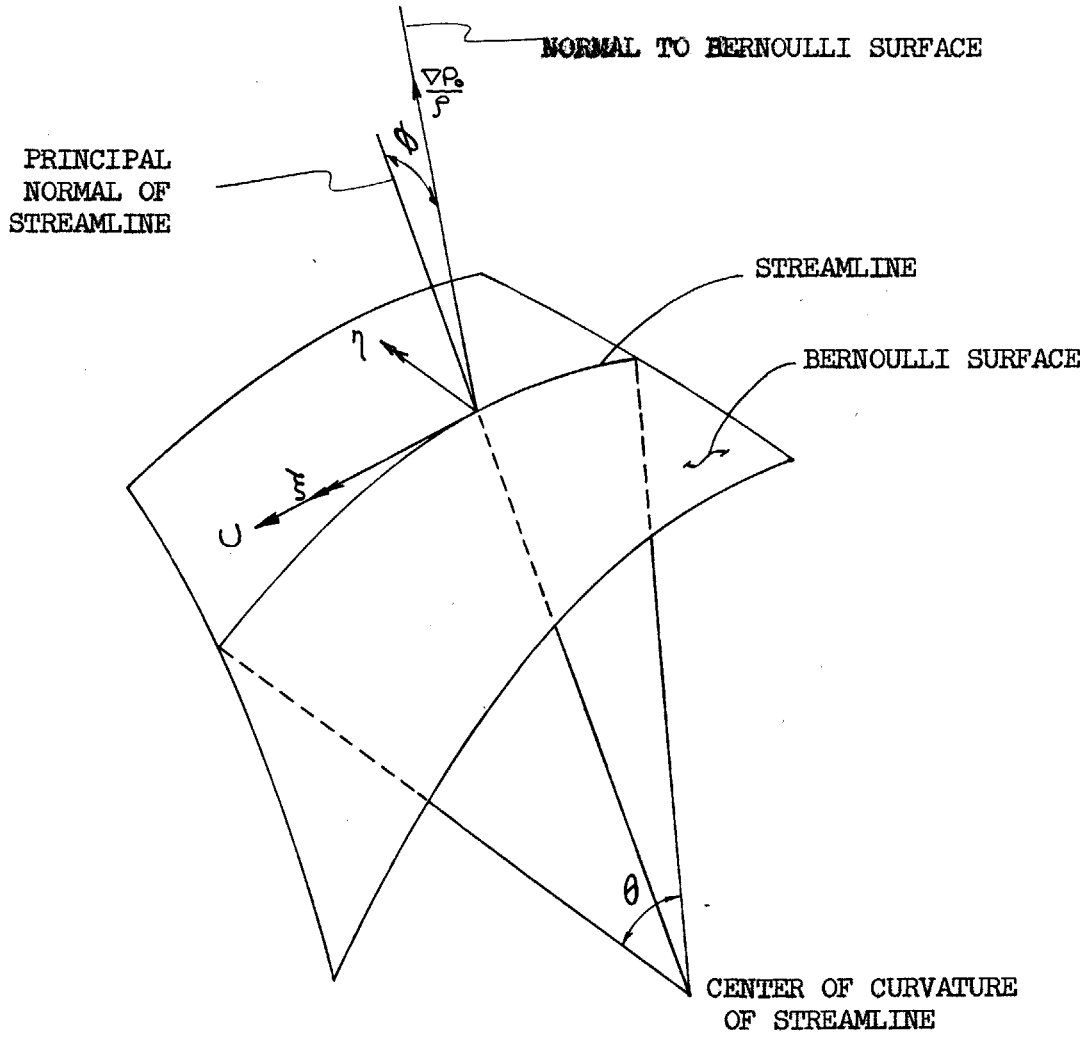

where ξ = vorticity component tangent to a streamline

U = velocity

P_o = stagnation pressure

ρ = stream density

ϕ = angle between principle normal to streamline and to Bernoulli surface

θ = turning angle

Louis (45) integrated this formula under the following assumptions:

1) The vorticity component ξ_1, along a streamline at the inlet to the cascade is equal to zero, yielding $\xi_1 = 0$.

2) The vorticity is being transported by the two-dimensional flow through the cascade and not by the induced velocity.

3) The turning of the Bernouilli surfaces is small, giving $\sin \phi = 1$.

4) The stagnation pressure varies only in spanwise direction and is given by its value at the inlet of the cascade, yielding

$$\frac{\nabla P_o}{\rho} = \frac{\partial}{\partial z}\left(\frac{P_1}{\rho}\right) + U_1 \frac{dU_1}{dz}$$

5) The stream pressure is constant at the inlet to the cascade, yielding

$$\frac{\nabla P_o}{\rho} = U_1 \frac{dU_1}{dz}$$

6) Infinitely thin blades, yielding the continuity equation for the two-dimensional flow

$$U \sin \alpha = U_1 \sin \alpha_1 .$$

The result of the integration is (with the notation of this report):

$$\xi = -\frac{1}{\sin\alpha_1 \sin\alpha_2}\left[\alpha_2 - \alpha_1 - \frac{\sin 2\alpha_2 - \sin 2\alpha_1}{2}\right]\frac{dU_1}{dz} \qquad 4\text{-}3$$

Comparison of the formulae for ξ yields, with the data of this cascade

$$\alpha_1 = 45°$$

$$\alpha_2 = 64.4°,$$

that

$$\xi_L = 1.04\ \xi_{sw}$$

where

ξ_L is the secondary vorticity component given by 4-3

ξ_{sw} is the secondary vorticity component given by 4-1

As can be seen they give almost the same result in this case and will thus predict almost the same secondary flow.

A different integration of 4-2 based on other assumptions will be given here. Assumption (1), (2) and (3) in Louis' derivation will be retained here. Assumption (3) is supported by the result of the measurements of the rotation and warping of the Bernouilli surfaces.

Assume now:

The stagnation pressure varies only in spanwise direction based on the fact that the rotation of the Bernouilli surfaces is small and that the broadening of the wake is slow.

therefore $$\frac{\nabla P_o}{\rho} = \frac{\partial}{\partial z}\left(\frac{p}{\rho}\right) + U\frac{\partial U}{\partial z}$$

The measurements show that the variation of the stream pressure in spanwise direction is small downstream of the cascade and is probably small

upstream too as the pressure variation through a wake is in general small. The variation is greater inside the cascade but is till small compared to $U\frac{\partial U}{\partial z}$. Therefore neglect $\frac{\partial}{\partial z}\left(\frac{p}{\rho}\right)$ compared to $U\frac{\partial U}{\partial z}$ yielding

$$\frac{\nabla p_0}{\rho} = U\frac{\partial U}{\partial z} \qquad 4\text{-}4$$

4-2 then becomes

$$\xi_2 = -2U_2\int_{'}^{2}\frac{1}{U}\frac{\partial U}{\partial z}\,d\theta \qquad 4\text{-}5$$

The velocity gradient $\frac{\partial U}{\partial z}$ varies as the flow moves through the cascade as can be seen from the measurements and is thus a function of Θ. In order to simplify the integration, $\frac{\partial U}{\partial z}$ is assumed to be constant and the average value between inlet and outlet is chosen

$$\frac{\partial U}{\partial z} = \frac{1}{2}\frac{\partial}{\partial z}(U_1 + U_2) \qquad 4\text{-}6$$

Assuming infinitely thin blades, the continuity equation for the two-dimensional flow through the cascade yields

$$U \sin\alpha = U_1 \sin\alpha_1 \qquad 4\text{-}7$$

Combining 4-5, 4-6 and 4-7 and integrating yields:

$$\xi_2 = -\left(1 + \frac{\sin\alpha_1}{\sin\alpha_2}\right)\frac{\cos\alpha_1 - \cos\alpha_2}{\sin\alpha_2}\,\frac{dU_1}{dz} \qquad 4\text{-}8$$

This formula looks quite different from Squire and Winter's expression but it can be shown that the two formulas coincide as $\alpha_2 \longrightarrow \alpha_1$ i.e. for infinitely small turning.

The proof is given below:

4-8 can also be written as

$$\xi_2 = -\left(1 + \frac{\sin\alpha_1}{\sin\alpha_2}\right)\frac{2\sin\frac{\alpha_1+\alpha_2}{2}\sin\frac{\xi}{2}}{\sin\alpha_2}\cdot\frac{dU_1}{dz}$$

As $\alpha_2 \longrightarrow \alpha_1$

$$\sin \frac{\alpha_1+\alpha_2}{2} \longrightarrow \sin \alpha_2$$

$$2 \sin \frac{\varepsilon}{2} \longrightarrow \varepsilon$$

and so

$$\lim_{\alpha_2 \to \alpha_1} \xi_2 = -2\varepsilon \frac{dU_1}{dz}$$

Comparison between 4-8 and 4-1 for the actual values yields

$$\frac{\xi_2}{\xi_{2w}} = 0.80$$

The difference is appreciable and is due to the fact that formula 4-8 corrects for the pressure rise over the cascade.

In the following portion of this report the notation for ξ_2 according to 4-1 will be used. Also the results using 4-8 will be presented.

4.2.2 Determination of Secondary Velocities

Consider the flow in a plane perpendicular to the mainstream behind the cascade according to Figure 21. The rectangular boundaries of the plane are made up of the top and bottom walls of the cascade and two adjacent blade wakes from the two-dimensional flow. As the secondary vorticity vector is parallel to the flow direction the secondary velocities will be induced almost completely in the y, z - plane. Neglecting any velocities induced in the x - direction the continuity equation for the seconary flow becomes

$$\frac{\partial v}{\partial y} + \frac{\partial w}{\partial z} = 0 \qquad 4\text{-}9$$

The vorticity ξ may be expressed as

$$\frac{\partial w}{\partial y} - \frac{\partial v}{\partial z} = \xi \qquad 4\text{-}10$$

Introduce a stream function ψ for the secondary flow such that

$$v = \frac{\partial \psi}{\partial z}$$

$$w = -\frac{\partial \psi}{\partial y} \qquad 4\text{-}11$$

and which satisfies the continuity equation 4-9 identically. Combining 4-10 and 4-11 yields

$$\nabla^2 \psi = \frac{d^2\psi}{dy^2} + \frac{d\psi^2}{dz^2} = -\xi \qquad 4\text{-}12$$

where ξ is given by equation 4-1 and 4-8.

This is Poisson's equation which has to be solved for ψ together with appropriate boundary conditions.

Boundary conditions:

At the boundary the cross flow velocity components have to be zero. The flow is symmetrical about the midspan and so this can be taken as a boundary:

$$v = \frac{\partial \psi}{\partial z} = 0 \quad \text{for} \quad \begin{matrix} y = 0 \\ y = b \end{matrix} \qquad 4\text{-}13$$

$$w = -\frac{\partial \psi}{\partial y} = 0 \quad \text{for} \quad \begin{matrix} z = 0 \\ z = \ell \end{matrix} \qquad 4\text{-}14$$

These equations may be integrated yielding

$$\psi = \text{const at the boundaries}$$

As the constant is arbitrary it is chosen equal to zero. The boundary conditions are then

$$\psi = 0 \qquad 4\text{-}15$$

The equation 4-12 with the boundary conditions 4-15 has been solved analytically by Squire and Winter (17), Ehrich (26), Smith (24) and Hawthorne (29).

By using expression 4-1 for ξ and expressing ϵ in a Fourier series

$$\epsilon = \sum_{n=1,3,5\cdots}^{\infty} \frac{4\epsilon}{n\pi} \sin n\pi \frac{y}{b} \qquad 4\text{-}16$$

Hawthorne derived the following formula for ψ

$$\psi = \sum_{n=1,3,5\cdots}^{\infty} \psi_n(z) \sin n\pi \frac{y}{b} \qquad 4\text{-}17$$

where

$$\psi_n = \frac{-8\epsilon b}{(n\pi)^2} \left\{ \frac{\sinh n\pi z/b}{\sinh n\pi \ell/b} \int_z^{\ell} \frac{dU_1}{d\zeta} \sinh n\pi \frac{\ell-\zeta}{b} d\zeta + \right.$$

$$\left. + \frac{\sinh n\pi \frac{\ell-z}{b}}{\sinh n\pi \ell/b} \int_0^{z} \frac{dU_1}{d\zeta} \sinh n\pi \frac{\zeta}{\pi} d\zeta \right\} \qquad 4\text{-}18$$

In 4-18 ζ replaces z as a dummy variable.

The derivative of ψ_n with respect to z is

$$\psi_n' = \frac{d\psi_n}{dz} = \frac{-8\epsilon}{n\pi} \left\{ \frac{\cosh n\pi z/b}{\sinh n\pi \ell/b} \int_z^{\ell} \frac{dU_1}{d\zeta} \sinh n\pi \frac{\ell-\zeta}{b} d\zeta - \right.$$

$$\left. - \frac{\cosh n\pi \frac{\ell-z}{b}}{\sinh n\pi \ell/b} \int_0^{z} \frac{dU_1}{d\zeta} \sinh n\pi \frac{\zeta}{b} d\zeta \right\} \qquad 4\text{-}19$$

The secondary velocities v and w are then given by 4-13 and 4-14 which together with 4-17, 4-18 and 4-19 yields

$$V = \sum_{n=1,3,5\cdots}^{\infty} -\frac{8\varepsilon}{n\pi} \left\{ \frac{\cosh n\pi \frac{z}{b}}{\sinh n\pi \frac{l}{b}} \int_z^l \frac{dU_1}{d\zeta} \sinh n\pi \frac{l-\zeta}{b} d\zeta - \right.$$

$$\left. - \frac{\cosh n\pi \frac{l-\zeta}{b}}{\sinh n\pi \frac{l}{b}} \int_0^z \frac{dU_1}{d\zeta} \sinh n\pi \frac{\zeta}{b} d\zeta \right\} \sin n\pi \frac{y}{b} \qquad 4\text{-}20$$

$$w = \sum_{n=1,3,5\cdots}^{\infty} -\frac{8\varepsilon}{n\pi} \left\{ \frac{\sinh n\pi \frac{z}{b}}{\sinh n\pi \frac{l}{b}} \int_z^l \frac{dU_1}{d\zeta} \sinh n\pi \frac{l-\zeta}{b} d\zeta - \right.$$

$$\left. - \frac{\sinh n\pi \frac{l-\zeta}{b}}{\sinh n\pi \frac{l}{b}} \int_0^z \frac{dU_1}{d\zeta} \sinh n\pi \frac{\zeta}{b} d\zeta \right\} \sin n\pi \frac{y}{b} \qquad 4\text{-}21$$

4.2.2.1 The Transverse Velocity v and the Transverse Flow Deviation Angle β

The maximum value of the transverse velocity v at any position of z occurs at y = b/2 and is given by

$$V_{max} = \left(\frac{\partial \psi}{\partial z}\right)_{y=b/2} = -\sum_{n=1,3,5\cdots}^{\infty} (-1)^{\frac{n+1}{2}} \psi_n' \qquad 4\text{-}22$$

The transverse velocity v varies across the blade passage. It is of interest to find its average value in tangential direction. The y average is, however, equivalent to the tangential average because the secondary flow has been assumed not to vary in mainstream direction.

The average value of v at any z is then

$$\bar{V} = \frac{1}{b} \int_0^b V dy = \frac{2}{\pi} \sum_{n=1,3,5\cdots}^{\infty} \frac{\psi_n'}{n} \qquad 4\text{-}23$$

The transverse secondary flow component v causes a change β in transverse flow angle at the outlet of the cascade.

The maximum change in transverse flow angle β is given by

$$\tan\beta_{max} = \frac{V_{max}}{U_2} \qquad 4\text{-}24$$

which when combined with the two-dimensional continuity equation 4-7 yields

$$\tan\beta_{max} = \frac{V_{max}}{U_1}\,\frac{\sin\alpha_2}{\sin\alpha_1} \qquad 4\text{-}25$$

Similarly the average change in transverse flow angle β in tangential direction is

$$\tan\bar{\beta} = \frac{\bar{V}}{U_2} = \frac{\bar{V}}{U_1}\,\frac{\sin\alpha_2}{\sin\alpha_1} \qquad 4\text{-}26$$

A positive value of the transverse flow deviation angle indicates an underturning of the flow through the cascade.

4.2.2.2 The Spanwise Velocity w and Spanwise Flow Deviation Angle γ

The maximum value of the spanwise velocity w occurs at the blade wakes i.e. y = 0 and y = b and is

$$w_{max} = -\left(\frac{\partial\psi}{\partial y}\right)_{\substack{y=0\\ b}} = \mp \sum_{n=1,3,5\cdots}^{\infty} \frac{n\pi}{b}\,\psi_n \qquad 4\text{-}27$$

The average value of w over one blade spacing at any z position can be shown to be equal to zero.

The maximum spanwise flow deviation angle γ_{max} caused by the velocity w_{max} is given by

$$\tan \gamma_{max} = \frac{w_{max}}{U_2} = \frac{w_{max}}{U_1} \cdot \frac{\sin \alpha_2}{\sin \alpha_1} \qquad 4\text{-}28$$

Averaged over one blade spacing the spanwise flow deviation angle caused by the secondary flow is, of course, zero.

4.2.3 Mathematical Expression for the Velocity Distribution of the Wake at the Inlet to the Cascade

The velocity distribution in the wake could be described very well with two different mathematical expressions

$$\frac{U_1}{U_1} = 1 - 2a\left[1 - \left(\frac{z}{\delta}\right)^{\frac{3}{2}}\right] \qquad 4\text{-}29$$

$$\frac{U_1}{U_1} = 1 - a\left[1 + \cos \pi \frac{z}{\delta}\right] \qquad 4\text{-}30$$

where the notations are given in Figure 21.

The first expression 4-29 is given by H. Schlichting (46) for the velocity distribution in a two-dimensional wake. The second formula is given by Forstall in reference (48). When substituted in the formulae for Ψ_n and Ψ_n' the first expression 4-29 gave integrals that could not be integrated in closed forms. The second 4-30 gave simple integrals and so that was used in the calculations. See Figure 22.

The integrations of the expressions for Ψ_n and Ψ_n' have to be performed in two regions $0 \le z \le \delta$ and $\delta \le z \le l$ because $\frac{dU_1}{dz}$ is not

continuous over the whole region $0 \leq z \leq \ell$:

$$\frac{dU_1}{dz} \begin{cases} \neq 0 & \text{for } 0 < z < \delta \\ = 0 & \text{for } \delta < z < \ell \end{cases}$$

Inserting 4-30 in the formulae for ψ_n 4-18 and ψ_n' 4-19 and integrating yields

for $0 \leq z \leq \delta$

$$\psi_n = \frac{-8\varepsilon b}{(n\pi)^2} \frac{\bar{U}_1 a}{1+(n\frac{\delta}{b})^2} \left\{ n\frac{\delta}{b} \sin \pi \frac{z}{\delta} + \frac{\sinh n\pi \frac{\ell-\delta}{b}}{\sinh n\pi \ell/b} \sinh \left(n\frac{\delta}{b} \cdot \pi \frac{z}{\delta} \right) \right\} \qquad 4\text{-}31$$

$$\psi_n' = \frac{-8\varepsilon}{n\pi} \frac{\bar{U}_1 a}{1+(n\frac{\delta}{b})^2} \left\{ \cos \pi \frac{z}{\delta} + \frac{\sinh n\pi \frac{\ell-\delta}{b}}{\sinh n\pi \ell/b} \cosh \left(n\frac{\delta}{b} \cdot \pi \frac{z}{\delta} \right) \right\} \qquad 4\text{-}32$$

and for $\delta \leq z \leq \ell$

$$\psi_n = \frac{-8\varepsilon b}{(n\pi)^2} \frac{\bar{U}_1 a}{1+(n\frac{\delta}{b})^2} \frac{\sinh n\pi \delta/b}{\sinh n\pi \ell/b} \sinh n\pi \frac{\ell}{b} \left(1-\frac{z}{\ell}\right) \qquad 4\text{-}33$$

$$\psi_n' = \frac{8\varepsilon}{n\pi} \frac{\bar{U}_1 a}{1+(n\frac{\delta}{b})^2} \frac{\sinh n\pi \delta/b}{\sinh n\pi \ell/b} \cosh n\pi \frac{\ell}{b} \left(1-\frac{z}{\ell}\right) \qquad 4\text{-}34$$

Details of the integration can be found in Appendix A.

Remembering the expressions for the secondary velocity components v and w, 4-11, some conclusions can now be drawn about those velocities, caused by a wake described by 4-30.

Both components v and w are directly proportional to the turning angle ε and to the velocity defect $2\bar{U}a$ in the center of the wake. The expressions for the velocity componets are built up of non-dimensional factors:

$$\frac{l}{b} = \frac{\text{Blade height}}{\text{width of the blade passage at outlet}}$$

$$\frac{\delta}{b} = \frac{\text{half wake width}}{\text{width of the blade passage of the outlet}}$$

and $\frac{z}{l}$, $\frac{z}{\delta}$, and $\frac{y}{b}$ which are geometrical positions of the actual velocity components.

4.2.4 Comparison of Theory and Experiments

The actual values for the cascade configuration and the inlet flow (given in Appendix A) have been inserted in the formulas derived above and the transverse flow deviation angles and spanwise flow deviation angles have been calculated. In these calculations the three first terms in the series for ψ and ψ' have been retained i.e. n = 1, 3 and 5.

The results of these calculations and the experiments are given in Figures 23, 24, 25, and 26.

4.2.4.1 The Maximum Transverse Flow Deviation Angle, β_{max}.

The variation of the maximum transverse flow deviation angle β_{max} over the span is shown in Figure 23.

The position of both the maximum overturning and the maximum underturning was located on a vertical line at about midway between two adjacent bladewakes. The maximum overturning occurred at the center of the wake and amounted to 9.7° at 0.1 inches behind the cascade and 6.9° at 2.25 inches behind the cascade.

The maximum underturning at the cascade exit amounted to 2.8° and occurred at about 1.1 inches from the center of the wake which is also the spanwise position of the edge of the incoming wake. The position of the maximum underturning moved away from the wake center as the flow travelled downstream and was located at about 1.5 inches from the wake center at 2.25 inches behind the cascade. The magnitude of the underturning had only changed slightly.

The theory predicts that the location of both the maximum overturning and maximum underturning should occur at midway between two adjacent blade wakes and the experiments confirmed this.

Using expression 4-1 for the secondary vorticity gives a maximum overturning of 14.2° which is about 50% higher than the experiments showed and predicts an underturning of 3° which is very close to the measured value. The theoretical values are here compared with the measured values at the cascade exit plane as the theory is only applicable for this case.

Using expression 4-8 instead gives a maximum overturning of 11.2° which is about 15% higher than the experimental value and a maximum

underturning of 2.4° which is somewhat less than the measured value.

Both formulas predict the same locations for the extreme values namely the wake center for the maximum overturning and at about the edge of the incoming wake for the maximum underturning. The agreement with the experiments in this respect was excellent.

4.2.4.2 The Average Transverse Flow Deviation Angle $\bar{\beta}$

Figure 24 shows the variation of the average transverse flow deviation angles, $\bar{\beta}$, over the span.

The measured transverse flow angles were averaged over two blade spacings at each spanwise traversed position. The difference between these values and the average of the two-dimensional transverse flow angles is called the average transverse flow deviation angle $\bar{\beta}$. The shape of these curves agrees closely with the shape of the curves of maximum transverse flow deviation angles. They both show maximum overturning in the center of the wake. The maximum overturning at the cascade exit was 6.7° and 4.4° half a chord downstream. The position of the maximum underturning was located at about 1.3 inches from the center of the wake at the cascade exit and about 1.4 inches at half a chord downstream. The magnitude of the underturning was about 0.7° at the cascade exit and this value had increased to about 1.9° half a chord downstream. The shape of the curve outside the wake had changed too. The average value of the transverse flow angle differed about 2° in the free stream outside the wake on the two sides of the wake at cascade exit. This phenomenon can probably be traced back to the inlet conditions where a change in inlet angle of about the same magnitude on the two sides of the wake was noticed. Most of this difference had disappeared half a chord downstream

and this rearrangement of the flow may have caused the noted change in magnitude of the maximum underturning.

The predicted values using expressions 4-1 and 4-8 for the secondary vorticity are shown in Figure 24 and yield 11.6° and 9.8° respectively for the maximum overturning and 2.4° and 1.9° respectively for the maximum underturning. These values are to be compared with 6.7° and 0.7° respectively which were the measured values. Also in this case the values calculated by using 4-8 agree fairly well and are much closer to the experimental values than the ones that 4-1 predicts.

4.2.4.3 The Maximum Spanwise Flow Deviation Angle γ_{max}

The variation of the maximum spanwise flow deviation angle γ over the span is shown in Figure 25 and Figure 26. The average value over one blade spacing of the spanwise flow deviation angle due to the secondary flow should be zero at each spanwise position. However, the measurements showed an average angle variation over the span at the two different measuring positions. This is due to the diffusion of the wake as it moves downstream thus causing spanwise flows toward the center of the wake. This is brought out by the curve of the average spanwise flow deviation angle shown in Figure 26. The measured values of the spanwise flow deviation angle have therefore been corrected with the flow angle caused by the diffusion of the wake.

The measured maximum spanwise flow deviation angle at cascade exit was 5.8° and it was located very close to one of the blade wakes and about 0.5 inches from the center of the wake. About the same magnitude of the corrected maximum angle was found at both the pressure and the suction side of the blade wakes. The spanwise position of these maximum values was,

however, different. It was located closer to the center of the wake on the pressure side of the blade wake which can be seen in Figure 17 and Figure 18, and was caused by the spanwise flow which is directed toward the center of the wake on the pressure side and away from the center on the suction side of the blade wake. Half a chord downstream this angle had reduced to 3.5° at one side of the wake and to 4.7° at the other side and the spanwise positions for these maximum values had moved out to about 0.8 inches from the wake center.

The theory predicts the maximum spanwise flow deviation angle to occur at the blade wakes and the experiments confirmed this. The calculated value for the same angle is 7.8° when using formula 4-1 and 6.2° using 4-8. Even in this case formula 4-8 gives a value close to the experimental results while formula 4-1 gives too high a value. Both formulas predict the same spanwise position, about 0.6 inches for the maximum value which is slightly higher than the measured position on the pressure side, and slightly less than the measured position on the suction side. The spanwise position predicted by the theory agrees well with the average measured position on the two sides of the blade wake.

4.2.4.4 Conclusion

Close agreement between the measured and calculated values of the flow angle deviations at cascade exit due to the secondary flow is achieved when formula 4-8 is used to describe the distributed vorticity in streamwise direction behind the cascade. When formula 4-1 is used instead of 4-8, the predicted values are about 50% higher than the measured ones. The positions of the maximum flow angle deviations are predicted closely by the theory and both formulae predict identical positions.

4.3 Losses and Kinetic Energy of Secondary Flow

4.3.1 Results of Measurements

The magnitude of the velocity vector was computed at cascade exit plane by using the measured values of stagnation pressure and stream pressure. The stagnation pressure was measured 0.1 inches behind the cascade while the stream pressure was measured 0.35 inches behind. In these calculations, however, it was assumed that the stream pressure did not change between the two axial positions. When computing the corresponding values half a chord downstream it was assumed that the stream pressure was identical with the atmospheric pressure. Using the measured flow deviation angles and the computed magnitudes of the velocity vectors the secondary flow velocity components v and w were computed. The sum $\frac{1}{2}\rho(v^2+w^2)$ was formed at each measured point and these values were integrated and averaged over two blade spacings at constant spanwise positions. The values were divided by the value of the kinetic energy of the inlet flow and were plotted vs. distance over the span. The area under the curve was integrated. The resulting curves are shown in Figure 27. At cascade exit the following result was obtained

$$\frac{D}{KE_{inl.}} = 0.13\ \%$$

and half a chord downstream

$$\frac{D}{KE_{inl.}} = 0.07\ \%$$

The kinetic energy of the secondary flow had apparently decayed due to viscous action to about 50% of its value at cascade exit.

The curve of the kinetic energy of the secondary flow has two maximum points and one minimum point. The absolute maximum is located in

the wake center caused by the transverse component of the secondary flow which also has its maximum value there (= maximum overturning). The second maximum point which is lower than the first is located at about the same spanwise position as the edge of the incoming wake and this maximum is also caused by the transverse component of the secondary flow which has another extreme value here, namely maximum underturning.

Between these maxima there is a minimum point the location of which corresponds to the position of zero transverse velocity component of the secondary flow. See Figures 23 and 24.

The ratio of the kinetic energy of the spanwise flow and the total kinetic energy of the secondary flow was also evaluated.

This ratio was 0.57 at cascade exit and 0.50 half a chord downstream. The accuracy of the measurements and calculations does not permit a definite conclusion about their relative values.

The conclusion to draw is that the kinetic energy of the secondary flow is divided equally in the spanwise and transverse flow components and that this ratio is preserved as the flow moves downstream. This implies that the two velocity components of the secondary flow decay at the same rate.

4.3.2 Theoretical Calculation of the Kinetic Energy of the Secondary Flow

The kinetic energy per unit volume of the secondary flow is given by

$$D = \tfrac{1}{2}\rho \int_0^{\ell}\int_0^{b} (v^2 + w^2)\, dy\, dz \qquad 4\text{-}35$$

After some calculations this expression transforms into:

$$D = \frac{16}{\pi^2}\rho(\varepsilon b \bar{U}_1 a)^2 \sum_{n=1,3,5\ldots}^{\infty} \frac{1}{n^3\left[1+(n\frac{\delta}{b})^2\right]} \left\{ \frac{n\delta}{2b} + \right.$$

$$\left. + \frac{1}{\pi\left[1+(n\frac{\delta}{b})^2\right]} \frac{\sinh n\pi \frac{\ell-\delta}{b}}{\sinh n\pi \ell/b} \sinh n\pi \frac{\delta}{b} \right\} \qquad 4\text{-}36$$

Details of these calculations are given in Appendix F.

The expression for the kinetic energy per unit volume of the inlet flow to the cascade has been derived in Appendix F-2 and is

$$KE_{inl.} = \frac{1}{2}\rho \bar{U}_1 s\ell \sin\alpha_1 \left\{ 1 - \frac{\delta}{\ell}\left[1-(1-a)^2+\frac{a^2}{2}\right]\right\} \qquad 4\text{-}37$$

The ratio of the kinetic energy of the secondary flow and the kinetic energy of the incoming flow is then given by

$$\frac{D}{KE_{inl.}} = \frac{32}{\pi^2}\frac{s}{c}\frac{c}{\ell}\frac{\varepsilon^2 a^2}{1-\frac{\delta}{\ell}\left[1-(1-a)^2-\frac{a^2}{2}\right]}\frac{\sin^2\alpha_2}{\sin\alpha_1}\sum_{n=1,3,5\ldots}^{\infty}\frac{1}{n^3\left[1+(n\frac{\delta}{b})^2\right]}\left\{\frac{n\delta}{2b}+\right.$$

$$\left. + \frac{1}{\pi\left[1+(n\frac{\delta}{b})^2\right]}\frac{\sinh n\pi\frac{\ell-\delta}{b}}{\sinh n\pi \ell/b}\sinh n\pi\frac{\delta}{b}\right\} \qquad 4\text{-}38$$

Formula 4-38 expresses how much of the kinetic energy per unit volume of the incoming flow that has been used to produce the secondary flow. The kinetic energy per unit time instead of per unit volume is a more correct expression for the total transformation of incoming kinetic energy into secondary flow and would have been achieved if formula 4-35 had been multiplied by the transport velocity (= the axial velocity) before integrating. Correspondingly also, the expression 4-37 of the kinetic energy of the inlet flow. This would have reduced the magnitude of the ratio $D/K.E._{inl}$ since the transport velocity is lower in the wake where most of the

secondary flow is located. However, no simple expression such as 4-38 would have been achieved then and it was felt that a simplification was justified for two reasons:

The evaluation and processing of the experimental data was greatly facilitated.

The numerical value of the kinetic energy of the secondary flow was found to be very small and could be neglected compared to the losses.

The expression for the ratio D/KE_{inl} is formed by non-dimensional parameters. The most important of which are:

the turning angle ε of the flow

the magnitude, a, of the wake

the outlet angle α_2 in form of sin α_2, which all occur to the second power.

The actual values for this cascade configuration have been inserted in formula 4-39 and gave

$$\frac{D}{KE_{inl}} = 0{,}23\ \%$$

when formula 4-1 was used to express the secondary vorticity, and gave

$$\frac{D}{KE_{inl}} = 0.15\ \%$$

when formula 4-8 was used.

Good agreement between predicted and measured values of the kinetic energy of the secondary flow was obtained when formulae 4-38 and 4-8 were used. The combination of 4-38 and 4-1 yielded too high a value as might be expected since the deviation angles predicted by using 4-1 were also too high.

If 4-35 is integrated only over y i.e. in the tangential direction the following expression is obtained (see Appendix F-5).

$$D_z = \frac{\rho b}{4} \sum_{n=1,3,5\ldots} \left[\psi_n'^2 + \left(\frac{\pi}{b}\right)^2 \psi_n^2 \right] \qquad 4\text{-}39$$

This formula gives the spanwise distribution of the kinetic energy of the secondary flow and can be expanded further by substituting the expressions for ψ_n and ψ_n' given in 4-31 through 4-34 but as ψ_n and ψ_n' have to be computed in order to calculate the secondary flow these values are given as functions of z and it is convenient then to use 4-39.

The actual values for this flow have been substituted in formula 4-39 and the results of this calculation are shown as curves in Figure 27. Both formulae 4-1 and 4-8 have been used to express the vorticity. The theoretical curves have the same shapes as the measured ones with two maximum points and one minimum point. Formula 4-39 together with 4-1 however yields values that almost everywhere exceed the curve of the measured data. Formula 4-39 combined with 4-8 predicts too high a value at the wake center and too low values over the rest of the span. The agreement with experiments is, however, better for this curve.

4.3.3 Losses

The measured stagnation pressure defects have been area averaged over two blade spacings at constant spanwise positions at the two traversed planes and these averaged values have been plotted vs. distance over the span as shown in Figure 28.

The inlet wake has broadened and its maximum value has reduced as it moved through the cascade. Outside the wake the stagnation pressure defect is greater than zero. This is caused by the friction at the blade surfaces and is a measure of the two-dimensional cascade loss. A stagnation pressure loss is here defined as the decrease of stagnation pressure along a streamline. In a two-dimensional cascade flow the loss can easily be calculated as the average stagnation pressure defect over one blade spacing at a constant spanwise position since all the streamlines remain in the same spanwise plane. In a three-dimensional flow the streamline cannot be easily traced and a streamline entering the cascade at one spanwise position may leave it at another. The difference between the reference stagnation pressure upstream of the cascade and the stagnation pressure at a point downstream of the cascade is therefore called stagnation pressure defect at that point. However, the difference between the integrated stagnation pressure over the whole area upstream of the cascade and the integrated stagnation pressure over the whole area downstream of the cascade may be called the stagnation pressure loss for the cascade. In this case it includes all the three-dimensional effects on the losses.

The loss calculations were performed in the following way. The two-dimensional stagnation pressure defect outside the wake is assumed to maintain its value even inside the wake. This implies that the friction effect on the blade surfaces is larger in the wake than outside, as the dynamic head in the wake is lower than the reference dynamic head and also the stagnation pressure defects in the wake have been divided by the reference dynamic head. The pictures of the streamline traces in

carbon black indicate that this is true. The magnitude is, however, not known and cannot be calculated with any accuracy. This assumption will, however, not change the conclusions about the three-dimensional losses. The stagnation pressure defect in excess of this two-dimensional loss has been averaged over the total span, 16 inches, giving a mean value of

3.73% at cascade exit

and 3.72% half a chord downstream.

These two figures agree very well. However, the defect is greater at cascade exit than further downstream which violates the second law of thermodynamics. This depends, however, on the fact that the defects have been area averaged instead of mass averaged. The same situation occurred in the two-dimensional tests (3-2). If the average inlet stagnation pressure defect, 3.7%, is subtracted from the figures above there is left a stagnation pressure defect that may be called a complementary loss and accounts for the losses created by the secondary flow. These figures are very small, 0.03% and 0.02% respectively and comprise effects such as mixing of the wake and the free stream as the flow moves through the cascade. The secondary flow probably causes a more extensive mixing than would occur if the Bernoulli surfaces were not turned. The figures are, however, smaller than would be expected from pure mixing of a wake in an adverse pressure field. This depends on the fact that the above figures are the result of an area integration instead of a mass integration in which case the inlet mean value would have decreased proportionally more than the outlet mean value thus giving higher losses. However, the results show that there is only a very small contribution of the secondary flow to the overall losses created in the cascade.

In the above figures the kinetic energy of the secondary flow has not been treated as a loss. In an actual machine most of the kinetic energy of the transverse flow is probably recovered in the following stage. The kinetic energy of the spanwise flow may be lost.

Even if all the kinetic energy of the secondary flow is lost this is a fairly small value amounting to 0.13% of the kinetic energy of the inlet flow to the cascade and is only about 8% of the two-dimensional cascade loss.

4.4 The tangential Component of the Blade Force

4.4.1 Results of Measurements

Stream pressure on the blade surfaces were measured at 5 different spanwise positions. The positions were located 1/8", 3/8", 1 1/8", 2 1/8" and 4 1/8" from midspan.

The results of the measurements are presented in Figure 29A as plots of the tangential component of the blade force divided by the reference dynamic pressure called the tangential pressure coefficient C_T. A contour map of the pressure distribution is shown in Figure 30.

There seems to be remarkably little change in the pressure distribution in the wake region. However, the curves show that the stream pressure in the wake is reduced over most of the chord. The defect is greatest at the leading portion of the suction side and reduces toward the trailing edge where the defect is slight. This gives a lower pressure rise along the chord in the wake than in the free stream. The defect on the pressure side is less and almost constant over most of the chord.

This defect of the stream pressure in the wake results in a lower

tangential pressure coefficient C_T there, as can be seen in Figure 29B. The pressure coefficient is here based on the reference dynamic pressure and it changes from $C_T = 0.461$ in the free stream to $C_T = 0.382$ in the center of the wake.

If the pressure coefficient instead is based on the actual inlet dynamic pressure at the same spanwise position as the pressure measurements were taken C_T increases in the wake and equals 0.725 in the wake center. This cascade configuration has been tested in a uniform flow in another wind tunnel for different inlet angles covering also the stalled flow region. The onset of stall has here been defined as the inlet angle for which the two-dimensional cascade losses are twice the minimum loss. At this inlet angle the flow at the rear part of the suction surface is separated.

Substituting the measured angles from this test into the formula for C_T given in section 3.3 yields $C_T = 0.590$ for the onset of stall. At the wake center where $C_T = 0.725$ no separation could be detected. Cascades generally behave differently in different wind tunnels especially close to and inside the stalled flow region but the conclusion to draw is that values of C_T achieved from two-dimensional cascade data will not give the same information about the flow behaviour in a three-dimensional case.

4.4.2 Theoretical Calculation of the Tangential Component of the Blade Force

In Appendix G derivation of the formula for the tangential pressure coefficient, C_T, is presented:

$$C_T = 2\sin^2\alpha_1(\cot\alpha_1 - \cot\alpha_2)\left(1 - \frac{\theta}{l} - \frac{\delta^*}{l}\right) - \frac{D}{\varepsilon}\frac{\sin\alpha_1}{\frac{1}{2}\rho\bar{U}_1^2 s \cdot l} \qquad 4\text{-}40$$

This expression may be interpreted in the following way

(1) $2\sin^2\alpha_1(\cot\alpha_1 - \cot\alpha_2)$ is the tangential pressure coefficient if the flow is uniform over all the span

(2) $-2\sin^2\alpha_1(\cot\alpha_1 - \cot\alpha_2)\left(\frac{\theta}{t} + \frac{\delta^*}{t}\right)$ is the reduction in C_T due to the decreased mass flow in the wake

(3) $-\frac{D}{\varepsilon}\frac{\sin\alpha_1}{\frac{1}{2}\rho V_1^2 s.t}$ is the reduction in C_T due to the creation of secondary flow.

It is to be noted that only term (3) changes when the different expressions 4-1 and 4-8 are used to express the streamwise vorticity component.

The actual values for this flow including the measured value of D have been substituted in formula 4-40. The results of this calculation is given in the following table:

Term	Value
(1)	0.521
(2)	-0.018
(3)	-0.002
C_T	0.501

The decrease in C_T from its two-dimensional value is about 3.8% of which term (2) contributes 3.4% and term (3) about 0.4%. The contribution from the secondary flow is thus very small.

The measured free stream value of C_T was 0.461 to be compared to the calculated value 0.521.

The average value of C_T over the span was determined through a graphical integration of the area under the C_T curve and gave $C_T = 0.445$ compared to the calculated value of 0.501.

As can be seen the calculated values are about 12 % greater than

the measured ones. The decrease in C_T from its two-dimensional value is about 3.4% to be compared to a calculated figure of 3.8%. The theory predicts a greater decrease in C_T due to the wake flow than the measurements show but the agreement is good.

5. SKEWED FLOW

5.1 Results of Measurements

The results of the measurements have been presented as contour maps over the traversed areas showing stagnation pressures, stream pressures, transverse flow angles and spanwise flow deviation angles.

5.1.1 Upstream Conditions

5.1.1.1 Transverse Inlet Flow Angles

Figure 31 shows the transverse inlet angle variation over the traversed area upstream of the cascade. The angles varied between about 45° in the free stream to about 24° in the center of the skewed layer. The angle distribution was fairly uniform in tangential direction. The nonuniformity was larger in the free stream than in the skewed layer.

5.1.1.2 Stagnation Pressure

The stagnation pressure distribution over the traversed area is shown in Figure 32. The intention was to have a constant stagnation pressure over the whole area but due to the reasons mentioned in section 2.3 this could not be realized. Two wakes located about 1 inch on each side of the midspan and extending in tangential direction were created. The pressure defect in the centers of these wakes amounted to about 25% of

the dynamic pressure when the flow was adjusted so that there was no pressure defect of the skewed flow layer at midspan. The width of each of the wakes was about 1 inch at the base. The distribution was fairly uniform in tangential direction.

5.1.1.3 Stream Pressure

A contour map of the stream pressure distribution over the traversed area is shown in Figure 33. The stream pressure distribution around the blades of the cascade can clearly be seen as vertical contours modified by the pressure distribution in the skewed flow layer. A higher stream pressure was built up around each blade since the flow had a stagnation point at the leading edge of each blade. The stream pressure in the skewed flow layer was about the same as, or somewhat higher than, the stream pressure midway between two adjacent blades.

5.1.2 Downstream Conditions

5.1.2.1 Stagnation Pressure

Figures 34 and 35 show contour maps of the stangation pressure distribution at the two traversed areas downstream of the cascade.

The blades were heavily stalled in the skewed flow layer as can be seen in Figure 34. A real back flow was created at the suction side of the blades. This back flow was made visible by placing a thread glued to the end of a pin pointed stick in the flow. In the region of back flow the thread was blown in the direction from the trailing to the leading edge of the blade. At the transition region between the back flow and the free stream the flow was very unsteady. The limiting line on the contour maps between the back flow region and the through flow region may not be

considered to be very accurate. The region of back flow was much larger on the blade which had the pressure taps on its suction surface than on the blade with the pressure taps on the pressure side indicating the importance of the surface eveness in the stalled flow region.

The two wakes in the inlet flow to the cascade could be traced downstream of the cascade as two horizontal wakes seen in the center of the blade passage. The skewed flow impinged on the pressure side of the blades and spread out from the center toward the blade ends creating a secondary flow. This flow, made up of the high energy fluid in the spanwise center of the incoming skewed flow, distorted the two horizontal wakes towards the blade ends and reduced their magnitude on the pressure side of the blades.

An intensive mixing between the high energy flow at the pressure side of the blades and the low energy flow at the suction side of the blades effectively eliminated the back flow half a chord downstream. The flow was, however, very unsteady in the regions of previous back flow. The centers of low stagnation pressure had moved slightly away from the suction side of the blades toward the center of the blade passages. The centers of the high stagnation pressure at midspan had moved less, so that the blade wakes remained fairly straight. The Bernoulli surfaces were turned in different directions at the two sides of the blade wakes. The stalled flow regions blocked part of the blade passages and acted as obstacles around which the fluid had to flow causing the Bernoulli surfaces to turn. This effect persisted as the flow moved downstream.

The stalling of the blades effectively masked the influence of the

of the skewed flow on the behaviour of the cascade and made an interpretation of the flow measurements difficult.

5.1.2.2 Stream Pressure

The stream pressure distributions at the two traversed areas are shown in Figures 36 and 37.

The stream pressure in the wake was slightly lower than the surrounding atmospheric pressure at the exit plane. Within the wake there were regions of very low stream pressure located at the centers of the back flow. The pressure difference between these regions and the surrounding atmosphere amounted to 25% of the dynamic reference pressure. The size of the low stream pressure region was larger at the blade with the largest stall flow region which could be expected, since a separation reduces the turning of the flow and thus reduces the pressure rise over the cascade.

Half a chord downstream most of the pressure differences had vanished. The stream pressure in the wake was just slightly lower than the surrounding stream pressure indicating an overall spanwise flow toward midspan. The centers of the low pressure regions had moved only slightly from the suction side of the blades toward the centers of the blade passages and the pressure difference between these centers and the atmospheric pressure was only 4% of the reference dynamic pressure. As the low stream pressure changed very fast in streamwise direction these low pressure regions seem not to be caused by vortices in streamwise direction.

The stream pressure distribution around the blades which was clearly observable in the free stream at cascade exit had almost completely disappeared half a chord downstream giving a uniform stream pressure in tangential direction in the free stream flow.

5.1.2.3 Transverse Flow Angles

Contour maps of the transverse flow angles are shown in Figures 38 and 39. The distortion of the flow from the stalled flow regions is clearly shown at cascade exit. The blockage of the flow in the stalled regions acted as a solid boundary and thus effectively decreased the width of the through flow passages in the skewed layer flow region.

A strong underturning of the flow occurred in the skewed flow regions at cascade exit. The center of this region was located about in the center of the effective flow passage at midspan. This underturning indicates a strong transverse secondary flow at the spanwise center of the skewed flow directed toward the pressure side of the blades and reaching its maximum value at about the center of the effective through flow passage.

At the outer edge of the skewed flow layer there was a region of slight overturning indicating a secondary flow directed opposite to the secondary flow at midspan. The positions of the center of the regions of underturning were located somewhat differently at the two sides of midspan. One was located at about the center of the effective flow passage while the other was located closer to the pressure side of the blade. Apart from this, the flow showed good symmetry about midspan. The flow angles in the back flow region could not be measured.

Half a chord downstream the flow angles had changed differently in the regions close to the blade wakes at midspan. At the blade with the smaller back flow region (left blade in Figure 39) the center of the underturned flow region remained approximately at the same relative position to the blade wake when the flow moved downstream. On the other side of the

blade wake a new region of underturned flow was created, made up of the flow from the previous back flow region. Due to the separation on the suction side of the blade this flow had not been given an equal amount of tangential momentum as the rest of the flow in the cascade and so this flow was turned less. The two regions were partly separated by the blade wake. The position and magnitude of the overturned flow region remained almost the same as the flow moved downstream.

At the blade with the greater back flow region (right blade in Figure 39) a different behaviour of the flow was shown. The region of underturned flow in the adjacent flow passage at cascade exit had completely disappeared. It had moved across the blade wake and joined the flow from the previous back flow region at the suction side of this blade and the two flows had jointly formed a region of strongly underturned fluid. The cause of this was the strong low pressure region located at this position at cascade exit and which sucked in the flow from the opposite side of the blade wake. This low pressure region was larger than the one at the adjacent blade wake as can be seen in Figure 36.

A very interesting discovery made was that the average transverse outlet angle in the free stream flow was about 4°, greater than the angle measured in the two-dimensional cascade test. The reason for this may be the changed stream pressure distribution around the blades. A greater stream pressure difference between the blades and the blade passages was established in this case causing the flow to turn more. The strong spanwise stream pressure gradient may also have acted to force the boundary layer on the suction sides of the blades to flow toward midspan reducing its thickness and so

reducing the deviation between the blade profile outlet angle and the flow outlet angle. The pressure rise in the free stream was also lower in this case than in the two-dimensional cascade test and this too causes a reduction in boundary layer thickness on the suction side of the blades.

5.1.2.4 Spanwise Flow Deviation Angles

Figures 40 and 41 show contour maps of the spanwise flow deviation angles at the two traversed planes. In each blade passage four regions of large spanwise flow deviation angles were found at the cascade exit. They were located next to the junctions of the outer edges of the skewed flow layer and the blade wakes. At the suction side of the blades, however, the tangential positions were displaced toward the outer edges of the back flow regions and the regions were elongated along the edges of the back flow region, once more stressing the point that these back flow regions may be looked upon as solid obstacles in the blade passages. The secondary flow indicated by these angles was thus directed out from midspan at the pressure surfaces of the blades and toward midspan at the suction side of the blades. The secondary flow directions in the back flow regions were not measured.

At about two inches from midspan almost no spanwise flow was observed. The spanwise flow angle distributions at cascade exit showed great symmetry about midspan.

Half a chord downstream this symmetry began to disappear. The regions of spanwise flow at the pressure side of the blade wakes had only moved slightly toward the suction side of the blade wakes but the spanwise flow deviation angles in these regions had been greatly reduced. The fluid

in the regions of spanwise flow at the back flow regions behaved differently at the two sides of midspan as the flow moved downstream. Above midspan the spanwise flow region at cascade exit had separated into two regions half a chord downstream. One region, made up of the fluid in the skewed layer region, had moved over the blade passage toward the pressure side of the adjacent blade wake while the other region made up of the fluid just outside the skewed flow layer remained at its relative position and established a new center of spanwise secondary flow. The magnitude of the flow angles were greatly reduced in both regions.

Below midspan this division in two parts had not occured but the fluid in the skewed layer had moved toward the suction side of the adjacent blade wake while the fluid outside the skewed flow layer remained at its relative position thus elongating the region of spanwise flow. The magnitude of the spanwise flow deviation angles had, however, reduced considerably, more so than in the regions above midspan.

The spanwise position of the regions of maximum spanwise flow angles were about the same at the two traversed planes.

5.1.2.5 Streamline Traces in Carbon Black

Streamline traces in carbon black on the blade surfaces are shown in Figure 42 (pressure side) and Figure 43 (suction side).

The transition from laminar to turbulent boundary layer on the pressure side of the blades is indicated as a dark streak extending over the span and located at about 30% from the leading edge. The black streak is intercepted at midspan where the skewed flow layer impinges on the blade surface, creating a strong velocity gradient at the blade surface which

removes the carbon black. The streaks at the center part of the blade are pointing away from midspan indicating a spanwise flow out from midspan.

In order to detect the separation on the suction side of the blades two different techniques were used. The whole surface on one blade was painted while only a strip at the trailing edge of another blade was painted. When the wind tunnel was started the suspension in the strip moved toward the leading edge of the blade in the central part indicating a back flow over that part of the span. This can clearly be seen in Figure 43. The shape of this region was almost a semicircle and the leading edge of this semicircular area was dark indicating the strip separating the stalled flow region from the unstalled. The flow direction on the blade surface in this stalled region was pointing out from midspan. The information from the contour maps and the streamline traces in carbon black now allow us to draw the following picture of the secondary flow pattern in a blade passage. The flow pattern shows a similarity to the secondary flow pattern found for the wake flow in section 4.1.2.4. However, the flow direction is opposite to that created by the wake flow. Inside the back flow region an opposite flow is established.

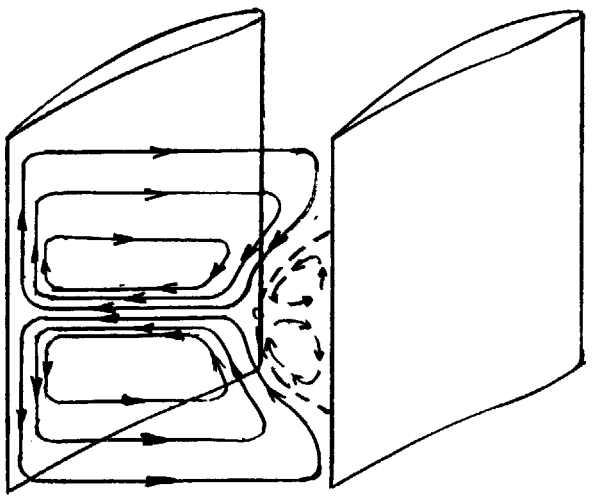

The mixing of this flow with the main flow further downstream may be the cause of the irregular spanwise flow deviation angle distribution found in Figure 41. The influence on the transverse flow angle distribution is less since the secondary flow in the back flow region is mostly in spanwise direction due to the shape of the region.

5.2 Analysis of the Secondary Flow

5.2.1 Statement of the Problem

The problem to be considered is the three-dimensional flow in a cascade caused by skewed flow at the inlet to the cascade. It may be specified as follows:

Given the velocity profile entering the cascade, determine the flow field inside and downstream of the cascade.

As the skewed flow is generated at midspan the influence of viscosity action is small except of course at the blade surfaces. The apparent friction due to turbulence can be of importance since the turbulence level in the skewed layer flow may be high. However, in order to simplify the problem mathematically it will be assumed that the flow is governed by inviscid flow equations of fluid mechanics. This implies that the flow losses in the cascade are not calculable. This approach is justified only by simplification of the theory and by the results obtained in the inviscid treatment of the wake flow (section 4). The Mach number of the flow is very low (about 0.1) and so the flow may be considered incompressible.

With these assumptions and assuming a steady flow, the flow field can be described by the momentum and continuity equations as follows:

$$\bar{v} \times \bar{\omega} = \frac{\nabla P_0}{\rho} \qquad 5\text{-}1$$

where

$$\bar{\omega} = \nabla \times \bar{V} \qquad 5\text{-}2$$

$$\nabla \cdot \bar{V} = 0 \qquad 5\text{-}3$$

In this case the stagnation pressure P_o is constant at the inlet to the cascade and since inviscid fluid is assumed, the stagnation pressure remains constant all over the flow field. This makes the right hand side of 5-1 equal to zero and so 5-1 becomes

$$\bar{V} \times \bar{\omega} = 0 \qquad 5\text{-}4$$

Substituting 5-2 in 5-4 and transforming the resulting equation we obtain

$$\nabla(\nabla \cdot \bar{V}) - \nabla^2 \bar{V} = 0 \qquad 5\text{-}5$$

which together with the continuity equation 5-3 yields

$$\nabla^2 \bar{V} = 0 \qquad 5\text{-}6$$

or equivilantly

$$\left.\begin{aligned} \nabla^2 V_1 &= 0 \\ \nabla^2 V_2 &= 0 \\ \nabla^2 V_3 &= 0 \end{aligned}\right\} \qquad 5\text{-}7$$

This system of Laplace equations, one equation for each velocity component, has to be solved together with appropriate boundary conditions. The boundary conditions are:

Upstream of the cascade the velocity distribution is prescribed

$\bar{V}$ = known function of space

Inside the cascade the velocity vectors at the blades surfaces have to be

parallel to the surfaces.

$$\bar{V} \cdot \nabla G(x,y,z) = 0$$

where

$G(x,y,z) = 0$ is the mathematical expression for the blade surfaces. Infinitely far downstream no changes in the velocity components take place.

$$\frac{\partial v_i}{\partial x_i} = 0 \qquad i = 1, 2, 3.$$

These boundary conditions make the problem so difficult that an analytical solution is impossible to obtain. Instead of trying to solve for the flow field over all space we therefore restrict ourselves to try to solve for the flow field just in a plane downstream of the cascade.

5.2.2 Approximate Solution

A solution to 5-4 is that the vorticity vector $\bar{\omega}$ is parallel with the velocity vector $\bar{v}$, i.e.

$$\bar{\omega} = k\bar{v} \qquad 5\text{-}8$$

where k is a scalar and may be a function of space

$$k = k(x,y,z) \qquad 5\text{-}9$$

Consider the flow in a plane behind the cascade, the plane being perpendicular to the direction of the two-dimensional outlet flow. The boundaries of the plane are made up of the two end walls of the cascade and the neighboring blade wakes from the two-dimensional flow. The axes and velocity components are chosen according to Figure 44.

In this coordinate system 5-8 and 5-3 are

$$\xi = \frac{\partial w}{\partial y} - \frac{\partial v}{\partial z} = ku \qquad 5\text{-}8a$$

$$\eta = \frac{\partial u}{\partial z} - \frac{\partial w}{\partial x} = kv \qquad 5\text{-}8b$$

$$\zeta = \frac{\partial v}{\partial x} - \frac{\partial u}{\partial y} = kw \qquad 5\text{-}8c$$

$$\frac{\partial u}{\partial x} + \frac{\partial v}{\partial y} + \frac{\partial w}{\partial z} = 0 \qquad 5\text{-}10$$

The velocity components are given by

$$u = U \cos\beta \cos\gamma \qquad 5\text{-}11a$$

$$v = U \sin\beta \cos\gamma \qquad 5\text{-}11b$$

$$w = U \sin\gamma \qquad 5\text{-}11c$$

where U is the magnitude of the velocity vector, and γ and β are the flow deviation angles caused by the skewed flow. For the pure two-dimensional flow u = U, γ and β are zero and their magnitude is a measure of the disturbance effect of the skewed flow on the two-dimensional flow. u, v and w are then secondary flow velocity components in accordance with the definition of secondary flow in the introduction of this report. Far behind the cascade the stream pressure is constant in space and since the stagnation pressure also is constant, U will be constant.

$$U = \text{constant} \qquad 5\text{-}12$$

Differentiating 5-11a, b, c with respect to x, y, and z, respectively

$$\frac{\partial u}{\partial x} = -U\left[\cos\gamma \sin\beta \frac{\partial \beta}{\partial x} + \cos\beta \sin\gamma \frac{\partial \gamma}{\partial x}\right] \qquad 5\text{-}13$$

$$\frac{\partial v}{\partial y} = U\left[\cos\gamma\cos\beta\frac{\partial\beta}{\partial y} - \sin\beta\sin\gamma\frac{\partial\gamma}{\partial y}\right] \qquad 5\text{-}14$$

$$\frac{\partial w}{\partial z} = U\cos\gamma\frac{\partial\gamma}{\partial z} \qquad 5\text{-}15$$

Assume the two dimensional flow through the cascade is disturbed by the skewed flow and that this distrubance is small. This implies that the flow deviation angles β and γ caused by the skewed flow, are small.

$$\left.\begin{aligned}\sin\beta &\approx \beta\\ \cos\beta &\approx 1\\ \sin\gamma &\approx \gamma\\ \cos\gamma &\approx 1\end{aligned}\right\} \qquad 5\text{-}16$$

5-13, 5-14 and 5-15 then become:

$$\frac{\partial u}{\partial x} \approx -U\left(\beta\frac{\partial\beta}{\partial x} + \gamma\frac{\partial\gamma}{\partial x}\right) = -\frac{U}{2}\frac{\partial}{\partial x}(\beta^2+\gamma^2) \qquad 5\text{-}17$$

$$\frac{\partial v}{\partial y} \approx U\left(\frac{\partial\beta}{\partial y} - \beta\gamma\frac{\partial\gamma}{\partial y}\right) \approx U\frac{\partial\beta}{\partial y} \qquad 5\text{-}18$$

$$\frac{\partial w}{\partial z} \approx U\frac{\partial\gamma}{\partial z} \qquad 5\text{-}19$$

From this it is seen that $\frac{\partial u}{\partial x}$ is of a smaller order of magnitude than $\frac{\partial v}{\partial y}$ and $\frac{\partial w}{\partial z}$.

$\frac{\partial u}{\partial x}$ may then be neglected in the continuity equation 5-10 yielding:

$$\frac{\partial v}{\partial y} + \frac{\partial w}{\partial z} = 0 \qquad 5\text{-}20$$

Equation 5-20 allows us to define a stream function ψ such that

$$v = \frac{\partial\psi}{\partial z} \qquad 5\text{-}21$$

$$w = -\frac{\partial \Psi}{\partial y} \qquad 5\text{-}22$$

Ψ is then the stream function for the secondary flow in the considered plane.

Introducing 5-21 and 5-22 in 5-8a we arrive at

$$-\xi = \frac{\partial^2 \Psi}{\partial y^2} + \frac{\partial^2 \Psi}{\partial z^2} = -ku \qquad 5\text{-}23$$

This is a Poisson's equation for Ψ.

Before solving this equation it may be of interest to study the order of magnitude of the vorticity components ξ, η and ζ.

From 5-8a, b, and c:

$$\xi = ku \qquad 5\text{-}8a$$

$$\eta = kv \qquad 5\text{-}8b$$

$$\zeta = kw \qquad 5\text{-}8c$$

Substituting 5-16 into 5-11 a, b and c, 5-8 a, b and c, may be written:

$$\xi \approx kU \qquad 5\text{-}24a$$

$$\eta \approx k\beta U \qquad 5\text{-}24b$$

$$\zeta \approx k\gamma U \qquad 5\text{-}24c$$

As can be seen η and ζ are of smaller order of magnitude than ξ.
This implies that the secondary flow will essentially be induced in the yz-plane.

To solve equation 5-23 for Ψ, either ξ or k has to be determined.

From above

$$\bar{\omega} = \nabla \times \bar{V} \qquad 5\text{-}2$$

$$\bar{\omega} = k\bar{V} \qquad 5\text{-}8$$

$$\nabla \cdot \bar{V} = 0 \qquad 5\text{-}3$$

The divergence of 5-2 and 5-8 yields:

$$\nabla \cdot \bar{\omega} = \nabla \cdot (\nabla \times \bar{V}) \equiv 0 \qquad 5\text{-}25$$

$$\nabla \cdot \bar{\omega} = \nabla \cdot (k\bar{V}) = k\nabla \cdot \bar{V} + \bar{V} \cdot \nabla k \qquad 5\text{-}26$$

Combining 5-25 and 5-26 yields, together with 5-3

$$\bar{V} \cdot \nabla k = 0 \qquad 5\text{-}27$$

Equation 5-27 expresses the fact that k is constant along a streamline (∇k has no component in the flow direction).

Along a streamline, 5-8 may now be written

$$\bar{\omega} = const \cdot \bar{V} \qquad 5\text{-}28$$

Note that the streamlines mentioned inconnection with 5-27 are not the same as those in 5-21 and 5-22. The streamlines in 5-21 and 5-22 are streamlines for the secondary flow in a specific plane behind the cascade while the streamlines in connection with 5-27 are streamlines for the complete flow in the whole field. No simplifications have been made in the derivation of equation 5-27 and thus equation 5-28 is exact for the flow considered.

k is thus a constant along each streamline. For the vorticity component ξ tangent to a streamline equation 5-28 becomes

$$\left(\frac{\xi}{U}\right)_2 = \left(\frac{\xi}{U}\right)_1 \qquad 5\text{-}29$$

where subscript 1 refers to the upstream plane and subscript 2 refers to the downstream plane. At the inlet plane upstream of the cascade, the velocity distribution is prescribed and thus the vorticity distribution is known. If we could trace the streamlines for the flow through the cascade we would then find the vorticity distribution behind the cascade. However, the streamline pattern of the flow is unknown and is, in fact, the one to be determined.

If the disturbance effect of the skewed flow on the two-dimensional flow is small, the induced velocities are small and we may assume the vorticity to be transported by the two-dimensional flow alone and not by the induced flow. 5-29 may now be written:

$$\xi_2 = \xi_1 \frac{u_2}{u_1} \qquad 5\text{-}30$$

where u_1 and u_2 are the velocity components of the undisturbed two-dimensional flow, and so

$$u_1 = U_1 \qquad u_2 = U_2 \qquad 5\text{-}31$$

ξ_1 is given by the flow conditions upstream of the cascade. The streamwise vorticity component decreases as it moves through a compressor cascade since the outlet velocity is lower than the inlet velocity. In a turbine cascade it would increase.

Equation 5-29 can be derived from Hawthorne's formula 4-2 when noting that $\nabla P_0 = 0$.
The flow at inlet is assumed to vary only in spanwise direction. ξ_1 is then given by 5-8a as

$$\xi_1 = -\frac{\partial v_1}{\partial z} \qquad 5\text{-}32$$

and

$$V_1 = - U_1 \sin \beta_1 \qquad 5\text{-}33$$

where β_1 is the angle between the skewed flow and the two-dimensional main flow.

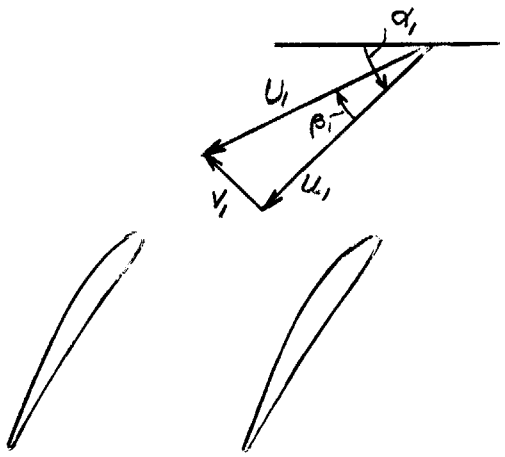

Substituting 5-33 in 5-32 and noting that U_1 is constant, yields:

$$\xi_1 = - U_1 \cos \beta_1 \frac{\partial \beta_1}{\partial z} \qquad 5\text{-}34$$

Combining 5-30 and 5-34 yields

$$\xi_2 = - U_2 \cos \beta_1 \frac{\partial \beta_1}{\partial z} \qquad 5\text{-}35$$

The previous assumptions imply β_1 to be small and so

$$\cos \beta_1 \approx 1$$

which yields

$$\xi_2 = - U_2 \frac{d\beta_1}{dz} \qquad 5\text{-}36$$

where the partial differential has been changed to the total differential since β_1 is a function of z only.

Substituting 5-36 into 5-23 yields

$$\frac{\partial^2 \psi}{\partial y^2} + \frac{\partial^2 \psi}{\partial z^2} = U_2 \frac{d\beta_1}{dz} \qquad 5\text{-}37$$

This equation has to be solved for Ψ together with appropriate boundary conditions.

Boundary conditions:

No cross flow occurs at the boundaries. The flow is symmetrical about mid-span and so this may be taken as a boundary. These boundary conditions are the same as the ones for the wake flow, section 4.2.2, and so we get

$$\Psi = 0 \qquad 5\text{-}38$$

at the boundaries.

The similarity between equations 5-37 and 4-12 and the boundary conditions in both cases make it possible to immediately write the solution of 5-37

$$\Psi = \sum_{n=1,3,5..}^{\infty} \Psi_n(z) \sin n\pi \frac{y}{b} \qquad 5\text{-}39$$

where

$$\Psi_n = -\frac{4U_2 b}{(n\pi)^2} \left\{ \frac{\sinh n\pi \frac{l-z}{b}}{\sinh n\pi \frac{l}{b}} \int_0^z \frac{d\beta_1}{d\zeta} \sinh n\pi \frac{\zeta}{b} \, d\zeta + \right.$$

$$\left. + \frac{\sinh n\pi \frac{z}{b}}{\sinh n\pi \frac{l}{b}} \int_z^l \frac{d\beta_1}{d\zeta} \sinh n\pi \frac{l-\zeta}{b} \, d\zeta \right\} \qquad 5\text{-}40$$

and

$$\Psi_n' = \frac{4U_2}{n\pi} \left\{ \frac{\cosh n\pi \frac{l-z}{b}}{\sinh n\pi \frac{l}{b}} \int_0^z \frac{d\beta_1}{d\zeta} \sinh n\pi \frac{\zeta}{b} \, d\zeta - \right.$$

$$\left. - \frac{\cosh n\pi \frac{z}{b}}{\sinh n\pi \frac{l}{b}} \int_z^l \frac{d\beta_1}{d\zeta} \sinh n\pi \frac{l-\zeta}{b} \, d\zeta \right\} \qquad 5\text{-}41$$

The secondary velocities v and w are then given by 5-21 and 5-22 which together with 5-39, 5-40 and 5-41 yield:

$$v = \sum_{n=1,3,5...}^{\infty} \frac{4U_2}{n\pi} \left\{ \frac{\cosh n\pi \frac{l-z}{b}}{\sinh n\pi \frac{l}{b}} \int_0^z \frac{d\beta_1}{d\zeta} \sinh n\pi \frac{\zeta}{b} \, d\zeta - \right.$$

$$\left. - \frac{\cosh n\pi \frac{z}{b}}{\sinh n\pi \frac{l}{b}} \int_z^l \frac{d\beta_1}{d\zeta} \sinh n\pi \frac{l-\zeta}{b} \, d\zeta \right\} \sin n\pi \frac{y}{b} \qquad 5\text{-}42$$

$$w = -\sum_{n=1,3,5..}^{\infty} \frac{4U_2}{n\pi} \left\{ \frac{\sinh n\pi \frac{l-z}{b}}{\sinh n\pi \frac{l}{b}} \int_0^z \frac{d\beta_1}{d\zeta} \sinh n\pi \frac{\zeta}{b} \, d\zeta + \right.$$

$$\left. + \frac{\sinh n\pi \frac{z}{b}}{\sinh n\pi \frac{l}{b}} \int_z^l \frac{d\beta_1}{d\zeta} \sinh n\pi \frac{l-\zeta}{b} \, d\zeta \right\} \cos n\pi \frac{y}{b} \qquad 5\text{-}43$$

5.2.3 The Transverse Velocity v and the Transverse Flow Deviation Angle β

The similarity between the equations for the wake flow and the skewed flow immediately permit us to write the following formulae:

$$V_{max} = \left(\frac{\partial \Psi}{\partial z}\right)_{y=b/2} = -\sum_{n=1,3,5..}^{\infty} (-1)^{\frac{n+1}{2}} \Psi_n' \qquad 5\text{-}44$$

$$\bar{V} = \frac{2}{\pi} \sum_{n=1,3,5..}^{\infty} \frac{\Psi_n'}{n} \qquad 5\text{-}45$$

$$\tan \beta_{max} = \frac{V_{max}}{U_1} \frac{\sin \alpha_1}{\sin \alpha_2} \qquad 5\text{-}46$$

$$\tan \bar{\beta} = \frac{\bar{V}}{U_1} \frac{\sin \alpha_1}{\sin \alpha_2} \qquad 5\text{-}47$$

5.2.4 The Spanwise Velocity w and the Spanwise Flow Deviation Angle γ

The formulae for the above quantities are the same in this case as in the wake flow case.

$$w_{max} = \sum_{n=1,3,5..}^{\infty} \frac{n\pi}{b} \Psi_n \qquad 5\text{-}48$$

$$\tan \gamma_{max} = \frac{w_{max}}{U_1} \cdot \frac{\sin \alpha_1}{\sin \alpha_2} \qquad 5\text{-}49$$

The average value of w over one blade spacing at any z-position is zero, and therefore the average spanwise flow deviation angle over one blade spacing caused by the secondary flow is zero.

5.2.5 Mathematical Expression for the Skewed Flow Angle Distribution at the Inlet of the Cascade

The transverse angle in the skewed flow at the inlet of the cascade varied slightly in tangential direction.

The measured inlet angle distributions in spanwise direction at five different, equally spaced, tangential positions were plotted and a curve was faired through these five different sets of data, see Figure 45. This curve, representing the average angle distribution in spanwise direction was mathematically represented by a Fourier series

$$\beta_1 = \sum_{m=0} A_m \cos m\pi \frac{z}{\delta} \qquad 5\text{-}50$$

The derivative of β_1 with respect to z is

$$\frac{d\beta_1}{dz} = -\frac{\pi}{b} \sum_{m=1} A_m \sin m\pi \frac{z}{\delta} \qquad 5\text{-}51$$

Note that this series starts with m = 1 while the series for β_1 starts with m = 0. However, the term corresponding to m = 0 is a constant and so its derivative is zero.

With $\frac{d\beta_1}{dz}$ given by 5-51 the integrations of ψ_n 5-40 and ψ_n' 5-41 may be performed. The integrations have to be performed in two regions $0 \leq z \leq \delta$ and $\delta \leq z \leq l$ because $\frac{d\beta_1}{dz}$ is not continuous

over the whole region $0 \leq z \leq \ell$.

$$\frac{d\beta_1}{dz} \begin{cases} \neq 0 & \text{for} \quad 0 \leq z \leq \delta \\ = 0 & \text{for} \quad \delta \leq z \leq \ell \end{cases}$$

The details of the integration may be found in Appendix B and the results are:

for $0 \leq z \leq \delta$

$$\psi_n = -\frac{4U_2 b}{(n\pi)^2} \sum_{m=1} \frac{A_m}{1+\left(\frac{n\delta}{mb}\right)^2} \left\{ \frac{\cos m\pi \sinh n\pi \frac{\ell-\delta}{b}}{\sinh n\pi \frac{\ell}{b}} \sinh\left(n\pi \frac{\delta}{b} \frac{z}{\delta}\right) - \frac{n\delta}{mb} \sin m\pi \frac{z}{\delta} \right\} \qquad 5\text{-}52$$

$$\psi_n' = \frac{4U_2}{n\pi} \sum_{m=1} \frac{A_m}{1+\left(\frac{n\delta}{mb}\right)^2} \left\{ \cos m\pi \frac{z}{\delta} - \cos m\pi \frac{\sinh n\pi \frac{\ell-\delta}{b}}{\sinh n\pi \frac{\ell}{b}} \cosh n\pi \frac{\delta}{b} \frac{z}{\delta} \right\} \qquad 5\text{-}53$$

and for $\delta \leq z \leq \ell$

$$\psi_n = -\frac{4U_2 b}{(n\pi)^2} \sum_{m=1} \frac{A_m}{1+\left(\frac{n\delta}{mb}\right)^2} \cos m\pi \frac{\sinh n\pi \frac{\delta}{b}}{\sinh n\pi \frac{\ell}{b}} \sinh n\pi \frac{\ell}{b} \left(1 - \frac{z}{\ell}\right) \qquad 5\text{-}54$$

$$\psi_n' = \frac{4U_2}{n\pi} \sum_{m=1} \frac{A_m}{1+\left(\frac{n\delta}{mb}\right)^2} \cos m\pi \frac{\sinh n\pi \frac{\delta}{b}}{\sinh n\pi \frac{\ell}{b}} \cosh n\pi \frac{\ell}{b} \left(1 - \frac{z}{\ell}\right) \qquad 5\text{-}55$$

These expressions and the corresponding ones for the wake flow 4-31, 4-32, 4-33 and 4-34 are nearly identical. From these expressions some conclusions can be drawn about the secondary flow velocity components v and w caused by the skewed flow described by 5-50.

Both velocity components are directly proportional to the outlet velocity U_2 and the inlet angle distribution described by the Fourier coefficients, Am.

The same non-dimensional factors appear identically as in the expressions of the velocity components for the wake flow (section 4-23). Therefore the same cascade parameters are of equal importance in the two different flows. The width of the wake is 2δ in the wake flow, while in the skewed flow 2δ is the width of the skewed flow layer.

5.2.6 Correlation of Theory and Experiments

A Fourier series, 5-50, using four terms m = 1, 2, 3 and 4 has been used to describe the inlet flow angle variation to the cascade, see Figure 45. The actual values of the cascade configuration parameters (given in Appendix B) have been substituted in the formulae derived previously, and the transverse and spanwise flow deviation angles have been calculated. In the calculations the first three terms in the series for Ψ and Ψ' have been retained, i.e. n = 1, 3 and 5. The magnitude of the inlet velocity was not constant but two wakes were generated at the ends of the skewed flow layer. The secondary flow caused by these two wakes has also been calculated. This calculation was performed as for a pure wake flow i.e the inlet angle distribution was assumed to be constant. Details of this calculation are given in Appendix C. The results of these calculations and of the experiments are presented as curves in Figures 47, 48 and 49.

5.2.6.1 The Maximum Transverse Flow Deviation Angle β_{max}

The variation of the maximum transverse flow deviation angle over the span is shown in Figure 47.

The position of the measured maximum underturning, 14°, was located at midspan and about at the center of the effective flow passage at cascade exit. The maximum overturning occured near the edges of the skewed flow layer

and was about 2° on one side of midspan and about 1° on the other side.

Half a chord downstream the magnitude and distribution of the maximum flow deviation angles were almost unchanged. The location of this distribution in the flow passage had, however, moved toward the pressure side of the blade wake.

The theory predicts the maximum underturnign to occur at the center of the flow passage between two adjacent blades at midspan. Dut to the stalling of the blades the effective flow passage did not coincide with the flow passage established by the blade geometry. The tests showed that the maximum underturning occurred at the center of the effective flow passage instead of at the geometric center.

The theory predicts the maximum underturning to be about 11° and to occur at midspan. The measured value was 14°. The shape of the theoretical curve at midspan is different from the shape of the measured one. The inlet transverse flow angle curve represented by a Fourier series had a defect at midspan (Figure 45) and the effect of this defect has been increased through the calculations as can be seen. If the correlation between the measured inlet angle curve and the curve represented by a Fourier series had been better the defect in the transverse flow deviation angle would have disappeared and the overall correlation been better.

The theory predicts an overturning of about 6.5° while the experiments showed only 2°. The experimental curves show another region of underturning located about 2 inches from midspan and with a magnitude of about 1°. The theory does not predict this. However, the outlet transverse angle outside the skewed flow region had increased about 4° above the value measured in the pure two-dimensional test. The transverse flow deviation angles have

been measured from the direction of this increased free stream outlet angle, since the theory used in the calculation is that of the effect of a small perturbation on the two-dimensional cascade flow. If the transverse flow deviation angles had been measured from the direction of the transverse outlet angle, measured in the two-dimensional test, the correlation between the theoretical and measured maximum overturning would have been close while the correlation of the maximum underturning would have been somewhat poorer, and a discrepancy of about 4° would have occurred between the theoretical and measured curves in the free stream.

Adding the influence of the secondary flow caused by the two wakes does not change the theoretical curve much. The maximum underturning increases about 1°, but the maximum overturning remains about the same. The spanwise position of the maximum overturning shifts slightly toward midspan.

5.2.6.2 The Average Transverse Flow Deviation Angle $\bar{\beta}$

The variation of the average transverse flow deviation angle over the span is shown in Figure 48.

Due to the back flow at the cascade exit no averaging of the measured angle distribution could be done there. Half a chord downstream the maximum average transverse flow deviation angle, 10°, occurred at midspan. No overturning occurred. This may be due to separation over the central part of the cascade. The flow in the separated region has a lower tangential momentum and is therefore turned less. When this flow moves downstream it mixes with the rest of the flow and reduces the average tangential momentum, thereby decreasing the average transverse outlet angles in the midspan region.

The theory predicts a maximum average underturning at midspan of about 7°. However, the same argument about this value and about the shape of the curve is valid here as it was in section 5.2.6.1. The theory also predicts a maximum average overturing of about 3.5° located near the outer edge of the skewed flow layer but the measurements do not show this. The explanation for this is given above.

Including the effect of the secondary flow due to the wake flow does not change the theoretical curve much. The maximum average underturning increases by 1° while the magnitude of maximum average overturning remains almost the same. The spanwise position of this maximum average overturning is shifted slightly toward midspan.

5.2.6.3 The Maximum Spanwise Flow Deviation Angle γ_{max}

Figure 49 shows the variation of the maximum spanwise flow deviation angle over the span.

The average value over a blade spacing of the spanwise flow deviation angle due to the secondary flow should be zero at each spanwise position (see section 4.2.2.2). However, the measurements half a chord downstream (no averaging could be done at cascade exit due to the back flow) showed an average-angle variation over the span. The axial velocity in the skewed layer upstream of the cascade was less than in the free stream due to the more nearly tangential direction of the skewed layer. After the cascade the difference between the angle of the skewed layer and the main stream was less and so the axial velocity discrepancy between the skewed layer and the free stream was less. This caused an overall spanwise flow toward midspan and was shown as a finite average-spanwise flow deviation angle. The

measured spanwise flow deviation angles should therefore be corrected with this average angle distribution before they are correlated with the theoretical curves. However, this can not be done for the measured curve at cascade exit, since no averaging could be done at that position. The general trend, however, has to be remembered when the correlation is done.

The measured maximum spanwise flow deviation angle at cascade exit was about 10° and 7° on either side of midspan. If they are corrected for the overall spanwise flow these values would probably increase by about 2°. The location of these maximum angles was about 1 inch on either side of midspan and very close to the pressure side of the blade wake. Half a chord downstream these values were reduced to 7° and 5°, respectively, or corrected for the overall spanwise flow to about 9° and 7°, respectively. The spanwise position for these maximum angles remained almost the same. The maximum average spanwise flow deviation angle was about 2°, located at about 1.2 inches from midspan.

The theory predicts the maximum flow deviation angle to occur at the blade wakes and this is confirmed by the measurements. The theory predicts the maximum angle to about 10° which agrees well with one of the two uncorrected measured values obtained at cascade exit. The position for this maximum angle agrees, also, with the measured value. Adding the influence of the secondary flow due to the wake flow increases the maximum angle to about 11° which also agrees farily well, and certainly better, with the corrected maximum angle due to the overall spanwise flow. The spanwise position of the maximum angle is changed only slightly toward midspan.

5.2.6.4 Conclusions

The partial stalling of the cascade has essentially disturbed the flow by blocking part of the cascade and thus changing the effective geometrical configuration. It has also reudced the turning of the flow in that part of the cascade and is probably responsible for the overturning of the flow in the free stream. Under these conditions a very close correlation between theory and experiment is not to be expected. Nevertheless the experiments did prove the general predictions of the theory and in some respects a good correlation between predicted and measured values was obtained. This was especially true for the positions of the extreme values of the flow deviation angles. The correlation for spanwise flow deviation angles was better than the correlation for transverse flow deviation angles. This is probably due to the fact that the partially stalling of the cascade has less influence on the flow in spanwise direction.

5.2.7 Actuator Disc Theory

5.2.7.1 Statement of the Problem

As the flow moves downstream from the cascade exit the streamlines shift their spanwise positions thereby causing a change in the transverse angle distribution. The problem can then be stated as follows: given the transverse angle distribution at cascade exit determine the distribution infinitely far downstream. As a means to do this an actuator disc approach will be applied.

5.2.7.2 Solution

The cascade is replaced by an actuator disc which may be essentially regarded as a cascade containing an infinite number of blades of infinitesimal

chord. This actuator disc produces an abrupt change in transverse velocity across the disc but permits a continuous variation of the axial and spanwise velocities across the disc. The nomenclature and coordinate system is shown in Figure 50.

Since the disc is uniform in transverse direction all properties are independent of y and so

$$\frac{\partial}{\partial y} = 0 \qquad 5\text{-}56$$

The equations 5-8a, b, and c and 5-10 are still valid in this case and inserting 5-56 in these equations yields:

$$\xi = -\frac{\partial v}{\partial z} = ku \qquad 5\text{-}57$$

$$\eta = \frac{\partial u}{\partial z} = kv \qquad 5\text{-}58$$

$$\zeta = \frac{\partial v}{\partial x} = kw \qquad 5\text{-}59$$

$$\frac{\partial u}{\partial x} + \frac{\partial w}{\partial z} = 0 \qquad 5\text{-}60$$

Multiplying 5-57 by -w and 5-59 by u and adding, the result yields:

$$u\frac{\partial v}{\partial x} + w\frac{\partial v}{\partial z} = 0 \qquad 5\text{-}61$$

This equation expresses the fact that v remains constant along a streamline.

From equation 5-27 (which is valid, in general, when $\nabla P_o = 0$) we know that k is constant along a streamline. Equation 5-58 then shows that η is constant along a streamline. It is to be noted that the results above are only valid in each of the flow regions separated by the disc and are not valid across the disc.

Multiplying 5-58 by u and 5-57 by v and subtracting the result

yields:

$$u\eta - v\xi = u\left(\frac{\partial u}{\partial z} - \frac{\partial w}{\partial x}\right) - v\frac{\partial v}{\partial z} = 0 \qquad 5\text{-}62$$

But $\frac{\partial w}{\partial x}$ is of a smaller order of magnitude than $\frac{\partial u}{\partial z}$ and so η may be written

$$\eta = \frac{\partial u}{\partial z} \qquad 5\text{-}63$$

Introducing 5-63 into 5-62 yields

$$u\frac{\partial u}{\partial z} + v\frac{\partial v}{\partial z} = 0 \qquad 5\text{-}64$$

At the disc 5-64 becomes

$$u_o\frac{\partial u_o}{\partial z} + v_o\frac{\partial v_o}{\partial z} = 0 \qquad 5\text{-}65$$

$\eta(x,z)$ is constant along a streamline. Assuming the spanwise shift of the streamlines small, $\eta(x,z)$ may be considered a function of z only, and so

$$\eta_o(z) = \eta_2(z) = \frac{\partial u_o}{\partial z} = \frac{\partial u_2}{\partial z} \qquad 5\text{-}66$$

Introducing 5-66 into 5-65 yields

$$u_o\frac{\partial u_2}{\partial z} + v_o\frac{\partial v_o}{\partial z} = 0 \qquad 5\text{-}67$$

But $v_o = u_o \cot \alpha_{o2}$ 5-68

which substituted in 5-67 yields

$$\frac{du_2}{dz} + \cot\alpha_{o2}\frac{d}{dz}(u_o\cot\alpha_{o2}) = 0 \qquad 5\text{-}69$$

The partial derivatives have been changed to total ones since u_o, u_2 and α_{o2} are functions of z only.

η is, to the approximations above, independent of x. This implies that the axial velocity at the disc (x = 0) is the mean of the values at x = -00 and x = +00

i.e. $u_o = \frac{1}{2}(u_1+u_2)$ 5-70

Introducing 5-70 into 5-69 and rearranging yields:

$$\frac{du_o}{dz} + \frac{u_o}{2}\frac{d}{dz}\ln(2+\cot^2\alpha_{o2}) = \frac{1}{2+\cot^2\alpha_{o2}}\frac{du_1}{dz} \qquad 5\text{-}71$$

This is a linear non-homogeneous differential equation with variable coefficients. It can easily be solved to yield

$$u_o = \frac{1}{\sqrt{2+\cot^2\alpha_{o2}}}\left[\frac{1}{\sqrt{2+\cot^2\alpha_{o2}}}\frac{du_1}{dz}dz + C\right] \qquad 5\text{-}72$$

where C may be found by applying the continuity equation. Equation 5-72 relates the axial velocity distribution at cascade exit to that upstream when the transverse angle distribution at cascade exit is known. The average transverse angle distribution found by the secondary flow analysis may be taken to represent the angle distribution at cascade exit. Since α_{o2} is given by a very complicated formula, a numerical solution of 5-72 has to be performed.

Using 5-70 the axial velocity distribution far downstream may be computed. Equation 5-61 showed that v is constant along a streamline. It was assumed that the shift in streamlines was small. This gives

$$V_{o2}(z) = V_2(z) \qquad 5\text{-}73$$

or $u_o \cot\alpha_{o2} = u_2 \cot\alpha_2$

and so

$$\cot\alpha_2 = \frac{u_o}{u_2}\cot\alpha_{o2} \qquad 5\text{-}74$$

This formula relates the transverse flow angle far downstream to the one at cascade exit. Due to the stalling of the cascade no average-transverse flow

angle distribution could be found at cascade exit and thus no check on the validity of the derived formulae could be performed.

5.3 Losses and Kinetic Energy of Secondary Flow

5.3.1 Results of Measurements

Due to the back flow at cascade exit no measurements of the kinetic energy of the secondary flow could be performed there. Half a chord downstream the magnitude of the velocity vector was computed using the measured values of stagnation pressure and stream pressure. Using this value of the magnitude of the velocity vector and the measured flow deviation angles, the kinetic energy of the secondary flow was computed and plotted in the same way as for the wake flow, section 4.3.1. The resulting curve is shown in Figure 51.

The curve has two maximum points. One at midspan caused by the large underturning of the flow there and one of much smaller magnitude located about 1.5 inches from midspan. This was caused by the flow deviation at that position. As was noted in sections 5.2.6.1 and 5.2.6.2 the maximum transverse flow deviation angles showed a slight overturning at this position while the average transverse flow deviation angles showed underturning. The overall result of this was a very slight increase of the kinetic energy of the secondary flow above the values at neighbouring spanwise positions.

The area integrated value of the kinetic energy of the secondary flow was

$$\frac{D}{KE_{inl}} = 0,14\ \%$$

The ratio of the kinetic energy of the secondary flow bound in the spanwise flow to the total kinetic energy of the secondary flow was 0.21. This is a much lower ratio than the one for the wake flow. It may be due to stalling of the blades at midspan which caused an additional region of underturned flow and thus increased the kinetic energy of the transverse secondary flow and also caused this flow to persist as it moved downstream while the spanwise velocity component decreased rapidly (see Figures 47 and 49).

5.3.2 Theoretical Calcualtion of the Kinetic Energy of the Secondary Flow

In Appendix F is given the derivation of the formula for the ratio of kinetic energy per unit volume of the secondary flow to the kinetic energy of the flow entering the cascade.

$$\frac{D}{KE_{inl}} = \frac{8}{\pi^2}\cdot\frac{s}{c}\cdot\frac{c}{\ell}\cdot\frac{\sin^2\alpha_2}{\sin\alpha_1}\,\frac{\overset{(1)}{\left(\frac{\sin\alpha_1}{\sin\alpha_2}\right)^2}\cdot f + \overset{(2)}{2a^2\varepsilon\cdot g} + \overset{(3)}{\frac{2a}{\pi}\frac{\sin\alpha_1}{\sin\alpha_2}\cdot h}}{1-2\left(\frac{\theta+\delta^*}{\ell}\right)} \qquad 5\text{-}75$$

where f, g and h are functions given in Appendix F.3.1.

This formula is composed of three parts.

1. the contribution from the skewed flow only
2. the contribution from the wake flow only
3. the contribution from the interaction between the skewed flow and the wake flow.

The comments made on the corresponding formula, 4-39, of the wake flow are applicable also for this formula.

The actual values for this test were substituted in 5-75 and gave as a result

$$\frac{D}{KE_{inl}} = 0.26\,\%$$

The contribution to this value from the three different terms in 5-75 were

1. 0.252%
2. 0.022%
3. -0.018%

The influence of the wake flow is almost negligible as most of it was cancelled by the "interaction term". This could be expected from the distribution of the flow deviation angles (Figures 47, 48 and 49) where it was shown that the influence of the wake flow was very small.

The theoretical value of 0.26% is to be compared to the measured value of 0.14% half a chord downstream. Half a chord downstream the measured underturning flow angles agreed well with the calculated ones but there was no correlation between the predicted overturning angles and those actually measured. The measured spanwise flow deviation angles were much less than the predicted ones. From this it would be expected that the measured kinetic energy of the secondary flow would be less than the theoretical, the discrepancy being greatest where the theory predicts overturning of the flow, which is also the case (Figure 51). The magnitude of the actual velocity vector is smaller than the theoretical one at midspan since the stalling of the cascade there reduces the stagnation pressure and so the velocity. This increases the discrepancy still more between the predicted and measured values of the kinetic energy. Noting these effects, the correlation between predicted and measured value of the kinetic energy of the secondary flow may be considered satisfactory.

The spanwise distribution of the kinetic energy of the secondary

flow has also been performed using the following formula derived in Appendix F5.

$$D_z = \frac{1}{4}\rho b \sum_n \left\{ \left[\psi_{sn}'^2 + \left(\frac{n\pi}{b}\right)^2 \psi_{sn}^2 \right] + \left[\psi_{wn}'^2 + \left(\frac{n\pi}{b}\right)^2 \psi_{wn}^2 \right] + 2\left[\psi_{sn}' \psi_{wn}' + \left(\frac{n\pi}{b}\right)^2 \psi_{sn} \psi_{wn} \right] \right\} \qquad 5\text{-}76$$

This formula is composed of three parts:

1. the contribution from the skewed flow only
2. the contribution from the wake flow only
3. the contribution from the interaction between 1 and 2.

The actual values for this test have been substituted in 5-76. The results are shown graphically in Figure 51.

The shape of the curves for the predicted and measured values is similar except at the midspan where the predicted curve has a defect. This defect is caused by the defect in the curve representing the inlet transverse flow angle and would have disappeared if one more term had been added to the Fourier series representing the inlet angle distribution. The predicted curve also confirms the statements about the discrepancy between measured and predicted values of the kinetic energy mentioned before.

5.3.3 Losses

Most of the discussion concerning the three-dimensional losses for the wake flow in section 4.3.3 is valid even for this case and will therefore not be repeated here.

The measured area averaged stagnation pressure defect distribution over the span, half a chord downstream, is shown in Figure 52. The maximum pressure defect amounted to 37.5% of the reference dynamic pressure. The two-dimensional loss outside the stalled region amounted to about 1.6% which was the value measured in the two-dimensional test (section 3.2). The stagnation pressure defect, in excess of this two-dimensional loss,

averaged over the span, 16 inches, was 6.6%. The inlet stagnation pressure defect, due to the two wakes, averaged over the span was 2.5%.

The difference between the averaged outlet ("in excess") and inlet stagnation pressure defect is called the complementary loss and was 4.1%. This is a large loss and is somewhat greater than the losses usually measured in an actual compressor stage and attributed there to secondary losses. However, its magnitude depends on the size of the span over which it is averaged. The energy of the secondary flow was 0.14% and is not included in the complementary loss above. As can be seen the kinetic energy of the secondary flow is almost negligible and is less than 10% of the two-dimensional loss. The conclusion from this result will be drawn in section 7.

5.4 The Tangential Component of the Blade Force

5.3.1 Results of Measurements

Stream pressure distribution on the blade surfaces was measured at 6 different spanwise positions located 1/8", 3/8", 5/8", 1 1/8", 2 1/8" and 4 1/8" from midspan.

The results of the measurements are presented as plots of the tangential component of the pressure distribution around the blade surfaces, and as the tangential pressure coefficient, C_T. The plots are shown in Figure 53 and a contour map of the pressure distribution is shown in Figure 54. The curves show a strong separation over most of the chord in the skewed flow region. The stream pressure there is almost the same as the stream pressure of the reference probe upstream of the cascade. The spanwise change of stream pressure on the pressure

side is slight over most of the chord. At the trailing edge the stream pressure drops in the skewed flow region while it is higher than the free stream value a short distance behind the leading edge. This is due to the increased angle of attack of the flow in the skewed layer, which moves the stagnation point away from the leading edge.

The defect of the stream pressure in the skewed flow region results in a lower tangential pressure coefficient there, as may be seen in Figure 55.

5.4.2 Theoretical Calculation of the Tangential Component of the Blade Force

In Appendix G the derivation of the formula for the tangential pressure coefficient, C_T is presented:

$$C_T = 2\sin^2\alpha_1(\cot\alpha_1 - \cot\alpha_2)\left(1 - 2\frac{\theta+\delta^*}{l}\right) + \left[1 - 2\cot\alpha_1(\cot\alpha_1 - \cot\alpha_2)\cdot\frac{\delta}{l}A_0 - \right.$$

$$\left. - \frac{\sin\alpha_1}{\rho\frac{\bar{U}_1^2}{2}s\cdot l}\left[\frac{D_W}{\varepsilon} + D_s\frac{2\sin\alpha_2}{\sin\alpha_1} + \frac{D_{SW}}{2}\left(\frac{1}{\varepsilon} + \frac{2\sin\alpha_2}{\sin\alpha_1}\right)\right]\right] \qquad 5\text{-}77$$

This expression may be interpreted as follows:

1. $2\sin^2\alpha_1(\cot\alpha_1 - \cot\alpha_2)$ is the tangential pressure coefficient if the flow is uniform over all the span;

2. $-2\frac{\theta+\delta^*}{l}\cdot 2\sin^2\alpha_1(\cot\alpha_1 - \cot\alpha_2)$ is a reduction due to the decreased mass flow in the two wakes;

3. $\frac{\delta}{l}A_0$ is an increase due to the increased flow angle of attack;

4. $-2\cot\alpha_1(\cot\alpha_1 - \cot\alpha_2)\frac{\delta}{l}A_0$ is a reduction due to the decreased mass flow in the skewed flow;

5. $-\frac{\sin\alpha_1}{\rho\frac{\bar{U}_1^2}{2}\cdot s\cdot l}\frac{D_W}{\varepsilon}$ is a reduction due to the secondary flow caused by the wake flow

6. $-\frac{\sin\alpha_1}{\frac{\rho\bar{U}_1^2}{2}s.l} \cdot D_s \frac{2\sin\alpha_2\cos\alpha_1}{\sin^2\alpha_1}$ is the same as 5 but caused by the skewed flow;

7. $-\frac{\sin\alpha_1}{\frac{\rho\bar{U}_1^2}{2}s.l} \cdot \frac{D_{sw}}{2}\left(\frac{1}{\varepsilon} + \frac{2\sin\alpha_2\cos\alpha_1}{\sin^2\alpha_1}\right)$ is an increase caused by the interaction of the wake flow and the skewed flow.

The actual values for this test have been substituted in formula 5-77. The results of this calcualtion are given in the following table.

TERM	VALUE		PERCENTAGE	
1	0.52088	0.51283		
2	-0.00815		-1.55%	
3	0.04345	0.00181	8.34	-0.35
4	-0.04526		-8.69	
5	-0.00056	-0.00469	-0.11	-0.79
6	-0.00448		-0.86	
7	0.00035		0.07	
C_T	0.50633		Sum: -2.69%	

The decrease in C_T from its two-dimensional value is thus 2.7%, of which term (2) contributes more than half. The reduction due to the secondary flow is small. The measured reduction is 4.9%, to be compared with the calculated value of 2.7%. A reason for this discrepancy is the partial stalling of the cascade which reduces the tangential momentum, and which is not accounted for in the theoretical value.

In the calculation leading to the above results the two-dimensional value of the transverse outlet angle of 64.4° has been used instead of the measured free stream value of 68.4°. This gives $C_T = 0.521$ in the free stream (term (1) in the table above) to be compared with the

measured value of $C_T = 0.508$ which agrees favorably with the value measured in the two-dimensional test (section 3.3). The calcualted value is 2.5% greater than the measured one. Using the measured outlet angle, 68.4°, gives $C_T = 0.604$ which shows the rapid change in C_T with α_2. This calculated value is 19 % greater than the measured one. In deriving formula 5-77 a two-dimensional flow was assumed, where the streamlines do not shift position in spanwise direction. In the investigated flow this was not the case. Boundary layer growth on the end walls, partial blockage of the cascade through stalling, and secondary flow shift the streamlines and change the axial velocity profile, thereby violating the assumptions above and causing great errors in the calculation of the free stream tangential pressure coefficient. The reduction from its two-dimensional value of the average tangential pressure coefficient due to the secondary flow is, despite the violations of the assumptions, fairly well predicted. This will also be demonstrated in the skewed wake flow case.

6 SKEWED WAKE FLOW

6.1 Results of Measurements

The results of measurements are presented as contour maps over the traversed areas showing stagnation pressures, stream pressures, transverse flow angles and spanwise flow deviation angles.

6.1.1 Upstream Conditions

6.1.1.1 Transverse Inlet Flow Angles

Figure 56 shows the transverse inlet flow angle variation over the traversed area upstream of the cascade. The angles varied between about 45° in the free stream and about 20° in the center of the skewed flow layer. There was a variation of the inlet angle of about 4° in tangential direction in the center of this layer, over the traversed area. This disturbed the assumption of tangential uniformity.

6.1.1.2 Stagnation Pressure

The stagnation pressure distribution over the traversed area is shown in Figure 57. The stagnation pressure defect in the center of the skewed wake flow amounted to about 55% of the dynamic reference pressure. The distribution was fairly uniform in tangential direction. The spanwise width of the wake was about 3.5 inches. The spanwise profile of the wake was wave shaped. The pressure defect was slightly greater half an inch from either side of midspan than at midspan itself thus giving rise to two small wakes inside the big wake all three extending in tangential direction.

6.1.1.3 Stream Pressure

Figure 58 shows the variation of the stream pressure over the traversed area. The stream pressure distribution for this flow is very similar to the one for the skewed flow. The stream pressure distribution around the blades of the cascade can clearly be seen as vertical contour lines modified by the pressure distribution in the skewed wake flow layer. Also this distribution showed a slight lack of uniformity in tangential direction.

6.1.2 Downstream Conditions

6.1.2.1 Stagnation Pressure

The stagnation pressure distributions at the two areas traversed are shown in Figures 59 and 60.

The blades were heavily stalled over a large part of the central span as can be seen in Figure 59. The right-hand blade of the two that were investigated was more heavily stalled than the other due to the uneven suction side surface. A constant back flow was created at the suction side of the blades around midspan. The back flow was traced in the same way as it was in the skewed flow case so that the limiting line on the contour map between the back flow region and the through flow region may not be considered very accurate. The back flow did, however, extend over a greater part of the span in this case than in the skewed flow case.

The spanwise width of the wake was reduced close to the pressure side of the blades at cascade exit indicating a spanwise flow toward midspan at this position. The Bernoulli surfaces were slightly turned from the horizontal, partly because of the secondary flow and partly due to stalling, which reduced the flow passage area.

Half a chord downstream, Figure 60, the back flow had disappeared leaving a region of low stagnation pressure in its previous position, and the skewed wake had diffused slightly. The distortion of the Bernoulli surfaces persisted, being greatest in the region of previous back flow. The two small wakes, inside the big wake, in the inlet flow were traced as two horizontal wakes at about the center of the blade

passage at midspan. The centers of low stagnation pressure had moved slightly away from the suction side of the blade wakes toward the centers of the blade passages.

6.1.2.2 Stream Pressure

Figures 61 and 62 show the stream pressure distributions at the two traversed areas.

In each flow passage at cascade exit, defined by two adjacent blade wakes, there was a region of low stream pressure located close to the suction side of the blade wake and with two minimums, each located about 1.5 inches from midspan. The pressure defect in these minimums ranged between 14 and 20% of the reference dynamic pressure. The low pressure in these regions was caused by the partial stalling of the blades which reduced the turning of the flow through the cascade and thus reduced the pressure rise over the cascade in this region. Close to the pressure side of the blade wake at midspan was a region of stream pressure slightly higher than ambient. The pressure defect here was about 6%. This is the region where the secondary flow should have a stagnation point. Another stagnation point should be located at the suction side of the blade wake at midspan. The stream pressure here was slightly higher than further away from the midspan.

Half a chord downstream the shape of the pressure distribution remained the same but the magnitude of the greatest pressure defects had been reduced to about half their values at cascade exit. The locations of the pressure defect minimums remained almost unchanged relative to the flow passages between the blade wakes. These two low stream pressure

regions persisted fairly well as the flow moved downstream. This indicates that they were the centers of two vortices extending in streamwise direction.

6.1.2.3 Transverse Flow Angles

The transverse flow angle distributions at the two traversed areas are shown in Figures 63 and 64.

The strong distortion of the flow due to the stalled flow region makes an interpretation of the contour map at cascade exit difficult. The transverse flow angles in the skewed wake flow region at cascade exit differed very much from the two-dimensional values. The angles varied from a slight underturning at the pressure side to a strong overturning (axial flow direction) close to the back flow region. The flow angles in the back flow region could not be measured. This overturning was caused by the back flow region with its low stream pressure and is not to be attributed to the secondary flow. Due to the low dynamic pressure in this region the transverse velocity components were small despite the large flow deviation angles.

There were two regions of slight underturning located symmetrically about 2.5 inches from midspan and midway between two adjacent blade wakes, thus indicating a secondary transverse flow from the suction side of one blade wake to the pressure side of the adjacent blade.

Half a chord downstream the flow picture had changed radically. There was now strong underturning in the flow regions where previously there had been back flow with strong overturning. This proves that the overturning in the back flow region at the cascade exit was not caused

by the secondary flow but by the stalling of the blades. This fluid had been given less tangential momentum in the cascade due to the separation and was thus turned less. At cascade exit this was masked by the back flow. Around midspan between the regions of underturned flow the transverse flow angle remained fairly constant and was almost the same as in the free stream. The disappearance of the strongly overturned flow is evidence that this flow was due to stalling and was not caused by the secondary flow. As a summary of these measurements we may say that the variation of the transverse flow angle due to the secondary flow was small but the partial stalling of the cascade caused a large distortion of the flow angles.

6.1.2.4 Spanwise Flow Deviation Angles

Figures 65 and 66 show contour maps of the spanwise flow deviation angles at the two traversed areas.

A very complex flow angle distribution was found at cascade exit. Several regions of large spanwise flow deviation angles were located in the skewed wake flow layer.

Two of these were located at opposite sides of midspan about 1.5 inches apart and close to the pressure side of the blade wakes. The angles there indicated a spanwise secondary flow toward midspan.

There were also two regions of spanwise flow, located symmetrically about 3 inches from midspan at the edges of the back flow region, with the flow directed away from midspan. The positions of these regions agreed with the positions of the stream pressure minimums. Closer to midspan and slightly away from the back flow regions were two other regions in which the flow was directed toward midspan.

Half a chord downstream the regions of spanwise flow deviation angles at the pressure side of the blade wakes persisted and the magnitude of the angles there was almost unchanged while most of the other spanwise flow deviation angle regions had disappeared. Whether these spanwise flows were created by the secondary flow or by the partial stalling of the cascade could not be determined. It seems, however, they were not due to the secondary flow since then the spanwise flow toward midspan at the pressure side of the blade wakes would be followed by a spanwise flow away from midspan at the other side of the blade wake. The flow angles in the two regions would then be almost the same, the only difference being caused by an overall spanwise flow toward midspan from the smoothing out of the skewed wake.

6.1.2.5 Streamline Traces in Carbon Black

Streamline traces in carbon black on the blade surfaces are shown in Figure 67 (pressure side) and 68 (suction side).

The dark region behind the leading edge of the pressure side, extending in spanwise direction, indicates a transition from laminar to turbulent boundary layer terminating at the outer edges of the skewed wake flow layer. At these positions the flow was very turbulent due to the interaction between the skewed flow and the free stream. The magnitude of the velocity was almost the same as in the free stream thus the skin friction at the blade surface was high, removing the carbon black. Inside the skewed wake flow layer the velocity was low resulting in low skin friction indicated by the dark region there. The streaks at midspan position are pointing toward midspan indicating a spanwise flow in this direction.

The stalled flow region was separated from the unstalled flow region on the suction side by a dark line, visible in Figure 68. The stalled flow region was triangular in shape with its tip toward the leading edge and its base along the trailing edge, where it covered a large part of the span. Due to the low velocities in this region the direction at the blade surface was difficult to determine. It seems, however, that the flow was directed away from midspan.

6.2 Analysis of the Secondary Flow

6.2.1 Statement of the Problem

The problem to be considered is the three-dimensional flow in a cascade caused by a skewed wake flow at the inlet of the cascade. The problem is thus the same as the one of the skewed flow, however, the inlet conditions are different and more complicated in this case. The general assumptions made about the flow in the skewed flow case are valid here. An exact analytical solution of the flow field of the skewed flow was shown not to be feasible and thus the same will hold true for this case. Even in this case we must restrict ourselves to try to solve just for the flow in a plane downstream of the cascade.

6.2.2 Determination of the Distributed Streamwise Vorticity Component Downstream of the Cascade

To solve the problem, a small perturbation theory will be applied. Consider the flow in a plane perpendicular to the direction of the two-dimensional flow behind the cascade. The similarity between this problem and the one of the skewed flow permits the use of the same coordinate system and the same notations (see Figure 44).

The equations for the vorticity components are

$$\xi = \frac{\partial w}{\partial y} - \frac{\partial v}{\partial z} \qquad 6\text{-}1$$

$$\eta = \frac{\partial u}{\partial z} - \frac{\partial w}{\partial x} \qquad 6\text{-}2$$

$$\zeta = \frac{\partial v}{\partial x} - \frac{\partial u}{\partial y} \qquad 6\text{-}3$$

Considering the secondary flow in the selected plane the continuity equation becomes

$$\frac{\partial v}{\partial y} + \frac{\partial w}{\partial z} = 0 \qquad 6\text{-}4$$

Define a stream function Ψ for the secondary flow such that

$$v = \frac{\partial \Psi}{\partial z}$$

$$w = -\frac{\partial \Psi}{\partial y}$$

and which satisfies the continuity equation identically and transforms 6-1 to

$$\frac{\partial^2 \Psi}{\partial y^2} + \frac{\partial^2 \Psi}{\partial z^2} = -\xi \qquad 6\text{-}5$$

where

ξ = distributed vorticity component along a streamline. This must be calculated before equation 6-5 can be solved. However, ξ is given by formula 4-2 which was derived by Hawthorne (20) and is applicable for this case.

$$\left(\frac{\xi}{U}\right)_2 - \left(\frac{\xi}{U}\right)_1 = -2\int_1^2 \frac{|\nabla P_0|}{\rho}\,\frac{\sin\phi}{U^2}\,d\theta \qquad 4\text{-}2$$

The notation in this formula are explained in section 4.2.1. The integral has to be evaluated along a streamline from upstream of the cascade (where the flow is defined) through the cascade, to the considered plane behind it. However, at this stage the streamline pattern is not known and so an exact integration of 4-2 cannot be performed. In order to get a solution, we now assume the vorticity to be transported by the two-dimensional flow instead of being transported by the induced velocity and then integrate along a two-dimensional streamline. This method has been used in the two previous flow cases and is applicable only if the effect of the perturbation of the skewed wake flow on the two-dimensional flow is small.

The vorticity component ξ_1 is given by the inlet condition

$$\xi_1 = \frac{\partial w_1}{\partial y} - \frac{\partial v_1}{\partial z} \qquad 6\text{-}6$$

But

$$w_1 = 0 \qquad 6\text{-}7$$

and

$$v_1 = U_1 \sin\beta_1 \qquad 6\text{-}8$$

thus

$$\xi_1 = -\frac{\partial}{\partial z}(U_1 \sin\beta_1) \qquad 6\text{-}9$$

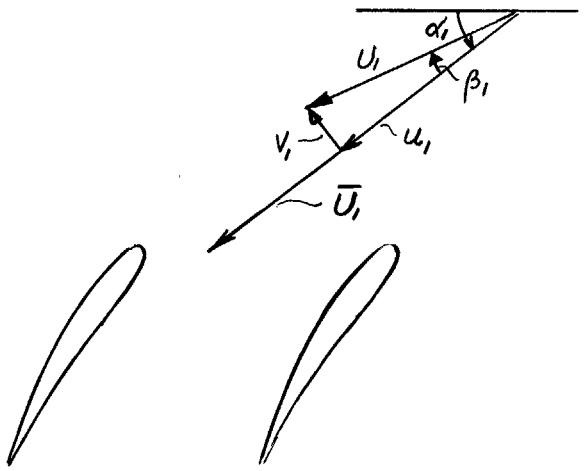

Substituting 6-9 in 4-2 and rearranging gives

$$\xi_2 = -\frac{U_2}{U_1}\frac{d}{dz}(U_1 \sin\beta_1) - 2U_2 \int_1^2 \frac{|\nabla\beta|}{\rho}\,\frac{\sin\phi}{U^2}\,d\theta \qquad 6\text{-}10$$

where the partial derivative has been changed to the total since U_1 and β_1 are functions of z only.

The integral in 6-10 may be evaluated to yield either formula 4-1 or 4-8. However, formula 4-8 showed better correlation of theory and experiment in the wake flow case and will therefore be used here.

Substituting 4-8 in 6-10 gives

$$\xi_2 = -\frac{U_2}{U_1}\frac{d}{dz}(U_1 \sin\beta_1) - \left(1 + \frac{\sin\alpha_1}{\sin\alpha_2}\right)\frac{\cos\alpha_1 - \cos\alpha_2}{\sin\alpha_1}\cdot\frac{U_2}{U_1}\frac{dU_1}{dz} \qquad 6\text{-}11$$

Let

$$\left(1 + \frac{\sin\alpha_1}{\sin\alpha_2}\right)\frac{\cos\alpha_1 - \cos\alpha_2}{\sin\alpha_1} \equiv K \qquad 6\text{-}12$$

6-11 then becomes

$$\xi_2 = -\frac{U_2}{U_1}\frac{d}{dz}\left[U_1 \sin\beta_1 + K\right] \qquad 6\text{-}13$$

But

$$U_1 = \overline{U}_1 - \Delta U_1 \qquad 6\text{-}14$$

where

$$\Delta U_1 \ll \overline{U}_1 \qquad 6\text{-}15$$

and

$$\sin\beta_1 \approx \beta_1 \qquad 6\text{-}16$$

Substituting 6-14 and 6-16 in 6-13 and neglecting second order terms

$$\xi_2 = -\frac{U_2}{U_1}\frac{d}{dz}\left[\overline{U}_1\beta_1 + K U_1\right] \qquad 6\text{-}17$$

The continuity equation is

$$U_1 \sin\alpha_1 = U_2 \sin\alpha_2 \qquad 6\text{-}18$$

which combined with 6-17 gives

$$\xi_2 = -U_2 \frac{d\beta_1}{dz} - \frac{\sin\alpha_1}{\sin\alpha_2} K \frac{dU_1}{dz} \qquad 6\text{-}19$$

or substituting the expression for K

$$\xi_2 = -U_2 \frac{d\beta_1}{dz} - \left(1 + \frac{\sin\alpha_1}{\sin\alpha_2}\right) \frac{\cos\alpha_1 - \cos\alpha_2}{\sin\alpha_2} \frac{dU_1}{dz} \qquad 6\text{-}20$$

This expression for the secondary vorticity, ξ_2, is a superposition of the secondary vorticity for the skewed flow (5-36) and the wake flow (4-8). The solutions obtained in sections 4 and 5 may thus be superposed to give the solution of this flow problem.

If 4-1 is used instead of 4-8, ξ_2 would then become

$$\xi_2 = -U_2 \frac{d\beta_1}{dz} - 2\varepsilon \frac{dU_1}{dz} \qquad 6\text{-}21$$

Equation 6-5 together with 6-13, 6-20 or 6-21 with the pertinent boundary conditions may now be solved. The boundary conditions in this case are the same as the ones for the wake flow and the skewed flow, i.e.

$$\Psi = 0 \qquad 6\text{-}22$$

for y = 0, y = b, z = 0, and z = 1

Before solving equation 6-5 it will be of interest to study the expression for ξ_2.

6.2.3 Requirement for No Secondary Flow

The magnitude of the streamwise vorticity component, ξ_2, is a measure of the generated secondary flow. If $\xi_2 = 0$, no secondary flow

will be established behind the cascade since in this case equation 6-5 changes from a Poisson's equation to a Laplace's equation, which together with the boundary conditions $\Psi = 0$, along the boundaries, gives only the solution $\Psi = 0$ over the whole plane. The requirement for no secondary flow behind the cascade then becomes using 6-13

$$\frac{d}{dz}\left[U_1(\sin\beta_1 + K)\right] = 0 \qquad 6\text{-}23$$

which may be integrated to yield

$$U_1(\sin\beta_1 + K) = C = \text{constant} \qquad 6\text{-}24$$

where C is given by the boundary condition:

at the edge of the skewed wake flow

$$\beta_1 = 0 \quad \text{for} \quad U_1 = \bar{U}_1 \qquad 6\text{-}25$$

Substituting the value of C determined from 6-25 and 6-24 into 6-24 yields

$$\sin\beta_1 = K\left(\frac{\bar{U}_1}{U_1} - 1\right) \qquad 6\text{-}26$$

Assuming β_1 and ΔU_1 to be small and substituting the value of K yields

$$\beta_1 = \left(1 + \frac{\sin\alpha_1}{\sin\alpha_2}\right)\frac{\cos\alpha_1 - \cos\alpha_2}{\sin\alpha_1}\left(1 - \frac{U_1}{\bar{U}_1}\right) \qquad 6\text{-}27$$

Using 6-21 instead of 6-13 gives

$$\beta_1 = 2\varepsilon\frac{\sin\alpha_1}{\sin\alpha_2}\left(1 - \frac{U_1}{\bar{U}_1}\right) \qquad 6\text{-}28$$

If the velocity distribution and the angle of attack at the inlet to the cascade correlate according to formulae 6-27 or 6-28 no secondary flow will be established behind the cascade.

6.2.4 Mathematical Expressions for the Inlet Flow Conditions

The magnitude of the velocity in the center of the skewed wake flow was set so that, according to formula 6-28, no secondary flow would be created at midspan. The reason for using 6-28 instead of the more correct formula, 6-27, was that the latter had not been derived when this experiment was made. A complete absence of secondary flow behind the cascade could not be expected since the velocity profile could not be varied to correlate with (equation 6-28) the inlet angle distribution everywhere over the span.

The transverse flow angle distribution upstream of the cascade varied slightly in tangential direction. In order to get a distribution that might represent the average condition a faired curve was drawn through the measured data (Figure 69). This curve was closely represented by a 4-term Fourier series as shown in Figure 69.

In the same manner the stagnation pressure distribution was represented by a faired curve as shown in Figure 70. From this faired curve the velocity distribution was calculated with the assumption that the stream pressure was constant over the span. This is a fairly valid assumption as shown in Figure 58. This velocity distribution was then closely represented by a 4-term Fourier series as shown in Figure 71. The same base width, $2\delta = 3.5$ inches, of the two mathematical curves representing the angle and velocity distribution, was used. A better correlation between the mathematical curves and the measurements would have been obtained if different base widths had been used i.e. $2\delta = 3.2$ inches for the angle distribution and $2\delta = 3.8$ inches for the velocity distribution. The reason for using the same value for the

two curves was that it reduced the numerical calculations considerably and this was justified by the fact that the severe stalling of the cascade effectively masked the secondary flow caused by the skewed wake flow, so that an accurate correlation of theory and experiment would not be expected.

Two different calculations have been made. In the first, a skewed flow and a wake flow were calculated separately using the inlet conditions represented by the two previous Fourier series. Their results were superposed to give the secondary flow deviation angles due to the skewed wake flow. Formulae 4-8 and 5-36 were used to represent the streamwise vorticity component. The values used in the numerical calculations are shown in Appendix D and the results are shown graphically in Figures 73, 74 and 75.

In the second calculation the more accurate expression, 6-11 for the streamwise vorticity component has been used. The function $U_1 (\sin \beta_1 + K)$, in this expression, was calculated from values taken from the faired curves of the inlet angle distribution and the velocity distribution, and was represented by a 4-term Fourier series as shown in Figure 72. The values used in the numerical calculations are shown in Appendix E and the results are shown graphically in Figures 73, 74 and 75. In all the calculations the first three terms in the series for Ψ and Ψ' have been retained, i.e. n = 1, 3 and 5.

6.2.5 Correlation of Theory and Experiment

The partial stalling of the cascade disturbed the flow severely, effectively masked the secondary flow caused by the skewed wake flow, and

made a correlation of theory and experiments very difficult. The cascade was also partially stalled in the skewed flow case but the stalled flow region was smaller and the secondary flow much stronger, thus making a correlation easier. The secondary flow was assumed to be very small in the present case.

6.2.5.1 Maximum Transverse Flow Deviation Angle, β_{max}

Referring to section 6.1.2.3 the only conclusion to be drawn about the measured maximum transverse flow deviation angle due to the secondary flow is that it is small.

The calculated spanwise distribution of the transverse flow deviation angle is shown in Figure 73.

The first method, superposing the solutions of a wake flow and a skewed flow, gives a maximum underturning of about 5.5° at midspan and a maximum overturning of about 1.5° at the outer edge of the skewed wake flow layer.

The second method gives two locations for maximum underturning, one at midspan and one about 1.2 inches from midspan. The magnitude of the underturning is about the same, 2.5°, at each position. There are also two locations of maximum overturning, one located about 0.7 inches from midspan and the other about 1.8 inches from midspan, both having the same amount of overturning (less than 1°).

The cross product term which is neglected in the first method is responsible for the difference between the two results and it may not be neglected in a case where the inlet distortions are great.

6.2.5.2 Average Transverse Flow Deviation Angle, $\bar{\beta}$

The variation of the measured average-transverse flow deviation angle over the span half a chord downstream of the cascade, together with the calculated distributions are shown in Figure 73.

The measured curve shows an underturning over the central part of the span. This is mainly caused by the separation of the blades over this region. In this region of general underturning there are three peaks of underturning, one at midspan and one on either side of midspan located about 4 inches apart. They are all of about the same magnitude, 3.5°. Between these peaks of underturning there are two regions of smaller underturning located at about 1 inch on either side of midspan. The underturning in one of them is about 2° and is almost zero in the other.

The average flow angle in the free stream had increased by about 1.5° above the value measured in the pure two-dimensional test. The two calculated curves have the same general shape and show flow deviation angles of the same order of magnitude as the measured one, but due to the influence of the stalling on the measured data no correlation may be made.

6.2.5.3 Maximum Spanwise Flow Deviation Angle, γ_{max}

Figure 74 shows the calculated curves of the maximum spanwise flow deviation angle distribution.

The first method gives a maximum angle of 3° while the second method predicts 1.5°. The locations of these maximum values also differ. According to the first method the maximum should be located about 0.7

inches from midspan while the other method places it 1.5 inches from midspan.

6.2.5.4 Conclusions

The partial stalling of the cascade has essentially disturbed the flow by blocking a large part of the cascade and thus changing its effective geometrical configuration. It has reduced the turning of the flow in the stalled part of the cascade and is probably responsible for the overturning in the free stream. The stalling of the cascade effectively masked the secondary flow caused by the skewed wake flow. A close correlation of theory and experiment may not be expected under these circumstances and the only conclusion to draw is that the measured secondary flow downstream of the cascade caused by the skewed wake flow was very small, which was predicted by the theory.

6.3 Losses and Kinetic Energy of Secondary Flow

6.3.1 Results of Measurements

The experimental data; flow deviation angles, stream pressure, and stagnation pressure, were used to calculate the kinetic energy of the secondary flow in the same way as for the skewed flow (section 5.3.1). The result is shown in Figure 76. The curve has two maximum points. One located at midspan, caused by the transverse flow at this position. The other, located about 2 inches from midsapn, is of greater magnitude than the first and is caused by the underturning at this position as may be seen in Figure 74. The amount of underturning is about the same at this position as at midspan, however, the magnitude of the velocity vector is much smaller at midspan due to the wake and so the kinetic energy of the secondary flow is smaller at midspan.

The area integrated value of the kinetic energy of the secondary flow is

$$\frac{D}{KE_{in}} = 0{,}13\,\%$$

The ratio of the kinetic energy bound in the spanwise flow to the total kinetic energy of the secondary flow was about 0.3.

6.3.2 Theoretical Calculation of the Kinetic Energy of the Secondary Flow

An Appendix F is given the derivation of the formula for the ratio of the kinetic energy per unit volume of the secondary flow to the kinetic energy of the flow entering the cascade:

$$\frac{D}{KE_{in}} = \frac{8}{\pi}\,\frac{s}{c}\,\frac{c}{\ell}\,\frac{\sin^2\alpha_2}{\sin\alpha_1}\,\frac{\left(\frac{\sin\alpha_1}{\sin\alpha_2}\right)^2 \cdot f + 4\varepsilon^2 \cdot g - 4\varepsilon\,\frac{\sin\alpha_1}{\sin\alpha_2}\cdot h}{1 - \frac{\Theta + \delta^*}{\ell}} \qquad \text{F-46}$$

where f, g and h are functions given by formula F-31, F-40 and F-41 in Appendix F-4.

For convenience the meaning of the three terms in F-46 is repeated here.

1. is the contribution from the skewed flow only
2. is the contribution from the wake flow only
3. is the contribution from the interaction between the skewed flow and the wake flow.

The actual values for this test were substituted in F-46 and gave

$$\frac{D}{KE_{in}} = 0.05\,\%$$

The contribution to this figure from the three terms in F-46 was

1. 0.41%
2. 0.18
3. -0.54

The predicted value of 0.05% is to be compared to the measured one of 0.13% half a chord downstream. It would be expected that the predicted value should be greater than the one measured half a chord downstream since the secondary flow has been diminished. However, the measured value includes the effect of the stalling of the cascade which results in increased flow deviation angles, and thus in higher measured kinetic energy of the flow in the plane studied. The result of this part of the investigation can therefore be summed up: the kinetic energy of the flow due to the secondary flow and to stalling are of the same order of magnitude, and the kinetic energy of the secondary flow is very small.

The spanwise distribution of the kinetic energy of the secondary flow has also been calculated using formula F-49, derived in Appendix F-5. The result is shown in Figure 76.

The predicted curve shows three maximum points due to maximum flow deviations at these locations. The minimum point located about 1.2 inches from midspan is caused by the fact that there is no transverse flow deviation and only a very small spanwise flow deviation at this position. The theory predicts the kinetic energy distribution to be concentrated more around midspan than was actually measured.

6.3.3 Losses

Most of the discussion concerning the three-dimensional losses for the wake flow in section 4.3.3 is valid for this case and will therefore not be repeated here.

The measured area averaged stagnation pressure defect distribution over the span half a chord downstream of the cascade is shown in

Figure 77. The maximum stagnation pressure defect amounted to 48% of the reference dynamic pressure. The two-dimensional loss outside the stalled region amounted to about 1.6% which was the value measured in the two-dimensional test (section 3.2). The stagnation pressure defect in excess of this two-dimensional loss, averaged over the whole span (16 inches) amounted to 11.4%. The inlet stagnation pressure defect, due to the wake, averaged over the span was 5.7%.

The difference between the averaged-outlet stagnation pressure defect (in excess of the two-dimensional defect) and the inlet one is called the complementary loss and amounted to 5.7%. This is a large loss and is greater than that part of the loss usually attributed to secondary flow in an actual compressor.

The measured kinetic energy of the secondary flow and the flow deviations due to the stalling, amounting to 0.13%, has not been included in the complementary loss for the reasons mentioned in section 4.3.3. This kinetic energy is negligible compared to the complementary losses. The conclusion of this result will be drawn in section 7.

6.4 The Tangential Component of the Blade Force

6.4.1 Results of Measurements

Stream pressure distribution on the blade surface was measured at the same spanwise positions as in the skewed flow case (5.4.1) and the results have been plotted in the same way.

The variation of C_T over the span is shown in Figure 55, the projected stream pressure on the blade surfaces in Figure 78, and a contour map of the pressure distribution in Figure 79. The curves show a

very strong separation over most of the suction surface in the skewed wake flow region. The pressure peak at the leading edge was reduced in the skewed wake flow due to the reduced dynamic pressure there. The stream pressure on the pressure side was lower in the skewed wake flow than in the free stream and remained almost constant over a very large portion of the chord.

6.4.2 Theoretical Calculation of the Tangential Component of the Blade Force

The derivation of the formula for the tangential pressure coefficient C_T is given in Appendix G together with an interpretation of it. (The reader is referred to that when interpreting the results given below.) The actual values for this test were substituted in formula G-41:

Term	Value		Percentage of (1)
(1)	0.52088	0.47993	
(2)	-0.04095		-7.86%
(3)	0.04962	0.00207	9.53
(4)	-0.05169		-9.92
(5)	-0.00260	0.00033	-0.50
(6)	-0.00465		-0.89
(7)	0.00692		1.33
C_T	0.478		-8.31

The decrease in C_T from its two-dimensional value is thus 8.3%, of which term (2) contributes about 95%. The total effect of the changed angle of attack in the skewed layer (terms 3 and 4) on the tangential blade force was very small since the increased momentum due to the increased

inlet angle was cancelled by the decreased mass flow in the same region. The reduction due to the secondary flow (terms 5, 6 and 7) was also very small. The measured reduction was 10.2% to be compared to the predicted value of 8.3%. A reason for the discrepancy was the partial stalling of the cascade which reduced the tangential blade force and which had not been accounted for in the theoretical calculations.

In the calculations leading to the results above the two-dimensional value of the transverse outlet angle, 64.4°, was used instead of the measured free stream value of 66.0°. This gave $C_T = 0.521$ in the free stream (term 1 in the table above) to be compared to the measured value of $C_T = 0.520$. Using the measured value of 66.0° gave $C_T = 0.555$. In deriving formula G-41 by means of which these free stream values have been calculated, a two-dimensional layer flow was assumed, i.e. the streamlines do not shift position in spanwise direction. In the investigated flow this assumption was violated through the partial blocking of the cascade due to stalling and thus changed the velocity profile and therefore did not permit a good correlation. From Figure 55 it may be seen that the value of C_T in the free stream is about the same for the two-dimensional test, the skewed flow test, and the skewed wake flow test, but not for the wake flow test. It may be just a coincidence but it could also indicate that when only part of the flow is changed over the span, in a fixed cascade configuration, so that the cascade is partially stalled, the flow adjusts itself so that C_T remains constant while C_p varies in the free stream. There are, however, no obvious reasons for this to occur.

7 SUMMARY AND CONCLUSIONS OF THE INVESTIGATION AND THEIR APPLICATION TO COMPRESSOR DESIGN

We have investigated three ways in which secondary flow is generated behing a compressor cascade.

1.) Wake flow. The inlet flow is characterized by a constant inlet angle and a varying stagnation pressure over the span. It may be described by vortex sheets parallel to the top and bottom plates of the cascade and with the vorticity-vectors perpendicular to the streamlines. These vortex sheets turn when they move through the cascade so that the vorticity vectors then have components along the streamlines and thus a secondary flow is set up behind the cascade causing an overturning at the spanwise center of the wake, and a smaller underturning at the edges of the wake.

2.) Skewed flow. The inlet flow is characterized by constant stagnation pressure and varying inlet angle over the span. It may be described by vortex sheets parallel to the top and bottom plates of the cascade, with the vorticity vectors parallel to the streamlines. The vorticity vector changes proportionally with velocity vector along a streamline, and so the vorticity vector reduces its magnitude when moving through a compressor cascade and increases its magnitude through a turbine cascade.

An increased angle of attack in the skewed flow layer entering the cascade causes a secondary flow behind the cascade opposite to that caused by a wake flow.

3.) Skewed wake flow. The inlet flow is characterized by a variation of both stagnation pressure and inlet angle over the span, and may be considered as a superposition of a wake flow and a skewed flow for small variations of inlet angle and stagnation pressure. It may be described by vortex sheets parallel to the top and bottom plates of the cascade and with the vorticity vector at an angle to the streamline. This, in general, causes a secondary flow behind the cascade. The direction of the secondary flow is dependent on the inlet conditions. For a certain combination of inlet angle and stagnation pressure distribution (given in formula 6-11) no secondary flow is generated behind the cascade. There might be a secondary flow within the cascade but it is probably small.

The secondary flow generated in all three cases is concentrated in the vorticity region i.e. in the wake, the skewed flow layer, and the skewed wake flow layer, respectively. The secondary flow outside these regions is slight.

The difference in flow conditions, in this investigation of a straight compressor cascade, and an actual compressor is appreciable and the results from this investigation may only be applied to compressor design with great caution. Skin friction at the casings and radial pressure gradients in a compressor can greatly change the flow picture from that of this investigation. However, the skewed boundary layer on the casings of a compressor is qualitativley the same as the skewed wake flow, thus the secondary flow and the turning of the Bernoulli surfaces in a compressor may be expected to be small.

7.1 Flow Deviation Angles

The severe stalling at midspan in the skewed flow and skewed wake flow case disturbed the flow appreciably and made a correlation of the theory and experiment difficult. However, the flow deviation angles predicted by the theory were, in general, well confirmed by the experiments.

7.1.1 Transverse Flow Deviation Angles

In all investigated cases the maximum transverse flow deviation angle was located at midspan i.e. in the center of the wake and the center of the skewed flow layer respectively. The wake flow caused an overturning at this position while the skewed flow generated an underturning. At the edges of the wake and the skewed flow layer a smaller transverse flow was generated opposite to the direction of that at midspan. In the skewed wake flow case only a very small transverse flow was generated.

The main stream was turned more in the skewed flow and skewed wake flow cases than in the two dimensional test.

In an actual compressor the transverse flow deviation angles may be expected to be small and may show up as an overturning, or an underturning at the casings depending on the actual compressor design.

7.1.2 Spanwise Flow Deviation Angles

The maximum spanwise flow deviation angles were located close to the blade wakes and about halfway between the edge and the center of the wake, or skewed flow layer, respectively. The spanwise flow was in opposite directions in the wake flow and skewed flow cases.

The spanwise flow deviation angles due to secondary flow may also be expected to be small in an actual compressor.

7.2 Kinetic Energy of the Secondary Flow

The kinetic energy of the secondary flow was in all cases concentrated in regions of high vorticity i.e. in the wake and the skewed flow layers, respectively. The kinetic energy of the secondary flow was very small and may be neglected completely in an actual compressor design when considering the losses.

7.3 Losses

No losses created by secondary flow were found in the wake flow case.

In both the skewed flow and the skewed wake flow cases the cascade stalled over its midspan region. The stalled flow region extended further in spanwise direction in the skewed wake flow case than in the other case. Two vortices, one on either side of the midspan, where shed from the stalled flow region in the skewed wake flow case but not in the skewed flow case. The partial stalling of the cascade caused large losses, in fact they were greater than those usually measured in a well designed compressor blade row.

The flow in the stalled flow region was very unsteady and caused unsteadiness in the free stream. This was observed visually by placing a grid of streamers in the flow behind the cascade. Both the losses and the unsteadiness of the flow were greater in the skewed wake flow case than in the skewed flow case.

Applying the results of this part of the investigation to

an actual compressor design may only be done with great caution. However, secondary flow itself does not seem to give rise to any losses. The relative motion between the blade rows increases the velocity gradient at the casings increasing the skin friction and thus the losses there. Since the cascade stalled in the skewed flow and skewed wake flow cases, in this investigation, where there was no end wall and the angle of attack was less than can be expected in a real compressor, we may draw the conclusion that, in an actual compressor, the blades stall at the casings, the amount of stalling being dependent on the actual design. These losses caused by the partial stalling of the cascade in the skewed boundary layer regions at the casings may then be the losses that have been erroneously attributed to secondary flow. The separation will probably be smaller if the tangential velocity component has a finite value at the casing at entrance to the blade row considered (see Figure 1a). From this viewpoint shrouded stator blades will decrease the separation and losses at the hub of the rotor blade rows.

The stalling at the casings blocks that part of the cascade, changing its effective geometry and distorting the flow conditions in the main flow. It also changes the inlet conditions to the next blade row and gives rise to very unsteady inlet flow conditions to portions of the following blade row which may increase the losses there and also cause blade vibration.

A way to avoid this would be to twist the ends of the stator blades in tangential direction to reduce the angle of attack and so reduce, or eliminate, the stalling there. This would also reduce the angle of attack in the skewed boundary layer at the casings

in the following rotor blade row and thus also improve the flow conditions there.

7.4 The Tangential Component of the Blade Force

The stream pressure on the blade surfaces was reduced around midspan in all three flow cases. The reduction was greatest for the skewed wake flow and smallest for the wake flow. This was expressed by the tangential pressure coefficient, C_T, based on the dynamic reference pressure. The reduction in C_T due to secondary flow was very small and could be neglected compared to the reduction due to the decreased mass flow in the wakes. The partial stalling of the cascade also reduced C_T. This reduction was much smaller than the reduction due to the decreased mass flow in the wake, in the skewed wake flow case.

The increased tangential momentum per unit volume due to the increased angle of attack in the skewed flow layer was balanced by the reduced mass flow in the same region so that its total influence on C_T for the cascade was almost zero.

The local value of C_T actually obtained in the wake flow case is higher than can be obtained in a two-dimensional cascade without separation. This shows that values of C_T obtained from two-dimensional cascade data will not give the corresponding information about a three dimensional flow.

C_T in the main stream remained almost constant for the two-dimensional, the skewed flow, and the skewed wake flow tests but was reduced in the wake flow test. This may just be a coincidence but it

could also indicate that when only part of the flow is changed over the span, in a fixed cascade configuration, so that the cascade is partially stalled, the flow adjusts itself so that C_T remains essentially constant while C_P varies in the free stream. C_p decreases with increased stalling due to the increased losses. The effects above also show up as increased transverse outlet flow angles in the free stream, in the skewed and skewed wake flow cases.

Applying this part of the investigation to compressor design would imply that the stream pressure varies in spanwise direction through the skewed boundary layer on the casing. This being contrary to the generally accepted idea of a constant spanwise pressure in the boundary layer on the casings. The variation in pressure is dependent on the actual design.

The reduction in tangential momentum in the skewed boundary layers can be calculated just by correcting for the decreased mass flow there.

7.5 Correlation of Theory and Experiment

The partial stalling of the cascade in the skewed flow and skewed wake flow cases disturbed the flow appreciably and masked the effects of the secondary flow, making a correlation of theory and experiment difficult. Despite this, good and satisfactory correlation of theory and experiments were found in all cases investigated.

8 SUGGESTIONS FOR FURTHER WORK

This investigation could be extended as follows:

1.) Reduce the angle of attack in the skewed layer in order to unstall the blades. This would allow a better correlation of theory and experiment.

2.) Reduce the spanwise thickness of the skewed layer. It is felt that the spanwise variation of stream pressure and the stalling is dependent on the ratio of the skewed flow layer thickness to the chord.

3.) Twist the blades in the skewed flow layer in tangential direction to allow for the increased flow angle of attack. This would test the theory of reducing the losses.

4.) Insert a splitter board at midspan inside the cascade. This splitter board would simulate the casings in a real compressor.

5.) Tests 2 and 3 repeated with the splitter board.

6.) Tests in a real compressor

BIBLIOGRAPHY

1. Howell, A. R., "The Present Basis of Axial Flow Compressor Design", Part I, Theory and Performance, R and M No. 2095, Brit. ARC, June 1942.

2. Allen, H. W., Kofskey, M. G. and Chamness, R. E., "Experimental Investigation of Loss in an Annular Cascade of Turbine-Nozzles Blades of Free Vortex Design", NACA TN 2871, 1953.

3. Rohlik, H. E., Allen, H. W. and Herzig, H. Z., "Study of Secondary Flow Patterns in an Annular Cascade of Turbine Nozzle Blades with Vortex Design", NACA TN 2909, 1953.

4. Stanitz, J. D., Osborn, W. M. and Mizisin, J., "An Experimental Investigation of Secondary Flow in an Accelerating, Rectangular Elbow with 90° of Turning", NACA TN 3015, 1953.

5. Toline, F. R. and Watson, R. H., "The Effects of a Moving Wall on the Secondary Flow in a Cascade", S.M. Thesis, M.I.T., 1953.

6. Rohlik, H. E., Kofskey, M. G., Allen, H. W. and Herzig, H. Z., "Secondary Flows and Boundary Layer Accumulations in Turbine Nozzles", Rep. 1168 (Supersedes: TN 2871, TN 2909, TN 2989), 1954.

7. Armstrong, W. D., "The Secondary Flow in a Cascade of Turbine Blades", Dept. of Engng., Univ. of Cambridge, March 7, 1955.

8. Gersten, K., Part II, "Secondary Flow Losses of a Turbine Cascade for Different Velocities Profiles of Inflow", Institut fur Strömungsmechanik, Rep. No. 54/12a. Technische Hochschule Braunschweig, 1955.

9. Moore, R. W. and Richardson, D. L., "Skewed Boundary Layer Flow near the End Walls of a Compressor Cascade", Trans. ASME, Vol. 79, No. 8. 1957.

10. Herzig, H. Z., Hansen, A. G. and Costello, G. R., "Visualization of Secondary Flow Phenomena in Blade Row", NACA RM E52F19, 1952.

11. "Effect of Geometry on Secondary Flow in Blade Rows", NACA RM E52H26, 1952.

12. Hansen, A. G., Herzig, H. Z. and Costello, G. R., "Smoke Studies of Secondary Flows in Bends, Tandem Cascades, and High Turning Configurations", NACA RM E52L24a, 1952.

13. Herzig, H. Z., Hansen, A. G. and Costello, G. R., "A Visualization Study of Secondary Flows in Cascades", NACA Rep. 1163 (Supersedes TN 2947) 1954.

14. Kofskey, M. G. and Allen, H. W., "Smoke Study of Nozzle Secondary Flows in a Low-Speed Turbine", NACA TN 3260, 1954.

15. Allen, H. W. and Kofskey, M. G., "Visualization Study of Secondary Flows in Turbine Rotor Tip Regions", NACA TN 3519, 1955.

16. Carter, A. D. S., "Three-Dimensional Flow Theories for Axial Compressors and Turbines", War Emergy. Issue No. 41, Proceedings, The Institute of Mechanical Engineers.

17. Squire, H. B. and Winter, K. G., "The Secondary Flow in a Cascade of Air-foils in a Non-Uniform Stream", Journal Aeronautic Sciences, Vol. 18, No. 4, April 1945.

18. Von Karman, T., and Tsien, H. S., "Lifting Line Theory for a Wing in Non-Uniform Flow", Quarterly of Applied Mathematics, Vol III, April 1945.

19. Hausmann, G. E., "The Theoretical Induced Deflection Angle in Cascades having Wall Boundary Layers", Journal of the Aeronautic Sciences, Vol. 15, NO. 4, April 1951.

20. Hawthorne, W. R., "Secondary Circulation in Fluid Flow", Proceedings of the Royal Society, A, Volume 206, 1951.

21. Kronauer, R., "Secondary Flow in Fluid Dynamics", Ph.D. Thesis, Harvard University, 1951.

22. Eichenberger, H. P., "Shear Flow in Bends", D.Sc. Thesis, M.I.T., 1952.

23. Van Le, Nguyen, "Three-Dimensional Flow in a Cascade", D.Sc. Thesis, M.I.T., 1952.

24. Smith, L. H. jr., "Three-Dimensional Flow in Axial Flow Turbo-Machinery", Part I. Theoretical Determination of Secondary Flow, Rep. 1-14, Part II. Experimental Investigations, Rep. 1-16. John Hopkins University, Air Force Contract AF-33(616)-152, Expenditure Order No. R-467-3BR1, R-467-3BR2.

25. Taylor, E. S., Stevenson, T. and Dean, R. C. , "The Control of Secondary Flow in the Wall Boundary Layers of Axial Turbo-Machines", M.I.T. G.T.L. Report No. 27-4.

26. Ehrich, F. F., "Secondary Flows in Cascades of Twisted Blades", Reprint No. 432, Inst. of Aero. Sciences, 1954.

27. Dean, R. C. jr., "Secondary Flow in Axial Compressors", M.I.T., G.T.L. Report.

28. Preston, J. H., "A Simple Approach to the Theory of Secondary Flows", The Aero. Quarterly, Vol. 5, Part 3, 1955.

29. Hawthorne, W. R., "Some Formulae for the Calculation of Secondary Flow in Cascades", Dept. of Engng., University of Cambridge, March 1955.

30. Hawthorne, W.R. and Armstrong, W. D., "Shear Flow Through a Cascade", Dept. of Engng., Univ. of Cambridge, Feb. 1955. Also the Aero. Quarterly, Vol. VIII, Nov. 1956.

31. Hawthorne, W. R., "The Growth of Secondary Circulation in Frictionless Flow", Proc. of the Cambridge Philosophical Soc., Vol. 51, Part 4, pp. 737-743, 1955.

32. Horlock, J. H., "Some Examples of Outlet Angle Variations in Cascade Wall Boundary Layers", Eng. Dept. Cambridge Univ., March 1955.

33. Hansen, A. G. and Herzig, H. Z., "Analysis of Particle Motions for a Class of Three-Dimensional, Incompressible Laminar Boundary Layers", NACA TN 3840.

34. Hansen, A. G. and Herzig, H. Z., "Cross Flows in Laminar Incompressible Boundary Layers," NACA TN 3651.

35. Herzig, H. Z. and Hansen, A. G., "Experimental and Analytical Investigations of Secondary Flows in Ducts", Inst. of Aero. Sciences, Journal of the Aero. Sciences, Reprint No. 593, 1956.

36. Soundrananyagam, S., "The Secondary Flow Behind a Cascade", JAS. Vol. 24, No. 9, 1957, p.706.

37. Turner, J. R., "An Investigation of the End-Wall Boundary Layer of a Turbine Nozzle Cascade", M.I.T. Gas Turbine Lab, Report No. 30.

38. Senoo, Y., "Three-Dimensional Laminar Boundary Layer in Curved Channels with Acceleration", M.I.T., Gas Turbine Lab Report No. 37, 1956.

39. Senoo, Y., "The Boundary Layer on the End Wall of a Turbine Nozzle Cascade", M.I.T. Gas Turbine Lab Report No. 35, 1956.

40. "Low Speed Cascades", Progress Reports on Project 2006, M.I.T. Gas Turbine Lab.

41. Mc Donald, J. W., "Development of a Skewed Velocity Profile for Compressor Cascade Research", S.M. Thesis, M.I.T., 1957.

42. Moore, R. W., Nelson, W. G., Prasad, A., Richardson, D. L. and Turner, J. R., "Experimental Techniques for Three-Dimensional Flow Research", M.I.T, Gas Turbine Lab Report No. 27-8, 1954.

43. Dean, R. C., "Aerodynamic Measurements", M.I.T., Gas Turbine Lab, 1953.

44. Mellor, G. L., "Theoretical Consideration of Secondary Flow", M.I.T. Gas Turbine Lab, Report No. 27-2, 1954.

45. Louis, J. F., "Rotational Viscous Flow", University of Cambridge, Dept. of Engng., March 1958.

46. Schlichting, H., "Boundary Layer Theory", McGraw Hill Book Co., Inc., New York, 1955.

47. Bragg, S. L., "The Flow of an Ideal Fluid through an Annular Cascade", S.M. Thesis, M.I.T., 1949.

48. Forstall, W., jr., "Material and Momentum Transfer in Coaxial Gas Streams", Sc.D. Thesis, M.I.T., 1949.

LIST OF SYMBOLS

l	blade height
c	chord
s	gap
$s_1 = s \cdot \sin\alpha_1$	blade passage width at inlet of cascade
$b = s \cdot \sin\alpha_2$	blade passage width at outlet of cascade
δ	half a width of wake, or half width of skewed flow layer
x, y, z	rectangular coordinates
$\bar{v}$	velocity vector
v	magnitude of velocity vector in perturbed flow region
$\bar{v}$	magnitude of velocity vector outside perturbed flow region
$\Delta v \equiv \bar{v} - v$	magnitude of velocity in wake
$2a$	magnitude of velocity defect at center of wake
u, v, w	velocity components along the x, y and z axes respectively
ψ	stream function
$\bar{\omega}$	vorticity vector
ξ	vorticity component along the x axis
η	vorticity component along the y axis
ζ	vorticity component along the z axis, also replaces z as dummy variable in certain integrals
ε	cascade turning angle
α	transverse flow angle for two-dimensional flow
α'	transverse flow angle for three-dimensional flow
β	transverse flow deviation angle

γ	spanwise flow deviation angle
θ	momentum thickness of half the wake
δ^*	displacement thickness of half the wake
KE_{inl}	kinetic energy per unit volume of the inlet flow
D	kinetic energy per unit volume of the complete secondary flow
D_z	kinetic energy per unit volume of the complete secondary flow at certain spanwise position
D_W	kinetic energy per unit volume of the secondary flow due to a wake flow
D_S	kinetic energy per unit volume of the secondary flow due to a skewed flow
D_{SW}	kinetic energy per unit volume of the secondary flow due to an interaction between wake flow and skewed flow
T	tangential component of blade force
C_T	tangential pressure coefficient
C_p	pressure coefficient
A_m, B_m, C_m	Fourier coefficients in the expressions for the inlet flow conditions
m, n	integers
k	scalar (given in 5-8)
K	dimensionless parameter (defined in 6-12)
f, g, h	functions (given by F-31, F-32, F-33, F-40 and F-41)

SUBSCRIPTS

1	upstream of cascade
2	downstream of cascade
0	at the actuator disc, also stagnation pressure when referred to P
02	at the actuator disc in the downstream region
r	reference value
s	skewed flow case
w	wake flow case
sw	interaction of skewed flow and wake flow
m	maximum

LIST OF FIGURES

19. Wakeflow. Streamline Traces in Carbon Black on the Blade Pressure Side.

20. Wakeflow. Streamline Traces in Carbon Black on the Blade Suction Side.

21. Wakeflow. Diagram of Notations.

22. Wakeflow. Velocity Profile at Cascade Inlet.

23. Wakeflow. Maximum Transverse Flow Deviation Angle.

24. Wakeflow. Average Transverse Flow Deviation Angle.

25. Wakeflow. Spanwise Flow Deviation Angle.

26. Wakeflow. Spanwise Flow Deviation Angle.

27. Wakeflow. Spanwise Distribution of the Kinetic Energy of the Secondary Flow.

28. Wakeflow. Stagnation Pressure Distribution.

29a Wakeflow. Projected Stream Pressure Distribution on the Blade Surfaces.

29b Wakeflow. Tangential Pressure Coefficient Distribution along the Span.

30. Wakeflow. Contours of Constant Stream Pressure on the Blade Surfaces.

31. Skewed Flow $\nabla P_0 = 0$. Contours of Constant Transverse Inlet Angles.

32. Skewed Flow $\nabla P_0 = 0$. Contours of Constant Stagnation Pressure Upstream of Cascade.

33. Skewed Flow $\nabla P_0 = 0$. Contours of Constant Stream Pressure Upstream of Cascade.

34. Skewed Flow $\nabla P_0 = 0$. Contours of Constant Stagnation Pressure. Axial Position: 0.1" Behind the Cascade.

35. Skewed Flow $\nabla P_0 = 0$. Contours of Constant Stagnation Pressure. Axial Position: 2.25" Behind the Cascade.

36. Skewed Flow $\nabla P_0 = 0$. Contours of Constant Stream Pressure. Axial Position: 0.35" Behind the Cascade.

37. Skewed Flow $\nabla P_0 = 0$. Contours of Constant Stream Pressure. Axial Position: 2.25" Behind the Cascade.

38. Skewed Flow $\nabla P_o = 0$. Contours of Constant Transverse Flow Angle. Axial Position: 0.1" Behind the Cascade.

39. Skewed Flow $\nabla P_o = 0$. Contours of Constant Transverse Flow Angle. Axial Position: 2.25" Behind the Cascade.

40. Skewed Flow $\nabla P_o = 0$. Contours of Constant Spanwise Flow Deviation Angle. Axial Position: 0.1" Behind the Cascade.

41. Skewed Flow $\nabla P_o = 0$. Contours of Constant Spanwise Flow Deviation Angle. Axial Position: 2.25" Behind the Cascade.

42. Skewed Flow. Streamline Traces in Carbon Black on the Blade Pressure Side.

43. Skewed Flow. Streamline Traces in Carbon Black on the Blade Suction Side.

44. Skewed Flow and Skewed Wakeflow. Diagram of Notations.

45. Skewed Flow. Transverse Inlet Angle Distribution over the Span for Various Tangential Positions.

46. Skewed Flow Velocity Profile at Cascade Inlet.

47. Skewed Flow. Maximum Transverse Flow Deviation Angle.

48. Skewed Flow. Average Transverse Flow Deviation Angle.

49. Skewed Flow. Spanwise Flow Deviation Angle.

50. Skewed Flow. Nomenclature of Actuator Disc Theory.

51. Skewed Flow. Spanwise Distribution of the Kinetic Energy of the Secondary Flow.

52. Skewed Flow. Spanwise Distribution of the Stagnation Pressure Defect Averaged over two Blade Spacings.

53. Skewed Flow. Projected Stream Pressure Distribution on the Blade Surfaces.

54. Skewed Flow $\nabla P_o = 0$. Contours of Constant Stream Pressure on the Blade Surfaces.

55. Spanwise Distribution of the Tangential Pressure Coefficient C_T.

56. Skewed Wakeflow $\nabla P_0 \neq 0$. Contours of Constant Transverse Inlet Angles.

57. Skewed Wakeflow. $\nabla P_0 \neq 0$. Contours of Constant Stagnation Pressure Upstream of Cascade.

58. Skewed Wakeflow $\nabla P_0 \neq 0$. Contours of Constant Stream Pressure Upstream of Cascade.

59. Skewed Wakeflow $\nabla P_0 \neq 0$. Contours of Constant Stagnation Pressure. Axial Position: 0.1" Behind The Cascade.

60. Skewed Wakeflow. $\nabla P_0 \neq 0$. Contours of Constant Stagnation Pressure. Axial Position: 2.25" Behind the Cascade.

61. Skewed Wakeflow $\nabla P_0 \neq 0$. Contours of Constant Stream Pressure Axial Position: 0.35" Behind the Cascade.

62. Skewed Wakeflow $\nabla P_0 \neq 0$. Contours of Constant Stream Pressure Axial Position: 2.25" Behind the Cascade.

63. Skewed Wakeflow $\nabla P_0 \neq 0$. Contours of Constant Transverse Flow Angle. Axial Position: 0.1" Behind the Cascade.

64. Skewed Wakeflow $\nabla P_0 \neq 0$. Contours of Constant Transverse Flow Angle. Axial Position: 2.25" Behind the Cascade.

65. Skewed Wakeflow. $\nabla P_0 \neq 0$. Contours of Constant Spanwise Flow Deviation Angle. Axial Position: 0.1" Behind the Cascade.

66. Skewed Wakeflow $\nabla P_0 \neq 0$. Contours of Constant Spanwise Flow Deviation Angle. Axial Position: 2.25" Behind the Cascade.

67. Skewed Wakeflow. Streamline Traces in Carbon Black on the Blade Pressure Side.

68. Skewed Wakeflow. Streamline Traces in Carbon Black on the Blade Suction Side.

69. Skewed Wakeflow. Transverse Inlet Angle Distribution over the Span for Various Tangential Positions.

70. Skewed Wakeflow. Inlet Stagnation Pressure Distribution over the Span for Various Tangential Positions.

71. Skewed Wakeflow. Inlet Velocity Distribution over the Span.

72. Skewed Wakeflow. Inlet Condition Used in Calculation for Secondary Flow.

73. Skewed Wakeflow. Maximum Transverse Flow Deviation Angle.

74. Skewed Wakeflow. Average Transverse Flow Deviation Angle.

75. Skewed Wakeflow. Spanwise Flow Deviation Angle.

76. Skewed Wakeflow. Spanwise Distribution of the Kinetic Energy of the Secondary Flow.

77. Skewed Wakeflow. Spanwise Distribution of the Stagnation Pressure Defect (Averaged over the Two Blades Spacings).

78. Skewed Wakeflow. Projected Stream Pressure Distribution on the Blade Surfaces.

79. Skewed Wakeflow. Contours of Constant Stream Pressure on the Blade Surfaces.

APPENDIX A

A.1 Integration of the Expressions for Ψ_n and Ψ_n' for the Wake Flow

The formulae for Ψ_n and Ψ_n' are:

$$\Psi_n = -\frac{8\varepsilon b}{(n\pi)^2}\left\{\frac{\sinh n\pi \frac{z}{b}}{\sinh n\pi \frac{l}{b}}\int_z^l \frac{dU_1}{d\zeta}\sinh n\pi \frac{l-\zeta}{b}\,d\zeta + \right.$$

$$\left. + \frac{\sinh n\pi \frac{l-z}{b}}{\sinh n\pi \frac{l}{b}}\int_0^z \frac{dU_1}{d\zeta}\sinh n\pi \frac{\zeta}{b}\,d\zeta\right\} \qquad 4\text{-}18$$

$$\Psi_n' = -\frac{8\varepsilon}{n\pi}\left\{\frac{\cosh n\pi \frac{z}{b}}{\sinh n\pi \frac{l}{b}}\int_z^l \frac{dU_1}{d\zeta}\sinh n\pi \frac{l-\zeta}{b}\,d\zeta - \right.$$

$$\left. \frac{\cosh n\pi \frac{l-z}{b}}{\sinh n\pi \frac{l}{b}}\int_0^z \frac{dU_1}{d\zeta}\sinh n\pi \frac{\zeta}{b}\,d\zeta\right\} \qquad 4\text{-}19$$

The velocity distribution is given by:

For $0 \le \zeta \le \delta$

$$\frac{U_1}{\bar{U}_1} = 1 - a\left(1 + \cos\pi\frac{\zeta}{\delta}\right) \qquad 4\text{-}30$$

For $\delta \le \zeta \le l$

$$U_1 = \bar{U}_1$$

Differentiating 4.30 with respect to ζ gives

$$\frac{dU_1}{d\zeta} = \bar{U}_1 a \frac{\pi}{\delta}\sin\pi\frac{\zeta}{\delta} \qquad A\text{-}1$$

valid in the wake, while

$$\frac{dU_1}{d\zeta} = 0 \qquad A\text{-}2$$

outside the wake.

Because $\frac{dU_1}{d\zeta}$ is not continuous over the whole region, $0 \le \zeta \le l$, the integrations of Ψ_n and Ψ_n' have to be performed in two regions, $0 \le \zeta \le \delta$ and $\delta \le \zeta \le l$

We then get

for $0 \le \zeta \le \delta$

$$\psi_n = -\frac{8\varepsilon b}{(n\pi)^2}\left\{\frac{\sinh n\pi z/b}{\sinh n\pi \ell/b}\int_z^\delta \frac{dU_1}{d\zeta}\sinh n\pi\frac{\ell-\zeta}{b}d\zeta + \right.$$

$$\left. + \frac{\sinh n\pi\frac{\ell-z}{b}}{\sinh n\pi \ell/b}\int_0^z \frac{dU_1}{d\zeta}\sinh n\pi\frac{\zeta}{b}d\zeta\right\} \qquad \text{A-3}$$

$$\psi_n' = -\frac{8\varepsilon}{n\pi}\left\{\frac{\cosh n\pi z/b}{\sinh n\pi \ell/b}\int_z^\delta \frac{dU_1}{d\zeta}\sinh n\pi\frac{\ell-\zeta}{b}d\zeta - \right.$$

$$\left. - \frac{\cosh n\pi\frac{\ell-z}{b}}{\sinh n\pi \ell/b}\int_0^z \frac{dU_1}{d\zeta}\sinh n\pi\frac{\zeta}{b}d\zeta\right\} \qquad \text{A-4}$$

and for $\delta \le \zeta \le \ell$

$$\psi_n = -\frac{8\varepsilon b}{(n\pi)^2}\frac{\sinh n\pi\frac{\ell-z}{b}}{\sinh n\pi \ell/b}\int_0^\delta \frac{dU_1}{d\zeta}\sinh n\pi\frac{\zeta}{b}d\zeta \qquad \text{A-5}$$

$$\psi_n' = \frac{8\varepsilon}{n\pi}\frac{\cosh n\pi\frac{\ell-z}{b}}{\sinh n\pi \ell/b}\int_0^\delta \frac{dU_1}{d\zeta}\sinh n\pi\frac{\zeta}{b}d\zeta \qquad \text{A-6}$$

Substituting A-1 in the integrals above and integrating by parts yields

$$\int_z^\delta \frac{dU_1}{d\zeta}\sinh n\pi\frac{\ell-\zeta}{b}d\zeta =$$

$$= \frac{\bar{U}_1 a}{1+(n\frac{\delta}{b})^2}\left\{\cos\pi\frac{z}{\delta}\sinh n\pi\frac{\ell-z}{b} + n\frac{\delta}{b}\sin\pi\frac{z}{\delta}\cosh n\pi\frac{\ell-z}{b} + \sinh n\pi\frac{\ell-\delta}{b}\right\} \qquad \text{A-7}$$

$$\int_z^\delta \frac{dU_1}{d\zeta}\sinh n\pi\frac{\zeta}{b}d\zeta =$$

$$= \frac{\bar{U}_1 a}{1+(n\frac{\delta}{b})^2}\left\{-\cos\pi\frac{z}{\delta}\sinh n\pi\frac{z}{b} + n\frac{\delta}{b}\sin\pi\frac{z}{\delta}\cosh n\pi\frac{z}{b}\right\} \qquad \text{A-8}$$

$$\int_0^{\delta} \frac{dU_1}{d\zeta} \sinh n\pi \frac{\zeta}{b}\, d\zeta = \frac{\bar{U}_1 a}{1+(n\frac{\delta}{b})^2} \sinh n\pi \frac{\delta}{b} \qquad \text{A-9}$$

Substituting A-7, A-8 and A-9 into A-3, A-4, A-5 and A-6 yields, after some rearrangement:

For $0 \le z \le \delta$

$$\psi_n = -\frac{8\varepsilon b}{(n\pi)^2} \frac{\bar{U}_1 a}{\left[1+(n\frac{\delta}{b})^2\right]} \left[n\frac{\delta}{b} \sin\pi\frac{z}{b} + \frac{\sinh n\pi \frac{\ell-\delta}{b}}{\sinh n\pi \ell/b} \sinh\left(\pi n \frac{\delta}{b}\cdot\frac{z}{\delta}\right)\right] \qquad \text{A-10}$$

$$\psi_n' = -\frac{8\varepsilon}{n\pi} \frac{\bar{U}_1 a}{\left[1+(n\frac{\delta}{b})^2\right]} \left[\cos\pi\frac{z}{b} + \frac{\sinh n\pi \frac{\ell-\delta}{b}}{\sinh n\pi \ell/b} \cosh\left(\pi n \frac{\delta}{b}\cdot\frac{z}{\delta}\right)\right] \qquad \text{A-11}$$

For $\delta \le z \le \ell$

$$\psi_n = -\frac{8\varepsilon b}{(n\pi)^2} \frac{\bar{U}_1 a}{\left[1+(n\frac{\delta}{b})^2\right]} \frac{\sinh n\pi \delta/b}{\sinh n\pi \ell/b} \sinh n\pi \frac{\ell}{b}\left(1-\frac{z}{\ell}\right) \qquad \text{A-12}$$

$$\psi_n' = \frac{8\varepsilon}{n\pi} \frac{\bar{U}_1 a}{\left[1+(n\frac{\delta}{b})^2\right]} \frac{\sinh n\pi \delta/b}{\sinh n\pi \ell/b} \cosh n\pi \frac{\ell}{b}\left(1-\frac{z}{\ell}\right) \qquad \text{A-13}$$

A.2 Numerical Calculations

The actual vlues for the cascade configuration and the inlet flow (given below) have been substituted in the previous derived formulae and the flow deviation angles have been calculated. In these calculations the first three terms in the series for ψ and ψ' have been retained i.e., n = 1,3, and 5.

The values used in the calculations were:

ℓ = 8.000"

δ = 1.130"

a = 0.137

α_1 = 45.0°

α_2 = 64.4°

ε = 19.4°

When formula 4.8 has been used instead of 4.1 to express the streamwise component of the distributed vorticity vector, 2ε, has been changed to $\left(1+\frac{\sin\alpha_1}{\sin\alpha_2}\right)\frac{\cos\alpha_1-\cos\alpha_2}{\sin\alpha_2}$ in the previous formulae (A-10 - A-13).

The results of the calculations are shown in Figures 23,24, and 25.

APPENDIX B

B.1 Integration of the Expressions for ψ_n and ψ_n' for the Skewed Flow

The formulae for ψ_n and ψ_n' are:

$$\psi_n = -\frac{4U_2 b}{(n\pi)^2}\left\{\frac{\sinh n\pi\frac{\ell-z}{b}}{\sinh n\pi \ell/b}\int_0^z \frac{dU_1}{d\zeta}\sinh n\pi\frac{\zeta}{b}\,d\zeta + \right.$$

$$\left. + \frac{\sinh n\pi z/b}{\sinh n\pi \ell/b}\int_z^\ell \frac{dU_1}{d\zeta}\sinh n\pi\frac{\ell-\zeta}{b}\,d\zeta\right\} \qquad 5\text{-}40$$

$$\psi_n' = \frac{4U_2}{n\pi}\left\{\frac{\cosh n\pi\frac{\ell-z}{b}}{\sinh n\pi \ell/b}\int_0^z \frac{dU_1}{d\zeta}\sinh n\pi\frac{\zeta}{b}\,d\zeta - \right.$$

$$\left. - \frac{\cosh n\pi z/b}{\sinh n\pi \ell/b}\int_z^\ell \frac{dU_1}{d\zeta}\sinh n\pi\frac{\ell-\zeta}{b}\,d\zeta\right\} \qquad 5\text{-}41$$

The inlet angle distribution is given by:

For $0 \le \zeta \le \delta$

$$\beta_1 = \sum_{m=0} A_m \cos m\pi\frac{\zeta}{\delta} \qquad 5\text{-}50$$

For $\delta \le \zeta \le \ell$

$$\beta_1 = 0 \qquad B\text{-}1$$

Differentiating 5.50 with respect to ζ gives

$$\frac{d\beta_1}{d\zeta} = -\frac{\pi}{\delta}\sum_{m=1} m A_m \sin m\pi\frac{\zeta}{\delta} \qquad B\text{-}2$$

valid in the skewed flow layer, while

$$\frac{d\beta_1}{d\zeta} = 0 \qquad B\text{-}3$$

outside the skewed flow layer.

Because $\frac{d\beta_1}{d\zeta}$ is not continuous over the whole region, $0 \le \zeta \le \ell$,
the integrations of ψ_n and ψ_n' have to be performed in two regions,
$0 \le \zeta \le \delta$ and $\delta \le \zeta \le \ell$

We then get

For $0 \le \zeta \le \delta$

$$\psi_n = -\frac{4U_2 b}{(n\pi)^2}\left\{\frac{\sinh n\pi\frac{\ell-z}{b}}{\sinh n\pi\,\ell/b}\int_0^z \frac{d\beta_1}{d\zeta}\sinh n\pi\frac{\zeta}{b}\,d\zeta + \right.$$
$$\left. + \frac{\sinh n\pi\, z/b}{\sinh n\pi\,\ell/b}\int_z^\delta \frac{d\beta_1}{d\zeta}\sinh n\pi\frac{\ell-\zeta}{b}\,d\zeta\right\} \qquad \text{B-4}$$

$$\psi_n' = \frac{4U_2}{n\pi}\left\{\frac{\cosh n\pi\frac{\ell-z}{b}}{\sinh n\pi\,\ell/b}\int_0^z \frac{d\beta_1}{d\zeta}\sinh n\pi\frac{\zeta}{b}\,d\zeta - \right.$$
$$\left. - \frac{\cosh n\pi\, z/b}{\sinh n\pi\,\ell/b}\int_z^\delta \frac{d\beta_1}{d\zeta}\sinh n\pi\frac{\ell-\zeta}{b}\,d\zeta\right\} \qquad \text{B-5}$$

and

for $\delta \le \zeta \le \ell$

$$\psi_n = -\frac{4U_2 b}{(n\pi)^2}\,\frac{\sinh n\pi\frac{\ell-z}{b}}{\sinh n\pi\,\ell/b}\int_0^\delta \frac{d\beta_1}{d\zeta}\sinh n\pi\frac{\zeta}{b}\,d\zeta \qquad \text{B-6}$$

$$\psi_n' = \frac{4U_2}{n\pi}\,\frac{\cosh n\pi\frac{\ell-z}{b}}{\sinh n\pi\,\ell/b}\int_0^\delta \frac{d\beta_1}{d\zeta}\sinh n\pi\frac{\zeta}{b}\,d\zeta \qquad \text{B-7}$$

Substituting B-2 in the integrals above and integrating by parts yields:

$$\int_0^z \frac{d\beta_1}{d\zeta}\sinh n\pi\frac{\zeta}{b}\,d\zeta =$$
$$\sum_{m=1}\frac{A_m}{1+\left(\frac{n\delta}{mb}\right)^2}\left\{\cos m\pi\frac{z}{\delta}\sinh n\pi\frac{z}{b} - \frac{n}{m}\frac{\delta}{b}\sin m\pi\frac{z}{\delta}\cosh n\pi\frac{z}{b}\right\} \qquad \text{B-8}$$

$$\int_0^{\delta} \frac{d\beta_1}{d\zeta} \sinh n\pi \frac{\zeta}{b}\, d\zeta = \sum_{m=1} \frac{A_m}{1+\left(\frac{n\delta}{mb}\right)^2} \cos m\pi \sinh n\pi \frac{\delta}{b} \qquad \text{B-9}$$

$$\int_z^{\delta} \frac{d\beta_1}{d\zeta} \sinh n\pi \frac{\ell-\zeta}{b}\, d\zeta =$$

$$= \sum_{m=1} \frac{A_m}{1+\left(\frac{n\delta}{mb}\right)^2} \left\{ \cos m\pi \sinh n\pi \frac{\ell-\delta}{b} - \cos m\pi \frac{z}{\delta} \sinh n\pi \frac{\ell-z}{b} - \right.$$

$$\left. - \frac{n\delta}{mb} \sin m\pi \frac{z}{\delta} \cosh n\pi \frac{\ell-z}{b} \right\} \qquad \text{B-10}$$

Substituting B-8, B-9 and B-10 into B-4, B-5, B-6 and B-7 and rearranging yields:

For $0 \le \zeta \le \delta$

$$\psi_n = -\frac{4U_2 b}{(n\pi)^2} \sum_{m=1} \frac{A_m}{1+\left(\frac{n\delta}{mb}\right)^2} \left\{ \cos m\pi \frac{\sinh n\pi \frac{\ell-\delta}{b}}{\sinh n\pi \ell/b} \sinh n\pi \frac{\delta}{b} \frac{z}{\delta} - \frac{n}{m} \frac{\delta}{b} \sin m\pi \frac{z}{\delta} \right\} \qquad \text{B-11}$$

$$\psi_n' = -\frac{4U_2}{n\pi} \sum_{m=1} \frac{A_m}{1+\left(\frac{n\delta}{mb}\right)^2} \left\{ \cos m\pi \frac{\sinh n\pi \frac{\ell-\delta}{b}}{\sinh n\pi \ell/b} \cosh n\pi \frac{\delta}{b} \frac{z}{\delta} - \cos m\pi \frac{z}{\delta} \right\} \qquad \text{B-12}$$

For $\delta \le \zeta \le \ell$

$$\psi_n = -\frac{4U_2 b}{(n\pi)^2} \sum_{m=1} \frac{A_m}{1+\left(\frac{n\delta}{mb}\right)^2} \frac{\cos m\pi \sinh n\pi \delta/b}{\sinh n\pi \ell/b} \sinh n\pi \frac{\ell}{b} \left(1-\frac{z}{\ell}\right) \qquad \text{B-13}$$

$$\psi_n' = \frac{4U_2}{n\pi} \sum_{m=1} \frac{A_m}{1+\left(\frac{n\delta}{mb}\right)^2} \frac{\cos m\pi \sinh n\pi \delta/b}{\sinh n\pi \ell/b} \cosh n\pi \frac{\ell}{b} \left(1-\frac{z}{\ell}\right) \qquad \text{B-14}$$

B.2 Numerical Calculations

The actual values for the cascade configuration and the inlet flow (given below) have been substituted in the previously derived formulae and the flow deviation angles have been calculated. In these calculations, the first three terms in the series for φ and φ' have been retained, i.e. n = 1,3, and 5.

The values used in the calculations were:

$l = 8.000"$

$\delta = 2.250"$

$\alpha_1 = 45.0°$

$\alpha_2 = 68.6°$

$A_1 = 0.19478$

$A_2 = 0.02731$

$A_3 = -0.02402$

$A_4 = -0.01122$

The results of the calculations are shown in Figures 47, 48 and 49.

APPENDIX C

C Correction of Flow Deviation Angles due to the Two Wakes in the Skewed Flow

C.1 General Procedure

The two wakes at the edges of the skewed layer cause a secondary flow in the cascade. This secondary flow will be calculated here under the assumption that the transverse inlet angle is constant over the span i.e. generated by a pure wake flow. The secondary flow due to this wake flow will then be added to the secondary flow caused by the skewed flow. The justification for this superposition is given in section 6.

The formulae developed in section 4 are applicable in this case and will be modified only according to the changed inlet conditions. The notations of equation 4.1 will be used to calcualte the secondary vorticity component in streamwise direction but the actual values will be calculated using equation 4.8.

C.2 Inlet Conditions

The inlet velocity profiles varied slightly in tangential direction. The velocity profile at the tangential center line of the cascade was chosen to represent the average velocity profile at cascade inlet. The velocity profile of each wake could be represented by a sinusoidal curve (see Figure 46). Since the conditions are symmetrical about midspan, only the flow conditions in one half of the span are studied.

Using the notations of Figure 46 the velocity profile is given by the following expressions

For $0 \leq z \leq \delta_1$

$$U_1 = \overline{U}_1$$

For $\delta_1 \leq z \leq \delta_2$

$$\frac{U_1}{\overline{U}_1} = 1 - a\left[1 + \cos\pi\left(\frac{z}{\delta_4} - \frac{\delta_3}{\delta_4}\right)\right] \qquad \text{C-1}$$

And for $\delta_2 \leq z \leq \ell$

$$U_1 = \overline{U}_1$$

C.3 Integration of the Expressions for ψ_n and ψ_n'

These integrations are performed in three regions

$0 \leq z \leq \delta_1$

$\delta_1 \leq z \leq \delta_2$

$\delta_2 \leq z \leq \ell$

because the function $\frac{dU_1}{dz}$ is not continuous over the whole region. There will then be three equations for both ψ_n and ψ_n', valid in their respective regions.

From section 4.2.2.

$$\psi_n = -\frac{8\varepsilon b}{(n\pi)^2}\left\{\frac{\sinh n\pi\, z/b}{\sinh n\pi\, \ell/b}\int_z^{\ell}\frac{dU_1}{d\zeta}\sinh n\pi\,\frac{\ell-\zeta}{b}\,d\zeta + \right.$$

$$\left. + \frac{\sinh n\pi\,\frac{\ell-z}{b}}{\sinh n\pi\,\ell/b}\int_0^{z}\frac{dU_1}{d\zeta}\sinh n\pi\,\frac{\zeta}{b}\,d\zeta\right\} \qquad 4\text{-}18$$

$$\psi_n' = -\frac{8\varepsilon}{n\pi}\left\{\frac{\cosh n\pi\, z/b}{\sinh n\pi\, \ell/b}\int_z^{\ell}\frac{dU_1}{d\zeta}\sinh n\pi\,\frac{\ell-\zeta}{b}\,d\zeta - \right.$$

$$\left. - \frac{\cosh n\pi\,\frac{\ell-z}{b}}{\sinh n\pi\,\ell/b}\int_0^{z}\frac{dU_1}{d\zeta}\sinh n\pi\,\frac{\zeta}{b}\,d\zeta\right\} \qquad 4\text{-}19$$

For $0 \leq z \leq \delta_1$

Introducing the integration limits 0 and δ_1 in 4-18 and 4-19 yields:

$$\psi_n = -\frac{8\varepsilon b}{(n\pi)^2} \frac{\sinh n\pi z/b}{\sinh n\pi \ell/b} \int_{\delta_1}^{\delta_2} \frac{dU_1}{d\zeta} \sinh n\pi \frac{\ell-\zeta}{b} d\zeta \qquad \text{C-2}$$

$$\psi_n' = -\frac{8\varepsilon}{n\pi} \frac{\cosh n\pi z/b}{\sinh n\pi \ell/b} \int_{\delta_1}^{\delta_2} \frac{dU_1}{d\zeta} \sinh n\pi \frac{\ell-\zeta}{b} d\zeta \qquad \text{C-3}$$

For $\delta_1 \leq z \leq \delta_2$

In this region, 4-18 and 4-19 are

$$\psi_n = -\frac{8\varepsilon b}{(n\pi)^2} \left\{ \frac{\sinh n\pi z/b}{\sinh n\pi \ell/b} \int_{z}^{\delta_2} \frac{dU_1}{d\zeta} \sinh n\pi \frac{\ell-\zeta}{b} d\zeta + \right.$$
$$\left. + \frac{\sinh n\pi \frac{\ell-z}{b}}{\sinh n\pi \ell/b} \int_{\delta_1}^{z} \frac{dU_1}{d\zeta} \sinh n\pi \frac{\zeta}{b} d\zeta \right\} \qquad \text{C-4}$$

$$\psi_n' = -\frac{8\varepsilon}{n\pi} \left\{ \frac{\cosh n\pi z/b}{\sinh n\pi \ell/b} \int_{z}^{\delta_2} \frac{dU_1}{d\zeta} \sinh n\pi \frac{\ell-\zeta}{b} d\zeta - \right.$$
$$\left. - \frac{\cosh n\pi \frac{\ell-z}{b}}{\sinh n\pi \ell/b} \int_{\delta_1}^{z} \frac{dU_1}{d\zeta} \sinh n\pi \frac{\zeta}{b} d\zeta \right\} \qquad \text{C-5}$$

For $\delta_2 \leq z \leq \ell$

4-18 and 4-19 reduces in this region to

$$\psi_n = -\frac{8\varepsilon b}{(n\pi)^2} \frac{\sinh n\pi \frac{\ell-z}{b}}{\sinh n\pi \ell/b} \int_{\delta_1}^{\delta_2} \frac{dU_1}{d\zeta} \sinh n\pi \frac{\zeta}{b} d\zeta \qquad \text{C-6}$$

$$\psi_n' = \frac{8\varepsilon}{n\pi} \frac{\cosh n\pi \frac{\ell-z}{b}}{\sinh n\pi \ell/b} \int_{\delta_1}^{\delta_2} \frac{dU_1}{d\zeta} \sinh n\pi \frac{\zeta}{b} d\zeta \qquad \text{C-7}$$

The integrals in these formulae are to be evaluated using

$$\frac{dU_1}{d\zeta} = U_1 a \frac{\pi}{\delta_4} \sin \pi \left(\frac{\zeta}{\delta_4} - 2\right) \qquad \text{C-8}$$

which is derived from C-1 changing z to ζ as a dummy and substituting

$$\frac{\delta_3}{\delta_4} = 2$$

After some calculations the following expressions are then found:

$$\int_z^{\delta_2} \frac{dU_1}{d\zeta} \sinh n\pi \frac{\ell - \zeta}{b} d\zeta =$$

$$= -\frac{U_1 a}{1+(n\frac{\delta_4}{b})^2} \left[\cos \pi\left(\frac{\delta_2}{\delta_4} - 2\right) \sinh n\pi \frac{\ell - \delta_2}{b} - \cos \pi\left(\frac{z}{\delta_4} - 2\right) \sinh n\pi \frac{\ell - z}{b} + \right.$$

$$\left. + n\frac{\delta_4}{b} \sin \pi\left(\frac{\delta_2}{\delta_4} - 2\right) \cosh n\pi \frac{\ell - \delta_2}{b} - n\frac{\delta_4}{b} \sin \pi\left(\frac{z}{\delta_4} - 2\right) \cosh n\pi \frac{\ell - z}{b} \right] \qquad \text{C-9}$$

$$\int_{\delta_1}^{\delta_2} \frac{dU_1}{d\zeta} \sinh n\pi \frac{\ell - \zeta}{b} d\zeta =$$

$$= -\frac{U_1 a}{1+(n\frac{\delta_4}{b})^2} \left[\cos \pi\left(\frac{\delta_2}{\delta_4} - 2\right) \sinh n\pi \frac{\ell - \delta_2}{b} - \cos \pi\left(\frac{\delta_1}{\delta_4} - 2\right) \sinh n\pi \frac{\ell - \delta_1}{b} + \right.$$

$$\left. + n\frac{\delta_4}{b} \sin \pi\left(\frac{\delta_2}{\delta_4} - 2\right) \cosh n\pi \frac{\ell - \delta_2}{b} - n\frac{\delta_4}{b} \sin \pi\left(\frac{\delta_1}{\delta_4} - 2\right) \cosh n\pi \frac{\ell - \delta_1}{b} \right] \qquad \text{C-10}$$

$$\int_{\delta_1}^{z} \frac{dU_1}{d\zeta} \sinh n\pi \frac{\zeta}{b}\, d\zeta =$$

$$= \frac{\bar{U}_1 a}{1+(n\frac{\delta_4}{b})^2}\Big[-\cos\pi\left(\frac{z}{\delta_4}-2\right)\sinh n\pi\frac{z}{b} + \cos\pi\left(\frac{\delta_1}{\delta_4}-2\right)\sinh n\pi\frac{\delta_1}{b} +$$

$$+ n\frac{\delta_4}{b}\sin\pi\left(\frac{z}{\delta_4}-2\right)\cosh n\pi\frac{z}{b} - n\frac{\delta_4}{b}\sin\pi\left(\frac{\delta_1}{\delta_4}-2\right)\cosh n\pi\frac{\delta_1}{b}\Big] \qquad \text{C-11}$$

$$\int_{\delta_1}^{\delta_2} \frac{dU_1}{d\zeta} \sinh n\pi \frac{\zeta}{b}\, d\zeta =$$

$$= \frac{\bar{U}_1 a}{1+(n\frac{\delta_4}{b})^2}\Big[-\cos\pi\left(\frac{\delta_2}{\delta_4}-2\right)\sinh n\pi\frac{\delta_2}{b} + \cos\pi\left(\frac{\delta_1}{\delta_4}-2\right)\sinh n\pi\frac{\delta_1}{b} +$$

$$+ n\frac{\delta_4}{b}\sin\pi\left(\frac{\delta_2}{\delta_4}-2\right)\cosh n\pi\frac{\delta_2}{b} - n\frac{\delta_4}{b}\sin\pi\left(\frac{\delta_1}{\delta_4}-2\right)\cosh n\pi\frac{\delta_1}{b}\Big] \qquad \text{C-12}$$

Introducing the expression C-9 through C-12 into the formulae C-2 through C-7 and noting that $\frac{\delta_2}{\delta_4} = 3$ and $\frac{\delta_1}{\delta_4} = 1$ yields, after some rearrangement:

For $0 \le z \le \delta_1$

$$\psi_n = \frac{-8\varepsilon b \bar{U}_1 a}{(n\pi)^2\left[1+(n\frac{\delta_4}{b})^2\right]} \frac{-\sinh n\pi\frac{\ell-\delta_1}{b} + \sinh n\pi\frac{\ell-\delta_2}{b}}{\sinh n\pi\,\ell/b} \sinh n\pi\frac{\delta_1}{b}\,\frac{z}{\delta_1} \qquad \text{C-13}$$

$$\psi_n' = \frac{-8\varepsilon\bar{U}_1 a}{n\pi\left[1+(n\frac{\delta_4}{b})^2\right]} \frac{\sinh n\pi\frac{\ell-\delta_2}{b} - \sinh n\pi\frac{\ell-\delta_1}{b}}{\sinh n\pi\,\ell/b} \cosh n\pi\frac{\delta_1}{b}\frac{z}{\delta_1} \qquad \text{C-14}$$

For $\delta_1 \leq z \leq \delta_2$

$$\psi_n = \frac{-8\varepsilon b \bar{U}_1 a}{(n\pi)^2\left[1+\left(n\frac{\delta_4}{b}\right)^2\right]}\left\{\frac{\sinh n\pi\frac{\ell-\delta_2}{b}}{\sinh n\pi \ell/b}\sinh n\pi\frac{z}{b} - \right.$$

$$\left. - \frac{\sinh n\pi \delta_1/b}{\sinh n\pi \ell/b}\sinh n\pi\frac{\ell}{b}\left[1-\frac{z}{\ell}\right] + n\frac{\delta_4}{b}\sin\pi\left(\frac{z}{\delta_4}-2\right)\right\} \qquad \text{C-15}$$

$$\psi_n' = \frac{-8\varepsilon \bar{U}_1 a}{n\pi\left[1+\left(n\frac{\delta_4}{b}\right)^2\right]}\left\{\frac{\sinh n\pi\frac{\ell-\delta_2}{b}}{\sinh n\pi \ell/b}\cosh n\pi\frac{z}{b} + \right.$$

$$\left. + \frac{\sinh n\pi \delta_1/b}{\sinh n\pi \ell/b}\cosh n\pi\frac{\ell}{b}\left[1-\frac{z}{\ell}\right] + \cos\pi\left(\frac{z}{\delta_4}-2\right)\right\} \qquad \text{C-16}$$

And for $\delta_2 \leq z \leq \ell$

$$\psi_n = \frac{-8\varepsilon b \bar{U}_1 a}{(n\pi)^2\left[1+\left(n\frac{\delta_4}{b}\right)^2\right]}\;\frac{\sinh n\pi \delta_2/b - \sinh n\pi \delta_1/b}{\sinh n\pi \ell/b}\sinh n\pi\frac{\ell}{b}\left(1-\frac{z}{\ell}\right) \qquad \text{C-17}$$

$$\psi_n' = \frac{-8\varepsilon \bar{U}_1 a}{n\pi\left[1+\left(n\frac{\delta_4}{b}\right)^2\right]}\;\frac{-\sinh n\pi \delta_2/b + \sinh n\pi \delta_1/b}{\sinh n\pi \ell/b}\cosh n\pi\frac{\ell}{b}\left(1-\frac{z}{\ell}\right) \qquad \text{C-18}$$

The formulae given in section 4.2.2 and 4.2.2.1 for the secondary flow velocities and deviation angles are valid, as they stand, for this case.

C.4 Numerical Calculations

The actual values for the cascade configuration and the inlet flow (given below) have been substituted in the previous derived formulae and the flow deviation angles have been calculated. In these calculations the first three terms in the series for φ and φ' have been retained, i.e. n = 1,3 and 5.

The values used in the calculations were:

$l = 8"$

$\delta_1 = 0.5"$

$\delta_2 = 1.5"$

$\delta_3 = 1.0"$

$\delta_4 = 0.5"$

$b = 4.13856"$

$a = 0.070$

$\alpha_1 = 45.0°$

$\alpha_2 = 68.6°$

The results of the calculation are shown in Figures 47, 48 and 49.

APPENDIX D

D.1 Integration of the Expressions for ψ_n and ψ_n' for the Skewed Wake Flow

The skewed wake flow is in this case considered to be a superposition of a skewed flow only and a wake flow only.

D.1.1 Skewed Flow

The expressions for this case are given in Appendix B and are repeated here.

For $0 \leq z \leq \delta$

$$\psi_n = -\frac{4U_2 b}{(n\pi)^2} \sum_{m=1} \frac{A_m}{1+\left(\frac{n\delta}{mb}\right)^2} \left\{ \cos m\pi \frac{\sinh n\pi \frac{\ell-\delta}{b}}{\sinh n\pi \ell/b} \sinh n\pi \frac{\delta}{b}\cdot\frac{z}{\delta} - \frac{n}{m}\frac{\delta}{b} \sin m\pi \frac{z}{\delta} \right\} \quad \text{B-11}$$

$$\psi_n' = -\frac{4U_2}{n\pi} \sum_{m=1} \frac{A_m}{1+\left(\frac{n\delta}{mb}\right)^2} \left\{ \cos m\pi \frac{\sinh n\pi \frac{\ell-\delta}{b}}{\sinh n\pi \ell/b} \cosh n\pi \frac{\delta}{b}\cdot\frac{z}{\delta} - \cos m\pi \frac{z}{\delta} \right\} \quad \text{B-12}$$

For $\delta \leq z \leq \ell$

$$\psi_n = -\frac{4U_2 b}{(n\pi)^2} \sum_{m=1} \frac{A_m}{1+\left(\frac{n\delta}{mb}\right)^2} \cos m\pi \frac{\sinh n\pi \delta/b}{\sinh n\pi \ell/b} \sinh n\pi \frac{\ell}{b}\left(1-\frac{z}{\ell}\right) \quad \text{B-13}$$

$$\psi_n' = \frac{4U_2}{n\pi} \sum_{m=1} \frac{A_m}{1+\left(\frac{n\delta}{mb}\right)^2} \cos m\pi \frac{\sinh n\pi \delta/b}{\sinh n\pi \ell/b} \cosh n\pi \frac{\ell}{b}\left(1-\frac{z}{\ell}\right) \quad \text{B-14}$$

D.1.2 Wake Flow

We have

$$\psi_n = \frac{-8\varepsilon b}{(n\pi)^2}\left\{\frac{\sinh n\pi z/b}{\sinh n\pi \ell/b}\int_z^{\ell}\frac{dU_1}{d\zeta}\sinh n\pi\frac{\ell-\zeta}{b}\,d\zeta + \right.$$

$$\left. + \frac{\sinh n\pi\frac{\ell-z}{b}}{\sinh n\pi\,\ell/b}\int_0^{z}\frac{dU_1}{d\zeta}\sinh n\pi\frac{\zeta}{b}\,d\zeta\right\} \qquad 4\text{-}18$$

$$\psi_n' = -\frac{8\varepsilon}{n\pi}\left\{\frac{\cosh n\pi z/b}{\sinh n\pi\,\ell/b}\int_z^{\ell}\frac{dU_1}{d\zeta}\sinh n\pi\frac{\ell-\zeta}{b}\,d\zeta - \right.$$

$$\left. - \frac{\cosh n\pi\frac{\ell-z}{b}}{\sinh n\pi\,\ell/b}\int_0^{z}\frac{dU_1}{d\zeta}\sinh n\pi\frac{\zeta}{b}\,d\zeta\right\} \qquad 4\text{-}19$$

The velocity distribution is given by:

For $0 \le \zeta \le \delta_1$

$$U_1 = \overline{U}_1\left[1 - \sum_{m=0} B_m \cos m\pi\frac{\zeta}{\delta_1}\right] \qquad D\text{-}1$$

For $\delta_1 \le \zeta \le \ell$

$$U_1 = \overline{U}_1 \qquad D\text{-}2$$

Differentiating U_1 with respect to ζ gives

$$\frac{dU_1}{d\zeta} = \overline{U}_1\frac{\pi}{\delta_1}\sum_{m=1} m B_m \sin m\pi\frac{\zeta}{\delta_1} \qquad D\text{-}3$$

valid in the wake flow layer, while

$$\frac{dU_1}{d\zeta} = 0 \qquad D\text{-}4$$

outside the wake flow layer.

Because $\frac{dU_1}{d\zeta}$ is not continuous over the whole region, $0 \le \zeta \le \ell$, the integration of ψ_n and ψ_n' have to be performed in two regions, $0 \le \zeta \le \delta_1$ and $\delta_1 \le \zeta \le \ell$,

For $0 \le \zeta \le \delta_1$

$$\psi_n = -\frac{8\varepsilon b}{(n\pi)^2}\left\{\frac{\sinh n\pi \frac{\ell-z}{b}}{\sinh n\pi \ell/b}\int_0^z \frac{dU_1}{d\zeta}\sinh n\pi\frac{\zeta}{b}\,d\zeta + \right.$$

$$\left. + \frac{\sinh n\pi z/b}{\sinh n\pi \ell/b}\int_z^{\delta_1}\frac{dU_1}{d\zeta}\sinh n\pi\frac{\ell-\zeta}{b}\,d\zeta\right\} \qquad \text{D-5}$$

$$\psi_n' = \frac{8\varepsilon}{n\pi}\left\{\frac{\cosh n\pi \frac{\ell-z}{b}}{\sinh n\pi \ell/b}\int_0^z \frac{dU_1}{d\zeta}\sinh n\pi\frac{\zeta}{b}\,d\zeta - \right.$$

$$\left. - \frac{\cosh n\pi z/b}{\sinh n\pi \ell/b}\int_z^{\delta_1}\frac{dU_1}{d\zeta}\sinh n\pi\frac{\ell-\zeta}{b}\,d\zeta\right\} \qquad \text{D-6}$$

and for $\delta_1 \le \zeta \le \ell$

$$\psi_n = -\frac{8\varepsilon b}{(n\pi)^2}\,\frac{\sinh n\pi \frac{\ell-z}{b}}{\sinh n\pi \ell/b}\int_0^{\delta_1}\frac{dU_1}{d\zeta}\sinh n\pi\frac{\zeta}{b}\,d\zeta \qquad \text{D-7}$$

$$\psi_n' = \frac{8\varepsilon}{n\pi}\,\frac{\cosh n\pi \frac{\ell-z}{b}}{\sinh n\pi \ell/b}\int_0^{\delta_1}\frac{dU_1}{d\zeta}\sinh n\pi\frac{\zeta}{b}\,d\zeta \qquad \text{D-8}$$

Substituting D-3 in the integrals above and integrating by parts yields

$$\int_0^z \frac{dU_1}{d\zeta}\sinh n\pi\frac{\zeta}{b}\,d\zeta =$$

$$= U_1\sum_{m=1}\frac{B_m}{1+\left(\frac{n\delta_1}{mb}\right)^2}\left\{-\cos m\pi\frac{z}{\delta_1}\sinh n\pi\frac{z}{b} + \frac{n}{m}\frac{\delta_1}{b}\sin m\pi\frac{z}{\delta_1}\cosh n\pi\frac{z}{b}\right\} \qquad \text{D-9}$$

$$\int_0^{\delta_1} \frac{dU_1}{d\zeta} \sinh n\pi \frac{\zeta}{b}\, d\zeta = -\bar{U}_1 \sum_{m=1} \frac{B_m}{1+\left(\frac{n\delta_1}{mb}\right)^2} \cos m\pi \sinh n\pi \frac{\delta_1}{b} \qquad \text{D-10}$$

$$\int_z^{\delta_1} \frac{dU_1}{d\zeta} \sinh n\pi \frac{\ell-\zeta}{b}\, d\zeta =$$

$$= -\bar{U}_1 \sum_{m=1} \frac{B_m}{1+\left(\frac{n\delta_1}{mb}\right)^2} \left\{ \cos m\pi \sinh n\pi \frac{\ell-\delta_1}{b} - \cos m\pi \frac{z}{\delta_1} \sinh n\pi \frac{\ell}{b}\left(1-\frac{z}{\ell}\right) - \right.$$

$$\left. - \frac{n\delta_1}{mb} \sin m\pi \frac{z}{\delta_1} \cosh n\pi \frac{\ell}{b}\left(1-\frac{z}{\ell}\right) \right\} \qquad \text{D-11}$$

Substituting D-9, D-10 and D-11 into D-5, D-6, D-7 and D-8 and rearranging yields:

For $0 \le \zeta \le \delta_1$

$$\psi_n = \frac{8\varepsilon b \bar{U}_1}{(n\pi)^2} \sum_{m=1} \frac{B_m}{1+\left(\frac{n\delta_1}{mb}\right)^2} \left\{ \cos m\pi \frac{\sinh n\pi \frac{\ell-\delta_1}{b}}{\sinh n\pi \ell/b} \sinh n\pi \frac{\delta_1}{b} \frac{z}{\delta_1} - \frac{n}{m} \frac{\delta_1}{b} \sin m\pi \frac{z}{\delta_1} \right\} \qquad \text{D-12}$$

$$\psi_n' = \frac{8\varepsilon \bar{U}_1}{n\pi} \sum_{m=1} \frac{B_m}{1+\left(\frac{n\delta_1}{mb}\right)^2} \left\{ \cos m\pi \frac{\sinh n\pi \frac{\ell-\delta_1}{b}}{\sinh n\pi \ell/b} \cosh n\pi \frac{\delta_1}{b} \frac{z}{\delta_1} - \cos m\pi \frac{z}{\delta_1} \right\} \qquad \text{D-13}$$

For $\delta_1 \le \zeta \le \ell$

$$\psi_n = \frac{8\varepsilon b \bar{U}_1}{(n\pi)^2} \sum_{m=1} \frac{B_m}{1+\left(\frac{n\delta_1}{mb}\right)^2} \cos m\pi \frac{\sinh n\pi \delta_1/b}{\sinh n\pi \ell/b} \sinh n\pi \frac{\ell}{b}\left(1-\frac{z}{\ell}\right) \qquad \text{D-14}$$

$$\psi_n' = \frac{-8\varepsilon \bar{U}_1}{n\pi} \sum_{m=1} \frac{B_m}{1+\left(\frac{n\delta_1}{mb}\right)^2} \cos m\pi \frac{\sinh n\pi \delta_1/b}{\sinh n\pi \ell/b} \cosh n\pi \frac{\ell}{b}\left(1-\frac{z}{\ell}\right) \qquad \text{D-15}$$

D.2 Numerical Values

The actual values for the cascade configuration and the inlet flow (given below) have been substituted in the previous formulae and the flow deviation angles have been calculated. Formula 4-8 has been used instead of 4-1 to express the streamwise component of the distributed vorticity vector and so 2ε has been replaced by $\left(1+\frac{\sin\alpha_1}{\sin\alpha_2}\right)\frac{\cos\alpha_1-\cos\alpha_2}{\sin\alpha_2}$ in the previous formulae. In the calculations, the first three terms in the series for ψ and ψ' have been retained i.e. $n = 1,3,$ and 5.

The values used in the calculations were:

$l = 8.000"$

$\delta = \delta_1 = 1.750"$

$\alpha_1 = 45.0°$

$\alpha_2 = 66.0°$

$A_1 = 0.19684$

$A_2 = -0.04920$

$A_3 = -0.00646$

$A_4 = 0.01274$

$B_1 = 0.18000$

$B_2 = -0.06560$

$B_3 = -0.01665$

$B_4 = 0.01762$

The results of the calculations are presented in Figures 73, 74 and 75.

APPENDIX E

E.1 Integration of the Expressions for ψ_n and ψ_n' for the Skewed Wake Flow, Using the Complete Expressions for the Streamwise Vorticity Component

We have

$$\xi_2 = -\frac{U_2}{U_1}\frac{d}{dz}\left[U_1(\sin\beta_1 + K)\right] \qquad 6\text{-}13$$

where $$K \equiv \left(1+\frac{\sin\alpha_1}{\sin\alpha_2}\right)\frac{\cos\alpha_1 - \cos\alpha_2}{\sin\alpha_1} \qquad 6\text{-}12$$

Introducing the continuity equation

$$U_1\sin\alpha_1 = U_2\sin\alpha_2 \qquad 6\text{-}18$$

6-13 may be written

$$\xi_2 = -\frac{\sin\alpha_1}{\sin\alpha_2}\frac{d}{dz}\left[U_1(\sin\beta_1 + K)\right] \qquad E\text{-}1$$

Let

$$\frac{U_1}{\bar{U}_1}(\sin\beta_1 + K) \equiv q \qquad E\text{-}2$$

thus E-1 is

$$\xi_2 = -\bar{U}_1\frac{\sin\alpha_1}{\sin\alpha_2}\frac{dq}{dz} \qquad E\text{-}3$$

Compare this expression with the one for the skewed flow

$$\xi_2 = -\bar{U}_2\frac{d\beta_1}{dz} \qquad 5\text{-}36$$

The formulae E-3 and 5-36 look similar and so we may expect similar solutions. We can now immediately write down the expressions for ψ_n and ψ_n' for the skewed

wake flow by changing U_2 to $\overline{U}_1 \frac{\sin\alpha_1}{\sin\alpha_2}$ and $\frac{d\beta_1}{d\zeta}$ to $\frac{dq}{d\zeta}$ in 5-40 and 5-41. The formulae for ψ_n and ψ_n' then are:

$$\psi_n = -\frac{4\overline{U}_1 b}{(n\pi)^2}\frac{\sin\alpha_1}{\sin\alpha_2}\left\{\frac{\sinh n\pi\frac{\ell-z}{b}}{\sinh n\pi\,\ell/b}\int_0^z \frac{dq}{d\zeta}\sinh n\pi\frac{\zeta}{b}\,d\zeta + \right.$$

$$\left. + \frac{\sinh n\pi\, z/b}{\sinh n\pi\,\ell/b}\int_z^\ell \frac{dq}{d\zeta}\sinh n\pi\,\frac{\ell-\zeta}{b}\,d\zeta\right\} \qquad \text{E-4}$$

$$\psi_n' = \frac{4\overline{U}_1}{n\pi}\frac{\sin\alpha_1}{\sin\alpha_2}\left\{\frac{\cosh n\pi\frac{\ell-z}{b}}{\sinh n\pi\,\ell/b}\int_0^z \frac{dq}{d\zeta}\sinh n\pi\frac{\zeta}{b}\,d\zeta - \right.$$

$$\left. - \frac{\cosh n\pi\, z/b}{\sinh n\pi\,\ell/b}\int_z^\ell \frac{dq}{d\zeta}\sinh n\pi\,\frac{\ell-\zeta}{b}\,d\zeta\right\} \qquad \text{E-5}$$

In the skewed wake flow layer q is expressed in a Fourier series:

For $\quad 0 \le \zeta \le \delta$

$$q = \sum_{m=0} C_m \cos m\pi\frac{\zeta}{\delta} \qquad \text{E-6}$$

And for $\delta \le \zeta \le \ell$

$$q = \text{constant} \qquad \text{E-7}$$

Differentiating q with respect to ζ yields

$$\frac{dq}{d\zeta} = -\frac{\pi}{\delta}\sum_{m=1} m\,C_m \sin m\pi\frac{\zeta}{\delta} \qquad \text{E-8}$$

valid in the skewed wake flow, while

$$\frac{dq}{d\zeta} = 0 \qquad \text{E-9}$$

outside the skewed wake flow layer.

The similarity between 5-40 and E-4, 5-41 and E-5 and B-2 and E-8 allows us to write down the final expressions for ψ_n and ψ_n' :

For $0 \le \zeta \le \delta$

$$\psi_n = -\frac{4\overline{U}_1 b}{(n\pi)^2}\frac{\sin\alpha_1}{\sin\alpha_2}\sum_{m=1}\frac{C_m}{1+\left(\frac{n\delta}{mb}\right)^2}\left\{\cos m\pi\,\frac{\sinh n\pi\frac{\ell-\delta}{b}}{\sinh n\pi\,\ell/b}\sinh n\pi\frac{\delta}{b}\frac{z}{\delta} - \right.$$

$$\left. - \frac{n}{m}\frac{\delta}{b}\sin m\pi\frac{z}{\delta}\right\} \qquad \text{E-10}$$

$$\psi_n' = -\frac{4\bar{U}_1}{n\pi}\frac{\sin\alpha_1}{\sin\alpha_2}\sum_{m=1}\frac{C_m}{1+\left(\frac{n\delta}{mb}\right)^2}\left\{\cos m\pi\,\frac{\sinh n\pi\frac{\ell-\delta}{b}}{\sinh n\pi\,\ell/b}\cosh n\pi\frac{\delta}{b}\frac{z}{\delta} - \right.$$

$$\left. - \cos m\pi\frac{z}{\delta}\right\} \qquad \text{E-11}$$

And for $\delta \le \zeta \le \ell$

$$\psi_n = -\frac{4\bar{U}_1 b}{(n\pi)^2}\frac{\sin\alpha_1}{\sin\alpha_2}\sum_{m=1}\frac{C_m}{1+\left(\frac{n\delta}{mb}\right)^2}\cos m\pi\,\frac{\sinh n\pi\,\delta/b}{\sinh n\pi\,\ell/b}\sinh n\pi\frac{\ell}{b}\left(1-\frac{z}{\ell}\right) \qquad \text{E-12}$$

$$\psi_n' = \frac{4\bar{U}_1}{n\pi}\frac{\sin\alpha_1}{\sin\alpha_2}\sum_{m=1}\frac{C_m}{1+\left(\frac{n\delta}{mb}\right)^2}\cos m\pi\,\frac{\sinh n\pi\,\delta/b}{\sinh n\pi\,\ell/b}\cosh n\pi\frac{\ell}{b}\left(1-\frac{z}{\ell}\right) \qquad \text{E-13}$$

E.2 Numerical Values

The actual values for the cascade configuration and the inlet flow (given below) have been substituted in the previous formulae and the flow deviation angles have been calculated. In these calculations the first three terms in the series for ψ and ψ' have been retained, i.e. n = 1, 3, and 5.

The values used in the calculations were:

l	= 8.000"	α_2	= 66.0°	C_3	= 0.01839
δ	= 1.750"	C_1	= 0.00272	C_4	= -0.00470
α_1	= 45.0°	C_2	= 0.00430	K	= 0.65700

The results of the calculations are presented in Figures 73, 74 and 75.

APPENDIX F

F.1 Derivation of the General Formulae for the Kinetic Energy of the Secondary Flow

The kinetic energy per unit volume of the secondary flow, contained in one blade passage, over half the span is

$$D = \frac{1}{2}\rho \int_0^{\ell}\int_0^{b} (v^2 + w^2)\, dy\, dz \qquad \text{F-1}$$

Expressing the secondary flow velocity components as derivatives of the stream function ψ, of the secondary flow, and substituting in F-1 yields:

$$D = \frac{1}{2}\rho \int_0^{\ell}\int_0^{b} \left[\left(\frac{\partial \psi}{\partial y}\right)^2 + \left(\frac{\partial \psi}{\partial z}\right)^2\right] dy\, dz \qquad \text{F-2}$$

In the general case the secondary flow is caused by a superposition of a wake flow and a skewed flow and so the stream function ψ is the sum of the stream functions of the wake flow and the skewed flow. The justification for this is given in section 6.

Therefore

$$\psi = \psi_s + \psi_w \qquad \text{F-3}$$

where

ψ_s = stream function of the secondary flow caused by the skewed flow only

ψ_w = stream function of the secondary flow caused by the wake flow only

Substituting F-3 into F-2 yields

$$D=\frac{1}{2}\rho\int_0^{\ell}\int_0^{b}\left[\left(\frac{\partial\Psi_s}{\partial y}\right)^2+2\left(\frac{\partial\Psi_s}{\partial y}\frac{\partial\Psi_w}{\partial y}\right)+\left(\frac{\partial\Psi_w}{\partial y}\right)^2+\left(\frac{\partial\Psi_s}{\partial z}\right)^2+2\left(\frac{\partial\Psi_s}{\partial z}\frac{\partial\Psi_w}{\partial z}\right)+\left(\frac{\partial\Psi_w}{\partial z}\right)^2\right]dy\,dz \qquad \text{F-4}$$

Consider the expresssion

$$\int_0^{\ell}\int_0^{b}\left[\left(\frac{\partial\Psi_s}{\partial y}\right)^2+2\left(\frac{\partial\Psi_s}{\partial y}\frac{\partial\Psi_w}{\partial y}\right)+\left(\frac{\partial\Psi_w}{\partial y}\right)^2\right]dy\,dz \qquad \text{F-5}$$

Integrating by parts yields:

$$\int_0^{\ell}\int_0^{b}\left[\left(\frac{\partial\Psi_s}{\partial y}\right)^2+2\left(\frac{\partial\Psi_s}{\partial y}\frac{\partial\Psi_w}{\partial y}\right)+\left(\frac{\partial\Psi_w}{\partial y}\right)^2\right]dy\,dz =$$

$$=\int_{z=0}^{z=\ell}\left[\Psi_s\cdot\frac{\partial\Psi_s}{\partial y}+2\Psi_s\cdot\frac{\partial\Psi_w}{\partial y}+\Psi_w\frac{\partial\Psi_w}{\partial y}\right]_{y=0}^{y=b}-$$

$$-\int_{z=0}^{z=\ell}\int_{y=0}^{y=b}\left[\Psi_s\frac{\partial^2\Psi_s}{\partial y^2}+2\Psi_s\frac{\partial^2\Psi_w}{\partial y^2}+\Psi_w\frac{\partial^2\Psi_w}{\partial y^2}\right]dy\,dz$$

But $\Psi_s = 0$ for $y = 0$ and $y = b$, and so:

$$\int_0^{\ell}\int_0^{b}\left[\left(\frac{\partial\Psi_s}{\partial y}\right)^2+2\left(\frac{\partial\Psi_s}{\partial y}\frac{\partial\Psi_w}{\partial y}\right)+\left(\frac{\partial\Psi_w}{\partial y}\right)^2\right]dy\,dz =$$

$$=-\int_0^{\ell}\int_0^{b}\left[\Psi_s\frac{\partial^2\Psi_s}{\partial y^2}+2\Psi_s\frac{\partial^2\Psi_w}{\partial y^2}+\Psi_w\frac{\partial^2\Psi_w}{\partial y^2}\right]dy\,dz \qquad \text{F-6}$$

The second part of F-4 may be integrated with respect to z in the same way: thus

$$D=\frac{1}{2}\rho\int_0^{\ell}\int_0^{b}\left[\Psi_s\left(\frac{\partial^2\Psi_s}{\partial y^2}+\frac{\partial^2\Psi_s}{\partial z^2}\right)+2\Psi_s\left(\frac{\partial^2\Psi_w}{\partial y^2}+\frac{\partial^2\Psi_w}{\partial z^2}\right)+\right.$$

$$\left.+\Psi_w\left(\frac{\partial^2\Psi_s}{\partial y^2}+\frac{\partial^2\Psi_s}{\partial z^2}\right)\right]dy\,dz \qquad \text{F-7}$$

The middle term in F-5 was integrated to yield $2\Psi_s\frac{\partial^2\Psi_w}{\partial y^2}$. By changing the order of integration this may also have been integrated

to yield $2\psi_w \frac{\partial^2 \psi_s}{\partial y^2}$, and the middle term in F-7 would then become

$$2\psi_w \left(\frac{\partial^2 \psi_s}{\partial y^2} + \frac{\partial^2 \psi_s}{\partial z^2} \right) \qquad \text{F-8}$$

leaving the other two terms unchanged.

Furthermore

$$\frac{\partial^2 \psi_s}{\partial y^2} + \frac{\partial^2 \psi_s}{\partial z^2} = \begin{cases} 0, \text{ for } \delta \le z \le \ell \\ -\xi_s, \text{ for } 0 \le z \le \delta \end{cases} \qquad \text{F-9}$$

$$\frac{\partial^2 \psi_w}{\partial y^2} + \frac{\partial^2 \psi_w}{\partial z^2} = \begin{cases} 0, \text{ outside the region } \delta_1 \le z \le \delta_2 \\ -\xi_w, \text{ inside the region } \delta_1 \le z \le \delta_2 \end{cases} \qquad \text{F-10}$$

The notations in F-10 are chosen from section 5 where the vorticity region is located between δ_1 and δ_2 , Formula F-10 is also valid for the skewed wake flow (section 6) if we make $\delta_1 = 0$. Substituting F-9 and F-10 into F-7 and changing the integration limits accordingly yields:

$$D = \tfrac{1}{2}\rho \Big[\underbrace{\int_0^b \int_0^{\delta} \psi_s \xi_s \, dy\, dz}_{(1)} + \underbrace{\int_0^b \int_{\delta_1}^{\delta_2} \psi_w \xi_w \, dy\, dz}_{(2)} + \underbrace{2 \int_0^b \int_{\delta_1}^{\delta_2} \psi_s \xi_w \, dy\, dz}_{(3)} \Big] \qquad \text{F-11}$$

This formula is composed of three terms.

(1) the kinetic energy of the secondary flow caused by the skewed flow only

(2) the kinetic energy of the secondary flow caused by the wake flow only

(3) the kinetic energy of the secondary flow caused by the interaction of the skewed flow and the wake flow (cross product term)

If the middle term in F-7 had been changed to F-8, the third term in F-11

would have been

$$2\int_0^b\int_0^\delta \psi_w \xi_s \, dy \, dz \qquad \text{F-12}$$

Since these two terms have to be the same we get:

$$\int_0^b\int_{\delta_1}^{\delta_2} \psi_s \xi_w \, dy \, dz = \int_0^b\int_0^\delta \psi_w \xi_s \, dy \, dz \qquad \text{F-13}$$

This relation will be used in the derivation of the tangential blade force in Appendix G.

Furthermore

$$\psi_s = \sum_n \psi_{sn} \sin n\pi \frac{y}{b} \qquad \text{F-14}$$

$$\psi_w = \sum_n \psi_{wn} \sin n\pi \frac{y}{b} \qquad \text{F-15}$$

$$\xi_s = - U_2 \frac{d\beta_1}{dz} \qquad \text{F-16}$$

$$\xi_w = - 2\varepsilon \frac{dU_1}{dz} \qquad \text{F-17}$$

where the notation of 4-1 is used in the expression for ξ_w. Substituting F-14, F-15, F-16 and F-17 into F-11 and integrating for y, between y = 0 and y = b yields:

$$D = -\rho \frac{b}{\pi}\Big[U_2 \underbrace{\int_0^\delta \frac{d\beta_1}{dz} \sum_n \frac{\psi_{sn}}{n} dz}_{(1)} + 2\varepsilon \underbrace{\int_{\delta_1}^{\delta_2} \frac{dU_1}{dz} \sum_n \frac{\psi_{wn}}{n} dz}_{(2)} + 4\varepsilon \underbrace{\int_{\delta_1}^{\delta_2} \frac{dU_1}{dz} \sum_n \frac{\psi_{sn}}{n} dz}_{(3)}\Big] \qquad \text{F-18}$$

Using the relation F-13 the third term in F-18 may be written as

$$4\varepsilon \int_{\delta_1}^{\delta_2} \frac{dU_1}{dz} \sum_n \frac{\psi_{sn}}{n} dz = 2U_2 \int_0^\delta \frac{d\beta_1}{dz} \sum_n \frac{\psi_{wn}}{n} dz \qquad \text{F-19}$$

With known functions of $\frac{d\beta_1}{dz}$, $\frac{dU_1}{dz}$, ψ_{sn} and ψ_{wn} formula F-18 may be integrated with respect to z.

In this report the expressions for ψ_{sn} and ψ_{wn} remain the same in the three investigated flows but the expression for $\frac{dU_1}{dz}$ differs in all three cases and so separate integrations of F-18 have to be performed, one for each case.

F.2 Wake Flow

F.2.1 Derivation of Formulae

In this case $\frac{d\beta_1}{dz}=0$ and so F-18 reduces to

$$D = -2\rho\varepsilon\frac{b}{\pi}\int_0^{\delta}\frac{dU_1}{dz}\sum_n\frac{\psi_n}{n}\,dz \qquad \text{F-20}$$

where the subscript w of ψ_n has been dropped.

From section 4.2.3.

$$\frac{U_1}{\overline{U}_1} = 1-a\left(1+\cos\pi\frac{z}{\delta}\right) \qquad 4\text{-}30$$

$$\psi_n = -\frac{8\varepsilon b}{(n\pi)^2}\frac{\overline{U}_1 a}{1+(n\frac{\delta}{b})^2}\left\{n\frac{\delta}{b}\sin\pi\frac{z}{\delta}+\frac{\sinh n\pi\frac{\ell-\delta}{b}}{\sinh n\pi\,\ell/b}\sinh\left(\pi n\frac{\delta}{b}\frac{z}{\delta}\right)\right. \qquad 4\text{-}31$$

Differentiating 4-30 with respect to z and substituting together with 4-31 into F-20 yields, after rearranging:

$$D=\frac{16}{\pi^2}\rho\frac{(\varepsilon a\overline{U}_1 b)^2}{\delta}\sum_n\frac{1}{n^3\left[1+(n\frac{\delta}{b})^2\right]}\int_0^{\delta}\left[n\frac{\delta}{b}\sin^2\pi\frac{z}{\delta}+\right.$$

$$\left.+\frac{\sinh n\pi\frac{\ell-\delta}{b}}{\sinh n\pi\,\ell/b}\sin\pi\frac{z}{\delta}\sinh\left(\pi n\frac{\delta}{b}\frac{z}{\delta}\right)\right]dz \qquad \text{F-21}$$

But

$$\int_0^{\delta} \sin^2 \pi \frac{z}{\delta}\, dz = \frac{\delta}{2} \qquad \text{F-22}$$

$$\int_0^{\delta} \sin \pi \frac{z}{\delta} \sinh n\pi \frac{\delta}{b} \frac{z}{\delta}\, dz = \frac{\delta/\pi}{1+\left(n\frac{\delta}{b}\right)^2} \sinh n\pi \frac{\delta}{b} \qquad \text{F-23}$$

and so

$$D = \frac{16}{\pi^2} \rho (\varepsilon a \bar{U}_1 b)^2 \sum_n \frac{1}{n^3\left[1+\left(n\frac{\delta}{b}\right)^2\right]} \left(\frac{n}{2}\frac{\delta}{b} + \frac{1}{\pi\left[1+\left(n\frac{\delta}{b}\right)^2\right]} \frac{\sinh n\pi \frac{\ell-\delta}{b}}{\sinh n\pi \ell/b} \sinh n\pi \frac{\delta}{b} \right) \qquad \text{F-24}$$

Formula F-24 gives the kinetic energy of the secondary flow due to a wake flow in terms of known quantities. However, still more interesting is the question: What percentage of the kinetic energy of the flow entering the cascade is converted into the kinetic energy of the secondary flow? To calculate this, the kinetic energy per unit volume of the flow entering the cascade has to be determined.

The expression for the kinetic energy per unit volume of the inlet flow to the cascade is:

$$KE_{inl.} = \frac{1}{2} \rho \int_0^{\ell} \int_0^{s_1} U_1^2\, dy\, dz \qquad \text{F-25}$$

Since U_1 is constant outside the wake and is also constant in transverse direction F-25 may be integrated to yield:

$$KE_{inl.} = \frac{1}{2} \rho \bar{U}_1 s_1 \ell \left[1 - \frac{\delta}{\ell} + \frac{1}{\ell} \int_0^{\delta} \left(\frac{U_1}{\bar{U}_1} \right)^2 dz \right] \qquad \text{F-26}$$

The integral in F-26 may be written as

$$\frac{1}{\ell} \int_0^{\delta} \left(\frac{U_1}{\bar{U}_1} \right)^2 dz = \frac{1}{\ell} \left[\int_0^{\delta} \frac{U_1}{\bar{U}_1} \left(1 - \frac{U_1}{\bar{U}_1} \right) dz - \int_0^{\delta} \left(1 - \frac{U_1}{\bar{U}_1} \right) dz + \int_0^{\delta} dz \right] = \frac{\delta}{\ell} - \frac{\theta}{\ell} - \frac{\delta^*}{\ell} \qquad \text{F-27}$$

where

δ = base width of half the wake

δ^* = displacement thickness of half the wake

θ = momentum thickness of half the wake

Substituting F-27 into F-26 yields:

$$KE_{inl.} = \frac{1}{2}\rho \bar{U}_1^2 s_1 \ell \left[1 - \frac{\delta^* + \theta}{\ell}\right] \qquad \text{F-28}$$

Substituting 4-30 into F-27 and integrating yields:

$$\frac{\delta^* + \theta}{\ell} = \frac{\delta}{\ell}\left[1 - (1-a)^2 + \frac{a^2}{2}\right] \qquad \text{F-29}$$

Combining F-24, F-28 and F-29 and noting that

$s_1 = s \sin \alpha_1$

$b = s \sin \alpha_2$

yields

$$\frac{D}{KE_{inl.}} = \frac{32}{\pi^2}\frac{s}{c}\frac{c}{\ell}\frac{\varepsilon^2 a^2}{\left\{1 - \frac{\delta}{\ell}\left[1-(1-a)^2-\frac{a^2}{2}\right]\right\}}\frac{\sin^2\alpha_2}{\sin\alpha_1}\sum_n \frac{1}{n^3\left[1+(n\frac{\delta}{b})^2\right]}\left[\frac{n}{2}\frac{\delta}{b} + \right.$$

$$\left. + \frac{1}{\pi\left[1+(n\frac{\delta}{b})^2\right]}\frac{\sinh n\pi\frac{\ell-\delta}{b}}{\sinh n\pi \ell/b}\sin n\pi\frac{\delta}{b}\right] \qquad \text{F-30}$$

F.2.2 Numerical Values

s	= 4.445"	δ	= 1.130"
c	= 4.500"	a	= 0.137
l	= 8.000"	α_1	= 45.0°
b	= 4.009"	α_2	= 64.4°

Both equations 4-1 and 4-8 have been used to describe the distributed vorticity component in streamwise direction. When 4-8 has been used, 2ε

in F-30 has been replaced by

$$\left(1+\frac{\sin\alpha_1}{\sin\alpha_2}\right)\frac{\cos\alpha_1-\cos\alpha_2}{\sin\alpha_2}$$

The calculation has been performed for n = 1, 3 and 5.

The results of this calculation are given in section 4.3.2.

F.3 Skewed Flow

F.3.1 Derivation of Formulae

In this case

$$\psi_{sn}=\frac{-4U_2b}{\pi^2n^2}\sum_{m}\frac{A_m}{1+\left(\frac{n\delta}{m\,b}\right)^2}\left\{\cos m\pi\,\frac{\sinh n\pi\frac{\ell-\delta}{b}}{\sinh n\pi\,\ell/b}\sinh\left(n\pi\frac{\delta}{b}\frac{z}{\delta}-\frac{n}{m}\frac{\delta}{b}\sin m\pi\frac{z}{\delta}\right)\right\} \quad 5\text{-}52$$

$$\psi_{wn}=\frac{-8\varepsilon b\,\bar{U}_1 a}{\pi^2n^2\left[1+\left(n\frac{\delta_4}{b}\right)^2\right]}\left\{\frac{\sinh n\pi\frac{\ell-\delta_2}{b}}{\sinh n\pi\,\ell/b}\sinh n\pi\frac{z}{b}-\right.$$

$$\left.-\frac{\sinh n\pi\frac{\delta_1/b}{\sinh n\pi\,\ell/b}}{\sinh n\pi\,\ell/b}\sinh n\pi\frac{\ell}{b}\left[1-\frac{z}{\ell}\right]+n\frac{\delta_4}{b}\sin\pi\left(\frac{z}{\delta_4}-2\right)\right\} \quad C\text{-}15$$

$$\frac{d\beta_1}{dz}=-\frac{\pi}{\delta}\sum_{m=1}m\,A_m\sin m\pi\frac{z}{\delta} \quad 5\text{-}51$$

$$\frac{dU_1}{dz}=\bar{U}_1 a\frac{\pi}{\delta_4}\sin\pi\left(\frac{z}{\delta_4}-2\right) \quad C\text{-}8$$

Consider the first term in F-18

$$(1) = U_2 \int_0^{\delta} \frac{d\beta_1}{dz} \sum \frac{\Psi_{sn}}{n} \, dz$$

Substituting 5-51 and 5-52 into (1) and rearranging yields:

$$(1) = \frac{4}{\pi} U_2^2 \frac{b}{\delta} \int_0^{\delta} \sum_n \sum_m \frac{m A_m^2}{n^3 \left[1+\left(\frac{n\delta}{mb}\right)^2\right]} \left\{ \cos m\pi \, \frac{\sinh n\pi \frac{\ell-\delta}{b}}{\sinh n\pi \ell/b} \sinh n\pi \frac{z}{b} \sin m\pi \frac{z}{\delta} - \right.$$

$$\left. - \frac{n}{m} \frac{\delta}{b} \sin^2 m\pi \frac{z}{\delta} \right\} dz$$

But

$$\int_0^{\delta} \sinh n\pi \frac{z}{b} \sin m\pi \frac{z}{\delta} \, dz = \frac{-\delta}{m\pi} \frac{1}{1+\left(\frac{n\delta}{mb}\right)^2} \cos m\pi \sinh n\pi \frac{\delta}{b}$$

$$\int_0^{\delta} \sin^2 m\pi \frac{z}{\delta} \, dz = \frac{\delta}{2}$$

Substituting these integrals into (1) and rearranging yields:

$$(1) = U_2 \int_0^{\delta} \frac{d\beta_1}{dz} \sum \frac{\Psi_{sn}}{n} \, dz =$$

$$= \frac{-4}{\pi} U_2^2 b \left\{ \sum_n \sum_m \frac{m A_m^2}{n^3 \left[1+\left(\frac{n\delta}{mb}\right)^2\right]} \left[\frac{1}{m\pi \left[1+\left(\frac{n\delta}{mb}\right)^2\right]} \sinh n\pi \frac{\delta}{b} \frac{\sinh n\pi \frac{\ell-\delta}{b}}{\sinh n\pi \ell/b} + \right.\right.$$

$$\left.\left. + \frac{n}{2m} \frac{\delta}{b} \right] \right\} \equiv -\frac{4}{\pi} U_2^2 b f \qquad \text{F-31}$$

where f is given by the double summation in F-31

Consider the second term in F-18

$$(2) = 2\varepsilon \int_{\delta_1}^{\delta_2} \frac{dU_1}{dz} \sum_n \frac{\Psi_{wn}}{n} \, dz$$

Substituting C-8 and C-15 into (2) and rearranging yields:

$$(2) = \frac{-8}{\pi}\frac{\varepsilon^2 b}{\delta_4}\bar{U}_1^2 a^2 \sum_n \frac{1}{n^3\left[1+\left(n\frac{\delta_4}{b}\right)^2\right]}\int_{\delta_1}^{\delta_2}\left\{\frac{\sinh n\pi\frac{\ell-\delta_2}{b}}{\sinh n\pi\,\ell/b}\sinh n\pi\frac{z}{b}\sin\pi\left(\frac{z}{\delta_4}-2\right)-\right.$$

$$\left.-\frac{\sinh n\pi\,\delta_1/b}{\sinh n\pi\,\ell/b}\sinh n\pi\frac{\ell}{b}\left(1-\frac{z}{\ell}\right)\sin\pi\left(\frac{z}{\delta_4}-2\right)+n\frac{\delta_4}{b}\sin^2\pi\left(\frac{z}{\delta_4}-2\right)\right\}dz$$

But

$$\int_{\delta_1}^{\delta_2}\sin\pi\left(\frac{z}{\delta_4}-2\right)\sinh n\pi\frac{z}{b}\,dz = \frac{\delta_4/\pi}{1+\left(n\frac{\delta_4}{b}\right)^2}\left\{-\cos\pi\left(\frac{\delta_2}{\delta_4}-2\right)\sinh n\pi\frac{\delta_2}{b}+\right.$$

$$\left.+\cos\pi\left(\frac{\delta_1}{\delta_4}-2\right)\sinh n\pi\frac{\delta_1}{b}+n\frac{\delta_4}{b}\sin\pi\left(\frac{\delta_2}{\delta_4}-2\right)\cosh n\pi\frac{\delta_2}{b}-n\frac{\delta_4}{b}\sin\pi\left(\frac{\delta_1}{\delta_4}-2\right)\cosh n\pi\frac{\delta_1}{b}\right\}$$

Substituting the actual values $\frac{\delta_2}{\delta_4}=3$, and $\frac{\delta_1}{\delta_4}=1$ into the above formula yields:

$$\int_{\delta_1}^{\delta_2}\sin\pi\left(\frac{z}{\delta_4}-2\right)\sinh n\pi\frac{z}{b}\,dz = \frac{\delta_4}{\pi}\frac{1}{1+\left(n\frac{\delta_4}{b}\right)^2}\left[\sinh n\pi\frac{\delta_2}{b}-\sinh n\pi\frac{\delta_1}{b}\right]$$

Similarly

$$\int_{\delta_1}^{\delta_2}\sin\pi\left(\frac{z}{\delta_4}-2\right)\sinh n\pi\frac{\ell}{b}\left(1-\frac{z}{\ell}\right)dz = \frac{\delta_4}{\pi}\frac{1}{1+\left(n\frac{\delta_4}{b}\right)^2}\left[-\sinh n\pi\frac{\ell-\delta_1}{b}+\sinh n\pi\frac{\ell-\delta_2}{b}\right]$$

$$\int_{\delta_1}^{\delta_2}\sin^2\pi\left(\frac{z}{\delta_4}-2\right)dz = \frac{\delta_2-\delta_1}{2}$$

Substituting these expressions into (2) yields:

$$(2) = 2\varepsilon \int_{\delta_1}^{\delta_2} \frac{dU_1}{dz} \sum_n \frac{\psi_{wn}}{n}\, dz =$$

$$= -\frac{8}{\pi}\varepsilon^2 b \bar{U}_1^2 a^2 \sum_n \frac{1}{n^3\left[1+\left(n\frac{\delta_4}{b}\right)^2\right]} \left\{ \frac{1}{\pi\left[1+\left(n\frac{\delta_4}{b}\right)^2\right]} \left[\frac{\sinh n\pi \frac{\ell-\delta_2}{b}}{\sinh n\pi \ell/b} \left(\sinh n\pi \frac{\delta_2}{b} - \sinh n\pi \frac{\delta_1}{b}\right) + \right.\right.$$

$$\left.\left. + \frac{\sinh n\pi \frac{\delta_1}{b}}{\sinh n\pi \ell/b} \left(\sinh n\pi \frac{\ell-\delta_1}{b} - \sinh n\pi \frac{\ell-\delta_2}{b}\right)\right] + \frac{n}{2}\frac{\delta_1-\delta_2}{b} \right\} \equiv \frac{-8}{\pi}\varepsilon^2 b \bar{U}_1^2 a^2 g \qquad \text{F-32}$$

where g is given by the summation in F-32

Consider the third term in F-18

$$(3) = 4\varepsilon \int_{\delta_1}^{\delta_2} \frac{dU_1}{dz} \sum \frac{\psi_{sn}}{n}\, dz$$

Substituting C-8 and 5-52 into (3) and rearranging yields:

$$(3) = \frac{-8}{\pi}\varepsilon \bar{U}_1 U_2 \frac{ab}{\delta_4} \int_{\delta_1}^{\delta_2} \sum_n \sum_m \frac{A_m}{n^3\left[1+\left(\frac{n\delta}{mb}\right)^2\right]} \left\{ \cos m\pi \; \frac{\sinh n\pi \frac{\ell-\delta}{b}}{\sinh n\pi \ell/b} \sinh n\pi \frac{z}{b} \sin\pi\left(\frac{z}{\delta_4}-2\right) - \right.$$

$$\left. - \frac{n}{m}\frac{\delta}{b} \sin m\pi \frac{z}{\delta} \sin\pi\left(\frac{z}{\delta_4}-2\right) \right\} dz$$

The first integral has already been solved and

$$\int_{\delta_1}^{\delta_2} \sin m\pi \frac{z}{\delta} \sin\pi\left(\frac{z}{\delta_4}-2\right) dz =$$

$$= \frac{1}{2\pi} \left\{ \frac{1}{\frac{1}{\delta_4}-\frac{m}{\delta}} \left[\sin\pi\left(\left[\frac{1}{\delta_4}-\frac{m}{\delta}\right]\delta_2 - 2\right) - \sin\pi\left(\left[\frac{1}{\delta_4}-\frac{m}{\delta}\right]\delta_1 - 2\right)\right] - \right.$$

$$\left. - \frac{1}{\frac{1}{\delta_4}+\frac{m}{\delta}} \left[\sin\pi\left(\left[\frac{1}{\delta_4}+\frac{m}{\delta}\right]\delta_2 - 2\right) - \sin\pi\left(\left[\frac{1}{\delta_4}+\frac{m}{\delta}\right]\delta_1 - 2\right)\right] \right\}$$

(3) then finally becomes:

$$(3) = 4\varepsilon \int_{\delta_1}^{\delta_2} \frac{dU_1}{dz} \sum_n \frac{\psi_{sn}}{n}\, dz =$$

$$= \frac{-8\varepsilon}{\pi^2}\, \bar{U}_1 U_2\, ab \sum_n \sum_m \frac{1}{n^3} \frac{A_m}{1+\left(\frac{n\delta}{mb}\right)^2} \left\{ \frac{\cos m\pi}{1+\left(n\frac{\delta_4}{b}\right)^2} \frac{\sinh n\pi \frac{\ell-\delta}{b}}{\sinh n\pi \ell/b} \left[\sinh n\pi \frac{\delta_2}{b} - \sinh n\pi \frac{\delta_1}{b}\right] - \right.$$

$$- \frac{n}{2m} \frac{\delta}{b} \frac{1}{\delta_4} \left\{ \frac{1}{\frac{1}{\delta_4} - \frac{m}{\delta}} \left[\sin\pi\left(\left[\frac{1}{\delta_4} - \frac{m}{\delta}\right]\delta_2 - 2\right) - \sin\pi\left(\left[\frac{1}{\delta_4} - \frac{m}{\delta}\right]\delta_1 - 2\right)\right] - \right.$$

$$\left.\left. - \frac{1}{\frac{1}{\delta_4} + \frac{m}{\delta}} \left[\sin\pi\left(\left[\frac{1}{\delta_4} + \frac{m}{\delta}\right]\delta_2 - 2\right) - \sin\pi\left(\left[\frac{1}{\delta_4} + \frac{m}{\delta}\right]\delta_1 - 2\right)\right] \right\} \right\}$$

$$\equiv \frac{-8\varepsilon}{\pi^2}\, \bar{U}_1 U_2\, abh \qquad \text{F-33}$$

where h is given by the double summation in F-33.

Substituting the expressions for (1), (2) and (3) into F-18 finally yields:

$$D = \frac{4}{\pi^2} \rho b^2 \left[U_2^2 f + 2\varepsilon^2 \bar{U}_1^2 a^2 g + \frac{2\varepsilon}{\pi} \bar{U}_1 U_2\, a h\right] \qquad \text{F-34}$$

Introducing the continuity equation,

$$\bar{U}_1 \sin\alpha_1 = U_2 \sin\alpha_2\ , \qquad \text{F-35}$$

into F-34 yields

$$D = \frac{4}{\pi^2} \rho \bar{U}_1^2 b^2 \left[\frac{\sin^2\alpha_1}{\sin^2\alpha_2} f + 2\varepsilon^2 a^2 g + \frac{2\varepsilon}{\pi} a \frac{\sin\alpha_1}{\sin\alpha_2} h\right]\ , \qquad \text{F-36}$$

where f, g and h are given by F-31, F-32 and F-33.

In calculating the kinetic energy per unit volume of the flow entering the cascade it is assumed that the flow enters at a constant inlet angle, α_1, which is the inlet angle of the free stream.

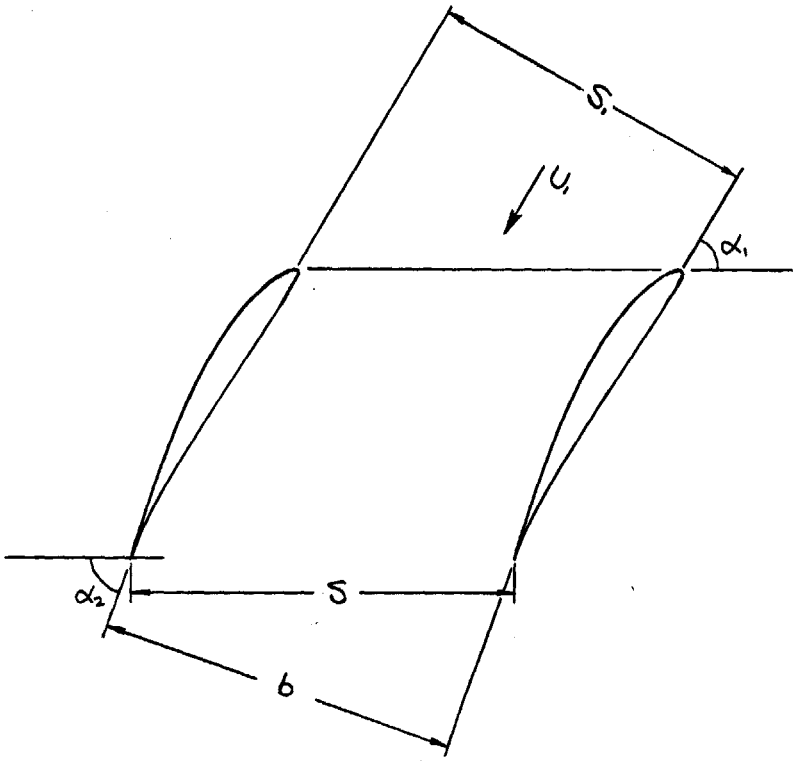

Under this assumption the formula F-25 is valid and may be integrated to yield

$$KE_{inl.} = \frac{1}{2}\rho \bar{U}_1^2 S_1 l \left[1 - 2\frac{\delta^* + \theta}{l}\right] \qquad \text{F-37}$$

which differs from F-28 only through the factor 2, inside the brackets. However, in this case the whole wake is inside the flow region and thus giving this factor of 2.

With notations of this flow, F-29 becomes

$$2\frac{\delta^* + \theta}{l} = \frac{2\delta_4}{l}\left[1 - (1-a)^2 - \frac{a^2}{2}\right] \qquad \text{F-38}$$

Combining F-36, F-37 and F-38 yields

$$\frac{D}{KE_{inl.}} = \frac{8}{\pi^2}\frac{S}{C}\frac{C}{\ell}\frac{\sin^2\alpha_2}{\sin\alpha_1}\frac{\left(\frac{\sin\alpha_1}{\sin\alpha_2}\right)^2 \cdot f + 2a^2\varepsilon^2 g + \frac{2a\varepsilon}{\pi}\frac{\sin\alpha_1}{\sin\alpha_2}\cdot h}{1-2\frac{\delta_4}{\ell}\left[1-(1-a)^2-\frac{a^2}{2}\right]} \qquad \text{F-39}$$

where f, g and h are given by F-31, F-32 and F-33.

F.3.2 Numerical Values

S	= 4.445"	δ_1	= 0.5"	α_2	= 68.6°
C	= 4.500"	δ_2	= 1.5"	A_1	= 0.19478
l	= 8.000"	δ_4	= 0.5"	A_2	= 0.02731
b	= 4.13856"	a	= 0.070	A_3	= -0.02402
δ	= 2.25"	α_1	= 45.0°	A_4	= -0.01122

Equation 4-8 has been used instead of 4-1 and so 2ε in F-39 was replaced by $\left(1+\frac{\sin\alpha_1}{\sin\alpha_2}\right)\frac{\cos\alpha_1-\cos\alpha_2}{\sin\alpha_2}$. The calculation has been performed for n = 1, 3, and 5. The result of the calculation is given in section 5.3.2.

F.4 Skewed Wake Flow

F.4.1 Derivation of Formulae

In this case

$$\psi_{sn} = \frac{-4U_2 b}{\pi^2 n^2}\sum_m \frac{A_m}{1+\left(\frac{n\delta}{mb}\right)^2}\left\{\cos m\pi\,\frac{\sinh n\pi\frac{\ell-\delta}{b}}{\sinh n\pi\ell/b}\sinh\left(n\pi\frac{\delta}{b}\frac{z}{\delta}\right)-\frac{n}{m}\frac{\delta}{b}\sin m\pi\frac{z}{\delta}\right\} \qquad 5\text{-}52$$

$$\psi_{wn} = \frac{8\varepsilon b\bar{U}_1}{\pi^2 n^2}\sum_m \frac{B_m}{1+\left(\frac{n\delta_1}{mb}\right)^2}\left\{\cos m\pi\,\frac{\sinh n\pi\frac{\ell-\delta_1}{b}}{\sinh n\pi\ell/b}\sinh\left(n\pi\frac{\delta_1}{b}\frac{z}{\delta_1}\right)-\frac{n\delta_1}{mb}\sin m\pi\frac{z}{\delta_1}\right\} \qquad \text{D-12}$$

$$\frac{d\beta_1}{dz} = -\frac{\pi}{\delta}\sum_{m=1} m A_m \sin m\pi\frac{z}{\delta} \qquad 5\text{-}51$$

$$\frac{dU_1}{dz} = \bar{U}_1\frac{\pi}{\delta_1}\sum_{m=1} m B_m \sin m\pi\frac{z}{\delta_1} \qquad D\text{-}3$$

The first term in F-18 will remain the same as in the skewed flow:

$$(1) = U_2\int_0^{\delta}\frac{d\beta_1}{dz}\sum_n \frac{\Psi_{sn}}{n}\,dz =$$

$$= \frac{-4}{\pi}U_2^2 b\left\{\sum_n\sum_m \frac{mA_m^2}{n^3\left[1+\left(\frac{n\delta}{mb}\right)^2\right]}\left[\frac{1}{m\pi\left[1+\left(\frac{n\delta}{mb}\right)^2\right]}\sinh n\pi\frac{\delta}{b}\,\frac{\sinh n\pi\frac{\ell-\delta}{b}}{\sinh n\pi\ell/b} + \frac{n}{2m}\frac{\delta}{b}\right]\right\} =$$

$$= \frac{-4}{\pi}U_2^2 bf \qquad F\text{-}31$$

Consider the second term in F-18

$$(2) = 2\varepsilon\int_0^{\delta_1}\frac{dU_1}{dz}\sum_n\frac{\Psi_{wn}}{n}\,dz$$

Substituting D-3 and D-12 into (2) and rearranging yields:

$$(2) = \frac{16}{\pi}\frac{\bar{U}_1^2\varepsilon^2 b}{\delta_1}\sum_n\sum_m \frac{m B_m^2}{n^3\left[1+\left(\frac{n\delta_1}{mb}\right)^2\right]}\int_0^{\delta_1}\left\{\cos m\pi\,\frac{\sinh n\pi\frac{\ell-\delta_1}{b}}{\sinh n\pi \ell/b}\sin m\pi\frac{z}{\delta_1}\sinh n\pi\frac{z}{b} - \right.$$

$$\left. - \frac{n\delta_1}{mb}\sin^2 m\pi\frac{z}{\delta_1}\right\} dz$$

But

$$\int_0^{\delta_1}\sin m\pi\frac{z}{\delta_1}\sinh n\pi\frac{z}{b}\,dz = \frac{-\frac{\delta_1}{m\pi}}{1+\left(\frac{n\delta_1}{mb}\right)^2}\cos m\pi\sinh n\pi\frac{\delta_1}{b}$$

$$\int_0^{\delta_1}\sin^2 m\pi\frac{z}{\delta_1}\,dz = \frac{\delta_1}{2}$$

Substituting the values of these integrals into (2) yields:

$$(2) = 2\varepsilon\int_0^{\delta_1}\frac{dU_1}{dz}\sum_n\frac{\Psi_{wn}}{n}\,dz =$$

$$= \frac{-16\bar{U}_1^2\varepsilon^2 b}{\pi}\sum_n\sum_m\frac{mB_m^2}{n^3\left[1+\left(\frac{n\delta_1}{mb}\right)^2\right]}\left\{\frac{1}{m\pi\left[1+\left(\frac{n\delta_1}{mb}\right)^2\right]}\,\frac{\sinh n\pi\frac{\ell-\delta_1}{b}}{\sinh n\pi\ell/b}\sinh n\pi\frac{\delta_1}{b} + \frac{n}{2m}\frac{\delta_1}{b}\right\} \equiv$$

$$\equiv \frac{-16}{\pi}\bar{U}_1^2\varepsilon^2 b\cdot g \qquad \text{F-40}$$

Consider the third term (3) in Figure F-18

$$(3) = 4\varepsilon\int_0^{\delta_1}\frac{dU_1}{dz}\sum_n\frac{\Psi_{sn}}{n}\,dz$$

Substituting D-3 and 5-52 into (3) and rearranging yields

$$(3) = \frac{-16}{\pi}\,\bar{U}_1 U_2\,\frac{\varepsilon b}{\delta_1}\sum_n\sum_m \frac{m A_m B_m}{n^3\left[1+\left(\frac{n\delta}{mb}\right)^2\right]}\int_0^{\delta_1}\left\{\cos m\pi\,\frac{\sinh n\pi\,\frac{\ell-\delta}{b}}{\sinh n\pi\,\ell/b}\sin m\pi\,\frac{z}{\delta_1}\sinh n\pi\,\frac{z}{b} - \right.$$

$$\left. -\frac{n}{m}\,\frac{\delta}{b}\sin m\pi\,\frac{z}{\delta}\sin m\pi\,\frac{z}{\delta_1}\right\} dz$$

The first integral has been evaluated before, and

$$\int_0^{\delta_1}\sin m\pi\,\frac{z}{\delta}\sin m\pi\,\frac{z}{\delta_1}\,dz = \frac{\sin m\pi\left(1-\frac{\delta_1}{\delta}\right)}{2m\pi\,\frac{1}{\delta_1}\left(1-\frac{\delta_1}{\delta}\right)} - \frac{\sin m\pi\left(1+\frac{\delta_1}{\delta}\right)}{2m\pi\,\frac{1}{\delta_1}\left(1+\frac{\delta_1}{\delta}\right)}$$

Note: If $\delta = \delta_1$, the integral above becomes $\frac{\delta_1}{2}$

In the numerical calculations $\delta = \delta_1$, and so the integral becomes $\frac{\delta_1}{2}$.

Then (3) becomes:

$$(3) = 4\varepsilon\int_0^{\delta_1}\frac{dU_1}{dz}\sum\frac{\Psi_{sn}}{n}\,dz =$$

$$= \frac{16}{\pi}\,\bar{U}_1 U_2\,\varepsilon b\sum_n\sum_m\frac{m A_m B_m}{n^3\left[1+\left(\frac{n\delta}{mb}\right)^2\right]}\left\{\frac{1}{m\pi\left[1+\left(\frac{n\delta_1}{mb}\right)^2\right]}\,\frac{\sinh n\pi\,\frac{\ell-\delta_1}{b}}{\sinh n\pi\,\ell/b}\sinh n\pi\,\frac{\delta_1}{b}+\frac{n}{2m}\,\frac{\delta_1}{b}\right\}\equiv$$

$$\equiv \frac{16}{\pi}\,\bar{U}_1 U_2\,\varepsilon b\cdot h \qquad \text{F-41}$$

Substituting the expressions for (1), (2) and (3) into F-18 gives

$$D = \frac{4}{\pi^2}\rho b^2\left[U_2^2\cdot f + 4\bar{U}_1^2\varepsilon^2\cdot g - 4\bar{U}_1 U_2\,\varepsilon\cdot h\right] \qquad \text{F-42}$$

or with the continuity equation F-35

$$D = \frac{4}{\pi^2} \rho \bar{U}_1^2 b^2 \left[\frac{\sin^2\alpha_1}{\sin^2\alpha_2} f + 4\varepsilon^2 g - 4\varepsilon \frac{\sin\alpha_1}{\sin\alpha_2} h \right] \qquad \text{F-43}$$

The same assumptions about the kinetic energy of the flow entering the cascade is made for this case as for the skewed flow case and so

$$KE_{inl.} = \frac{1}{2} \rho \bar{U}_1^2 s_1 \ell \left[1 - \frac{\delta^* + \theta}{\ell} \right] \qquad \text{F-44}$$

where

$$1 - \frac{\delta^* + \theta}{\ell} = 1 - \frac{\delta_1}{\ell} \left(B_0^2 + \frac{1}{2} \sum_m B_m^2 \right) \qquad \text{F-45}$$

Combining F-34, F-44 and F-45 yields

$$\frac{D}{KE_{inl.}} = \frac{8}{\pi^2} \frac{s}{c} \frac{c}{\ell} \frac{\sin^2\alpha_2}{\sin\alpha_1} \frac{\frac{\sin^2\alpha_1}{\sin^2\alpha_2} \cdot f + 4\varepsilon^2 g - 4\varepsilon \frac{\sin\alpha_1}{\sin\alpha_2} \cdot h}{1 - \frac{\delta_1}{\ell} \left(B_0^2 + \frac{1}{2} \sum_m B_m^2 \right)} \qquad \text{F-46}$$

where f, g and h are given by F-31, F-40 and F-41.

F.4.2 Numerical Values

The actual values for this flow are listed below

$s = 4.445"$	$\alpha_1 = 45.0°$	$B_1 = 0.18000$
$c = 4.500"$	$\alpha_2 = 64.4°$	$B_2 = -0.06560$
$l = 8.000"$	$B_0 = 0.21133$	$B_3 = -0.01665$
$\delta = \delta_1 = 1.750"$		$B_4 = 0.01762$

Equation 4-8 has been used instead of 4-1 and so 2ε in F-46 was replaced by $\left(1+\frac{\sin\alpha_1}{\sin\alpha_2}\right)\frac{\cos\alpha_1-\cos\alpha_2}{\sin\alpha_2}$. The calculations have been performed for n = 1, 3 and 5. The result of the calculations is given in section 6.3.2.

F.5 The Spanwise Distribution of the Kinetic Energy of the Secondary Flow

The kinetic energy per unit volume of the secondary flow averaged over one blade spacing at a constant spanwise position is:

$$D_z = \frac{1}{2}\rho\int_0^b (V^2+W^2)\,dy \qquad \text{F-47}$$

Expressing the secondary flow velocity components as derivatives of the stream function, ψ , of the secondary flow and substituting into F-47 gives

$$D_z = \frac{1}{2}\rho\int_0^b \left[\left(\frac{\partial\psi}{\partial y}\right)^2+\left(\frac{\partial\psi}{\partial z}\right)^2\right] dy \qquad \text{F-48}$$

Substituting F-3, F-14 and F-15 yields

$$D_z = \frac{1}{2}\rho\int_0^b \left\{\sum_n (\psi'_{sn}+\psi'_{wn})^2 \sin^2 n\pi\frac{y}{b}+\left(\frac{\pi}{b}\right)^2\sum_n (\psi_{sn}+\psi_{wn})^2 n^2\cos^2 n\pi\frac{y}{b}\right\} dy \qquad \text{F-49}$$

which may be integrated and rearranged to yield

$$D_z = \frac{1}{4}\rho b \sum_n \left\{ \underbrace{\left[\psi_{sn}'^2 + \left(\frac{\pi}{b}\right)^2 n^2 \psi_{sn}^2\right]}_{(1)} + \underbrace{\left[\psi_{wn}'^2 + \left(\frac{\pi}{b}\right)^2 n^2 \psi_{wn}^2\right]}_{(2)} + \right.$$

$$\left. + 2\left[\psi_{sn}' \psi_{wn}' + \left(\frac{\pi}{b}\right)^2 n^2 \psi_{sn}\psi_{wn}\right] \right\} \qquad \text{F-50}$$

This formula is composed of three parts

(1) is the contribution from the skewed flow only

(2) is the contribution from the wake flow only

(3) is the contribution from the interaction between (1) and (2) (cross product term)

Although this formula may be expanded further by substituting the values of ψ_n and ψ_n', it is of practical interest to stop here, since those expressions are very complicated and the values of ψ_n and ψ_n' are known from the calculations of the secondary flow velocity components.

In order to make D_z dimensionless F-50 is divided by the expressions for the kinetic energy of the energy of the flow entering the cascade, i.e. by F-28, F-37 or F-44 depending on the case under consideration.

APPENDIX G

The Tangential Component of the Blade Force

G.1 Derivation of Formulae

The tangential component, T, of the blade force over half of the span is given by the tangential component of the momentum equation:

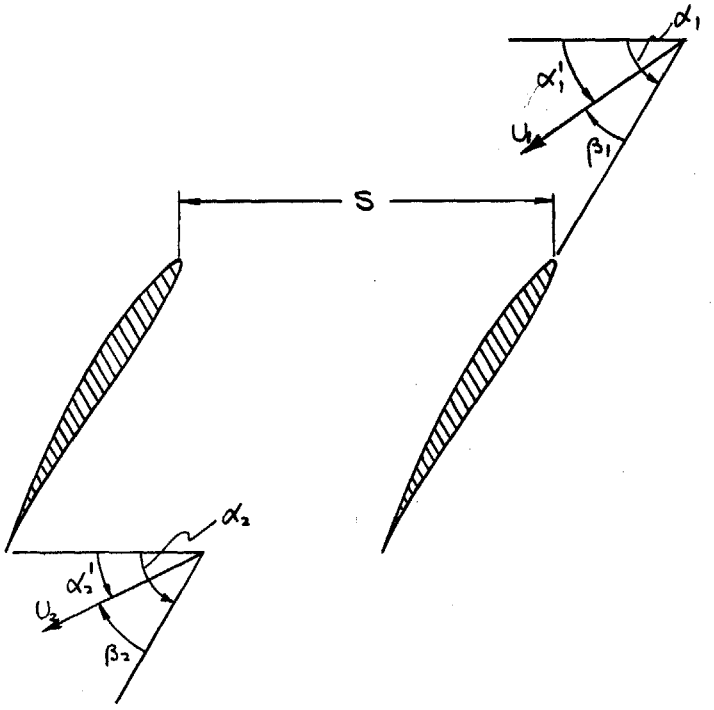

$$-T = \int_0^{\ell} s\rho U_1 \sin\alpha_1' \,(U_2\cos\alpha_2' - U_1\cos\alpha_1') \qquad \text{G-1}$$

where α_1' and α_2' are the total transverse flow angles, i.e.

$$\alpha_1' = \alpha_1 - \beta_1 \qquad \text{G-2}$$

$$\alpha_2' = \alpha_2 - \beta_2 \qquad \text{G-3}$$

where α_1 and α_2 are two-dimensional transverse flow angles, and β_1 and β_2 are the transverse flow deviation angles. Assuming no spanwise shift of

the streamlines through the cascade the continuity equation may be written

$$U_1 \sin \alpha_1' = U_2 \sin \alpha_2' \qquad \text{G-4}$$

This assumption is good only if the perturbation is small, i.e. a small secondary flow is created and no blockage effects in the cascade are created due to stalling. Substituting G-2 and G-3 into G-1 and rearranging yields

$$-T = s\rho \int_0^{\ell} U_1^2 \sin^2 \alpha_1' (\cot \alpha_2' - \cot \alpha_1') \, dz \qquad \text{G-5}$$

Assuming β_1 and β_2 to be small, the expressions in the paranthesis may be rewritten using G-2 and G-3.

$$\cot \alpha_2' = \cot (\alpha_2 - \beta_2) \approx \cot \alpha_2 + \beta_2 \qquad \text{G-6}$$

$$\cot \alpha_1' = \cot (\alpha_1 - \beta_1) \approx \cot \alpha_1 + \beta_1 \qquad \text{G-7}$$

Similarly

$$\sin^2 \alpha_1' = \sin^2 (\alpha_1 - \beta_1) \approx \sin^2 \alpha_1 (1 - 2\beta_1 \cot \alpha_1) \qquad \text{G-8}$$

Sibstituting G-6, G-7 and G-8 into G-5 neglecting second order terms and rearranging yields:

$$-T = s\rho \sin^2 \alpha_1 \left\{ (\cot \alpha_2 - \cot \alpha_1) \int_0^{\ell} U_1^2 \, dz - \right.$$

$$\left. -\left[1 + 2 \cot \alpha_1 (\cot \alpha_2 - \cot \alpha_1)\right] \int_0^{\ell} \beta_1 U_1^2 \, dz + \int_0^{\ell} \beta_2 U_1^2 \, dz \right\} \qquad \text{G-9}$$

Consider the integral of the first term in G-9. It may be written as

$$\int_0^\ell U_1^2\,dz = -\int_0^\ell U_1(\bar{U}_1 - U_1)\,dz - \bar{U}_1\int_0^\ell(\bar{U}_1 - U_1)\,dz + \bar{U}_1^2\int_0^\ell dz \equiv$$

$$\equiv -\theta\bar{U}_1^2 - \delta^*\bar{U}_1^2 + \ell\bar{U}_1^2 \qquad \text{G-10}$$

where

δ^* = displacement thickness of half of the wake

θ = momentum thickness of half of the wake

$$\delta^* = \int_0^\ell \left(1-\frac{U_1}{\bar{U}_1}\right)dz \qquad \text{G-11}$$

$$\theta = \int_0^\ell \frac{U_1}{\bar{U}_1}\left(1-\frac{U_1}{\bar{U}_1}\right)dz \qquad \text{G-12}$$

The first term G-9 then becomes:

$$(1) = S\rho\bar{U}_1^2\sin^2\alpha_1(\cot\alpha_2 - \cot\alpha_1)(\ell - \delta^* - \theta) \qquad \text{G-13}$$

Consider the integral of the second term G-9: $\int_0^\ell U_1^2\beta_1\,dz$

U_1 may be written

$$U_1 = \bar{U}_1 - \Delta U_1 \qquad \text{G-14}$$

where

ΔU_1 is the velocity decrease in the wake, less than the two-dimensional uniform flow $\bar{U}_1$.

If

$$\Delta U \ll \bar{U}_1 \qquad \text{G-15}$$

then

$$U_1^2 \approx \bar{U}_1^2 - 2\bar{U}_1\Delta U_1 \qquad \text{G-16}$$

and

$$\beta_1 U_1^2 \approx \beta_1 \bar{U}_1^2 - 2\bar{U}_1 \beta_1 \Delta U_1 \approx \beta_1 \bar{U}_1^2 \qquad \text{G-17}$$

The integral then becomes:

$$\int_0^{\ell} U_1^2 \beta_1 dz \approx \bar{U}_1^2 \int_0^{\ell} \beta_1 dz \qquad \text{G-18}$$

but

$$\beta_1 = \sum_{m=0} A_m \cos m\pi \frac{z}{\delta} \qquad \text{G-19}$$

for $0 \le z \le \delta$

and

$\beta_1 = 0$ for $\delta \le z \le \ell$ and therefore

$$\int_0^{\ell} \beta_1 dz = \int_0^{\delta} \beta_1 dz = A_0 \cdot \delta \qquad \text{G-20}$$

The second term in G-9 then becomes:

$$(2) = -s\rho \bar{U}_1^2 \sin^2\alpha_1 \left[1 + 2\cot\alpha_1 (\cot\alpha_2 - \cot\alpha_1)\right] \delta \cdot A_0 \qquad \text{G-21}$$

Consider the integral of the third term in G-9: $\int_0^{\ell} \beta_2 U_1^2 dz$

β_2 is the average transverse angle given by: (see for instance 4-23 and 4-26 and note that $\tan\beta_2 \approx \beta_2$)

$$\beta_2 = \frac{1}{U_2} \frac{2}{\pi} \sum_n \frac{\psi_n'}{n} \qquad \text{G-22}$$

Eliminating U_2 using G-4 yields

$$\beta_2 = \frac{2}{\pi}\frac{1}{U_1}\frac{\sin\alpha_2'}{\sin\alpha_1'}\sum\frac{\psi_n'}{n} \qquad \text{G-23}$$

In this formula

$$\psi_n' = \psi_{sn}' + \psi_{wn}' \qquad \text{G-24}$$

is the sum of the derivatives with respect to z of the two stream functions

$$\psi_{sn} \text{ and } \psi_{wn}.$$

Using G-2 and G-3 and noting that β_1 and β_2 are small gives

$$\frac{\sin\alpha_2'}{\sin\alpha_1'} \approx \frac{\sin\alpha_2}{\sin\alpha_1}(1+\beta_1\cot\alpha_1 - \beta_2\cot\alpha_2) \qquad \text{G-25}$$

Substituting G-25 into G-23 and dropping the last term in G-25 (as it implies a correction to a correction) gives

$$\int_0^\ell \beta_2 U_1^2\, dz =$$

$$= \frac{2}{\pi}\int_0^\ell U_1\frac{\sin\alpha_2}{\sin\alpha_1}(1+\beta_1\cot\alpha_1)\sum_n\frac{\psi_n'}{n}\,dz =$$

$$= \frac{2}{\pi}\frac{\sin\alpha_2}{\sin\alpha_1}\left[\int_0^\ell U_1\sum\frac{\psi_n'}{n}dz + \cot\alpha_1\int_0^\ell U_1\beta_1\sum\frac{\psi_n'}{n}\,dz\right] \qquad \text{G-26}$$

Consider the term $\int_0^\ell U_1\sum\frac{\psi_n'}{n}\,dz$ in G26

Integrating the parts yields:

$$\int_0^{\ell} U_1 \sum \frac{\psi_n'}{n} dz = \left[U_1 \sum \frac{\psi_n}{n}\right]_0^{\ell} - \int_0^{\ell} \frac{dU_1}{dz} \sum \frac{\psi_n}{n} dz \qquad \text{G-27}$$

The first term on right hand side is zero because

$$\psi_n = 0 \quad \text{for } z = 0 \quad \text{and} \quad z = \ell$$

Substituting

$$\psi_n = \psi_{sn} + \psi_{wn} \qquad \text{G-28}$$

in G-27 gives

$$\int_0^{\ell} U_1 \sum_n \frac{\psi_n'}{n} dz = -\int_0^{\ell} \frac{dU_1}{dz} \sum_n \frac{\psi_{sn}}{n} dz - \int_0^{\ell} \frac{dU_1}{dz} \sum \frac{\psi_{wn}}{n} dz \qquad \text{G-29}$$

But from the expressions of the kinetic energy of the secondary flow, F-18, we see that

$$\int_0^{\ell} \frac{dU_1}{dz} \sum \frac{\psi_{sn}}{n} dz = -\frac{\pi}{4} \frac{D_{sw}}{\rho \varepsilon b} \qquad \text{G-30}$$

$$\int_0^{\ell} \frac{dU_1}{dz} \sum \frac{\psi_{wn}}{n} dz = -\frac{\pi}{2} \frac{D_w}{\rho \varepsilon b} \qquad \text{G-31}$$

where

D_w = kinetic energy of the secondary flow due to the wake flow only

D_{sw} = kinetic energy of the secondary flow due to the coupling of the skewed flow and wake flow.

The first term of G-26 then becomes:

$$\frac{1}{\rho \varepsilon b} \frac{\sin \alpha_2}{\sin \alpha_1} \left(D_w + \frac{D_{sw}}{2} \right) \qquad \text{G-32}$$

Consider the term $\int_0^\ell U_1 \beta_1 \sum \frac{\psi_n'}{n} dz$ in G26

Using the same arguments as when deriving G-17 we get

$$U_1 \beta_1 \approx \bar{U}_1 \beta_1 \qquad \text{G-33}$$

and so

$$\int_0^\ell U_1 \beta_1 \sum \frac{\psi_n'}{n} dz \approx \bar{U}_1 \int_0^\ell \beta_1 \sum \frac{\psi_n'}{n} dz \qquad \text{G-34}$$

Integrating by parts as earlier and noting that

$\psi_n = 0$ for $z = 0$ and $z = \ell$ and substituting G-28 yields

$$\bar{U}_1 \int_0^\ell \beta_1 \sum \frac{\psi_n'}{n} dz = - \bar{U}_1 \int_0^\ell \frac{d\beta_1}{dz} \sum \frac{\psi_{sn}}{n} dz - \bar{U}_1 \int_0^\ell \frac{d\beta_1}{dz} \sum \frac{\psi_{wn}}{n} dz \qquad \text{G-35}$$

But from F-18 and F-19

$$\int_0^\ell \frac{d\beta_1}{dz} \sum \frac{\psi_{sn}}{n} dz = - \frac{\pi D_s}{\rho b U_2} \qquad \text{G-36}$$

$$\int_0^\ell \frac{d\beta_1}{dz} \sum \frac{\psi_{wn}}{n} dz = - \frac{\pi}{2} \frac{D_{sw}}{\rho b U_2} \qquad \text{G-37}$$

where

D_s = kinetic energy of the secondary flow due to the skewed flow only

D_{sw} = kinetic energy of the secondary flow due to the coupling of the skewed flow and the wake flow

The second term of G-26 becomes:

$$\frac{2\bar{U}_1}{\rho b U_2}\,\frac{\sin\alpha_2\cot\alpha_1}{\sin\alpha_1}\,\left(D_s+\frac{D_{sw}}{2}\right) \qquad \text{G-38}$$

Substituting G-4 for the main stream conditions into G-38

$$\bar{U}_1\sin\alpha_1=\bar{U}_2\sin\alpha_2$$

$$\frac{\bar{U}_1}{U_2}\,\frac{\sin\alpha_2}{\sin^2\alpha_1}=\frac{\bar{U}_2}{U_2}\,\frac{\sin^2\alpha_2}{\sin^3\alpha_1}\approx\frac{\sin^2\alpha_2}{\sin^3\alpha_1} \qquad \text{G-39}$$

Which yields

$$\frac{2}{\rho b}\,\frac{\sin^2\alpha_2}{\sin^2\alpha_1}\cot\alpha_1\,\left(D_s+\frac{D_{sw}}{2}\right) \qquad \text{G-40}$$

The third term in G-9 then becomes:

$$(3)=s\rho\sin^2\alpha_1\int_0^{\ell}\beta_2 U_1^2\,dz=$$

$$=s\sin\alpha_1\left[\frac{D_w}{\varepsilon}+D_s\frac{2\sin\alpha_2}{\sin\alpha_1}\cot\alpha_1+\frac{D_{sw}}{2}\left(\frac{1}{\varepsilon}+\frac{2\sin\alpha_2}{\sin\alpha_1}\cot\alpha_1\right)\right] \qquad \text{G-41}$$

Changing the sign for T and rearranging, G-9 finally becomes:

$$C_T=\frac{T}{\rho\frac{\bar{U}_1^2}{2}s\ell}=$$

$$=2\sin^2\alpha_1(\cot\alpha_1-\cot\alpha_2)\left(1-\frac{\delta^*+\theta}{\ell}\right)+\left[1-2\cot\alpha_1(\cot\alpha_1-\cot\alpha_2)\right]\frac{\delta}{\ell}A_0-$$

$$-\frac{\sin\alpha_1}{\rho\frac{\bar{U}_1^2}{2}s\ell}\left[\frac{D_w}{\varepsilon}+D_s\frac{2\sin\alpha_2\cos\alpha_1}{\sin^2\alpha_1}+\frac{D_{sw}}{2}\left(\frac{1}{\varepsilon}+2\frac{\sin\alpha_2\cos\alpha_1}{\sin^2\alpha_1}\right)\right] \qquad \text{G-42}$$

where

C_T = tangential pressure coefficient.

The expression for C_T may be interpreted as follows:

1) $2\sin^2\alpha_1 (\cot\alpha_1 - \cot\alpha_2)$ is the tangential pressure coefficient if the flow is uniform over all the span,

2) $-\frac{\delta^*+\theta}{\ell} 2\sin^2\alpha_1 (\cot\alpha_1 - \cot\alpha_2)$ is a reduction due to the decreased mass flow in the wake,

3) $\frac{\delta}{\ell} A_o$ is an increase due to the increased flow angle of attack,

4) $-2\cot\alpha_1 (\cot\alpha_1 - \cot\alpha_2) \frac{\delta}{\ell} A_o$ is a reduction due to the decreased mass flow in the skewed flow,

5) $-\frac{\sin\alpha_1}{\rho \frac{\bar{U}_1^2}{2} s\ell} \frac{D_w}{\varepsilon}$ is a reduction due to the secondary flow caused by the wake flow only,

6) $-\frac{\sin\alpha_1}{\rho \frac{\bar{U}_1^2}{2} s\ell} D_s \frac{2\sin\alpha_2 \cos\alpha_1}{\sin^2\alpha_1}$ same as 5 but caused by the skewed flow only, and

7) $-\frac{\sin\alpha_1}{\rho \frac{\bar{U}_1^2}{2} s\ell} \frac{D_{sw}}{2} \left(\frac{1}{\varepsilon} + 2\frac{\sin\alpha_2 \cos\alpha_1}{\sin^2\alpha_1}\right)$ is an increase caused by the interaction of the wake flow and the skewed flow.

G.2 Wake Flow

In this case G-42 reduces to

$$C_T = 2\sin^2\alpha_1 (\cot\alpha_1 - \cot\alpha_2)\left(1 - \frac{\delta^*+\theta}{\ell}\right) - \frac{\sin\alpha_1}{\rho \frac{\bar{U}_1^2}{2} s\ell} \frac{D_w}{\varepsilon} \qquad \text{G-43}$$

Numerical Values

The actual values for this flow are listed below:

$s = 4.445"$

$c = 4.500"$

$l = 8.000"$

$\delta = 1.130"$

$a = 0.137$

$\alpha_1 = 45.0°$

$\alpha_2 = 64.4°$

In the calculations formula 4-8 was used instead of 4-1 and so 2ε in the formula G-43 was replaced by

$$\left(1+\frac{\sin\alpha_1}{\sin\alpha_2}\right)\frac{\cos\alpha_1-\cos\alpha_2}{\sin\alpha_2}$$

The result of the calculation is given in section 4.4.2.

6.3 Skewed Flow

In this case G-42 becomes:

$$C_T = 2\sin^2\alpha_1\,(\cot\alpha_1-\cot\alpha_2)\left(1-2\,\frac{\delta^*+\theta}{\ell}\right)+\left[1-2\cot\alpha_1\,(\cot\alpha_1-\cot\alpha_2)\right]\frac{\delta}{\ell}A_o -$$

$$-\frac{\sin\alpha_1}{\rho\frac{\bar{U}_1^2}{2}s\ell}\left[\frac{D_w}{\varepsilon}+D_s\,\frac{2\sin\alpha_2\cot\alpha_1}{\sin^2\alpha_1}+\frac{D_{sw}}{2}\left(\frac{1}{\varepsilon}+2\,\frac{\sin\alpha_2\cot\alpha_1}{\sin^2\alpha_1}\right)\right] \qquad \text{G-44}$$

The only difference from G-42 being the factor of 2 in front of the term $\frac{\delta^* + \theta}{l}$. This comes from the fact that in this case the whole wake is inside the investigated region.

Numerical Values

The actual values for this flow are listed below

s	= 4.445"	δ_4	= 0.500"		
c	= 4.500"	a	= 0.070		
l	= 8.000"	α_1	= 45.0°		
δ	= 2.250"	α_2	= 68.6°	A_3	= -0.02402
δ_1	= 0.500"	A_o	= 0.15449	A_4	= -0.01122
δ_2	= 1.500"	A_1	= 0.19478		
δ_3	= 1.000"	A_2	= 0.02731		

In the calculation, formula 4-8 was used instead of 4-1, and so 2ε in formula G-44 was replaced by $\left(1 + \frac{\sin\alpha_1}{\sin\alpha_2}\right) \frac{\cos\alpha_1 - \cos\alpha_2}{\sin\alpha_2}$. The result of the calculations is given in section 5.4.2.

G.4 Skewed Flow

In this case formula G-42 is applicable without modification.

Numerical Values

The actual values for this flow are listed below:

s	= 4.445"	A_2	= -0.04920
c	= 4.500"	A_3	= -0.00646
l	= 8.000"	A_4	= 0.01274
δ	= δ_1 = 1.750"	B_0	= 0.21133
α_1	= 45.0°	B_1	= 0.18000
α_2	= 66.0°	B_2	= -0.06560
A_0	= 0.22685	B_3	= -0.01665
A_1	= 0.19684	B_4	= 0.01762

Formula 4-8 was used instead of 4-1 to express the streamwise component of the distributed vorticity vector and so $2\,\xi$ was replaced by

$$\left(1+\frac{\sin\alpha_1}{\sin\alpha_2}\right)\frac{\cos\alpha_1-\cos\alpha_2}{\sin\alpha_2}$$ in formula G-42.

The result of the calculations is given in section 6.4.2.

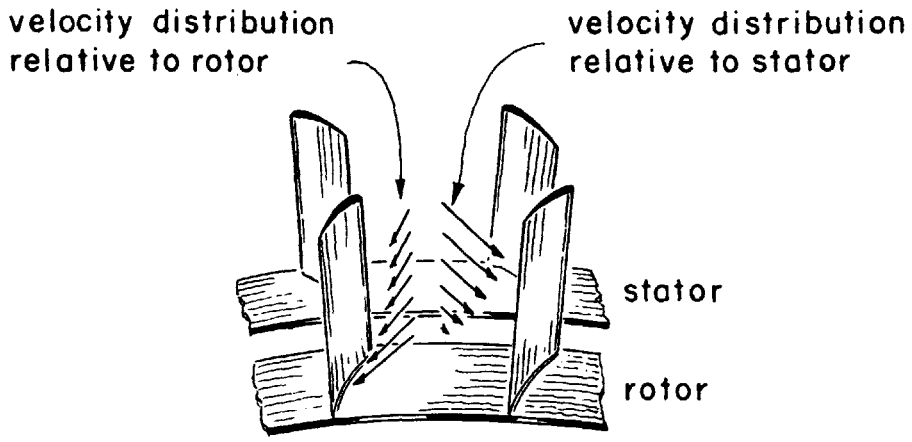

(A) Stator blades with shrouding

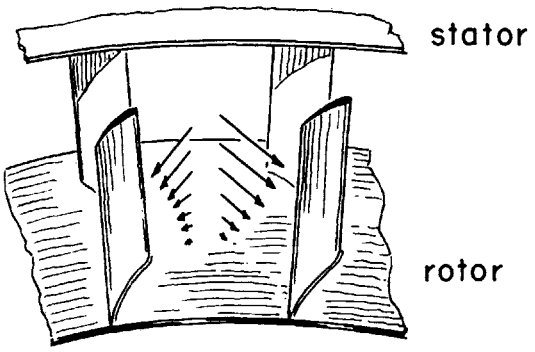

(B) Stator blades without shrouding

FIG. 1 INLET CONDITIONS AT THE HUB OF A COMPRESSOR ROTOR BLADE ROW

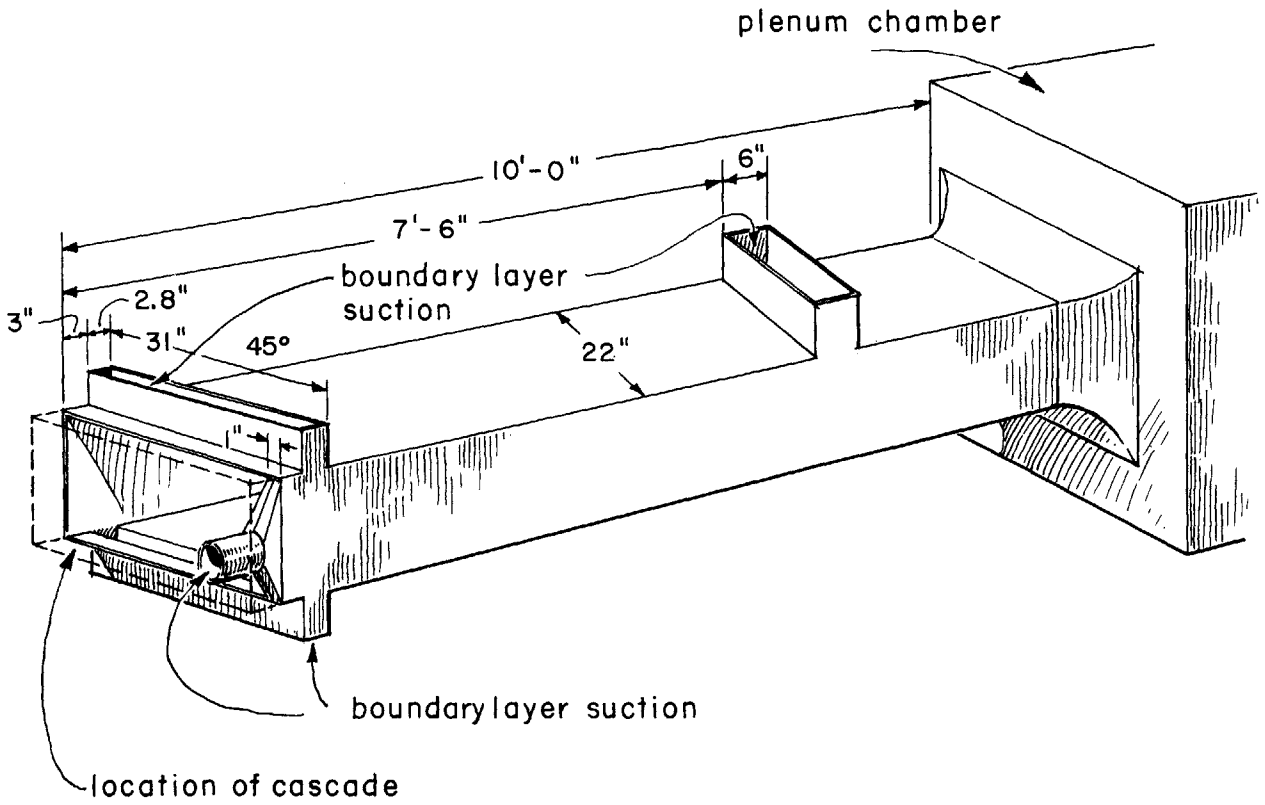

FIG. 2 SCHEMATIC OF THE WIND TUNNEL

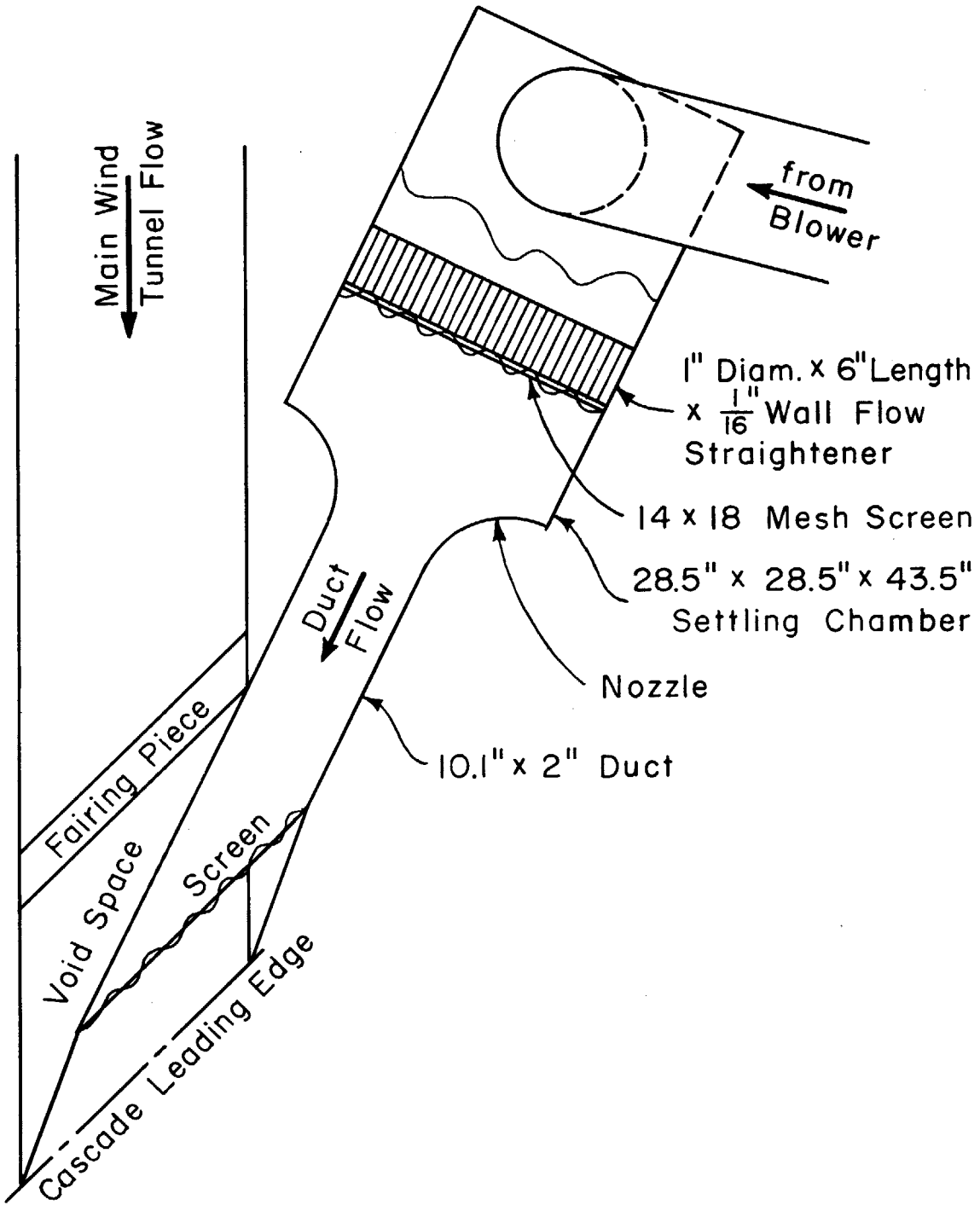

FIG. 3 DUCT SYSTEM SCHEMATIC

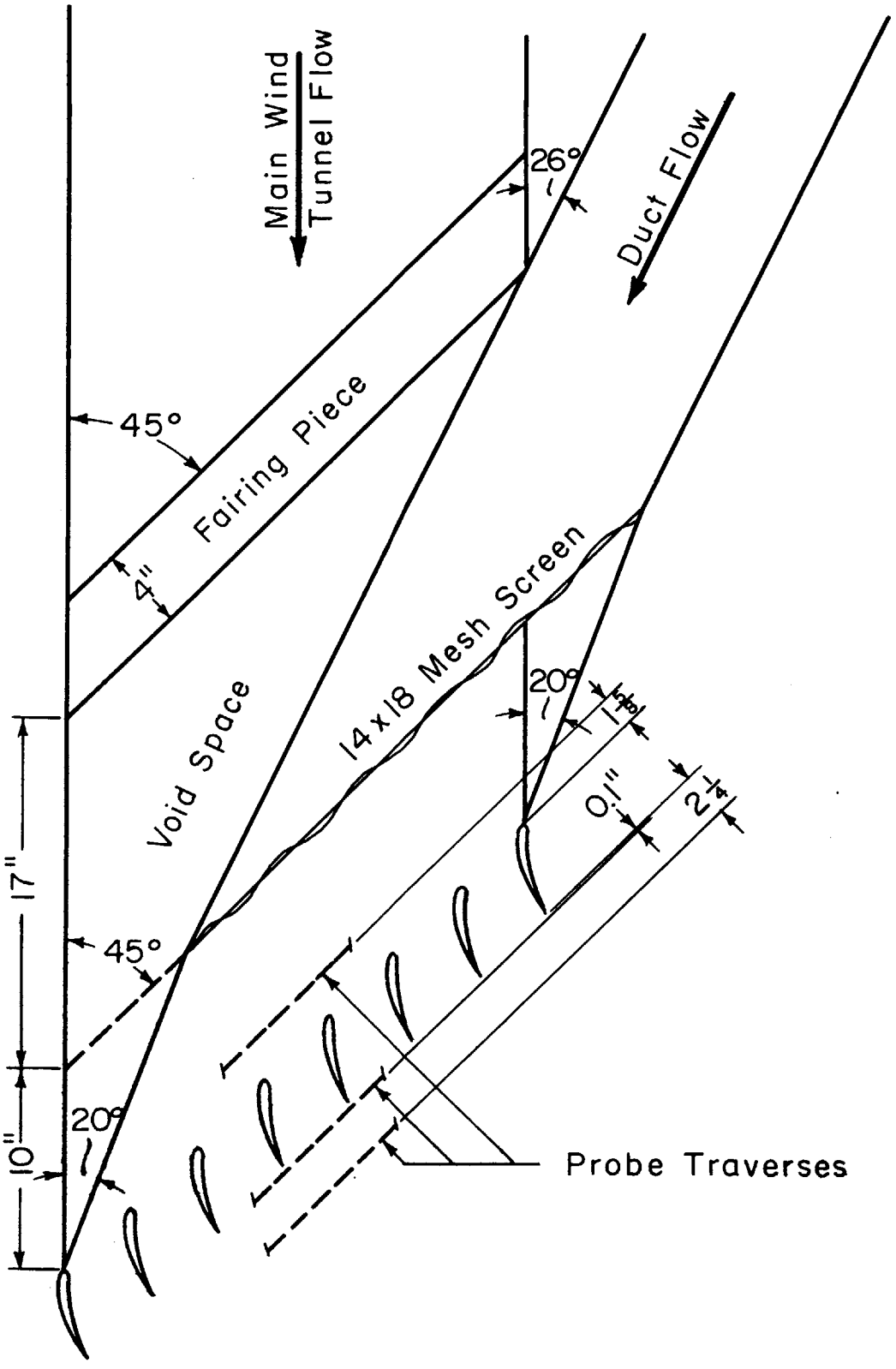

FIG. 4 DUCT SECTION

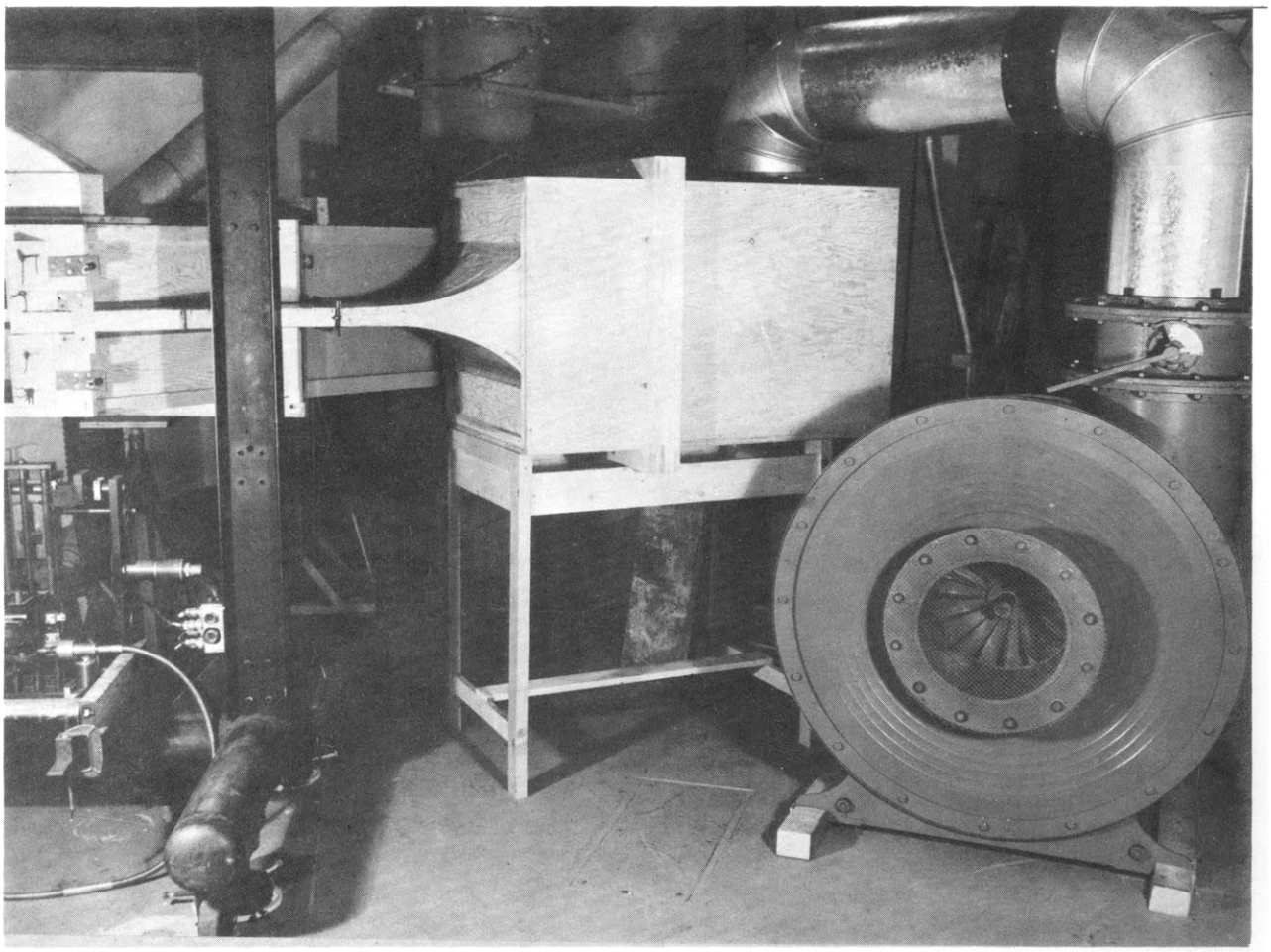

FIGURE 5 DUCT SYSTEM.

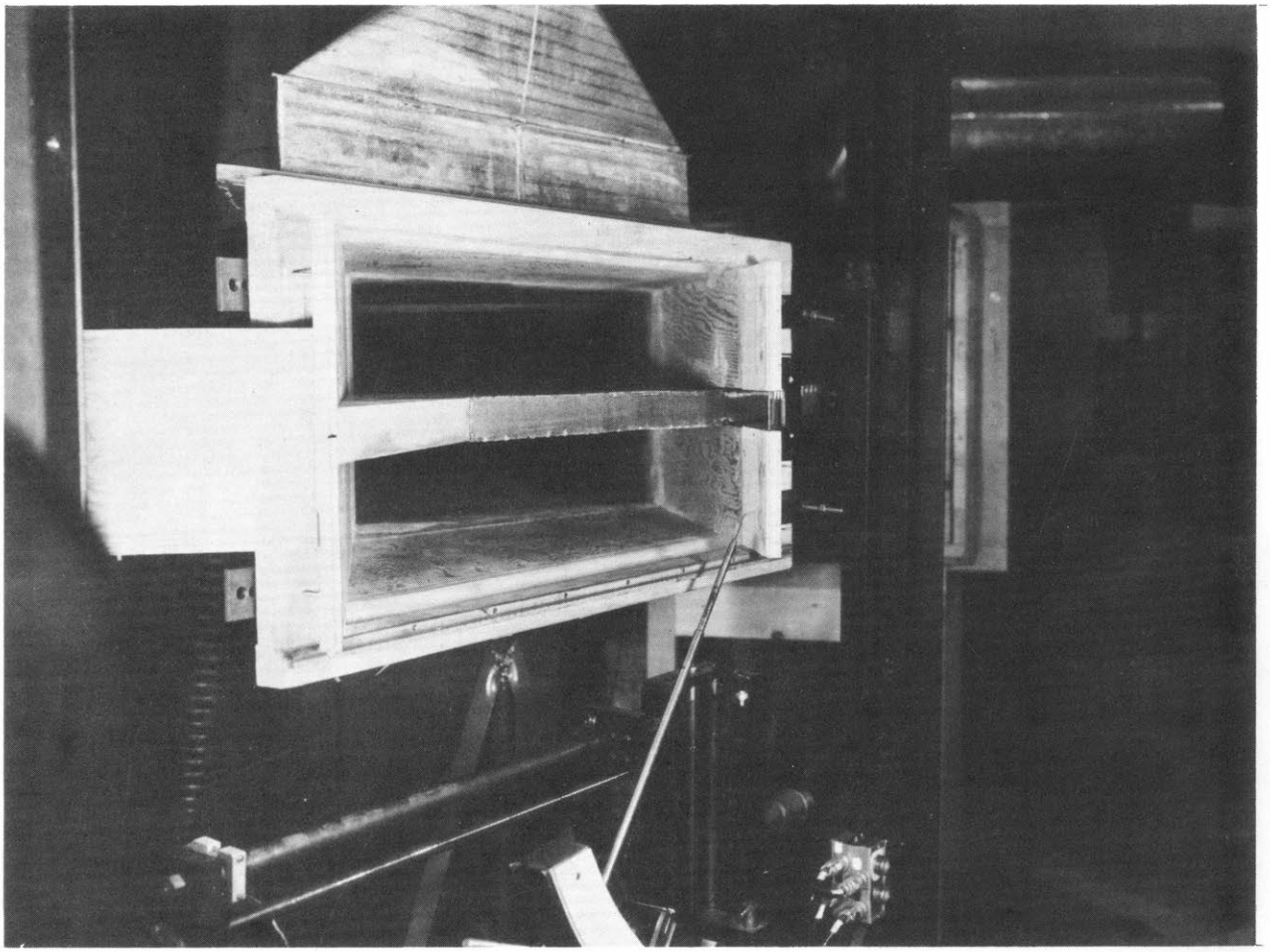

FIGURE 6 DUCT OUTLET.

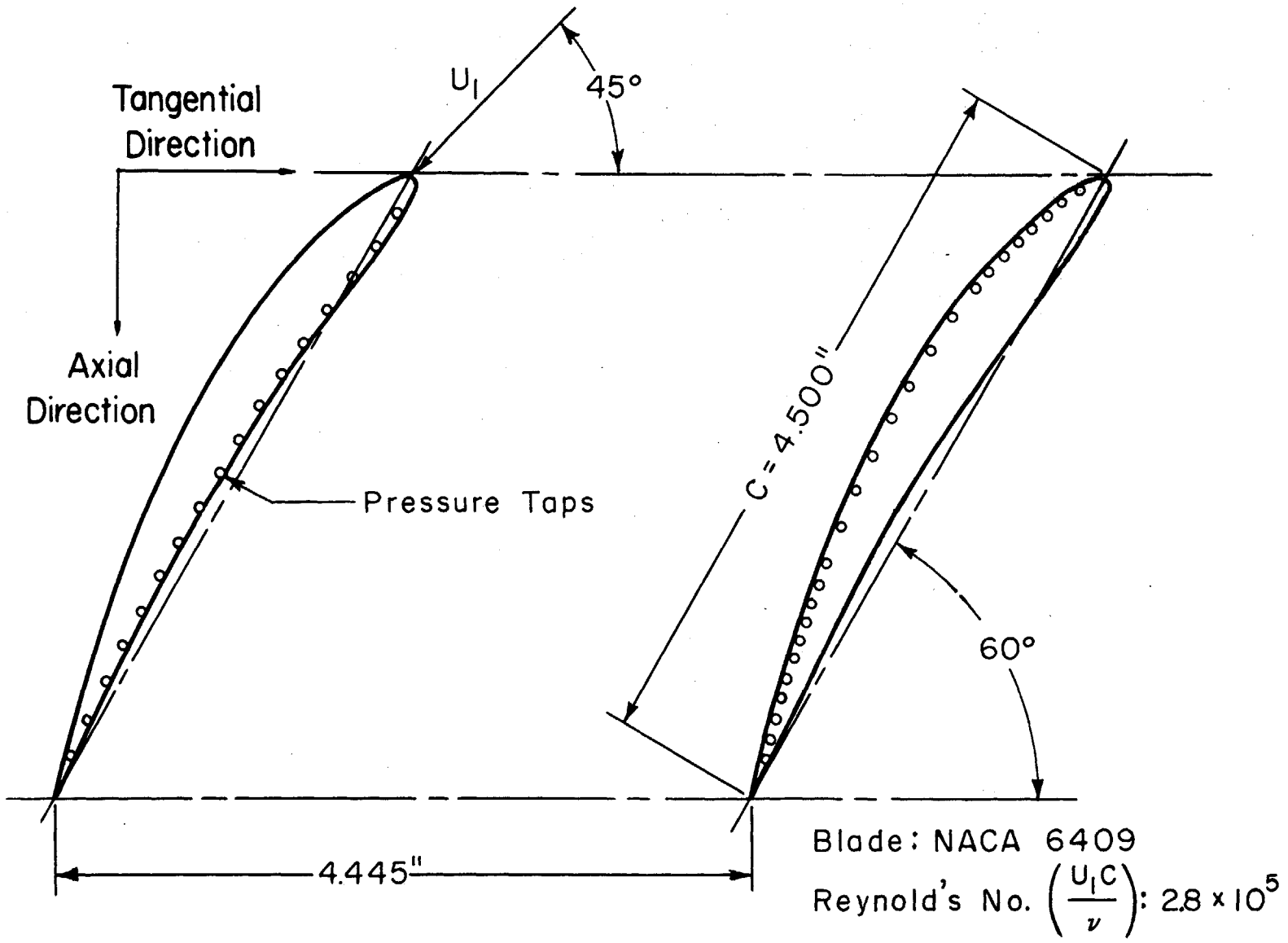

FIG. 7 CASCADE GEOMETRY

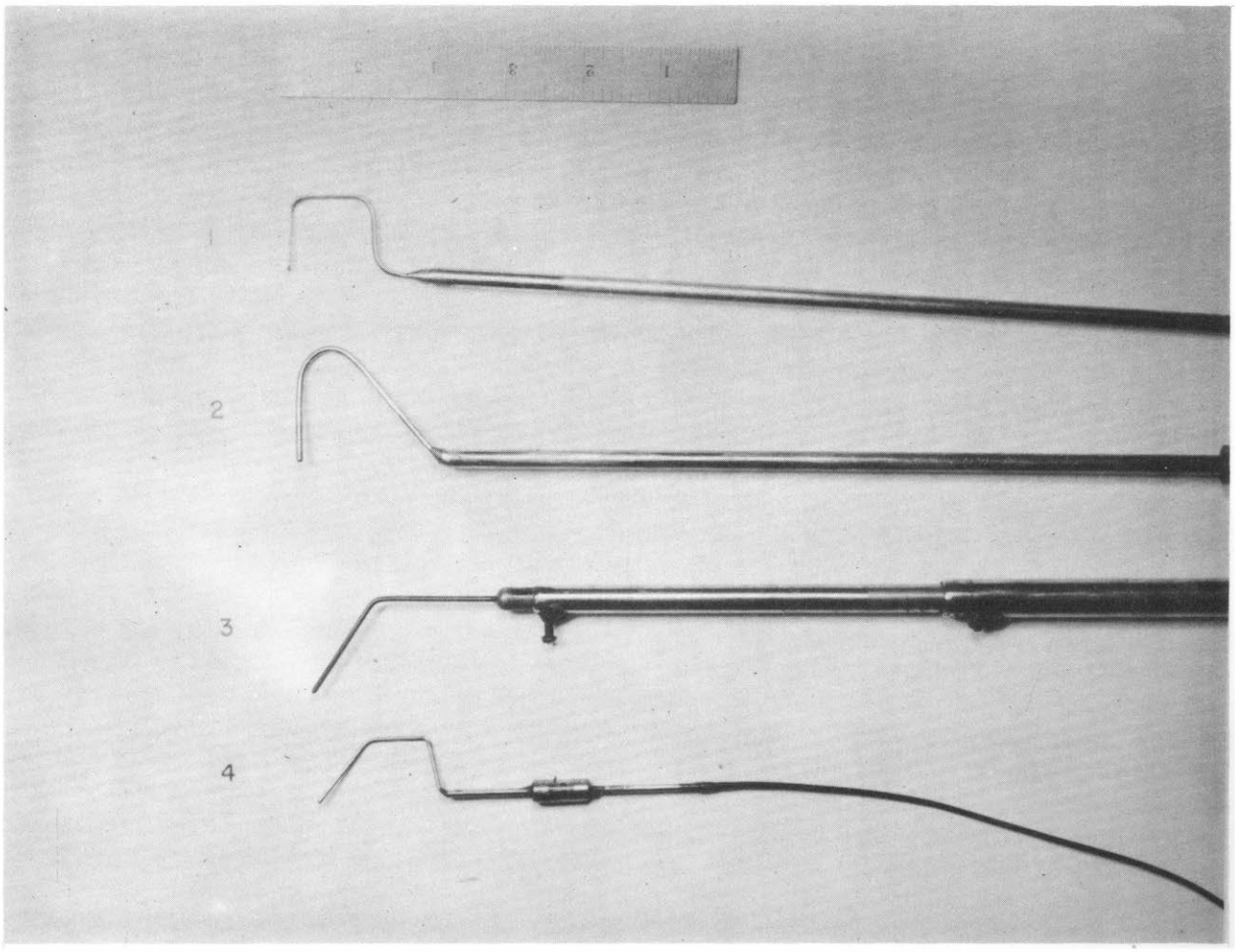

FIGURE 8 PROBES. UPSTREAM MEASURING PROBES:

1. 3-HOLE PROBE.
2. STREAM PRESSURE PROBE.

DOWNSTREAM MEASURING PROBES:

3. 5-HOLE PROBE.
4. STREAM PRESSURE PROBE.

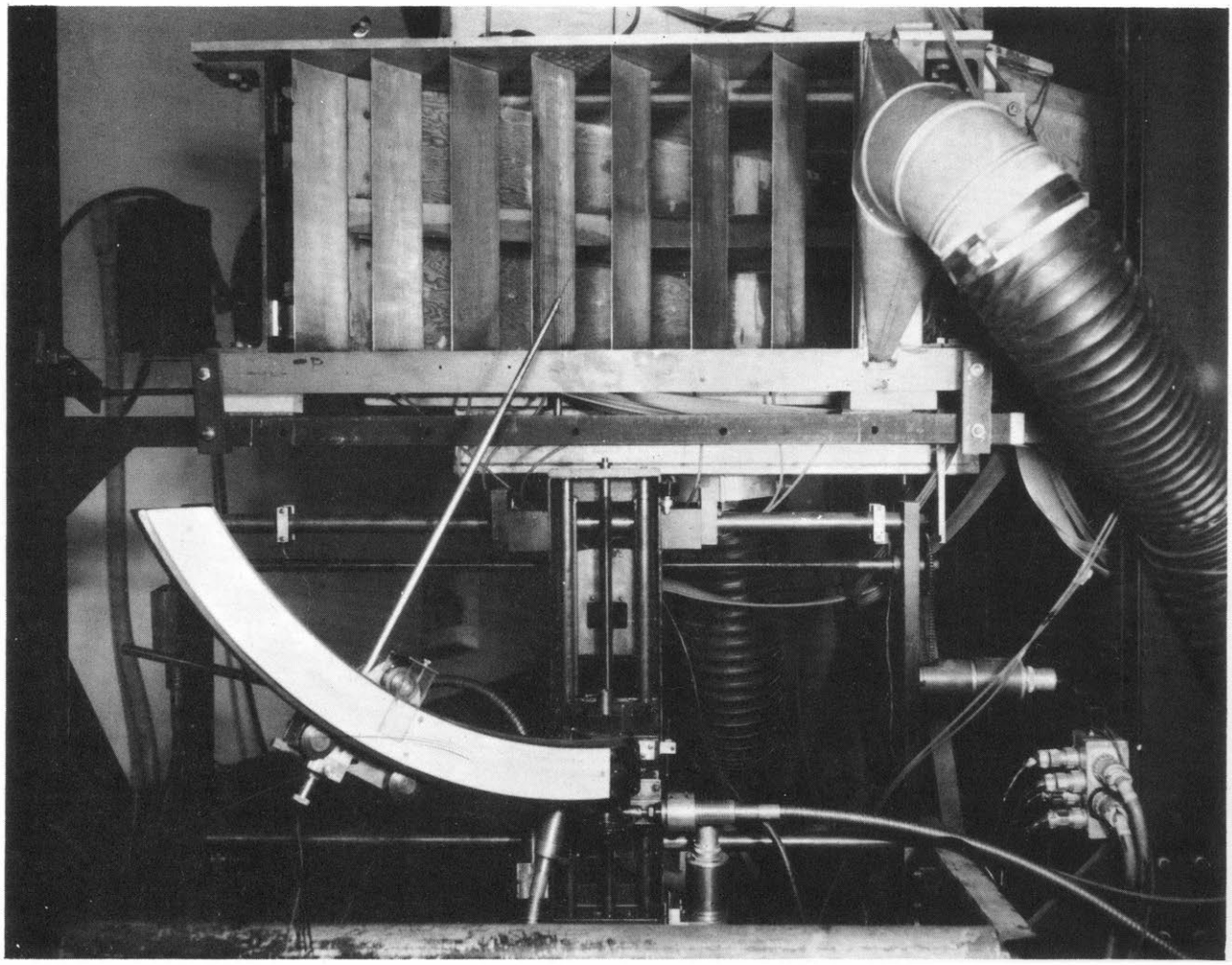

FIGURE 9 DOWNSTREAM TRAVERSING RIG.

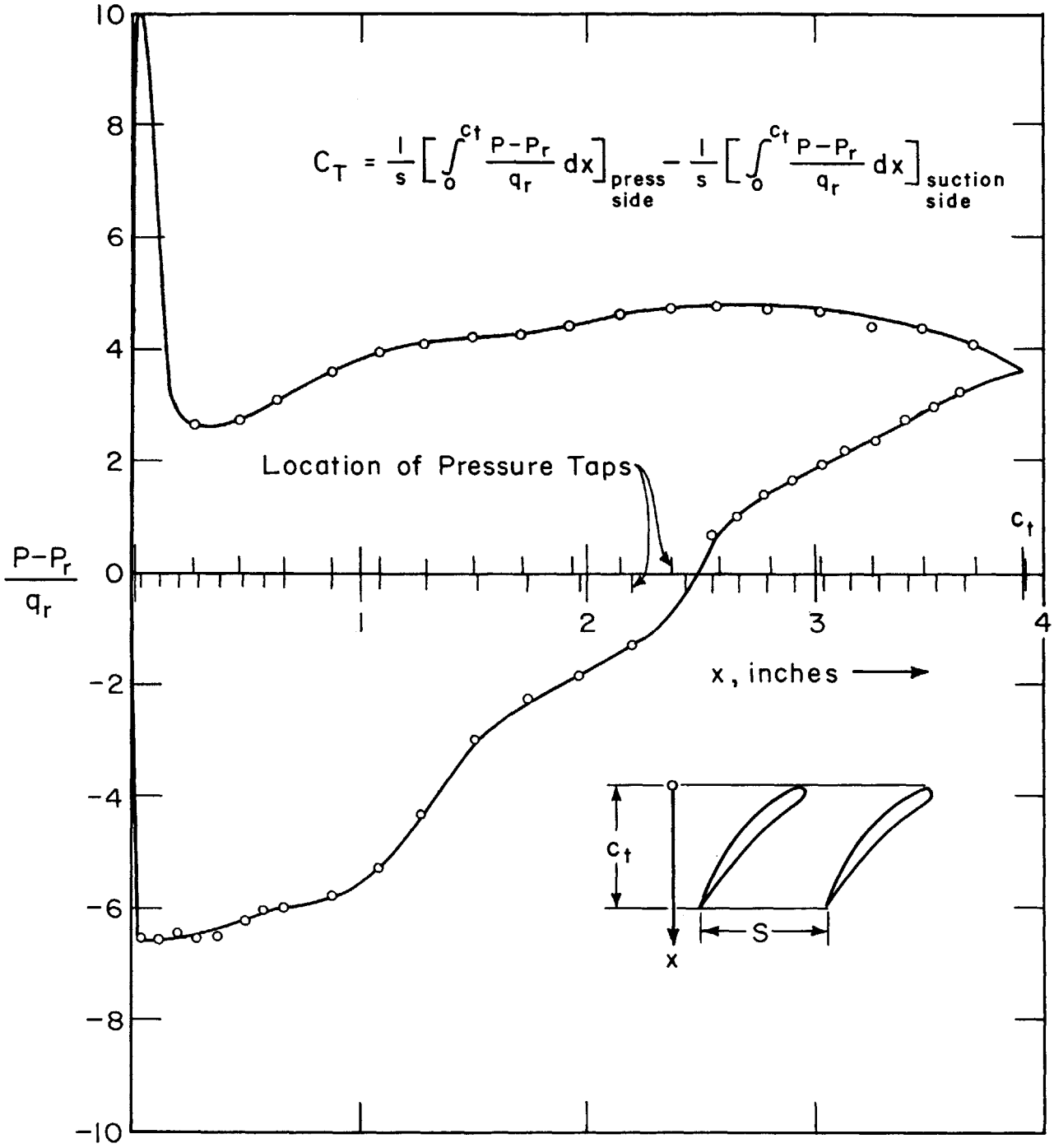

FIG. 10 TWO-DIMENSIONAL CASCADE FLOW PROJECTED STREAM PRESSURE DISTRIBUTION ON THE BLADE SURFACES

LOCATION: $\frac{1}{8}$" from Midspan

Tangential Pressure Coefficient $C_T = 0.508$

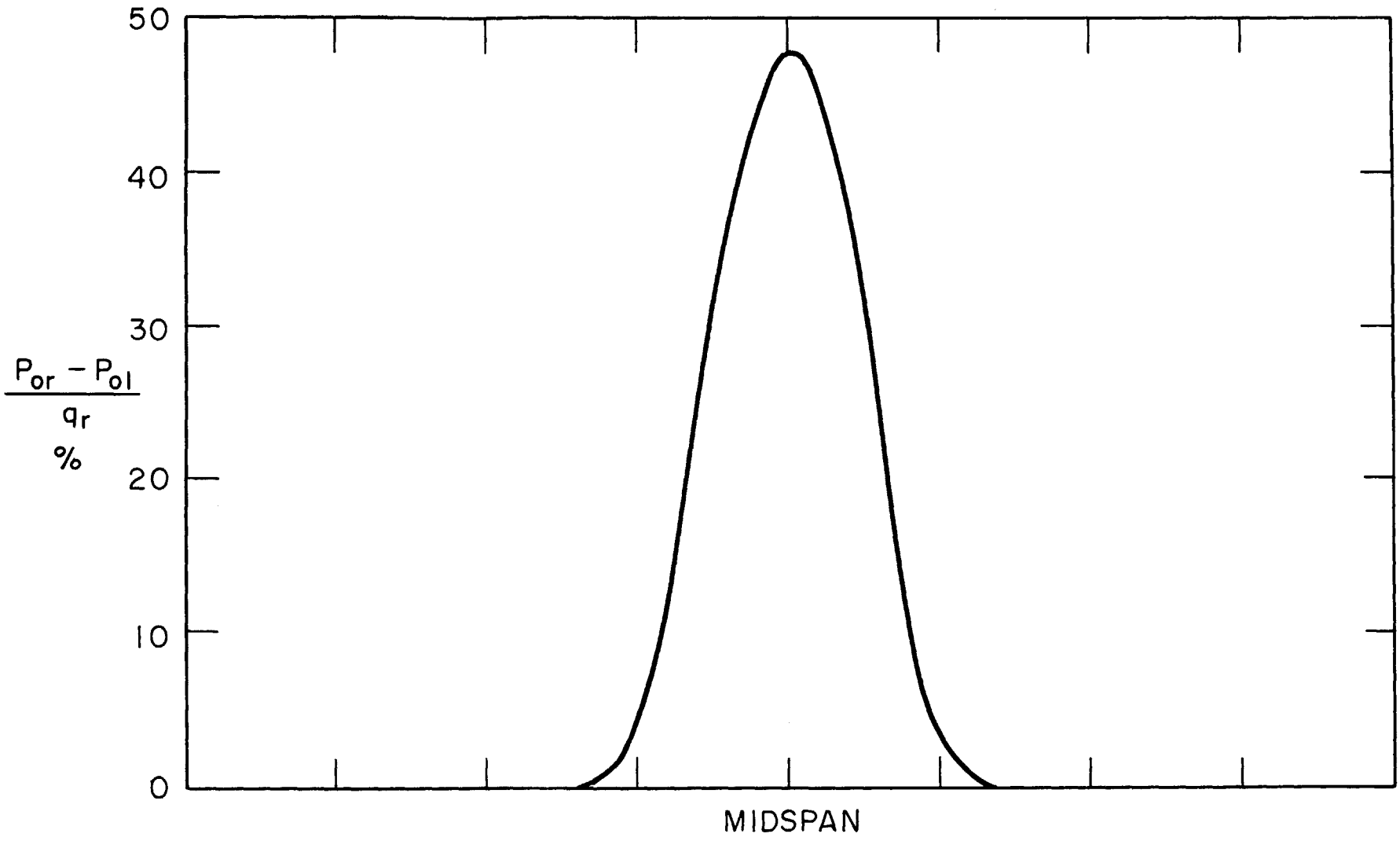

FIG. 11 WAKEFLOW INLET STAGNATION PRESSURE PROFILE
Scale Divisions Shown are in Inches

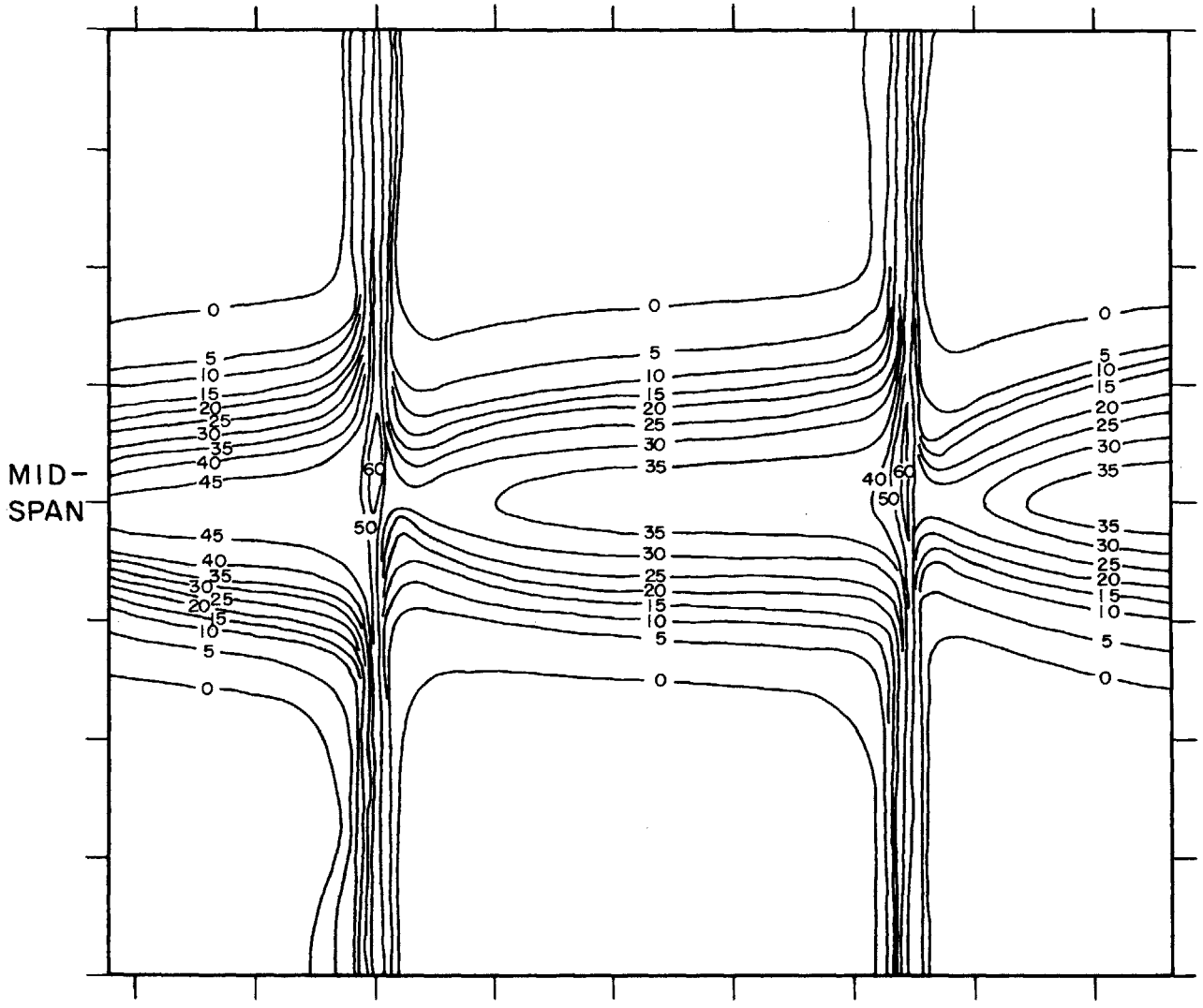

FIG. 12 WAKEFLOW CONTOURS OF CONSTANT STAGNATION PRESSURE

AXIAL POSITION : 0.1" behind the Cascade

Numbers on Contours Indicate Constant $\frac{P_{or} - P_{o2}}{q_r}$ in Percentage

Scale Divisions Shown are in Inches

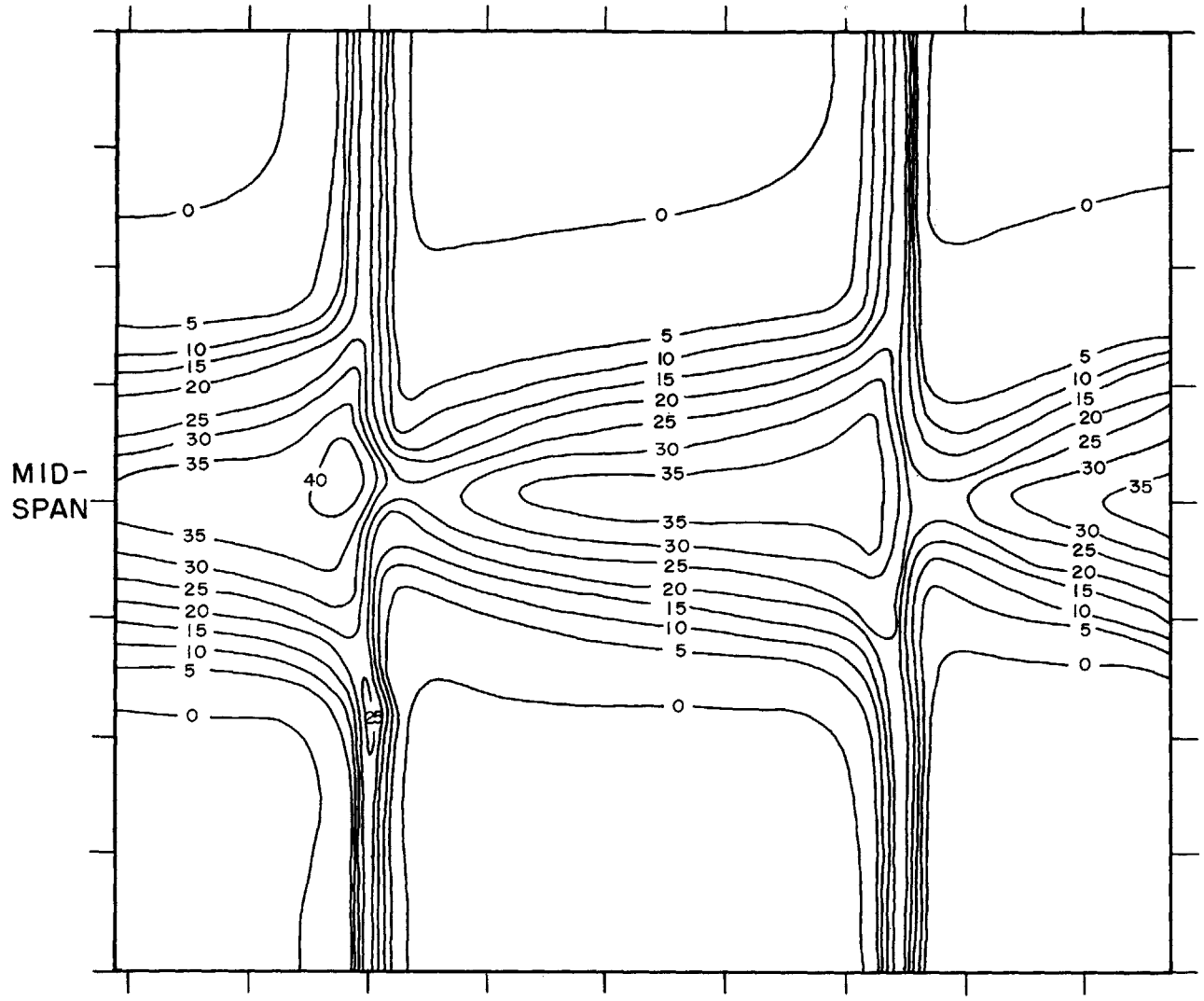

FIG. 13 WAKEFLOW CONTOURS OF CONSTANT STAGNATION PRESSURE

AXIAL POSITION: 2.25" behind the Cascade

Numbers on Contours Indicate Constant $\frac{P_{or} - P_{o2}}{q_r}$ in Percentage

Scale Divisions Shown are in Inches

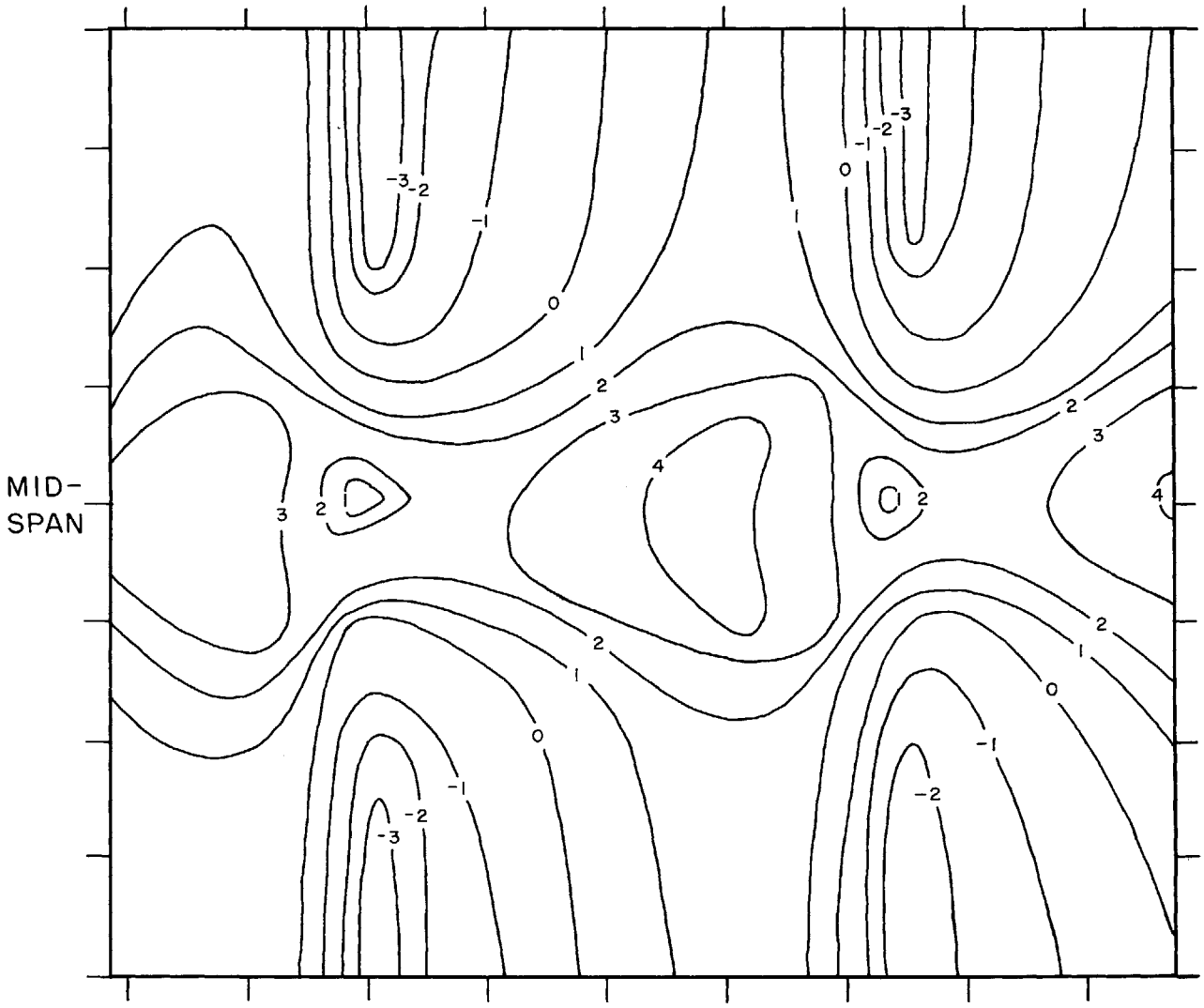

FIG. 14 WAKEFLOW CONTOURS OF CONSTANT STREAM PRESSURE

AXIAL POSITION: 0.35" behind the Cascade

Numbers on Contours Indicate Constant $\frac{P_{atm} - P}{q_r}$

Scale Divisions Shown are in Inches

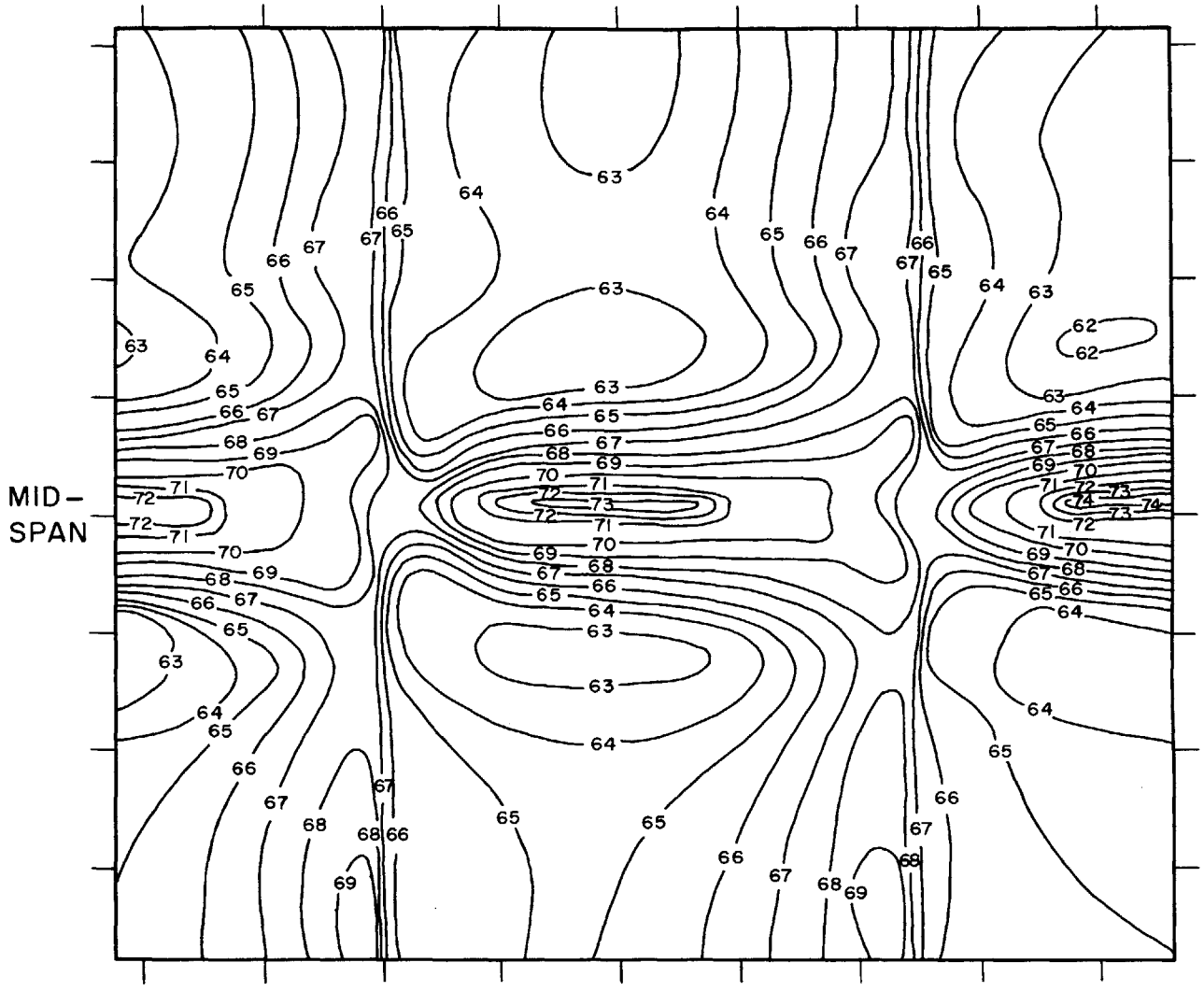

FIG. 15 WAKEFLOW CONTOURS OF CONSTANT TRANSVERSE FLOW ANGLE

AXIAL POSITION: 0.1" behind the Cascade

Numbers on Contours Indicate Constant Transverse Flow Angles Measured from Tangential Direction

Scale Divisions Shown are in Inches

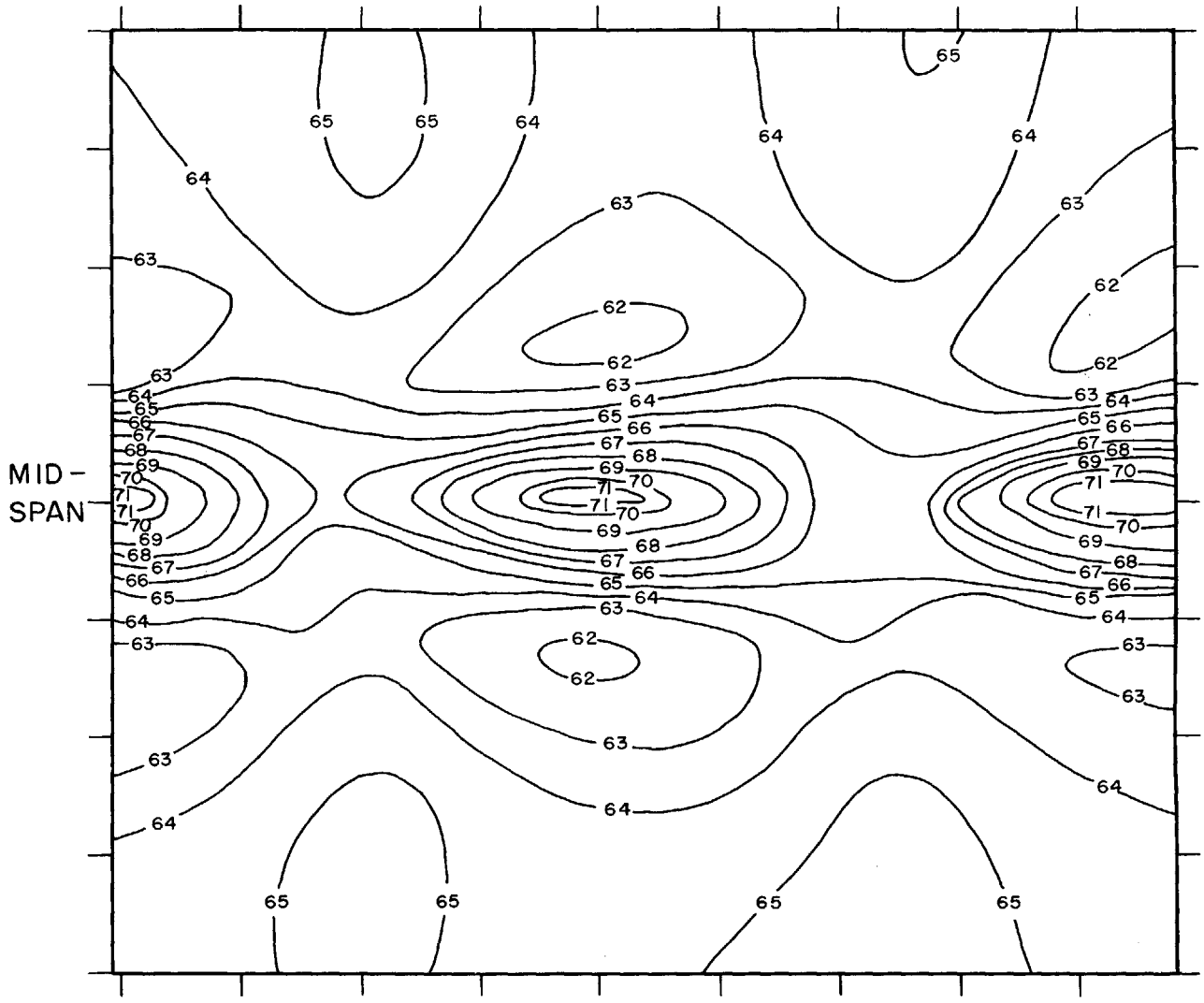

FIG. 16 WAKEFLOW CONTOURS OF CONSTANT TRANSVERSE FLOW ANGLE

AXIAL POSITION : 2.25" behind the Cascade

Numbers on Contours Indicate Constant Transverse Flow Angles Measured from Tangential Direction

Scale Divisions Shown are in Inches

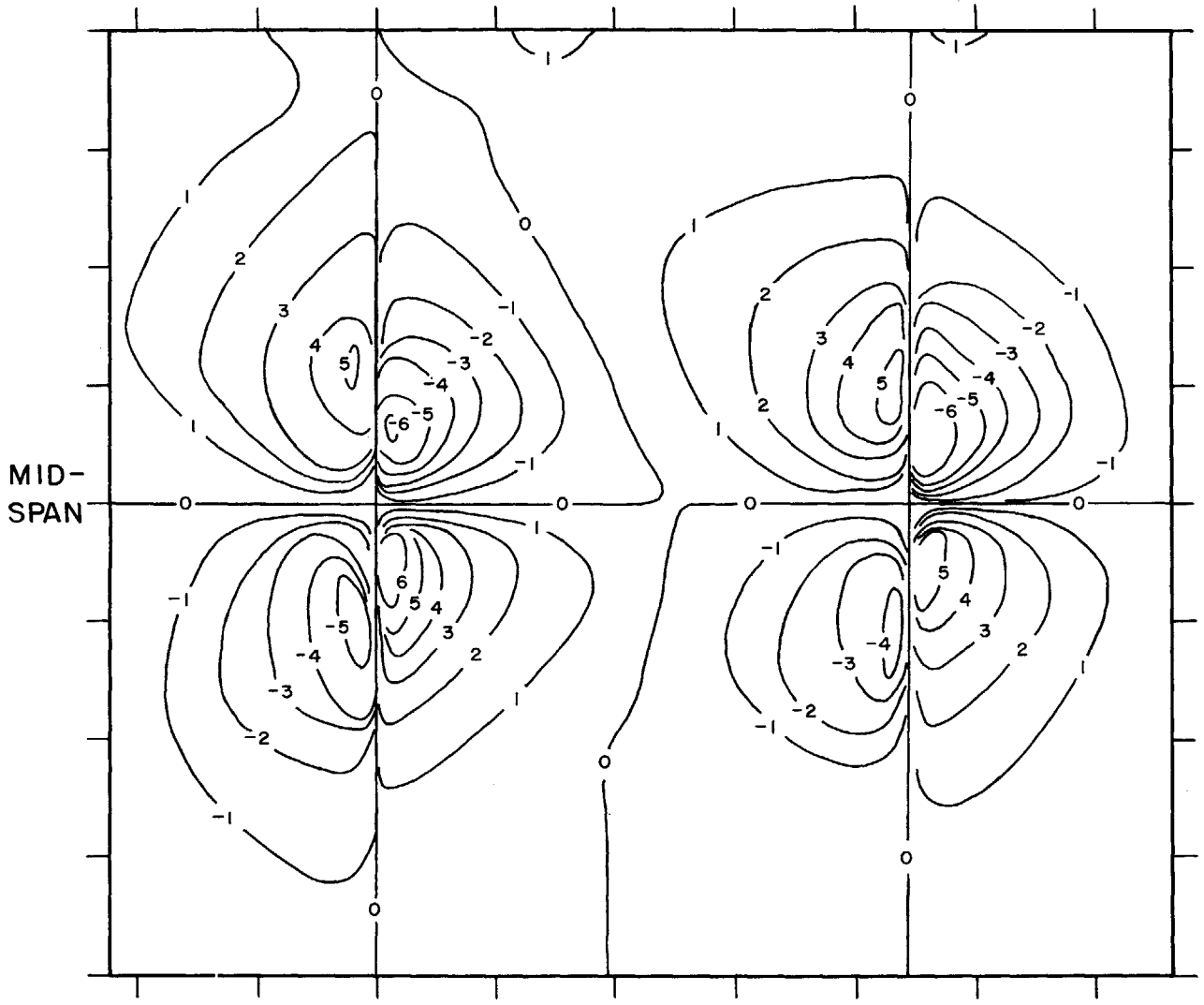

FIG. 17 WAKEFLOW CONTOURS OF CONSTANT SPANWISE FLOW DEVIATION ANGLES

AXIAL POSITION : 0.1" behind the Cascade

Numbers on Contours Indicate Constant Spanwise Flow Deviation Angles

Positive Numbers Indicate Flow Towards the Top of the Cascade

Scale Divisions Shown are in Inches

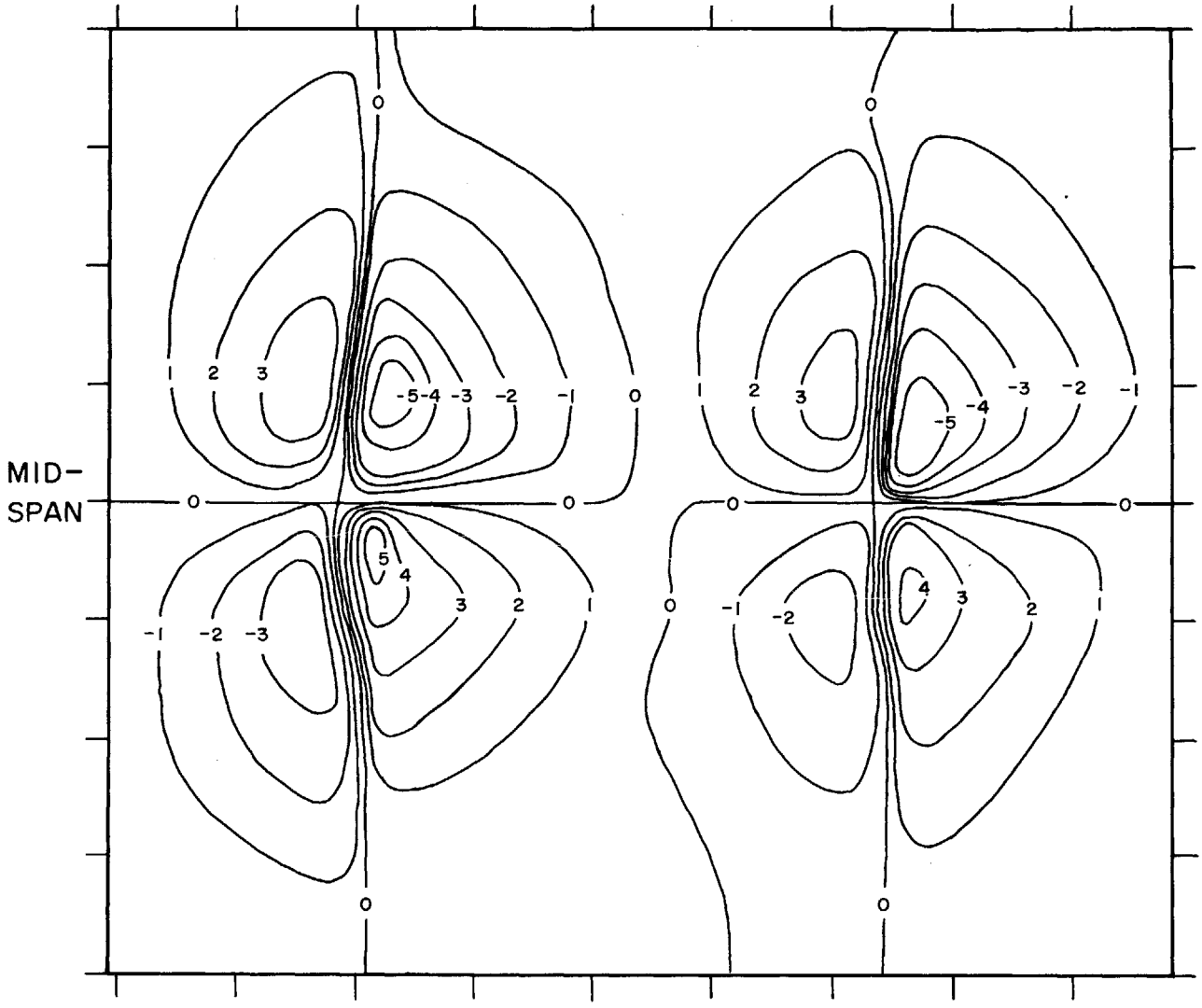

FIG. 18 WAKEFLOW CONTOURS OF CONSTANT SPANWISE FLOW DEVIATION ANGLES

AXIAL POSITION: 2.25" behind the Cascade

Numbers on Contours Indicate Constant Spanwise Flow Deviation Angles

Positive Numbers Indicate Flow Towards the Top of the Cascade

Scale Divisions Shown are in Inches

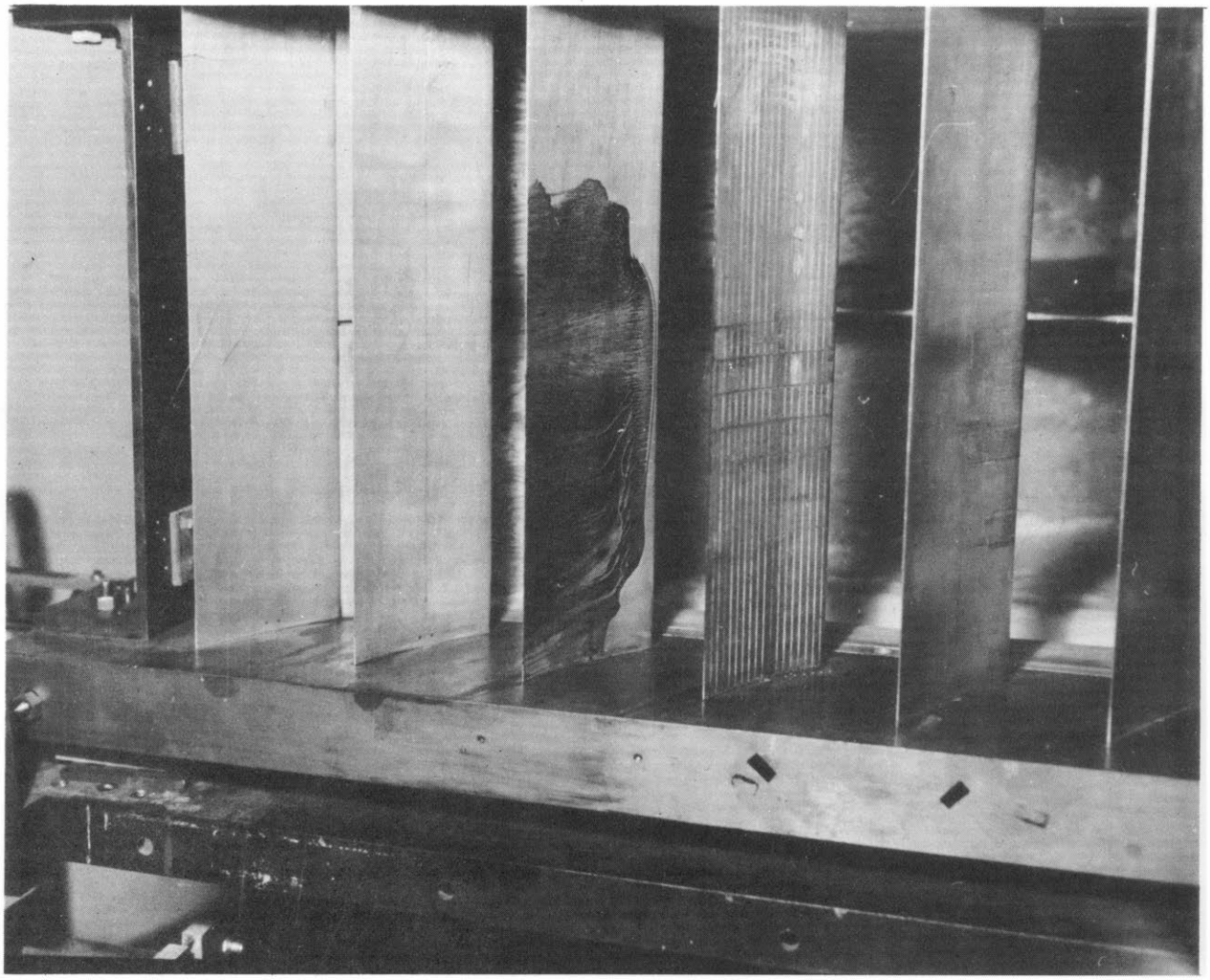

FIGURE 19 WAKE FLOW. STREAMLINE TRACES IN CARBON BLACK ON THE BLADE PRESSURE SIDE.

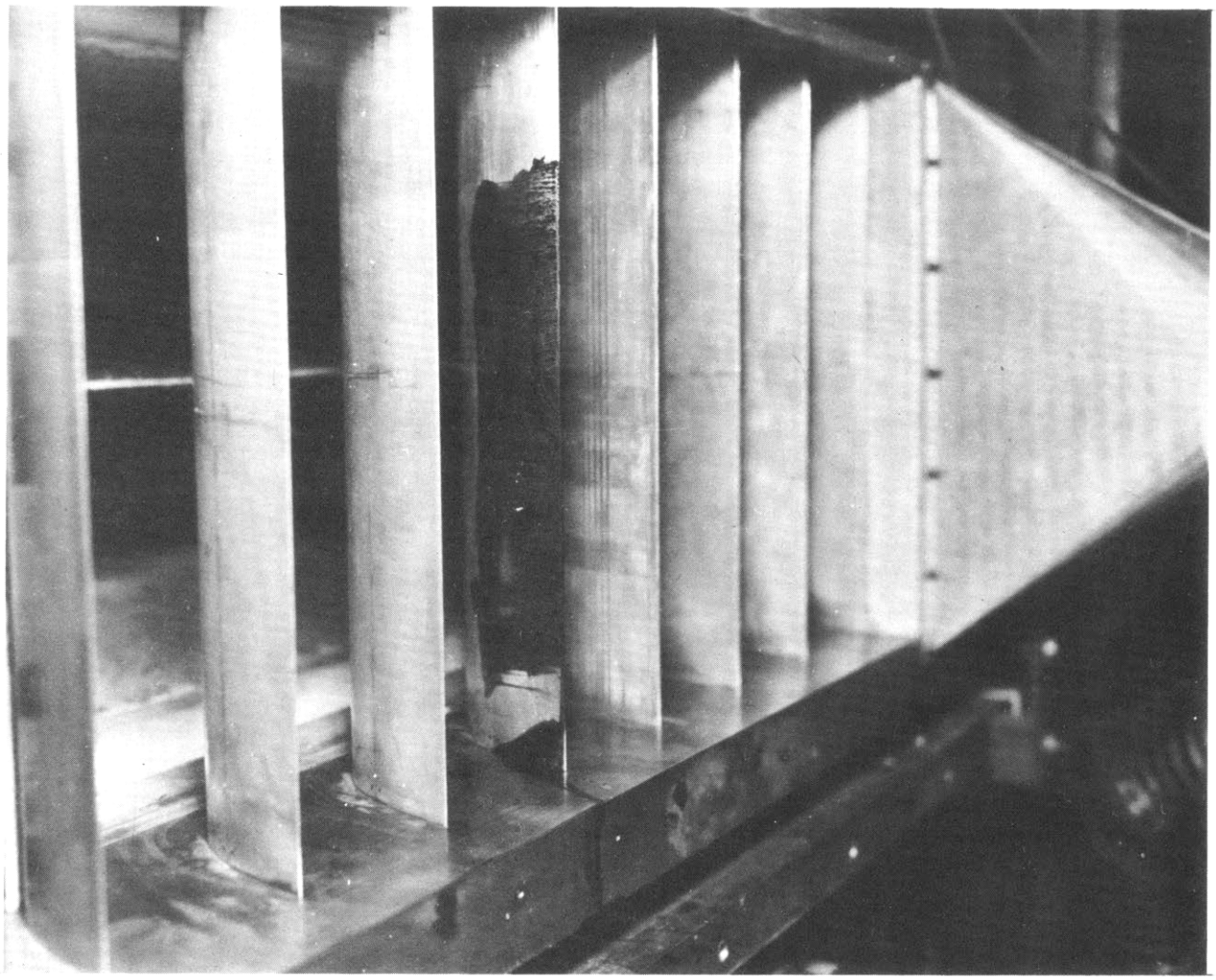

FIGURE 20 WAKE FLOW. STREAMLINE TRACES IN CARBON BLACK ON THE BLADE SUCTION SIDE.

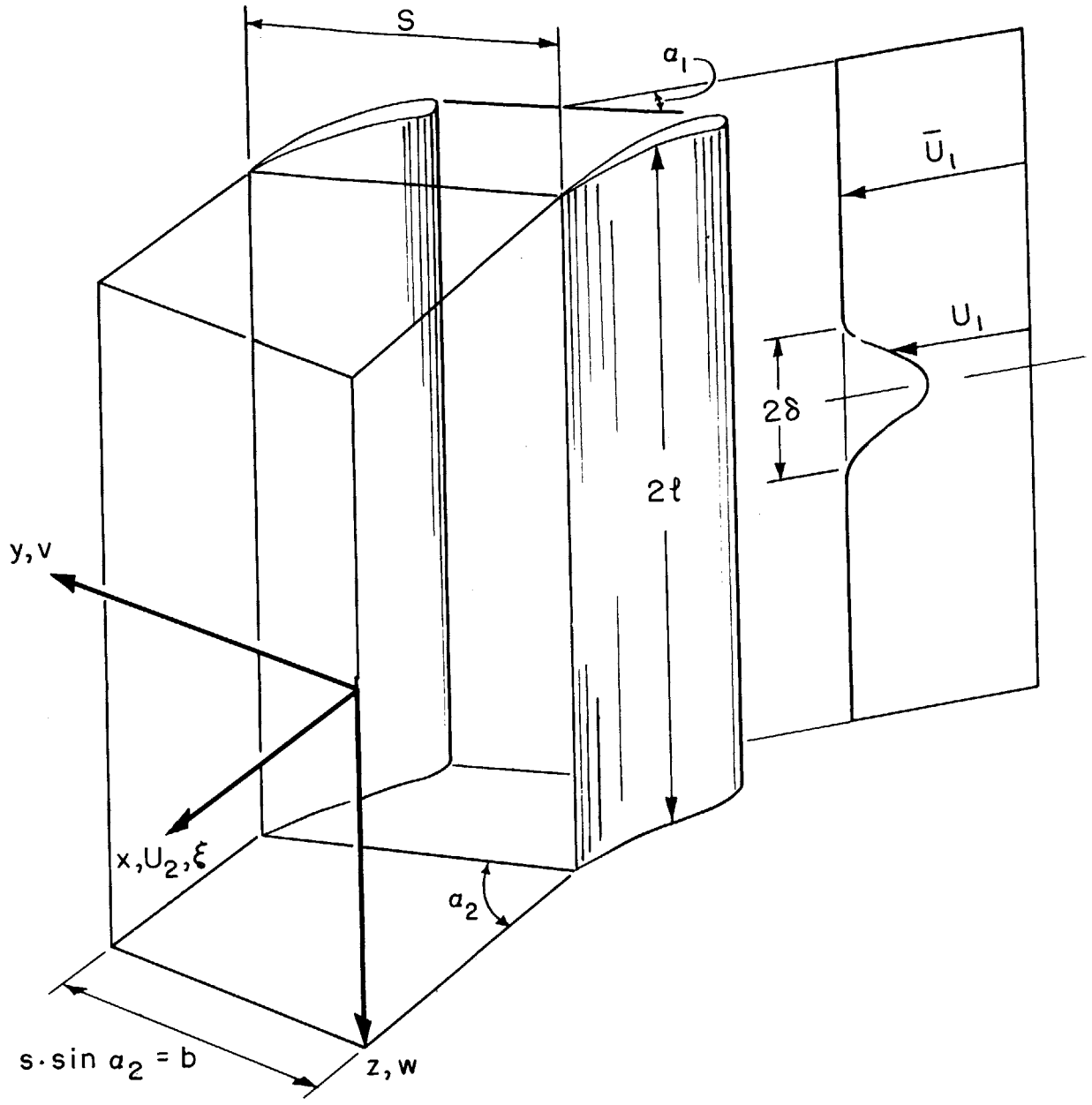

FIG. 21 WAKE FLOW - DIAGRAM OF NOTATIONS

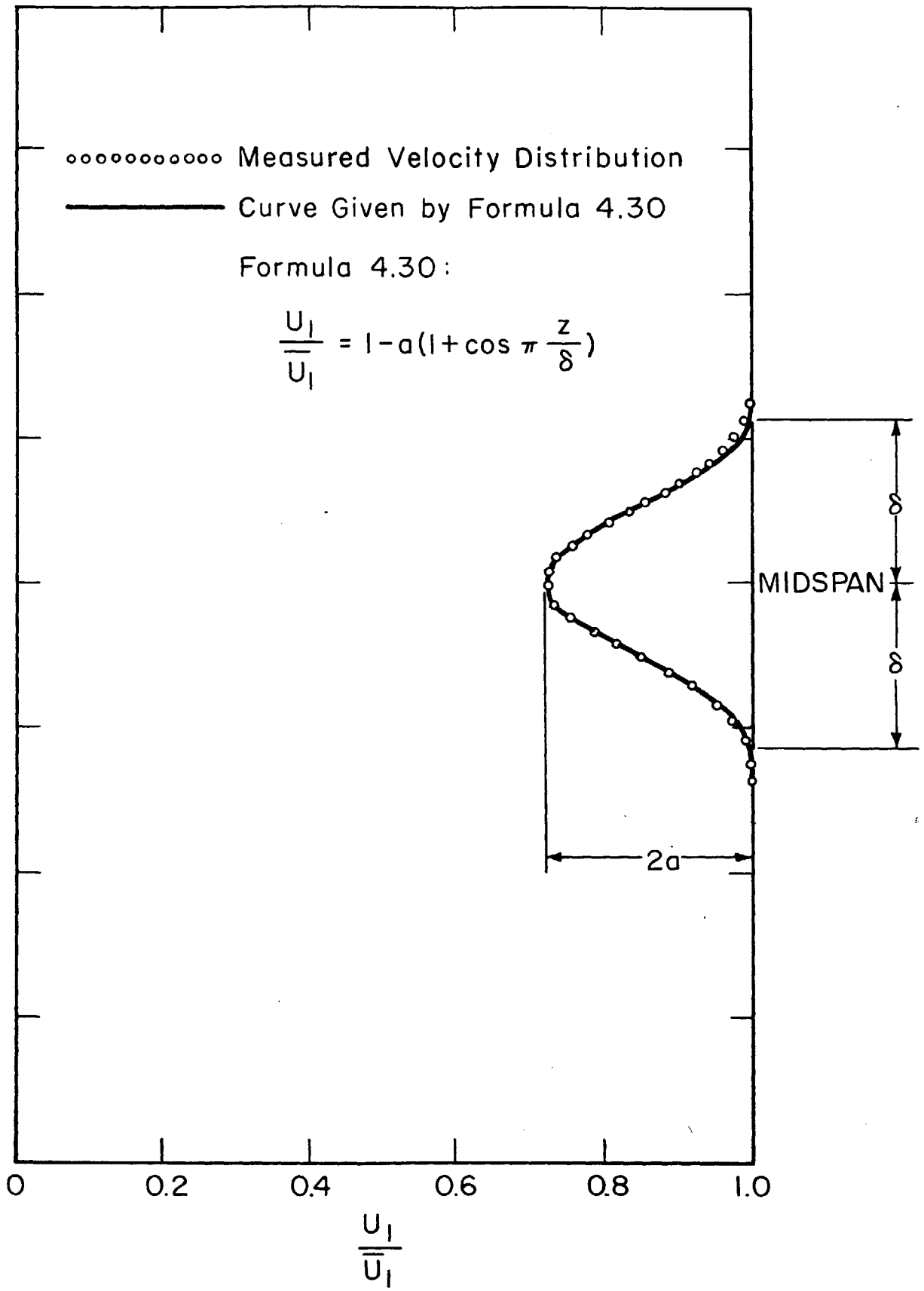

FIG. 22 WAKEFLOW VELOCITY PROFILE AT CASCADE INLET

Scale Divisions Shown are in Inches

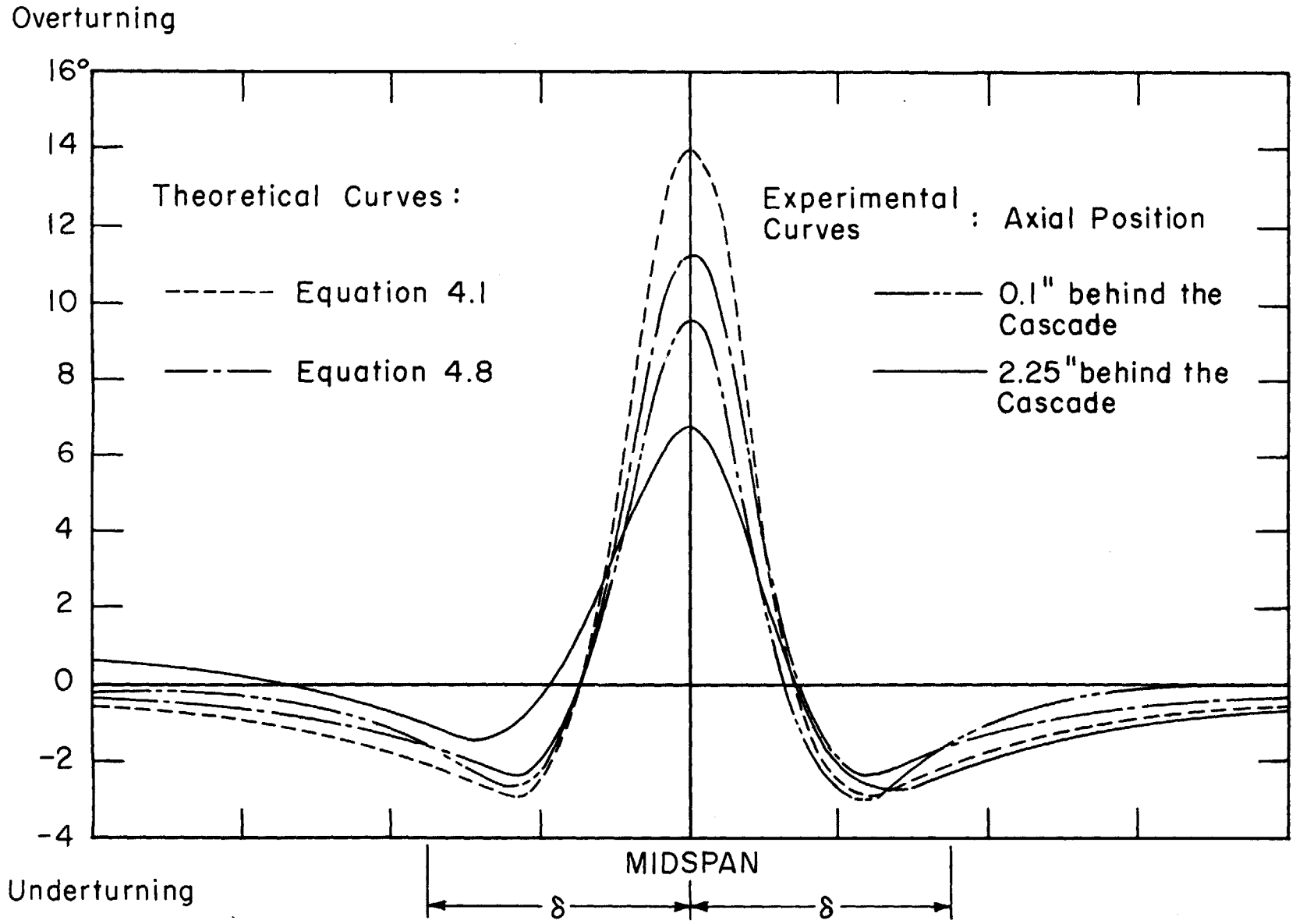

FIG. 23 WAKEFLOW MAXIMUM TRANSVERSE FLOW DEVIATION ANGLE
Scale Divisions Shown are in Inches.

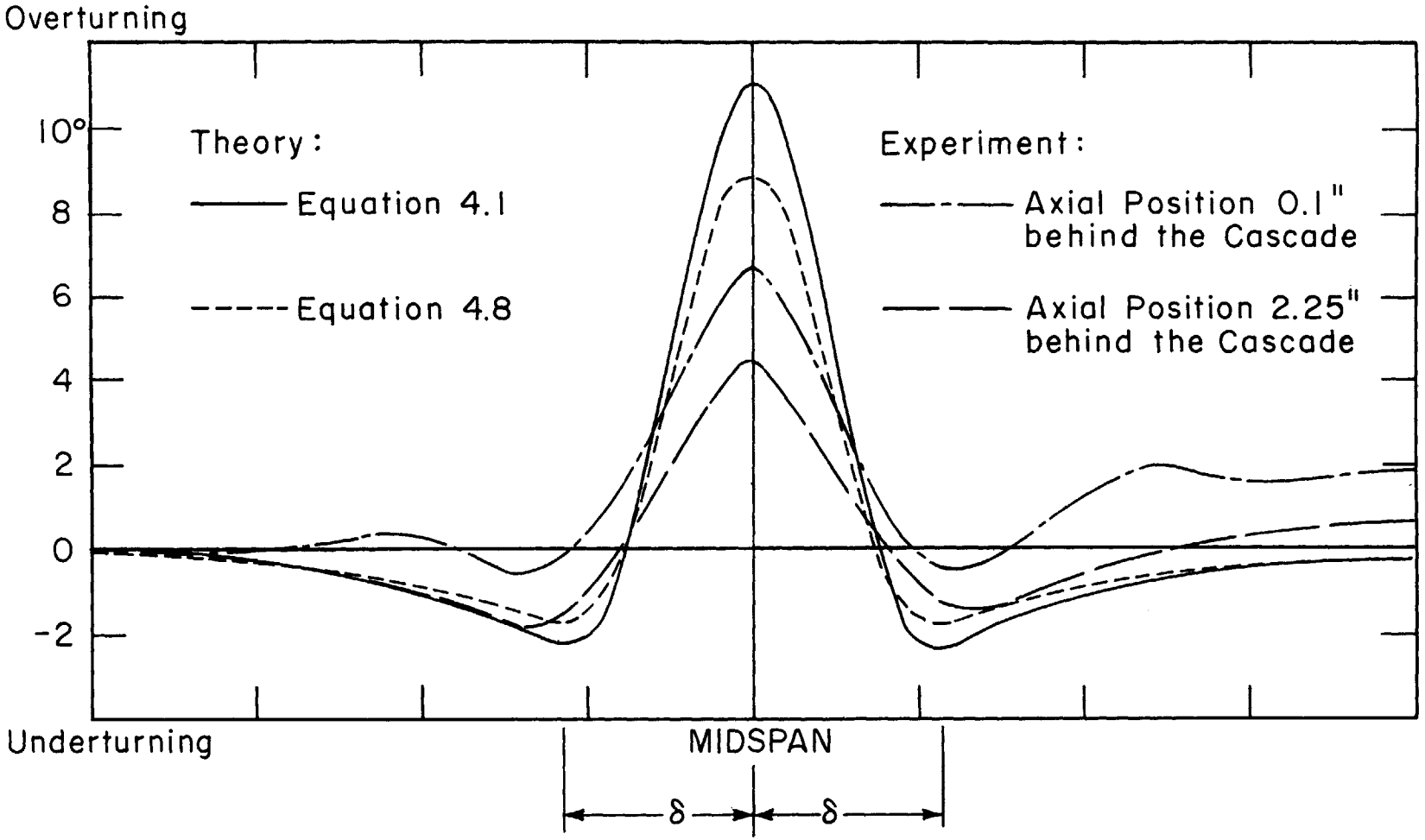

FIG. 24 WAKEFLOW AVERAGE TRANSVERSE FLOW DEVIATION ANGLE

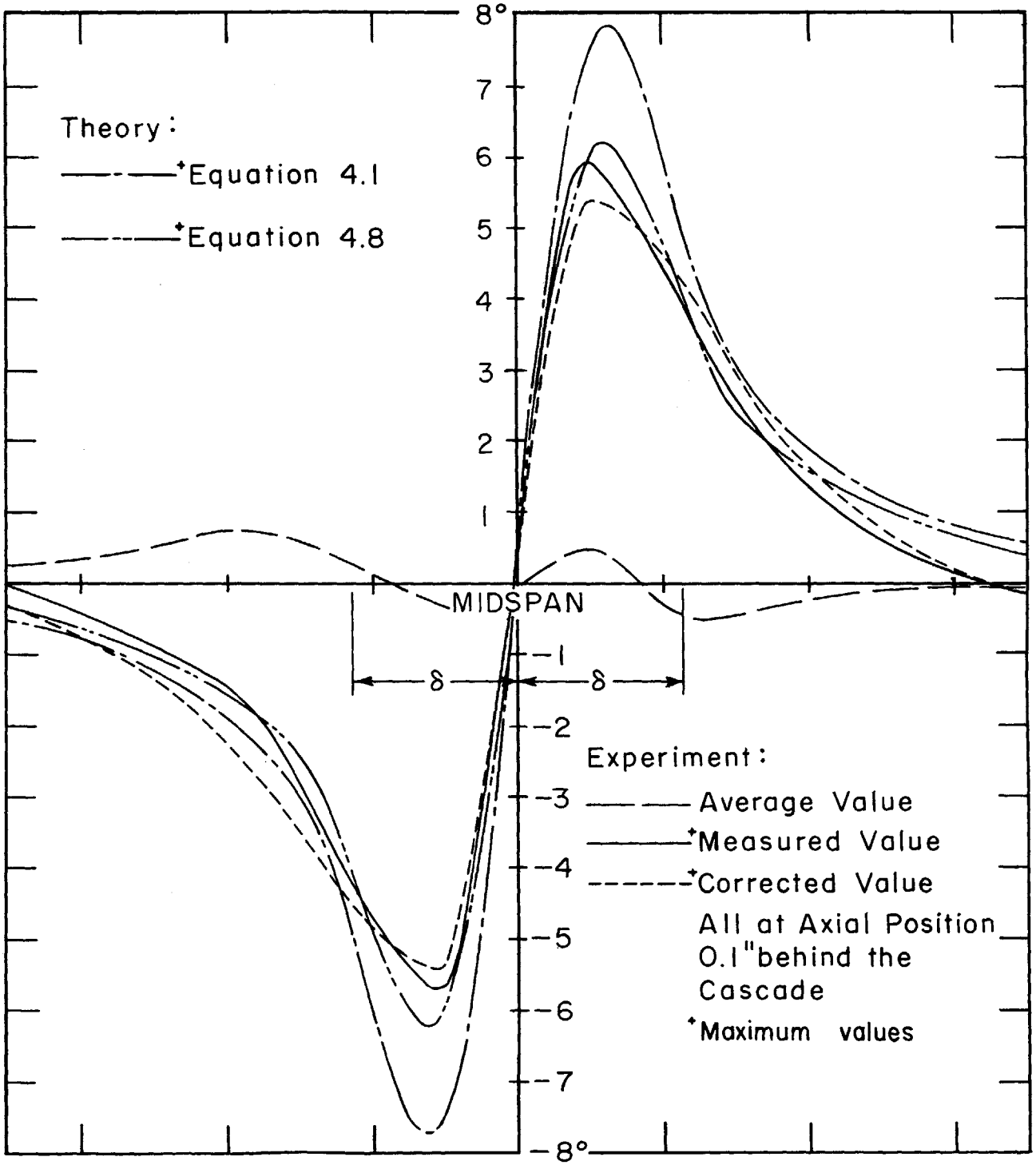

FIG. 25 WAKEFLOW SPANWISE FLOW DEVIATION ANGLE
Scale Divisions Shown are in Inches.

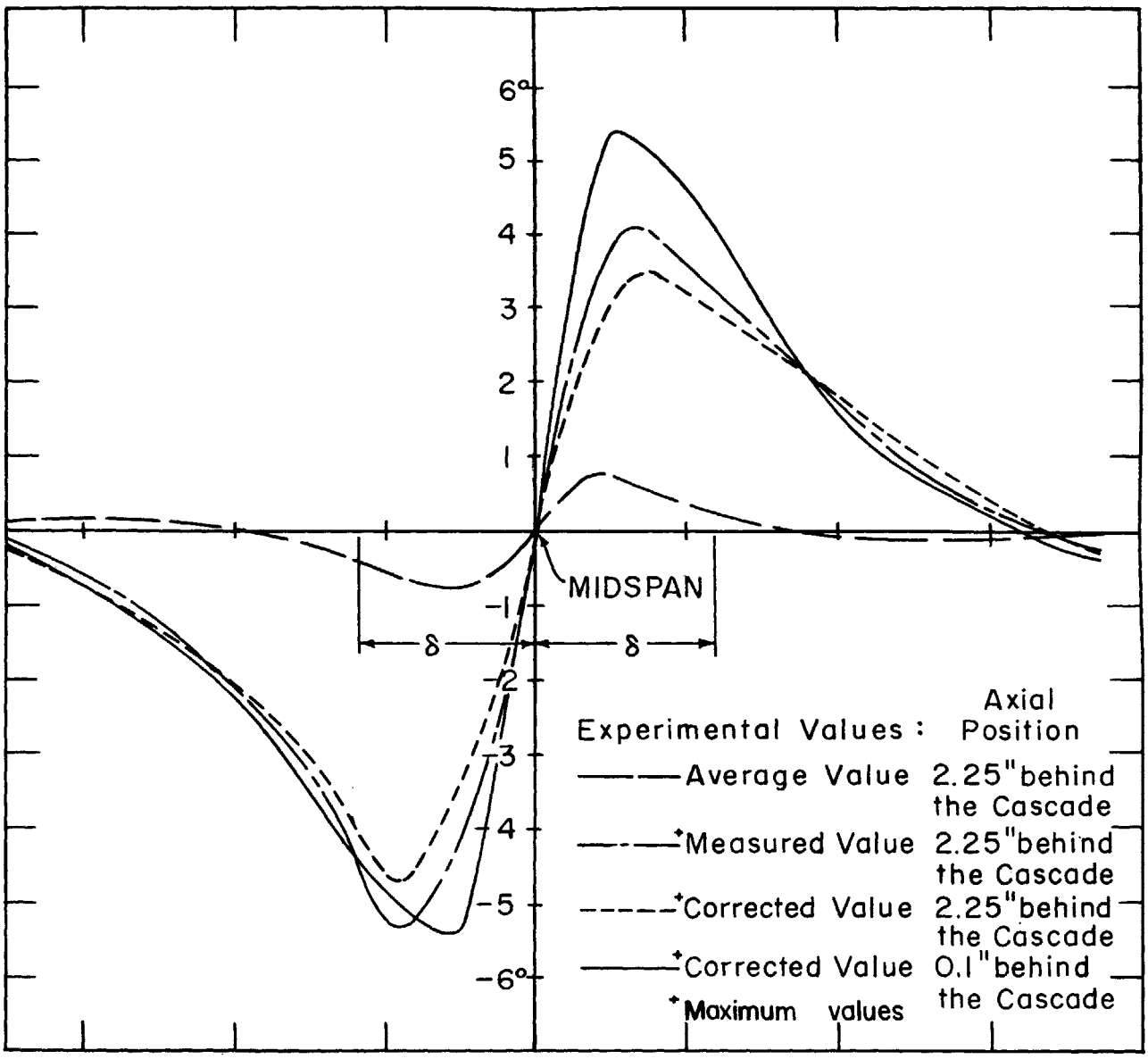

FIG. 26 WAKEFLOW SPANWISE FLOW DEVIATION ANGLE

Scale Divisions Shown are in Inches.

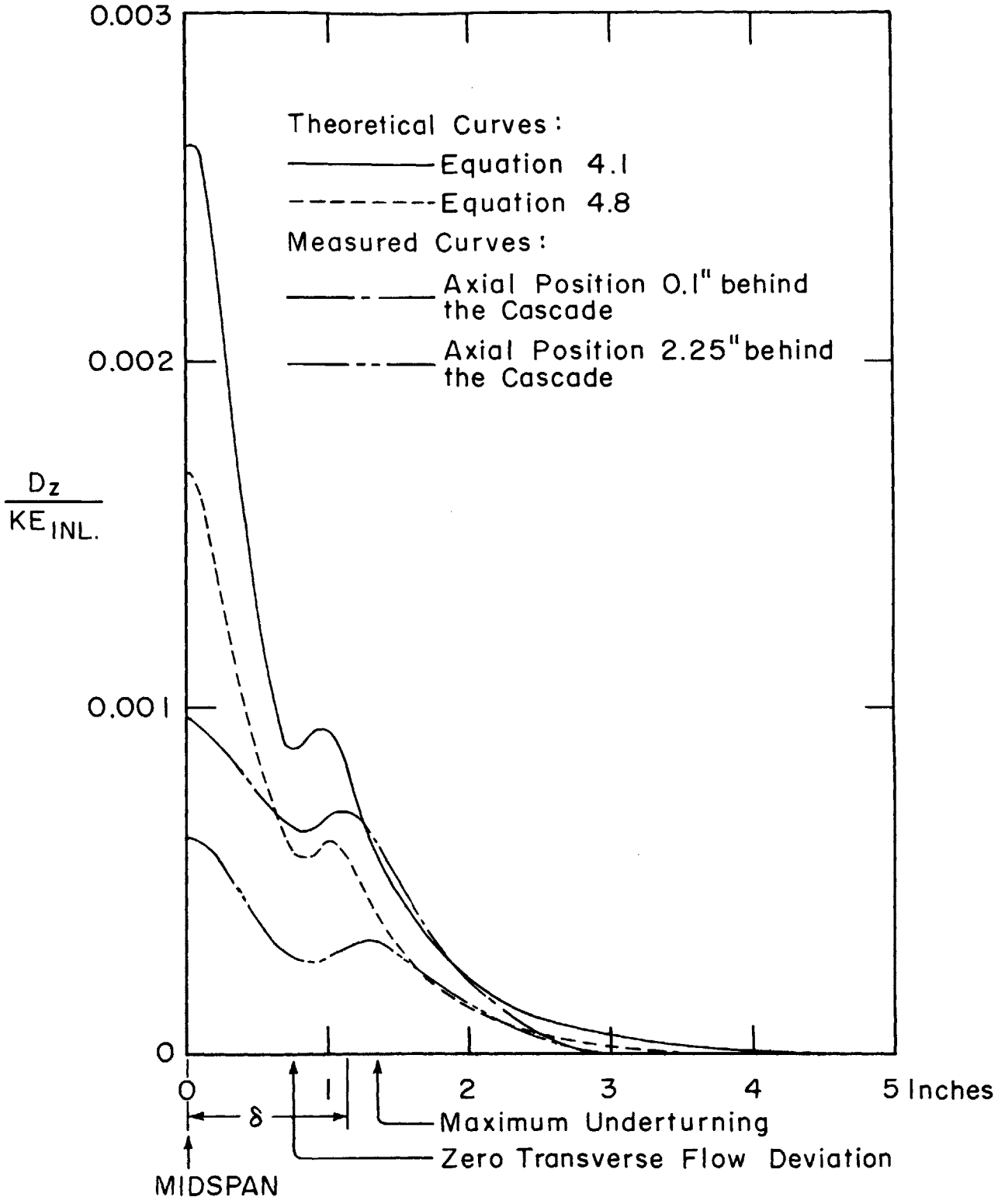

FIG. 27 WAKEFLOW SPANWISE DISTRIBUTION OF THE KINETIC ENERGY OF THE SECONDARY FLOW

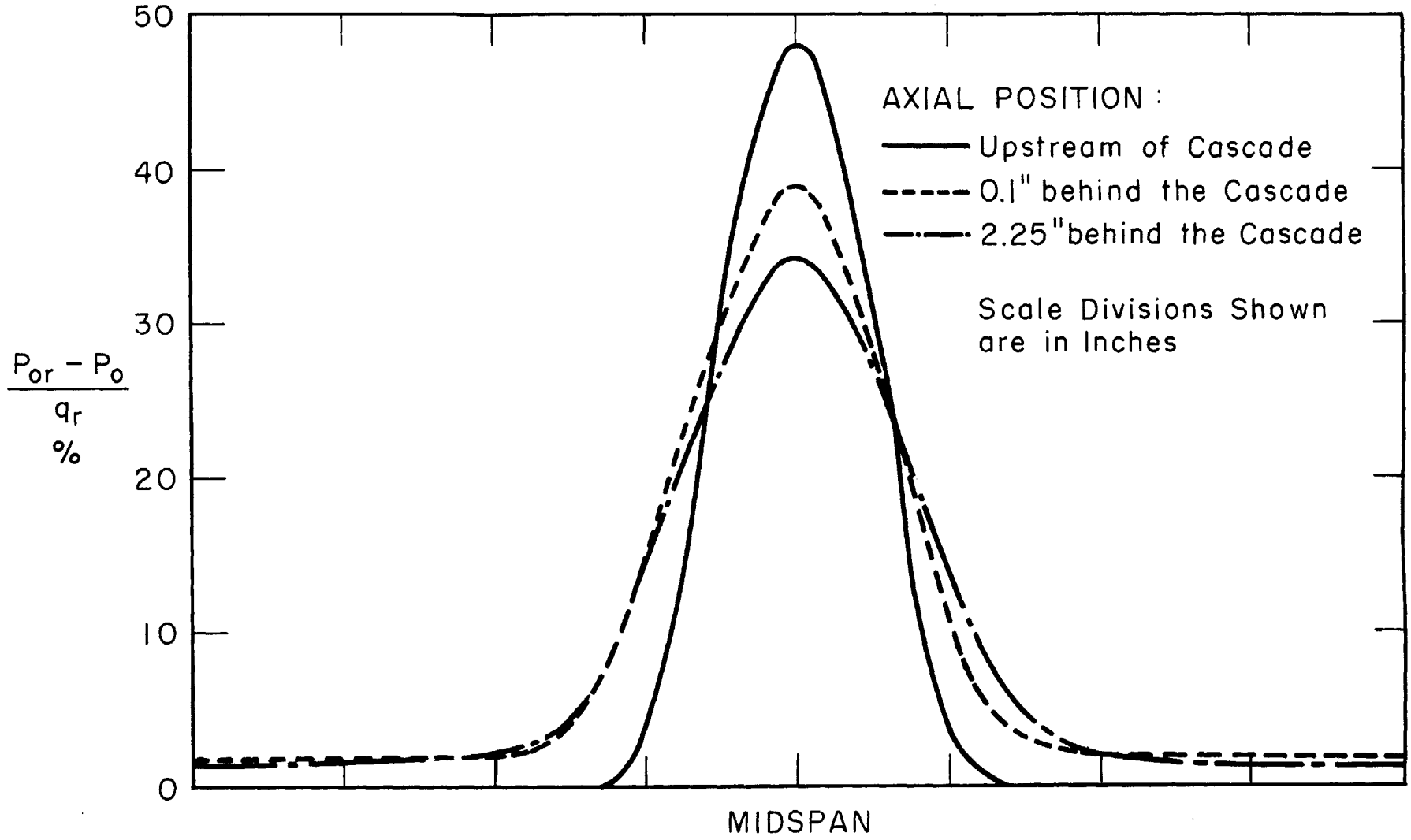

FIG. 28 WAKEFLOW STAGNATION PRESSURE DISTRIBUTION

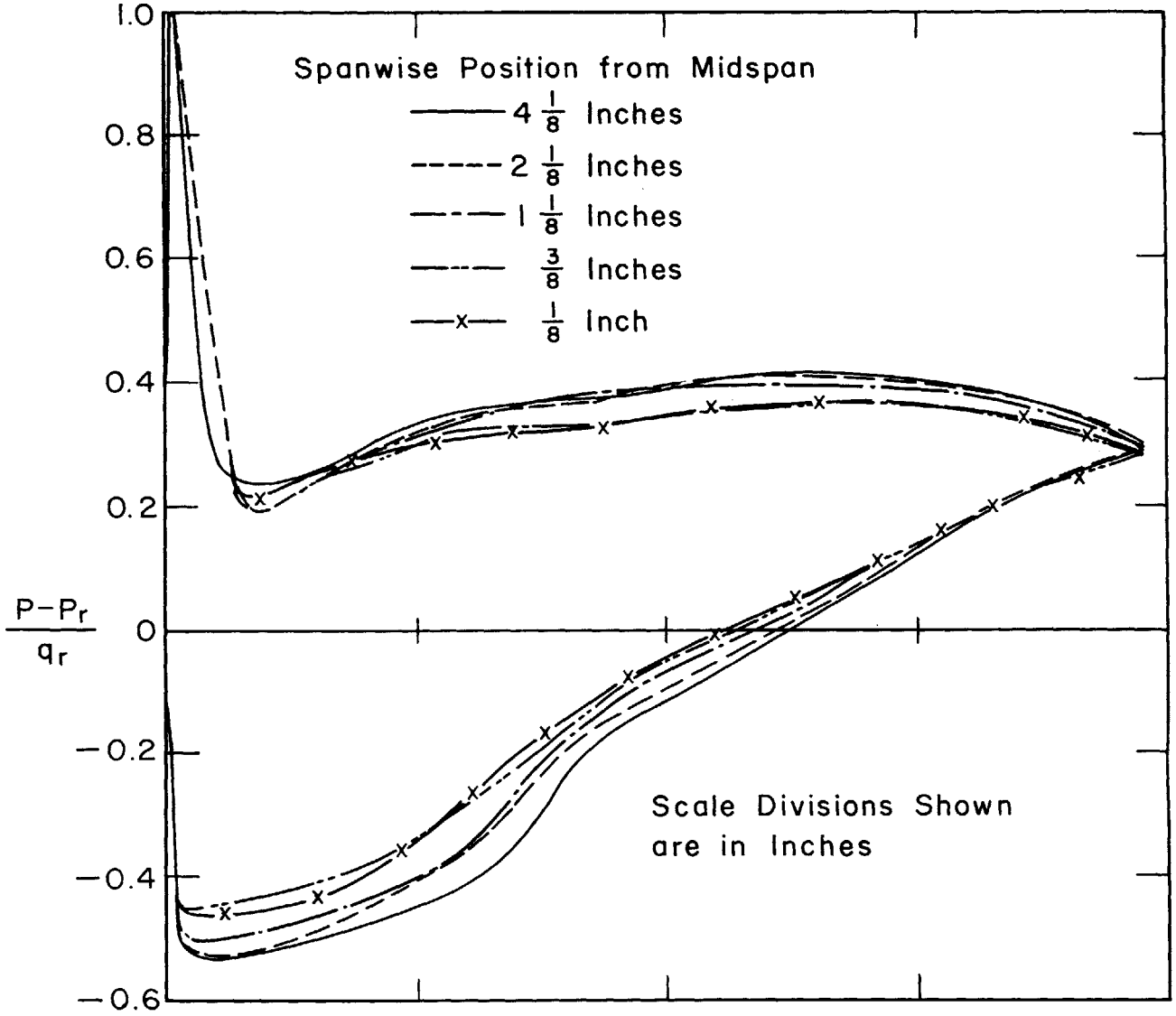

FIG. 29A WAKEFLOW PROJECTED STREAM PRESSURE DISTRIBUTION ON THE BLADE SURFACES

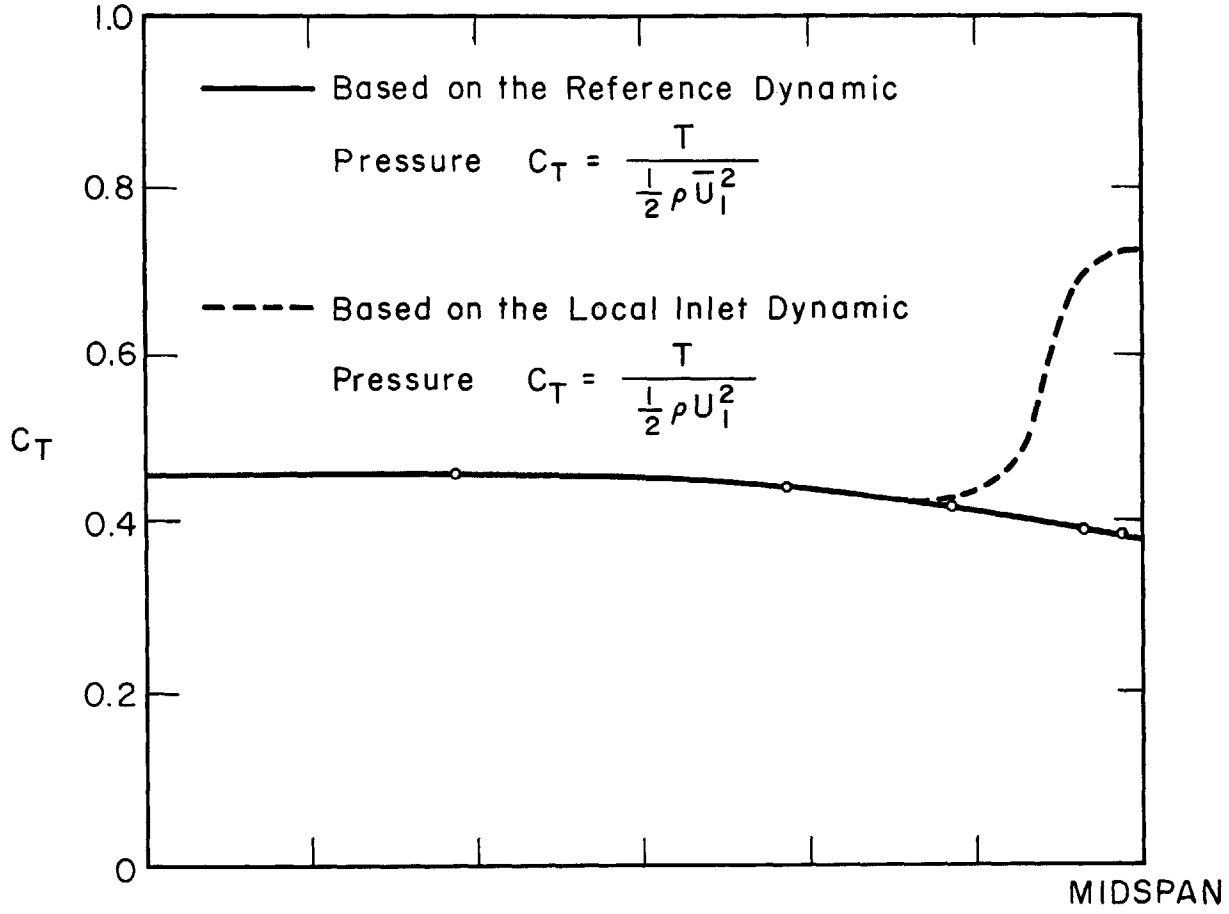

FIG. 29B WAKEFLOW TANGENTIAL PRESSURE COEFFICIENT DISTRIBUTION ALONG THE SPAN

Scale Divisions Shown are in Inches

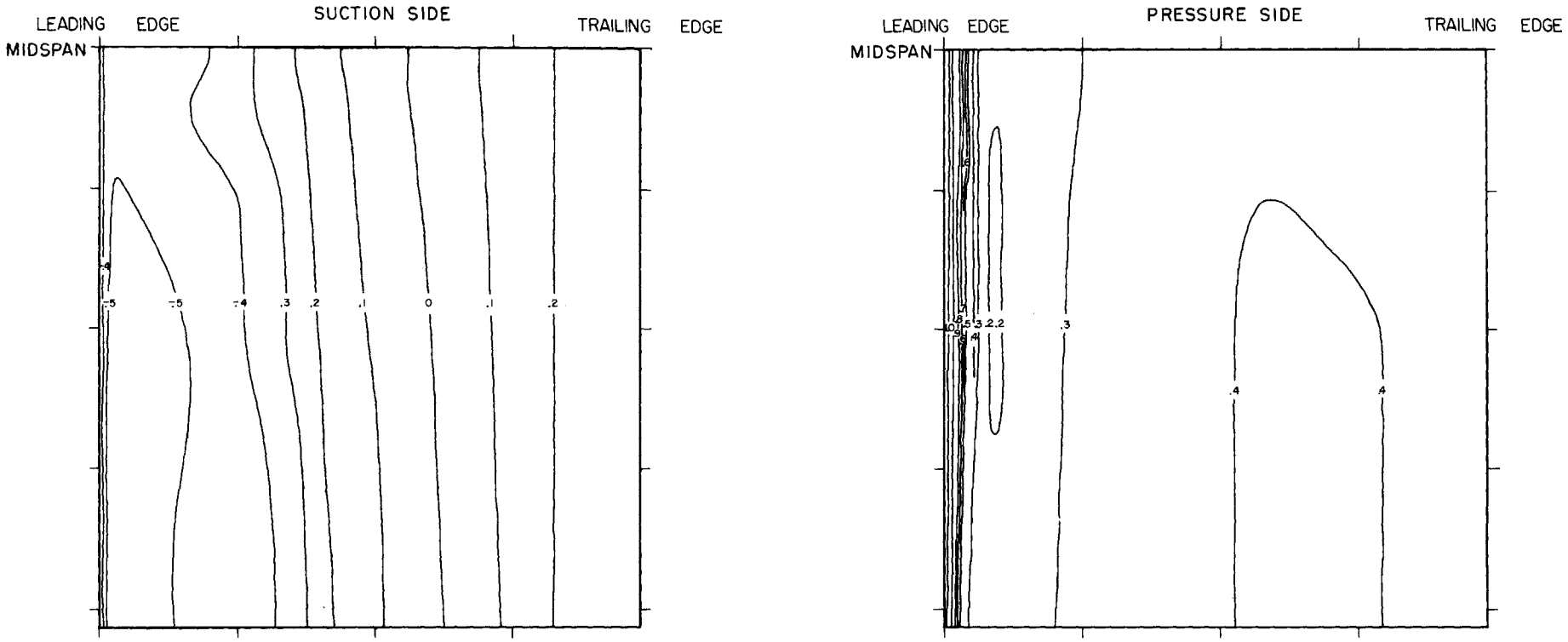

FIG. 30 WAKEFLOW CONTOURS OF CONSTANT STREAM PRESSURE ON THE BLADE SURFACES

Numbers on Contours Indicate $\frac{P - P_r}{q_r}$

Scale Divisions Shown are in Inches

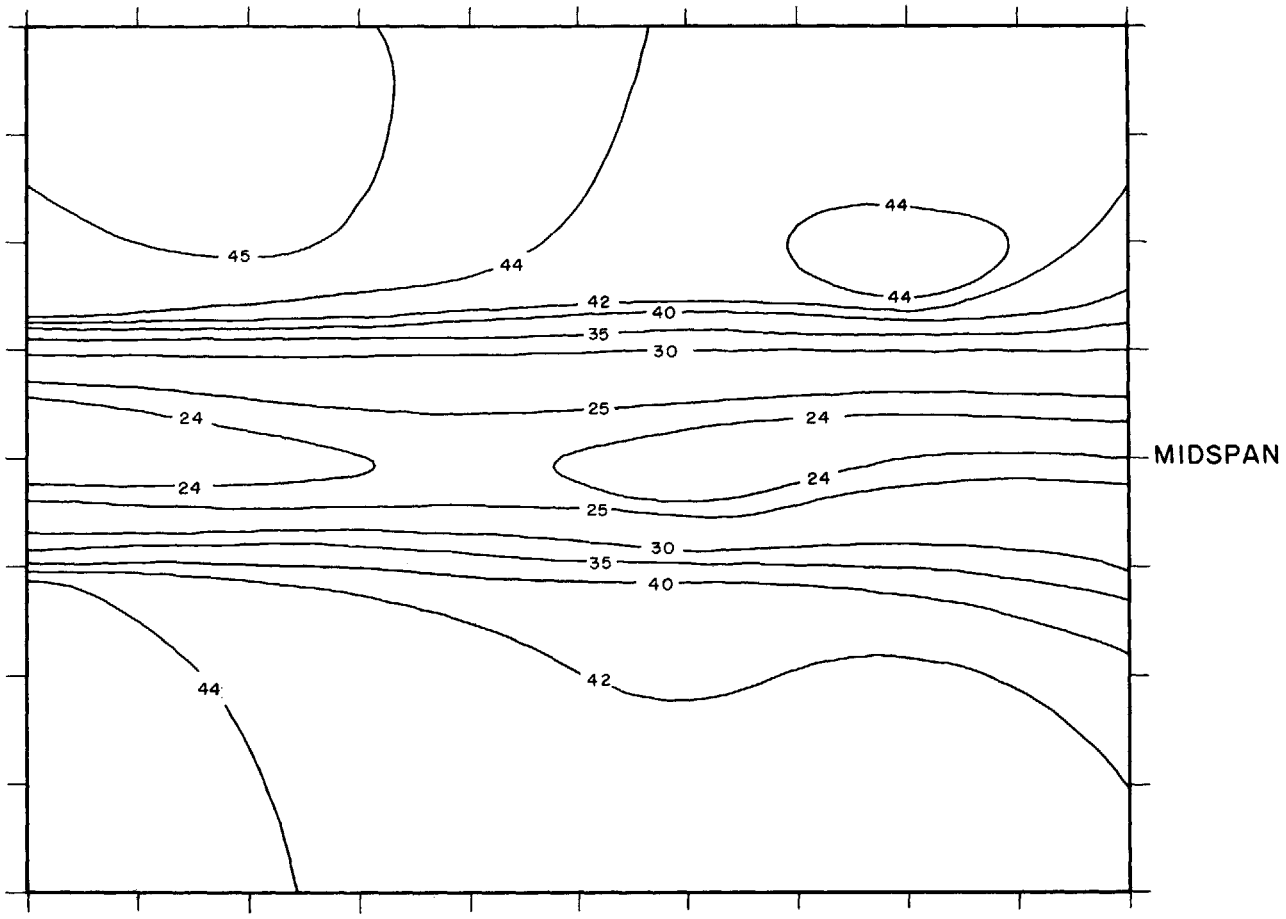

FIG. 31 SKEWED FLOW $\nabla P_0 = 0$. CONTOURS OF CONSTANT TRANSVERSE INLET ANGLES

Numbers on Contours Indicate Constant Inlet Angles

Scale Divisions Shown are in Inches

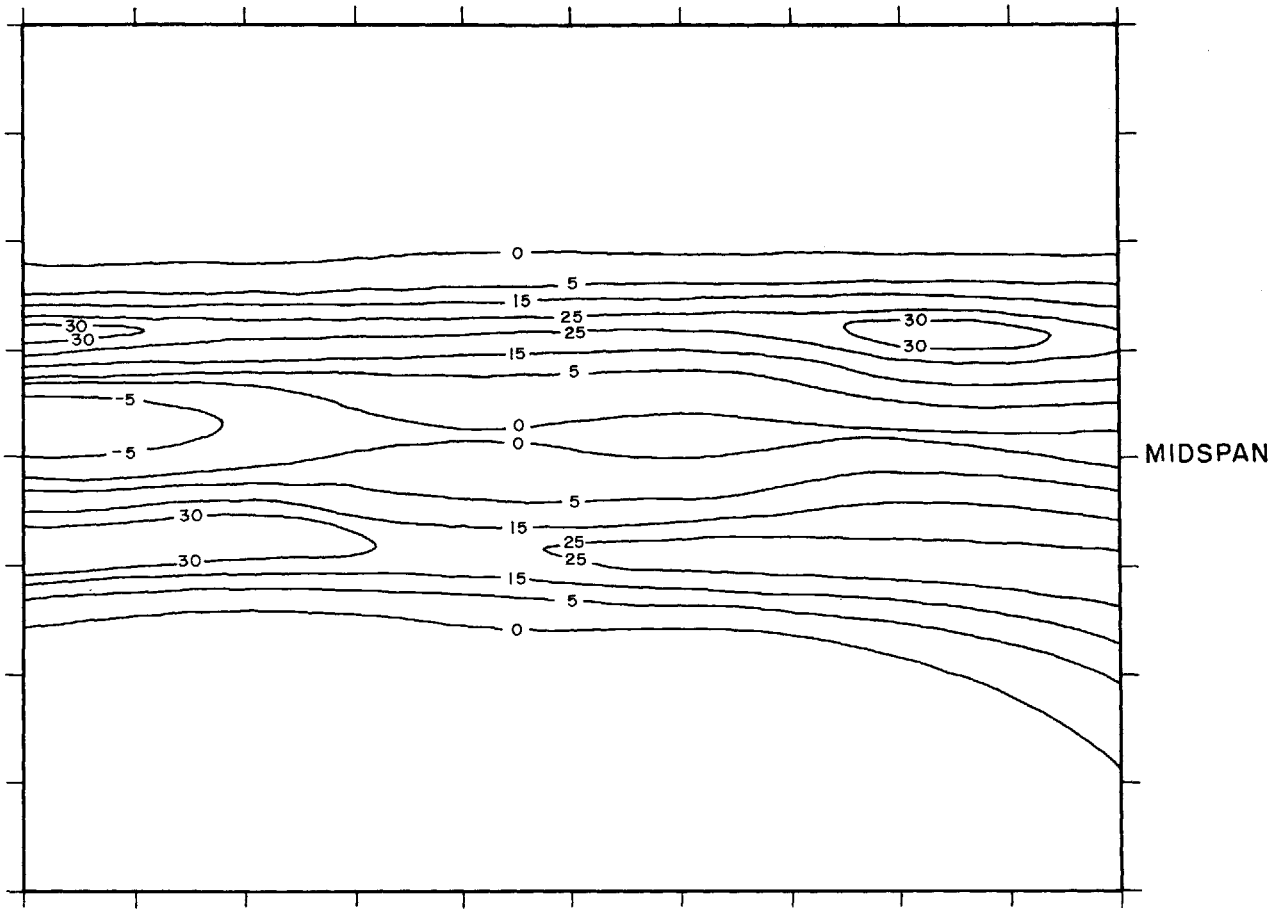

FIG. 32 SKEWED FLOW $\nabla P_0 = 0$. CONTOURS OF CONSTANT STAGNATION PRESSURE UPSTREAM OF CASCADE

Numbers on Contours Indicate $\frac{P_{or} - P_{o1}}{q_r}$ in Percentage

Scale Divisions Shown are in Inches

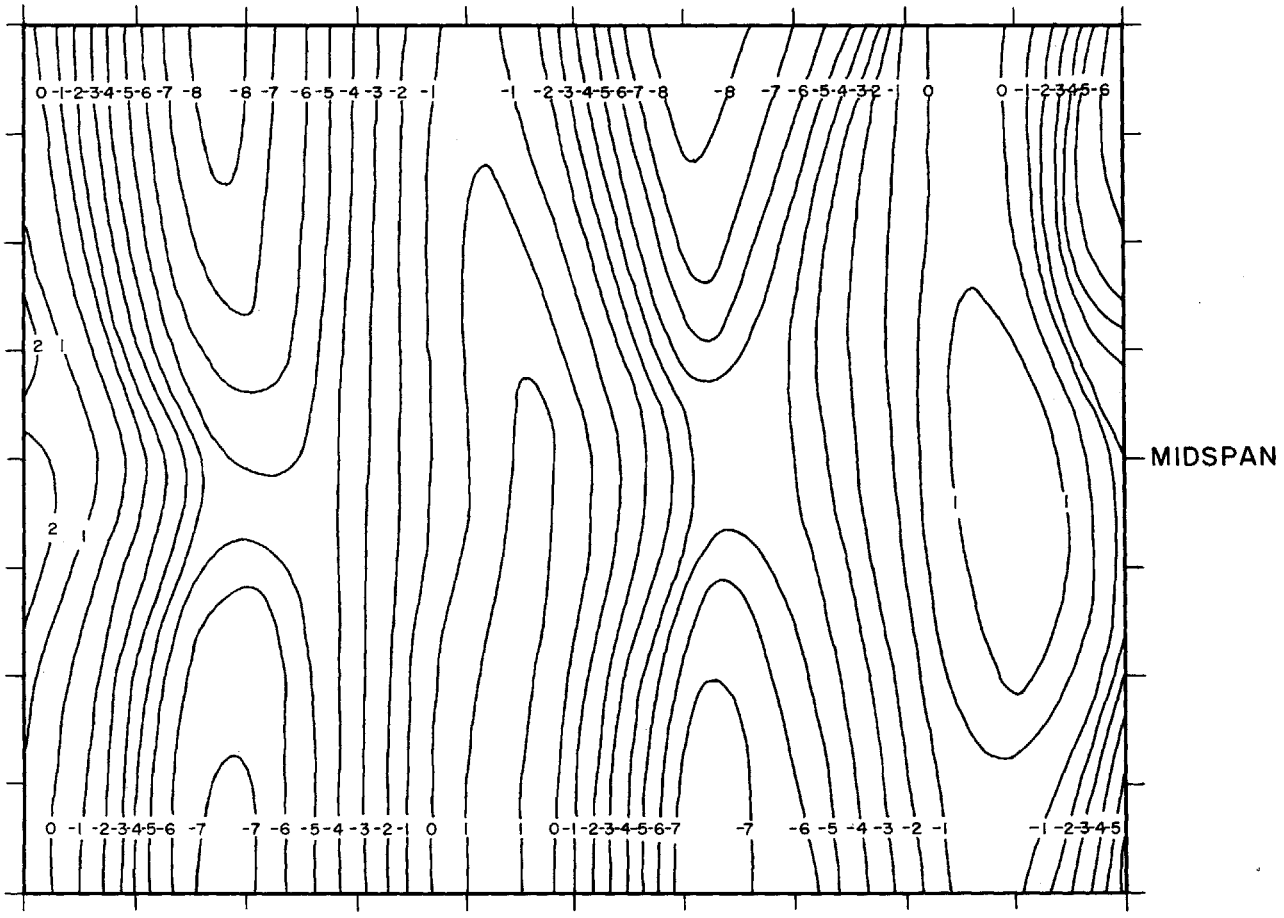

FIG. 33 SKEWED FLOW $\nabla P_0 = 0$. CONTOURS OF CONSTANT STREAM PRESSURE UPSTREAM OF CASCADE

Numbers on Contours Indicate $\frac{P_r - P}{q}$ in Percentage

Scale Divisions Shown are in Inches

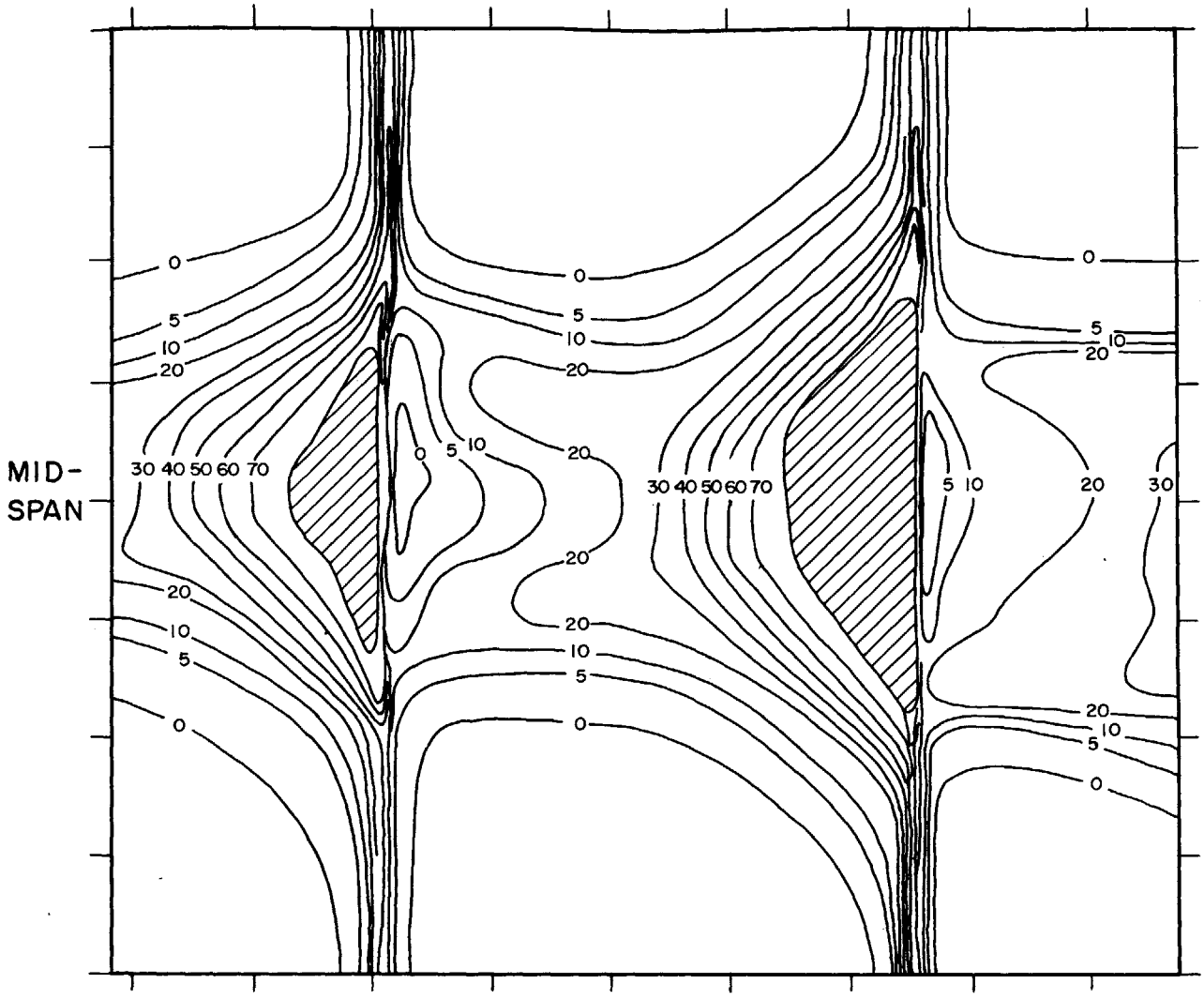

FIG. 34 SKEWED FLOW $\nabla P_o = 0$. CONTOURS OF CONSTANT STAGNATION PRESSURE

AXIAL POSITION : 0.1" behind the Cascade

Numbers on Contours Indicate Constant $\frac{P_{or} - P_{o2}}{q_r}$ in Percentage

Scale Divisions Shown are in Inches

Shaded Areas are Regions of Backflow

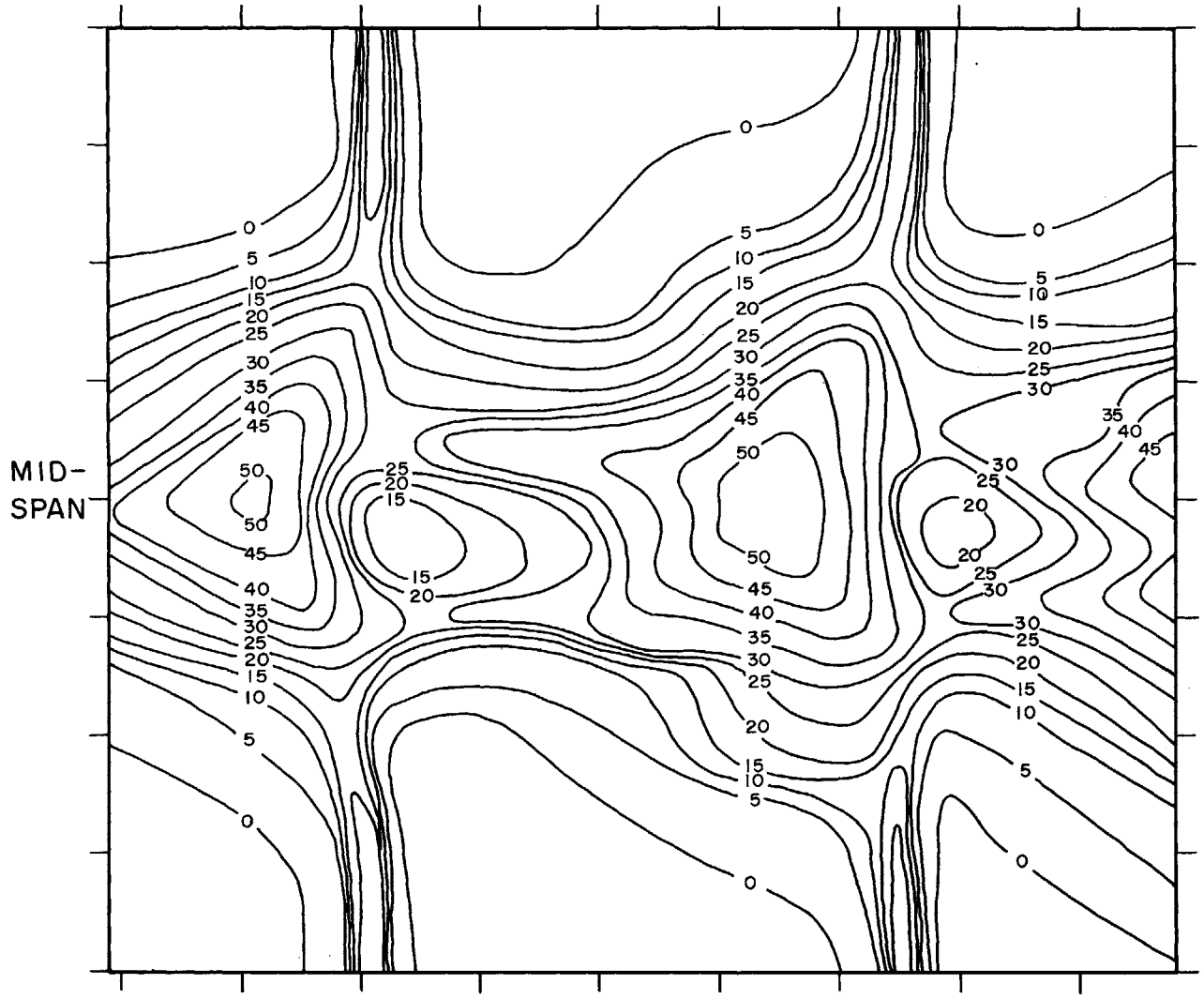

FIG. 35 SKEWED FLOW $\nabla P_0 = 0$. CONTOURS OF CONSTANT STAGNATION PRESSURE

AXIAL POSITION: 2.25" behind the Cascade

Numbers on Contours Indicate Constant $\frac{P_{or} - P_{o2}}{q_r}$ in Percentage

Scale Divisions Shown are in Inches

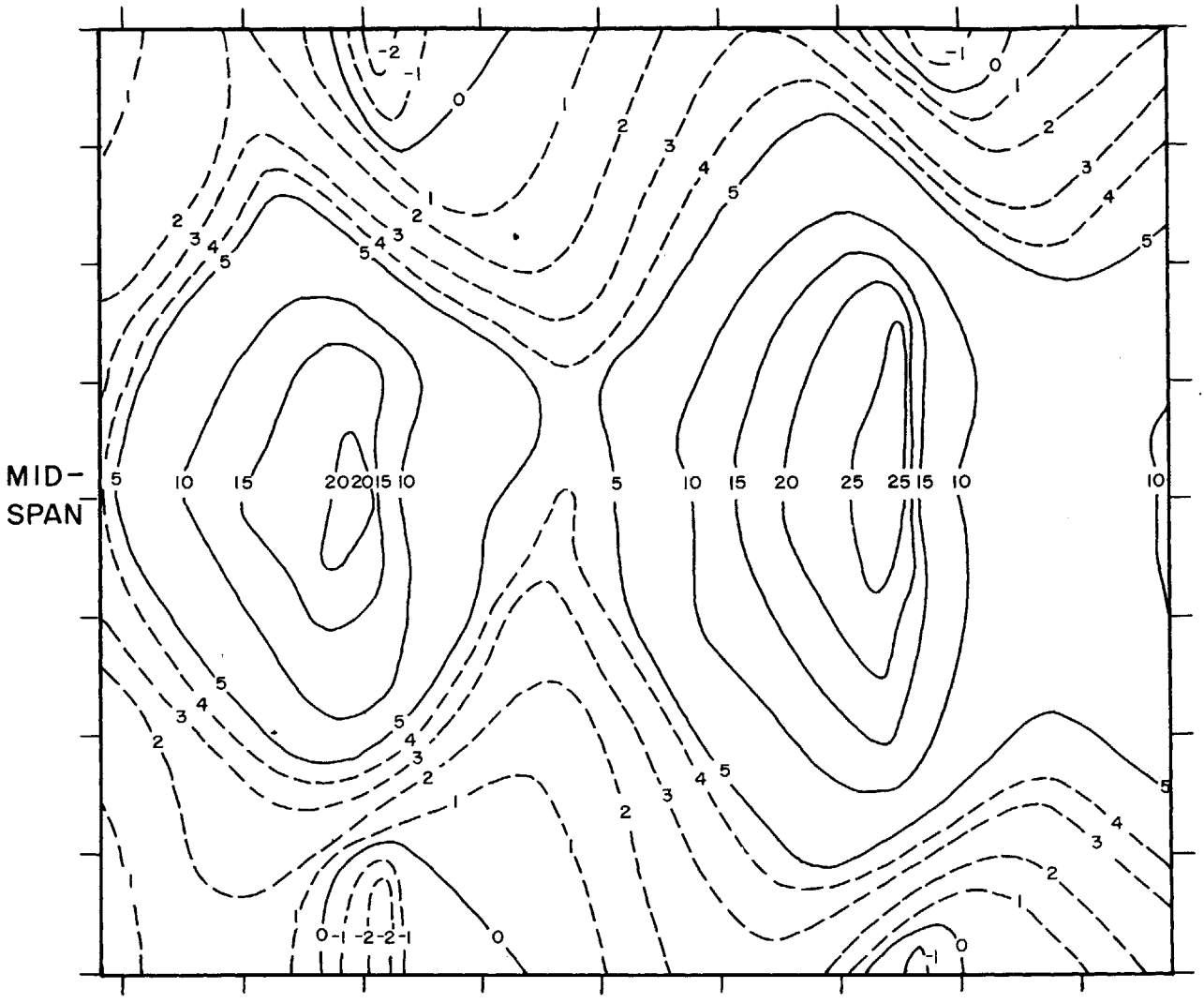

FIG. 36 SKEWED FLOW $\nabla P_0 = 0$. CONTOURS OF CONSTANT STREAM PRESSURE

AXIAL POSITION : 0.35" behind the Cascade

Numbers on Contours Indicate Constant $\frac{P_{atm} - P}{q_r}$

Scale Divisions Shown are in Inches

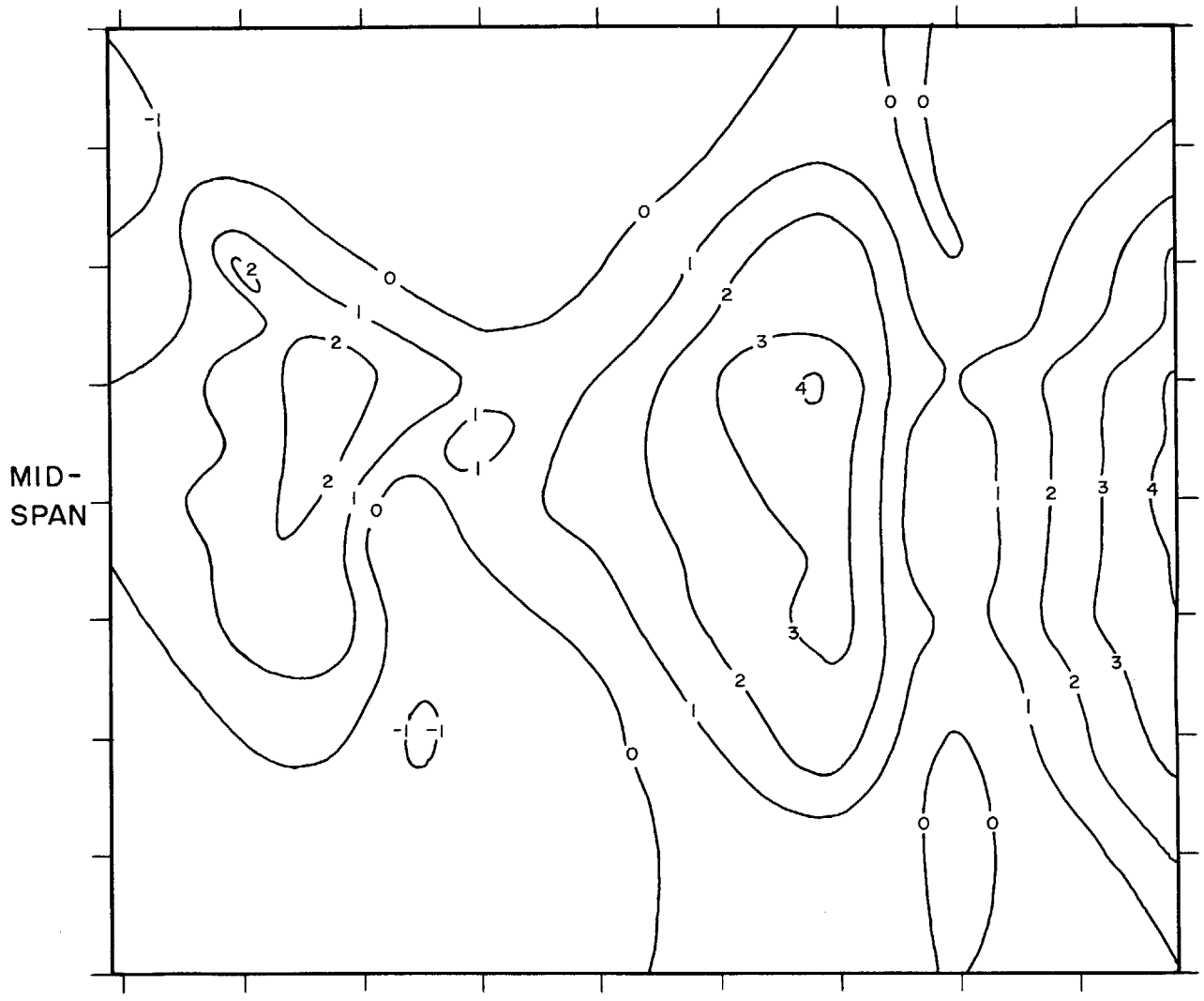

FIG. 37 SKEWED FLOW $\nabla P_0 = 0$. CONTOURS OF CONSTANT STREAM PRESSURE

AXIAL POSITION: 2.25" behind the Cascade

Numbers on Contours Indicate Constant $\frac{P_{atm} - P}{q_r}$

Scale Divisions Shown are in Inches

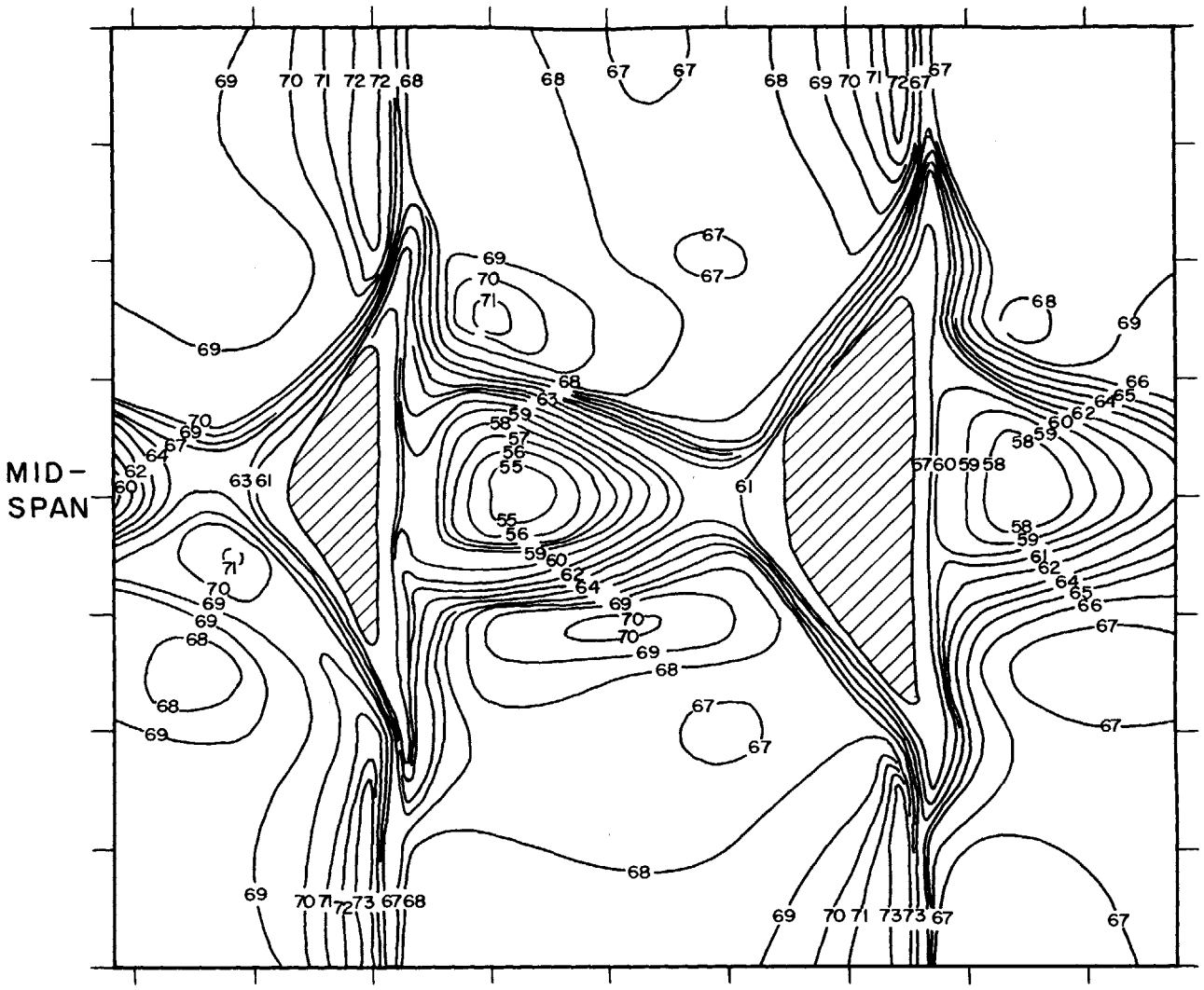

FIG. 38 SKEWED FLOW $\nabla P_o = 0$. CONTOURS OF CONSTANT TRANSVERSE FLOW ANGLE

AXIAL POSITION : 0.1 "behind the Cascade

Numbers on Contours Indicate Constant Transverse Flow Angles Measured from Tangential Direction

Scale Divisions Shown are in Inches

Shaded Areas are Regions of Backflow

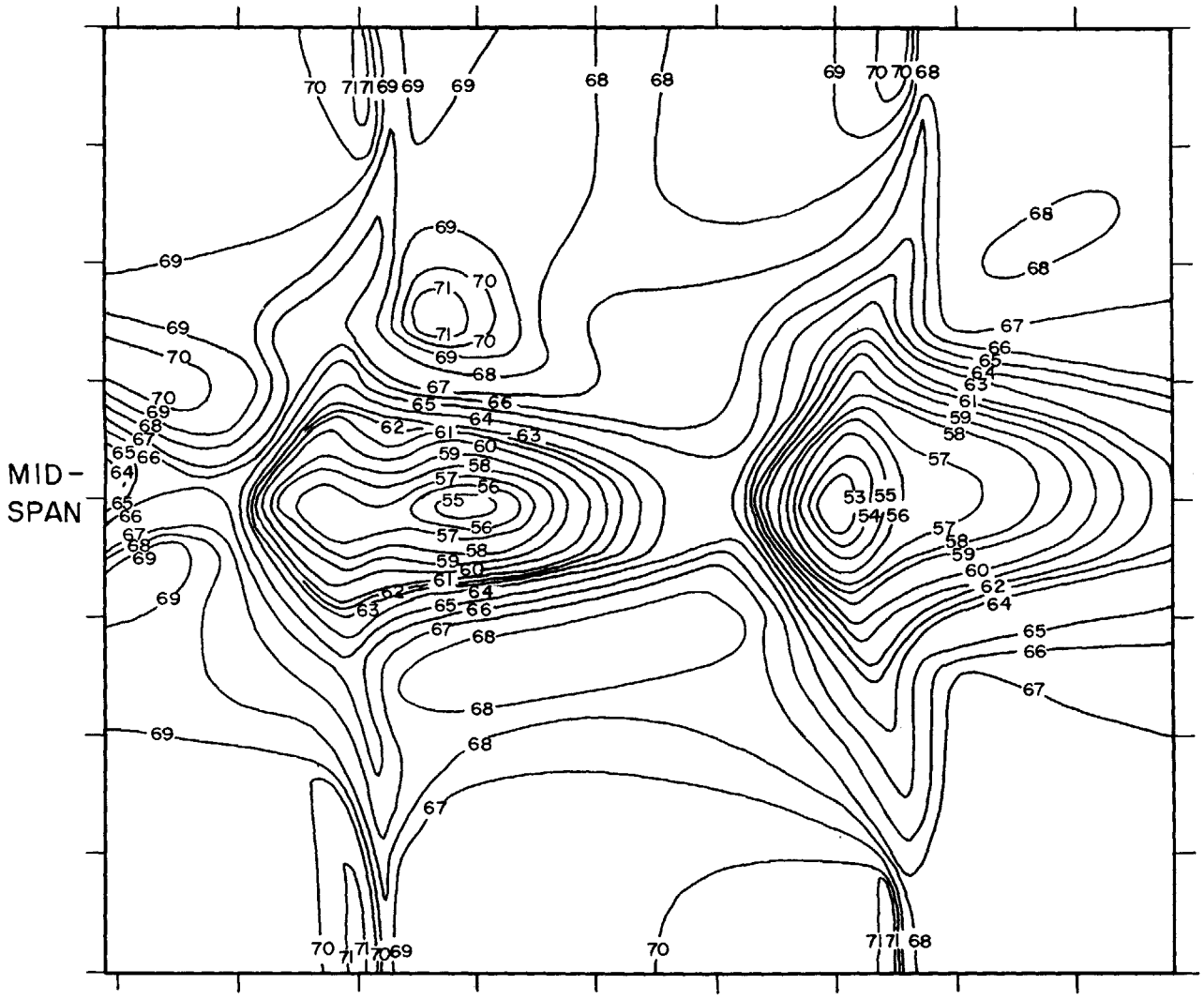

FIG. 39 SKEWED FLOW $\nabla P_o = 0$. CONTOURS OF CONSTANT TRANSVERSE FLOW ANGLE

AXIAL POSITION : 2.25" behind the Cascade

Numbers on Contours Indicate Constant Transverse Flow Angles Measured from Tangential Direction

Scale Divisions Shown are in Inches

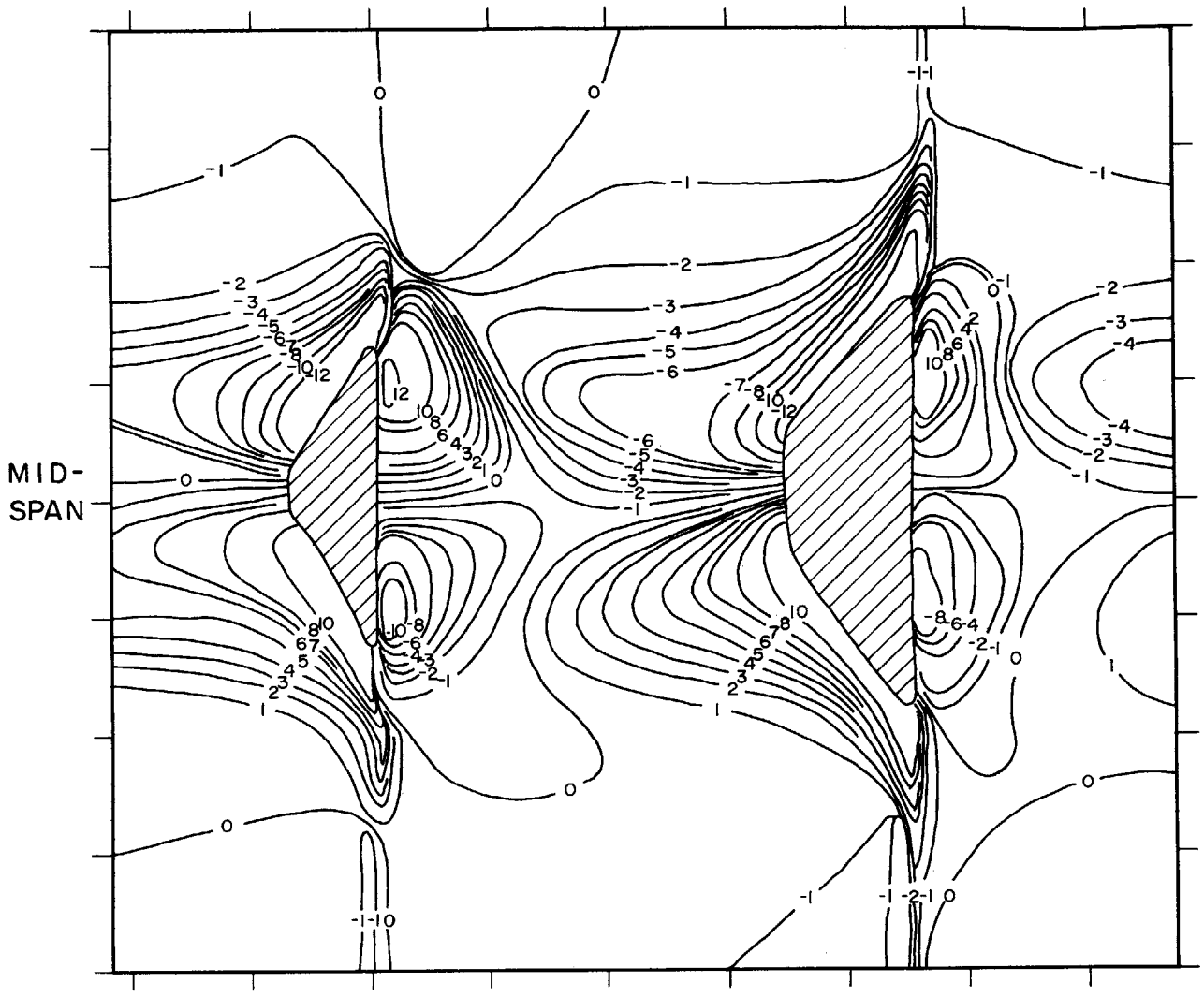

FIG. 40 SKEWED FLOW $\nabla P_0 = 0$. CONTOURS OF CONSTANT SPANWISE FLOW DEVIATION ANGLES

AXIAL POSITION: 0.1" behind the Cascade

Numbers on Contours Indicate Constant Spanwise Flow Deviation Angles

Positive Numbers Indicate Flow Towards the Top of the Cascade

Scale Divisions Shown are in Inches

Shaded Areas are Regions of Backflow

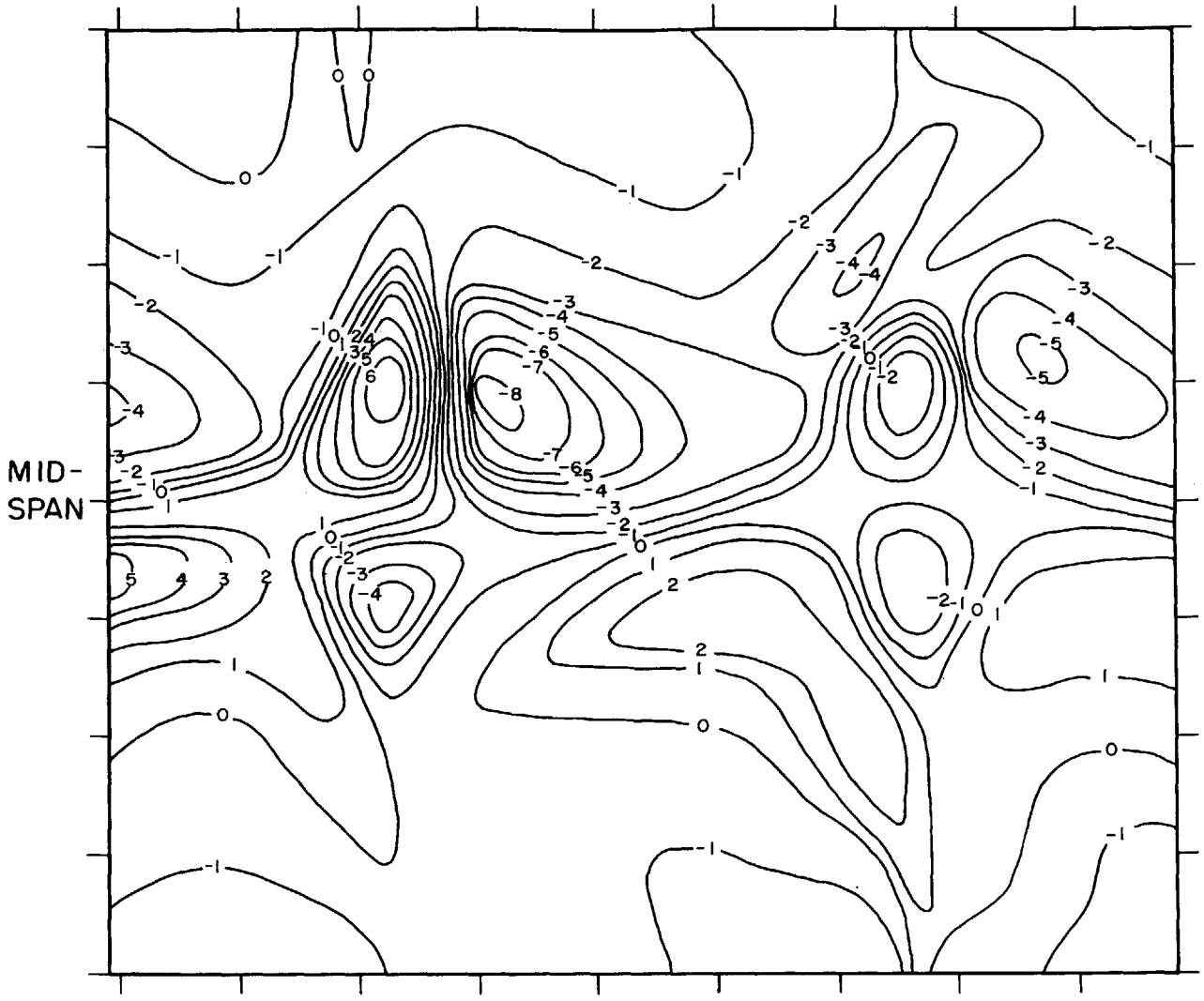

FIG. 41 SKEWED FLOW $\nabla P_o = 0$. CONTOURS OF CONSTANT SPANWISE FLOW DEVIATION ANGLES

AXIAL POSITION: 2.25" behind the Cascade

Numbers on Contours Indicate Constant Spanwise Flow Deviation Angles

Positive Numbers Indicate Flow Towards the Top of the Cascade

Scale Divisions Shown are in Inches

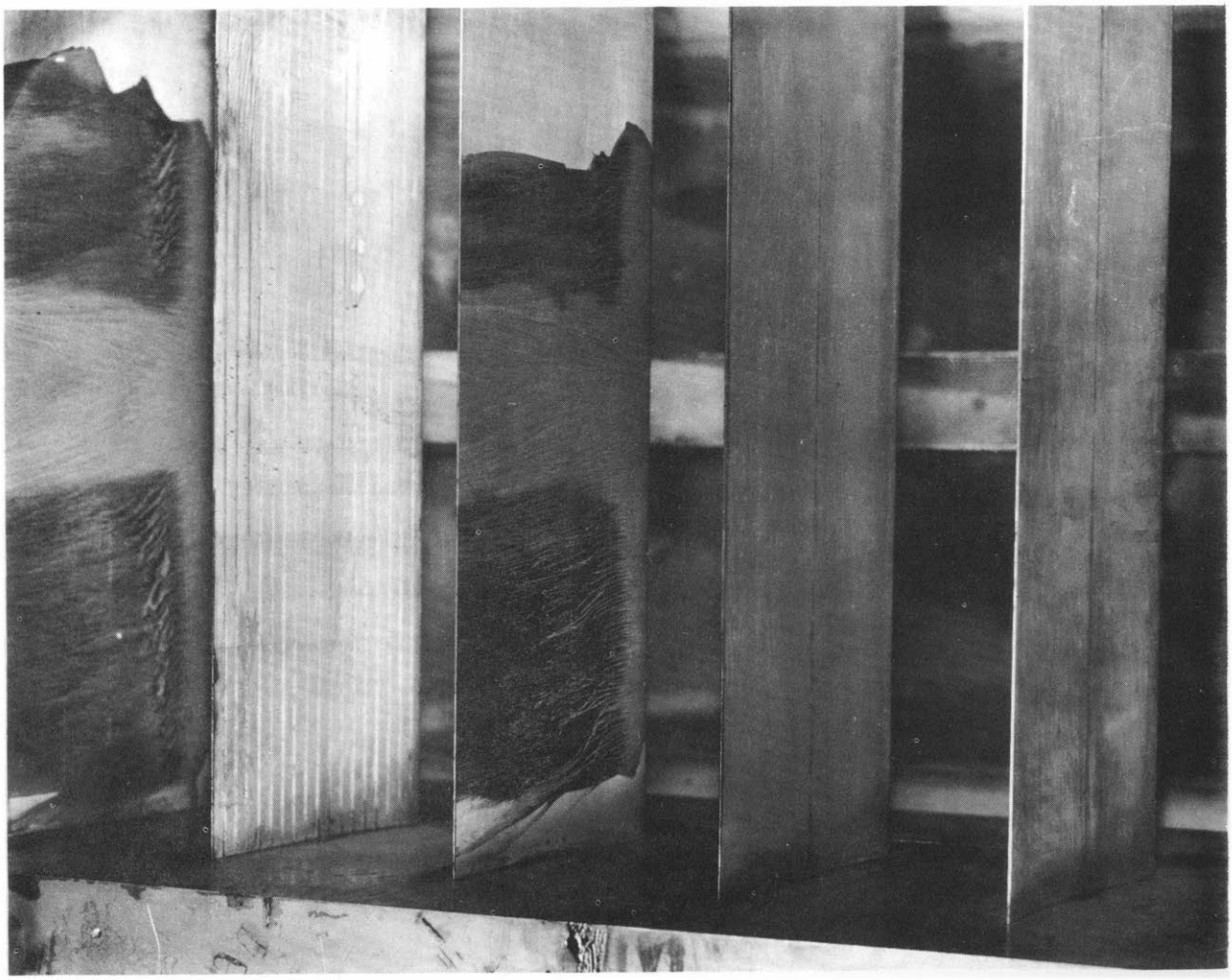

FIGURE 42 SKEWED FLOW. STREAMLINE TRACES IN CARBON BLACK ON THE BLADE PRESSURE SIDE.

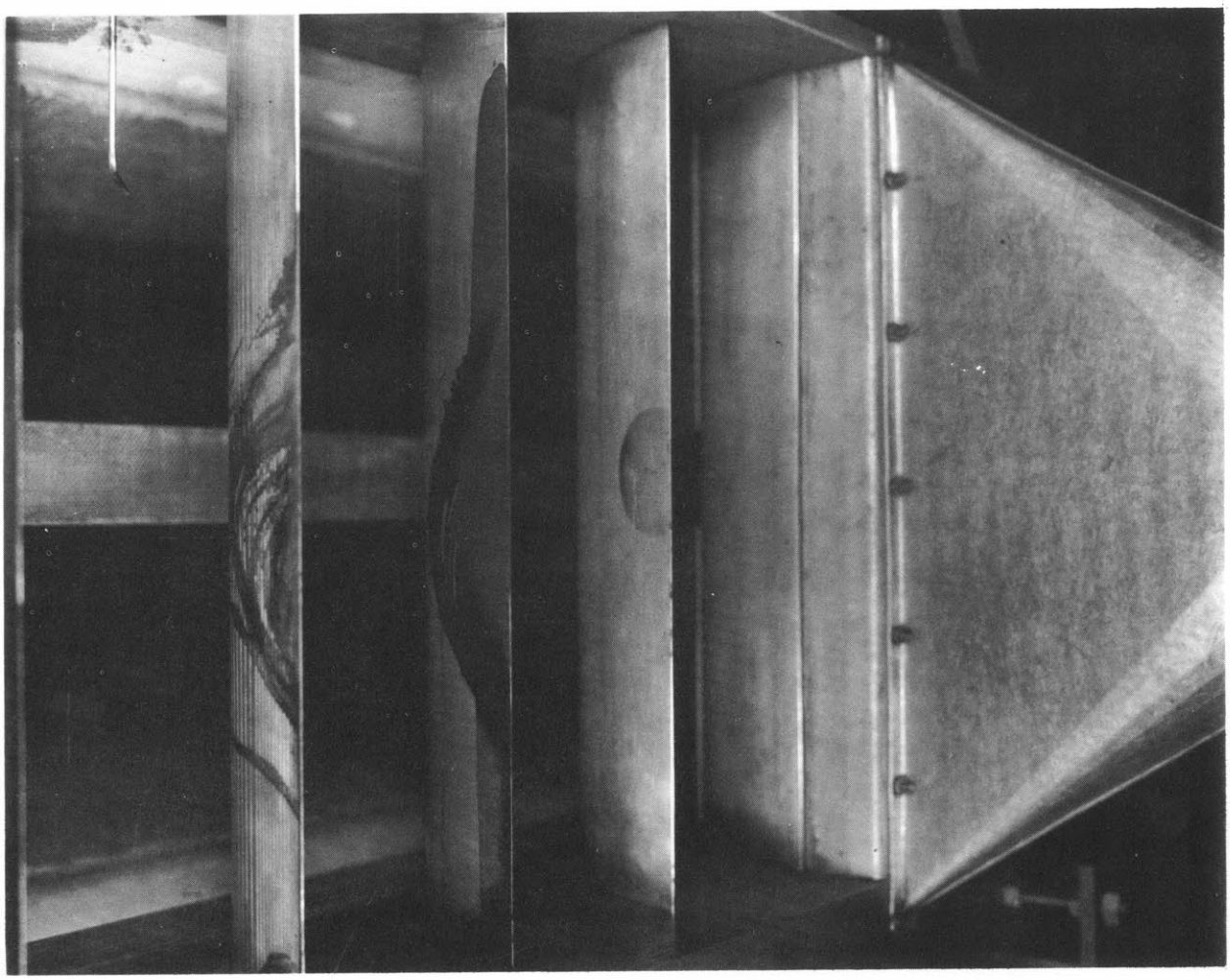

FIGURE 43 SKEWED FLOW. STREAMLINE TRACES IN CARBON BLACK ON THE BLADE SUCTION SIDE.

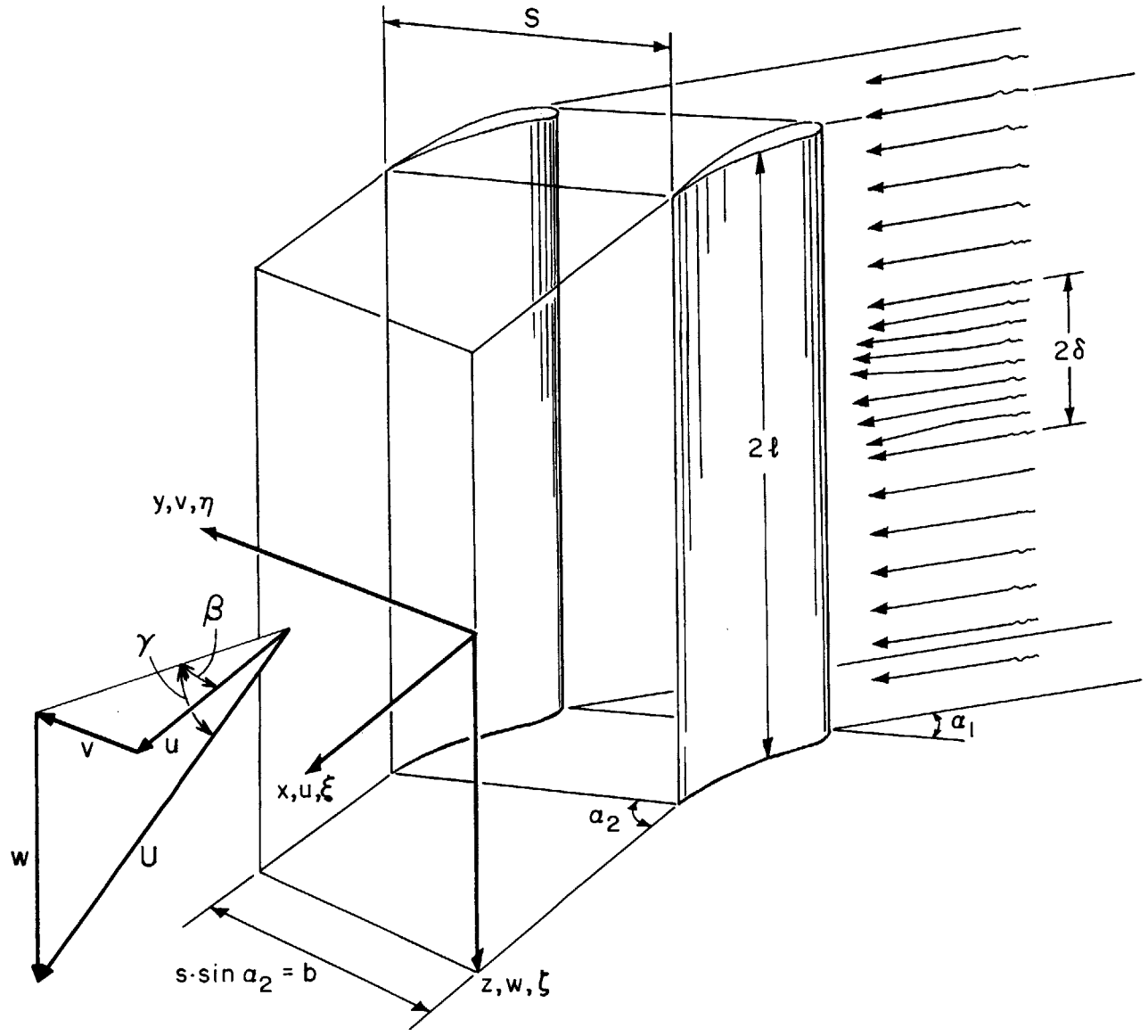

FIG. 44 SKEWED FLOW AND SKEWED WAKE FLOW DIAGRAM OF NOTATIONS

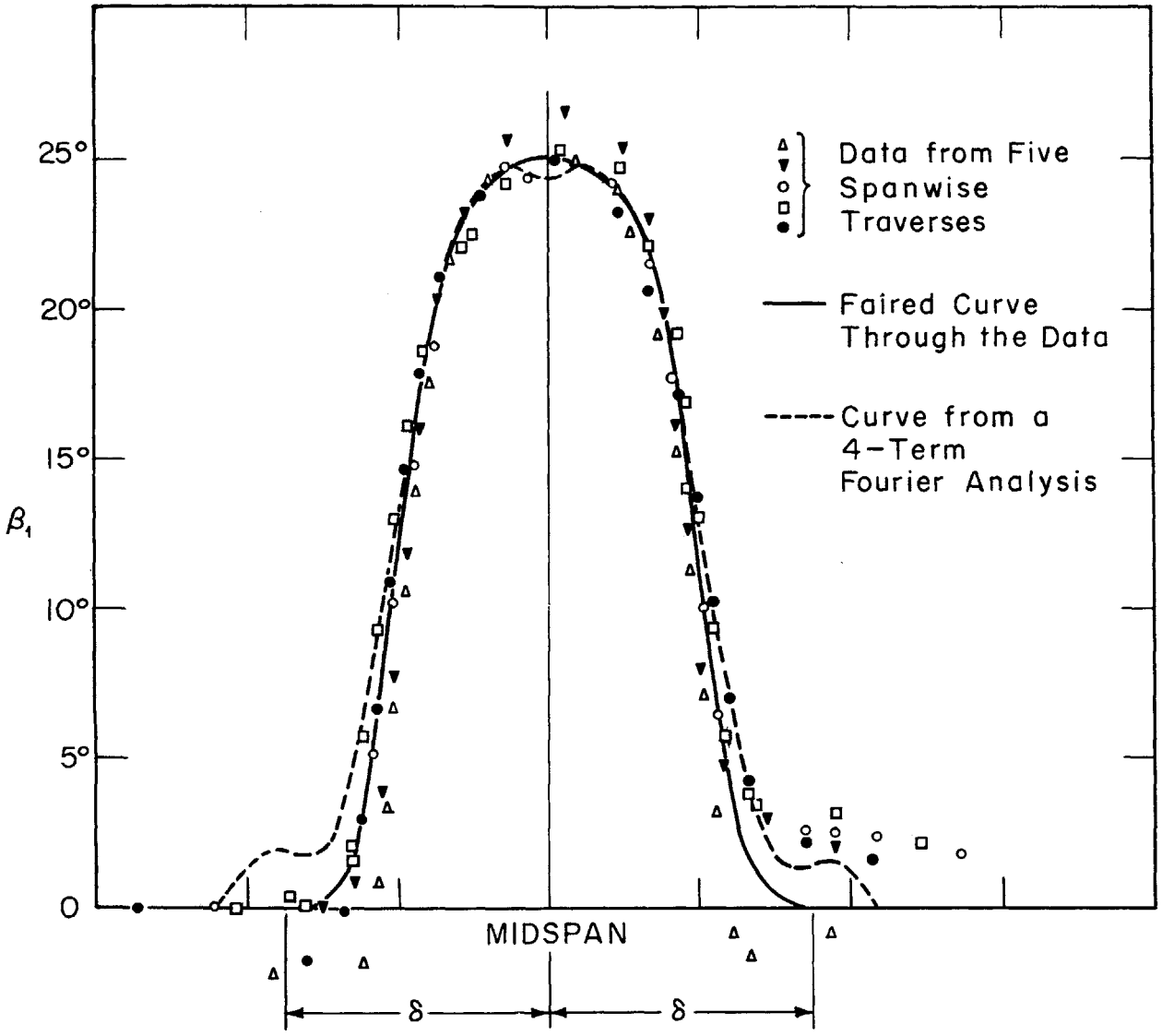

FIG. 45 SKEWED FLOW TRANSVERSE INLET ANGLE DISTRIBUTION OVER THE SPAN FOR VARIOUS TANGENTIAL POSITIONS

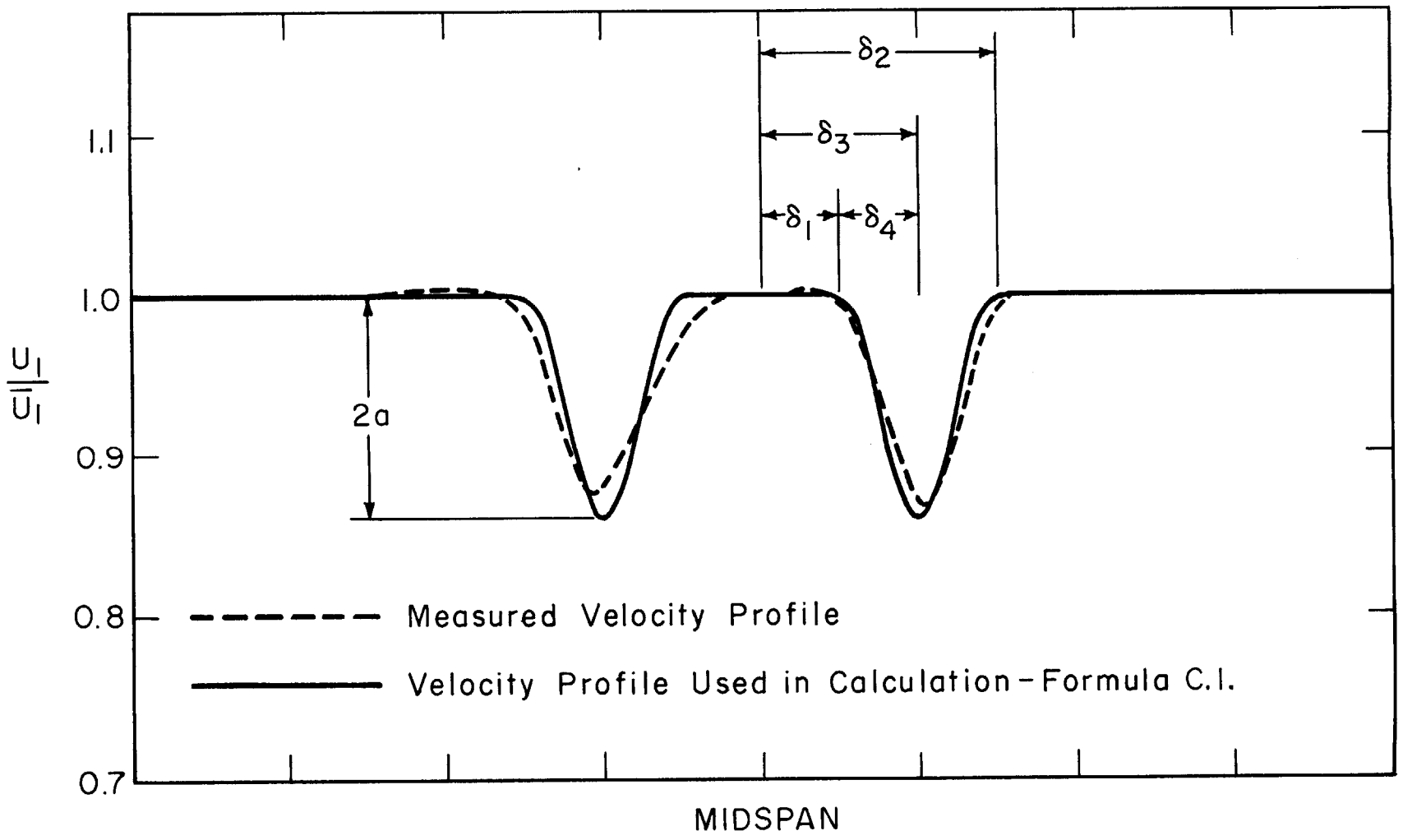

FIG. 46 SKEWED FLOW VELOCITY PROFILE AT CASCADE INLET

Scale Divisions Shown are in Inches

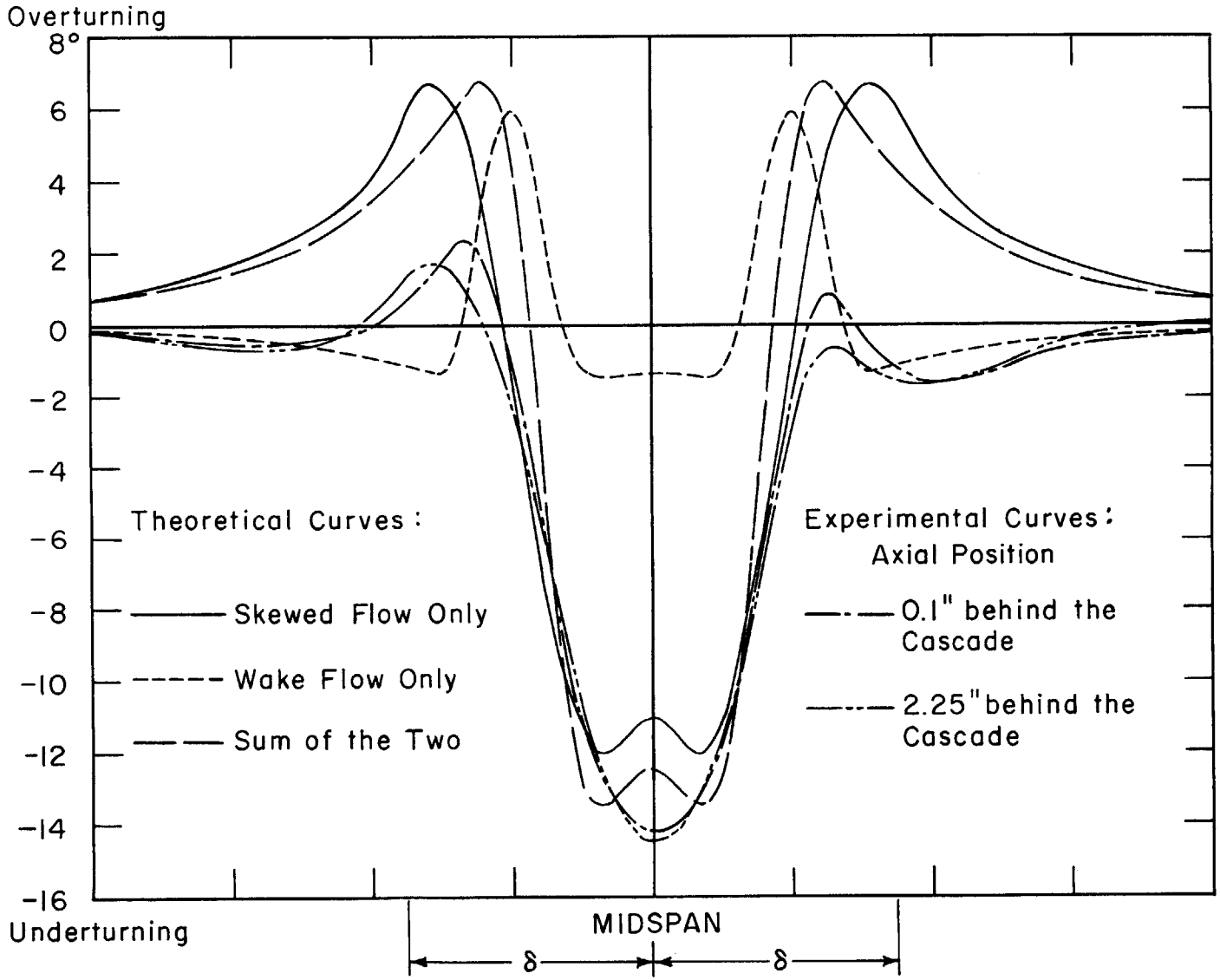

FIG. 47 SKEWED FLOW ANGLE MAXIMUM TRANSVERSE FLOW DEVIATION

Scale Divisions Shown are in Inches.

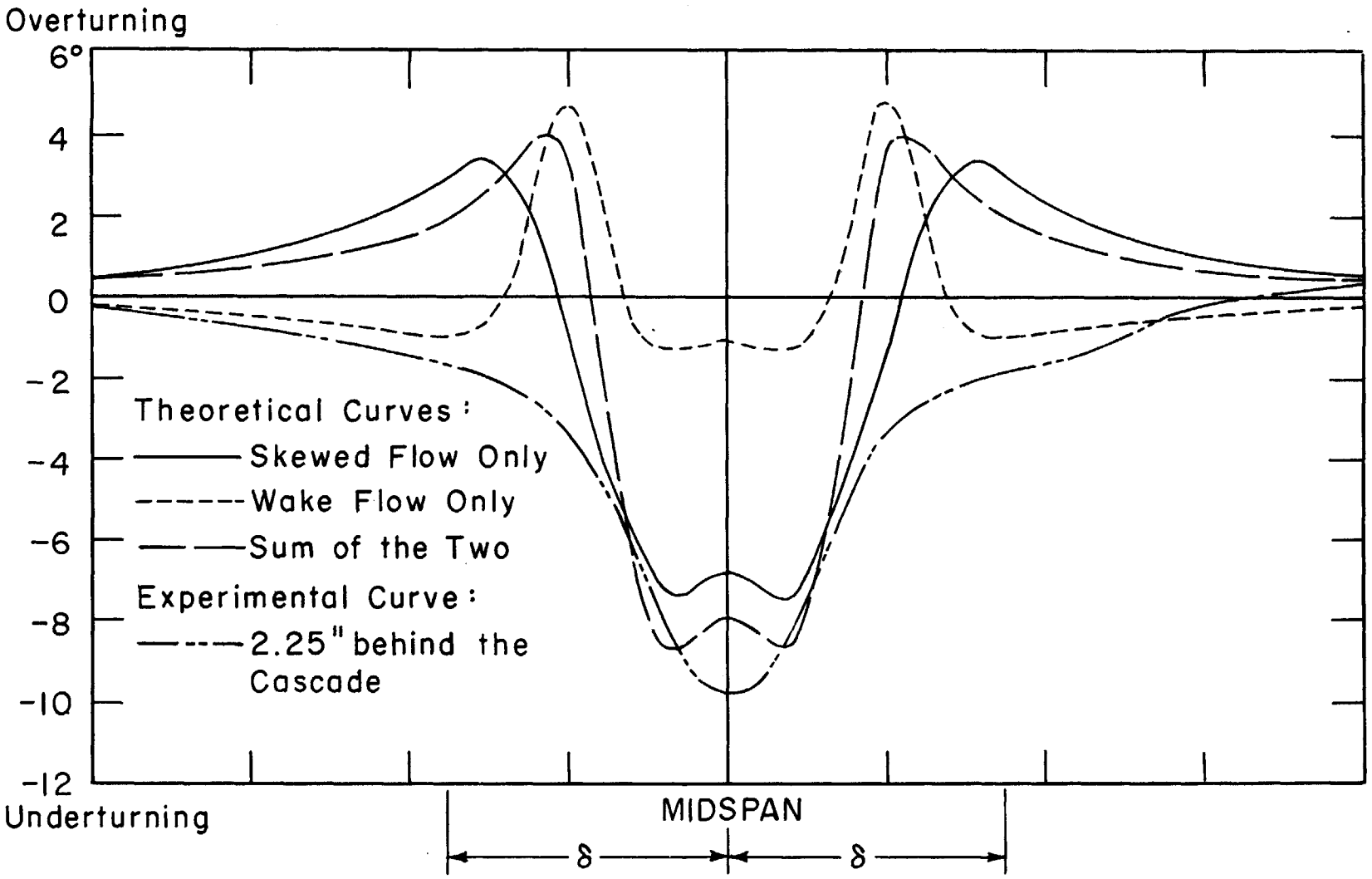

FIG. 48 SKEWED FLOW AVERAGE TRANSVERSE FLOW DEVIATION ANGLE

Scale Divisions Shown are in Inches.

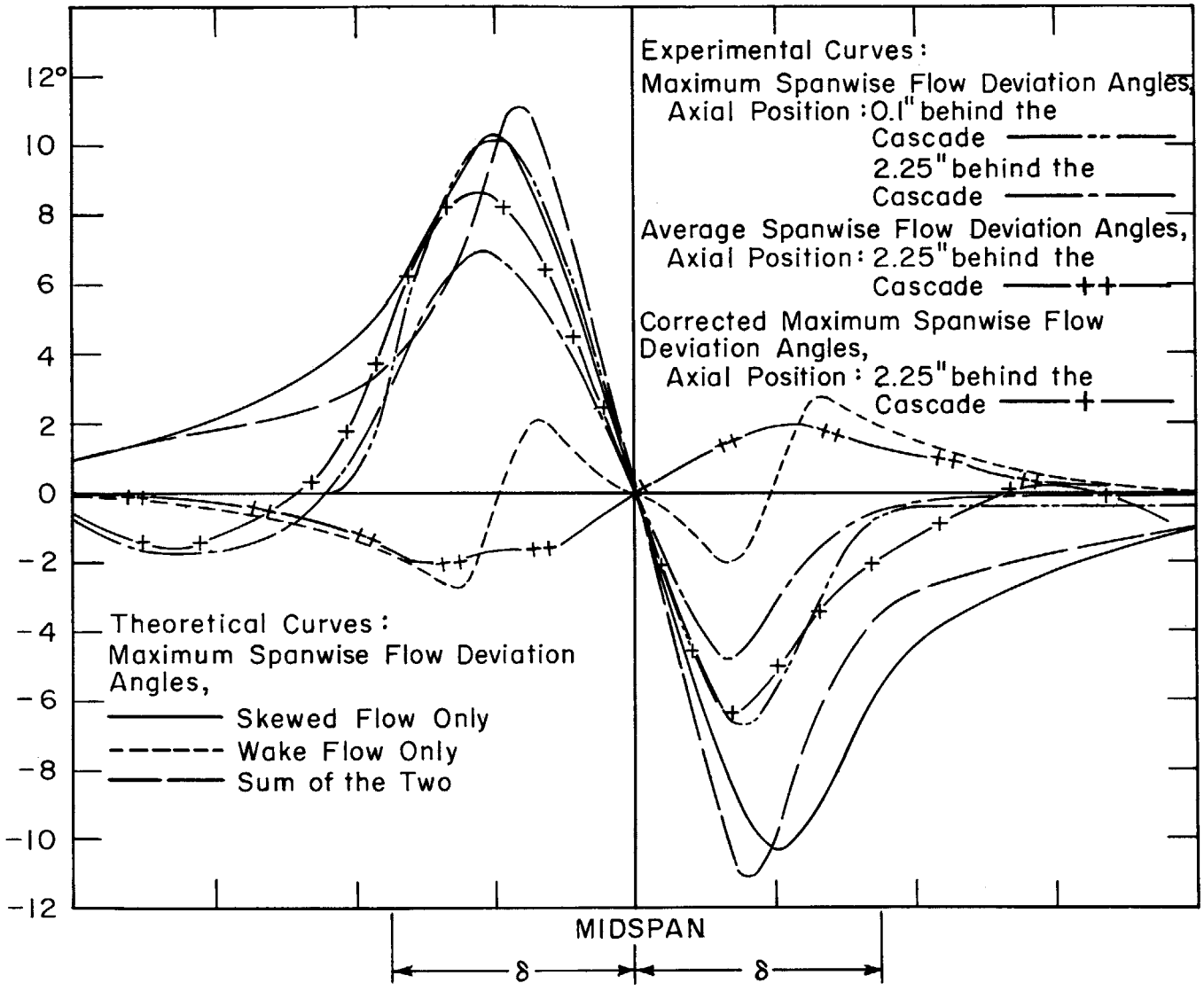

FIG. 49. SKEWED FLOW. SPANWISE FLOW DEVIATION ANGLE

Scale Divisions Shown are in Inches

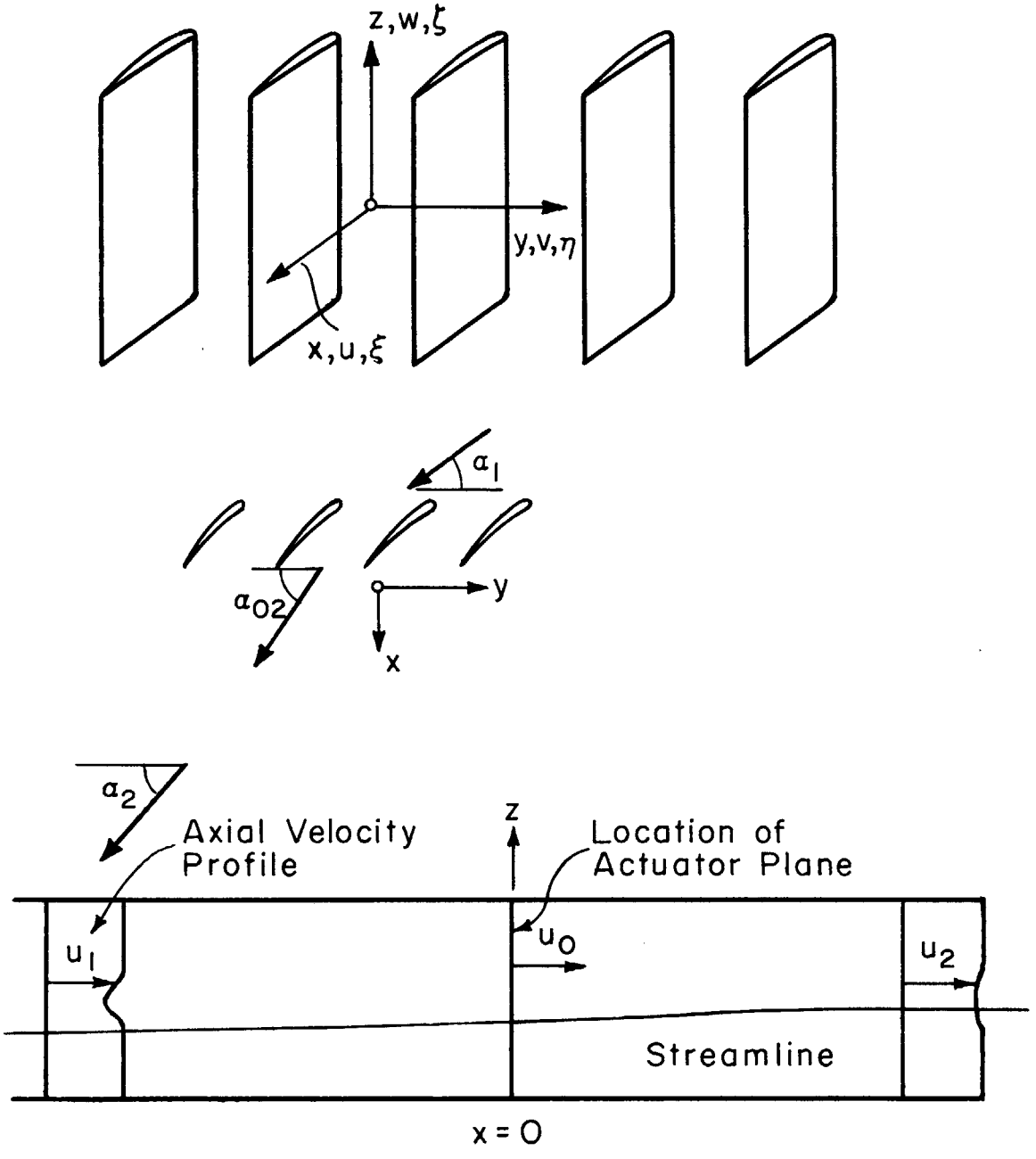

FIG. 50 SKEWED FLOW. NOMENCLATURE OF ACTUATOR DISC THEORY

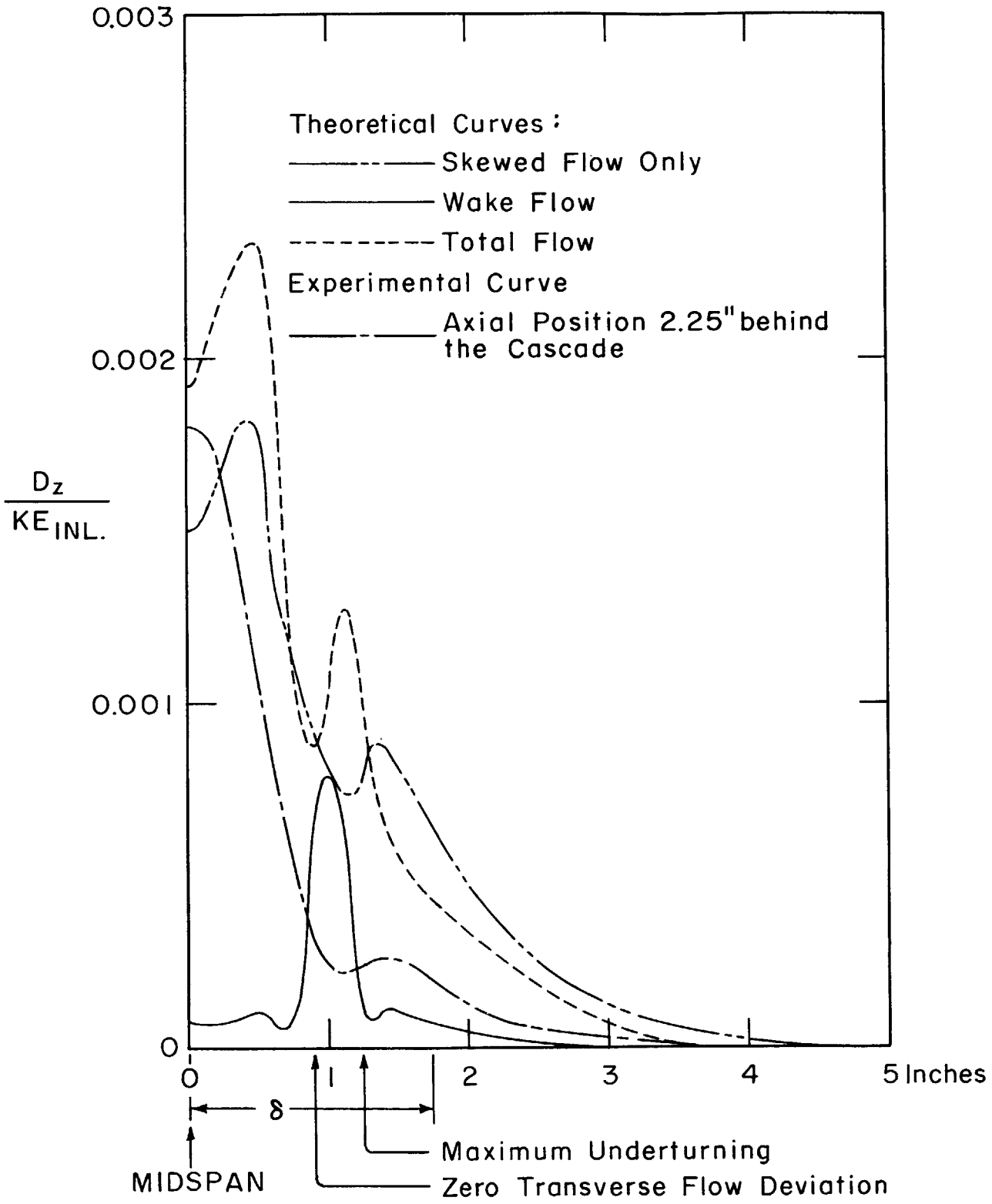

FIG. 51 SKEWED FLOW SPANWISE DISTRIBUTION OF THE KINETIC ENERGY OF THE SECONDARY FLOW

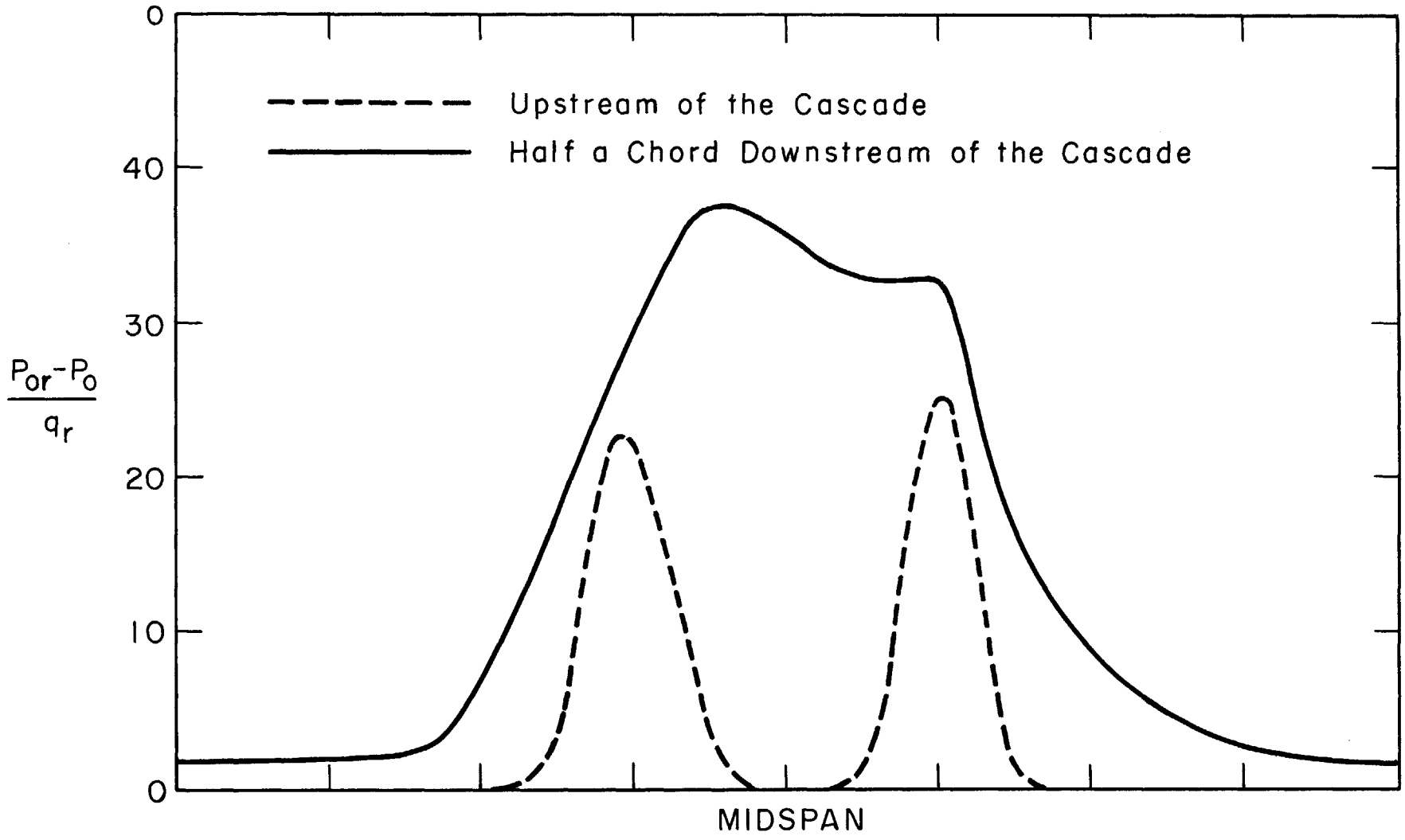

FIG. 52 SKEWED FLOW
SPANWISE DISTRIBUTION OF THE STAGNATION PRESSURE DEFECT AVERAGED OVER TWO BLADE SPACINGS
Scale Divisions Shown are in Inches

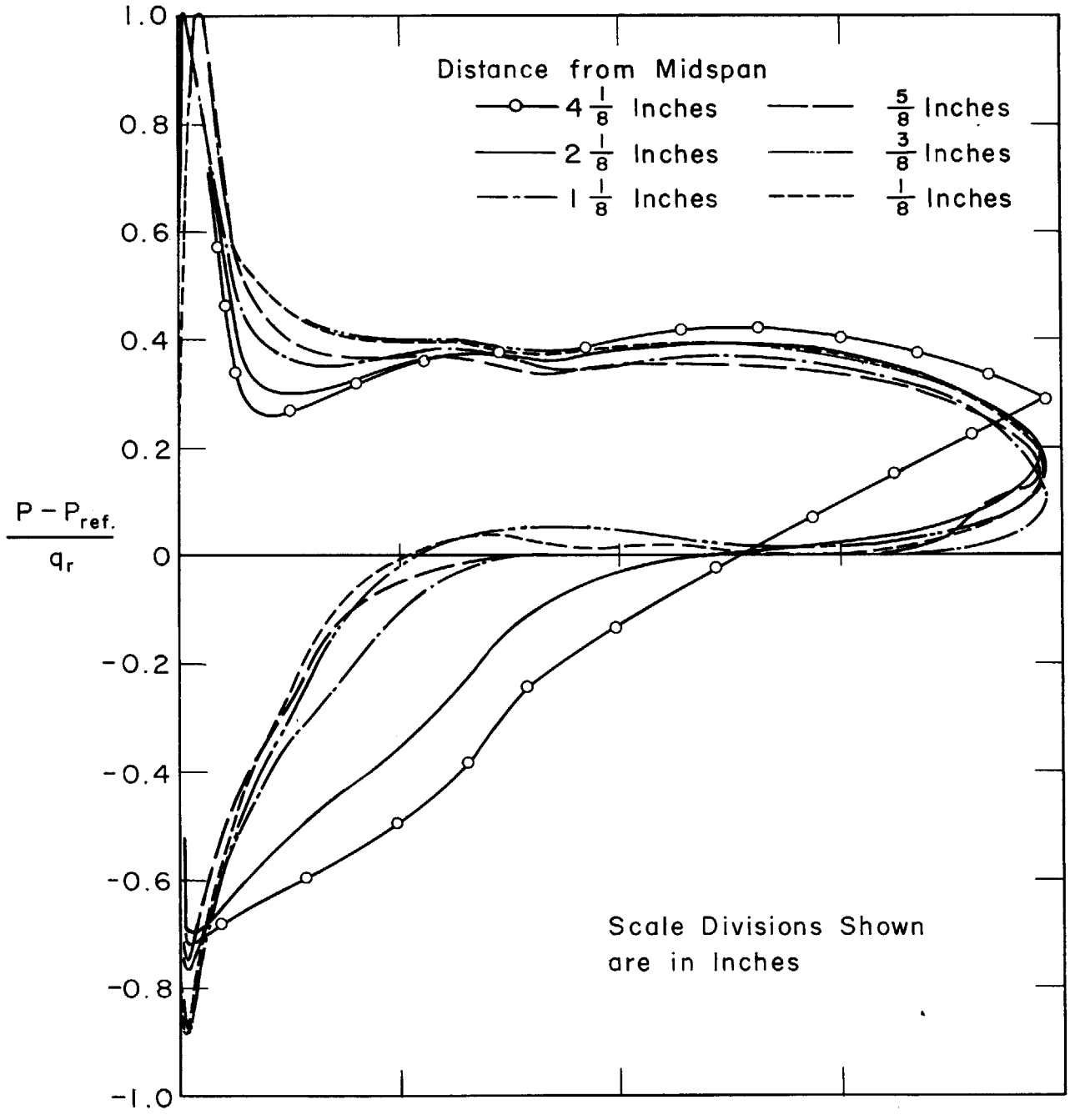

FIG. 53 SKEWED FLOW. PROJECTED STREAM PRESSURE DISTRIBUTION ON THE BLADE SURFACES

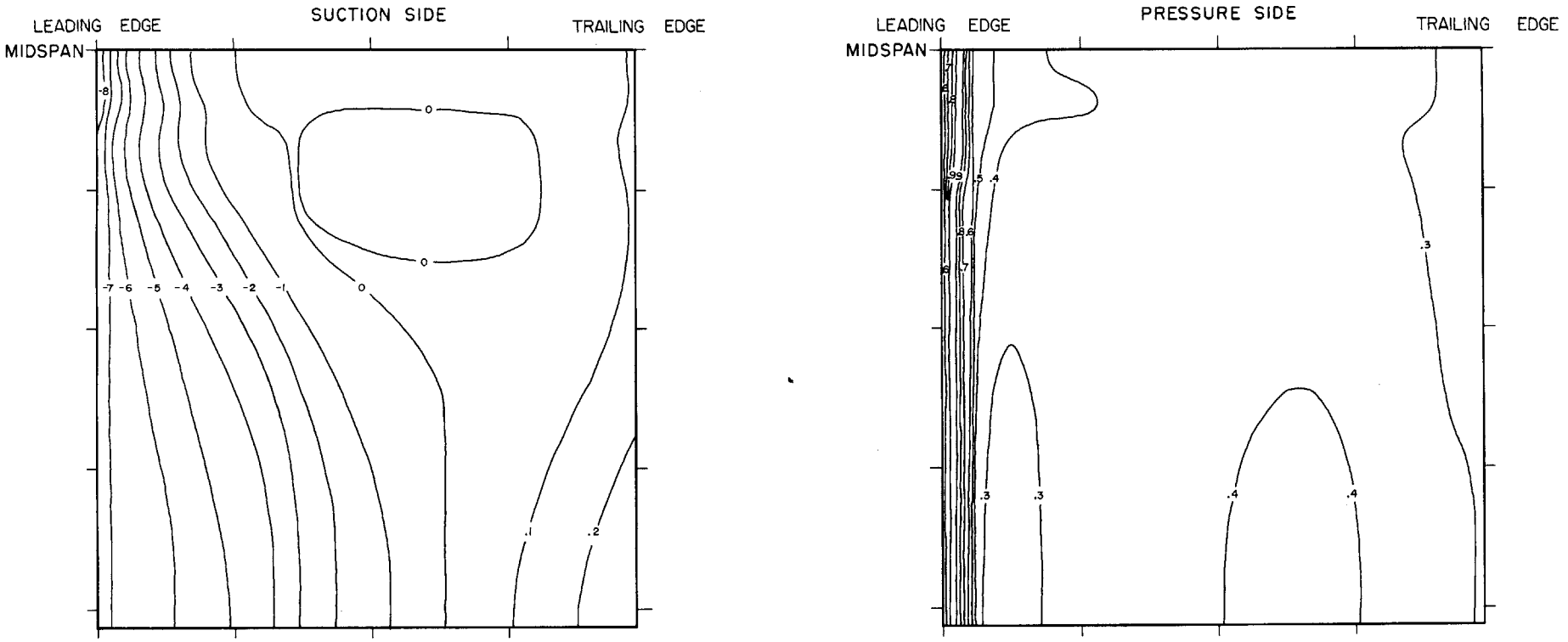

FIG. 54 SKEWED FLOW $\nabla P_o = 0$. CONTOURS OF CONSTANT STREAM PRESSURE ON THE BLADE SURFACES

Numbers on Contours Indicate $\frac{P - P_r}{q_r}$

Scale Divisions Shown are in Inches

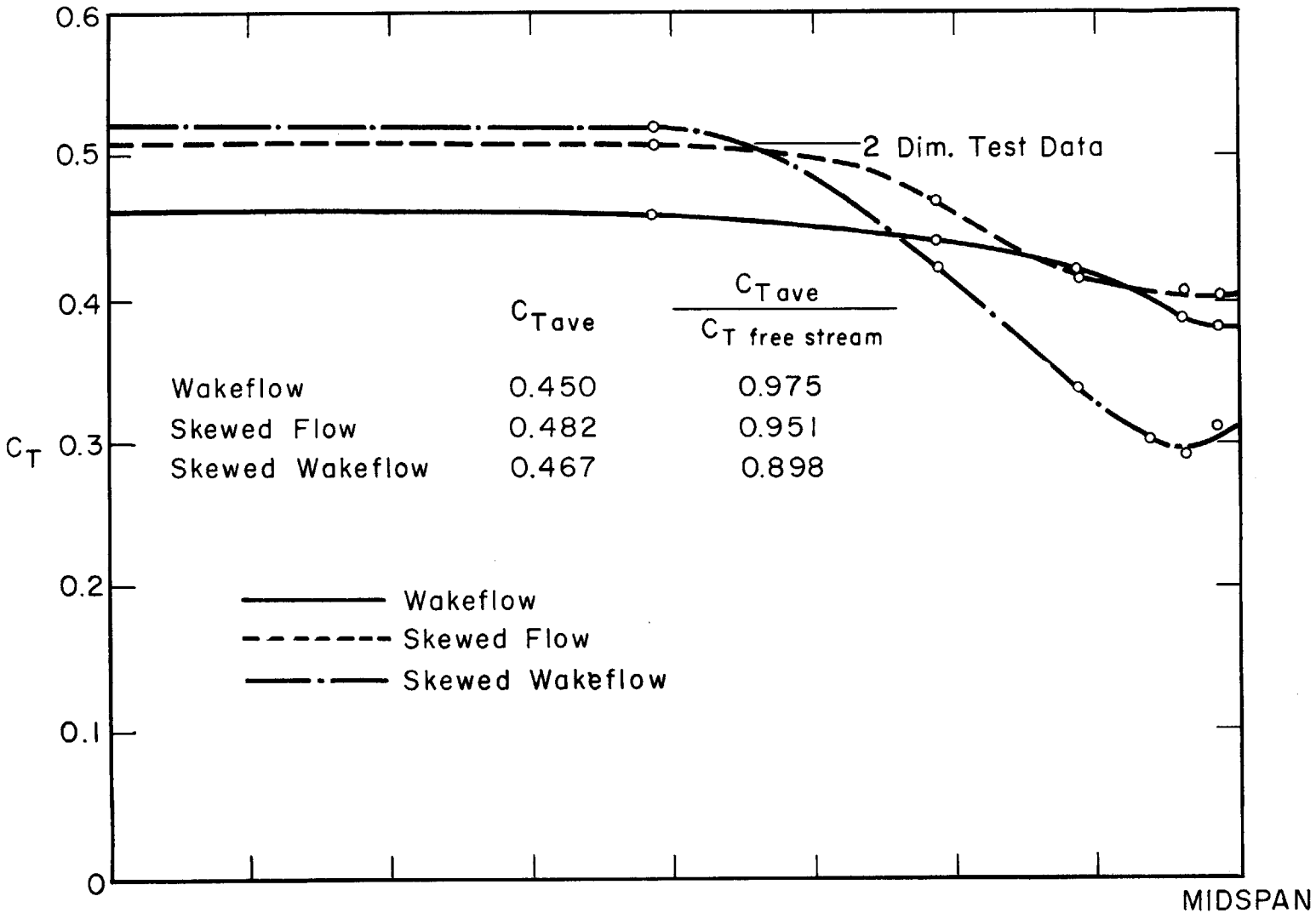

FIG. 55 SPANWISE DISTRIBUTION OF THE TANGENTIAL PRESSURE COEFFICIENT C_T

Scale Divisions Shown are in Inches

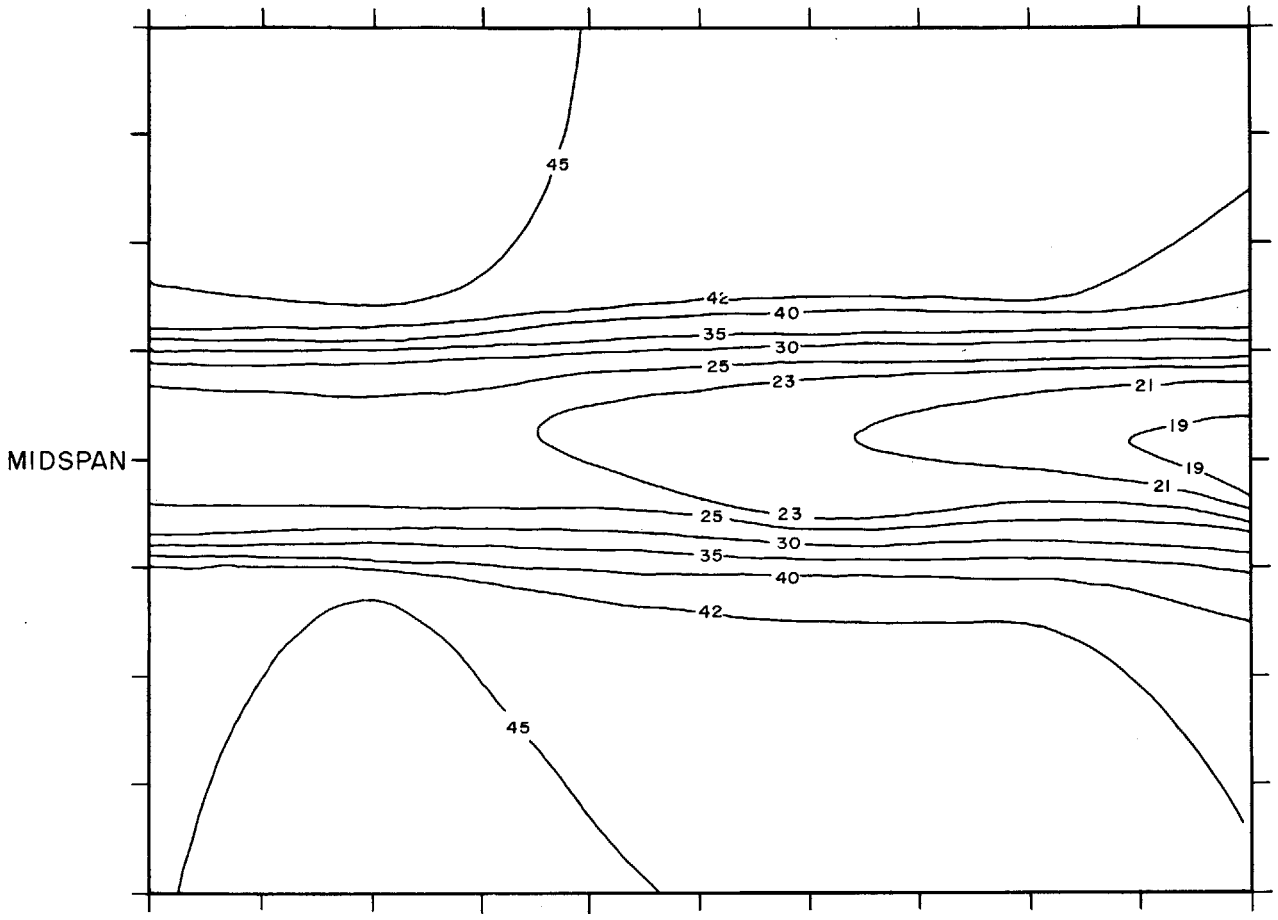

FIG. 56 SKEWED WAKEFLOW $\nabla P_0 \neq 0$. CONTOURS OF CONSTANT TRANSVERSE INLET ANGLES

Numbers on Contours Indicate Constant Transverse Inlet Angles

Scale Divisions Shown are in Inches

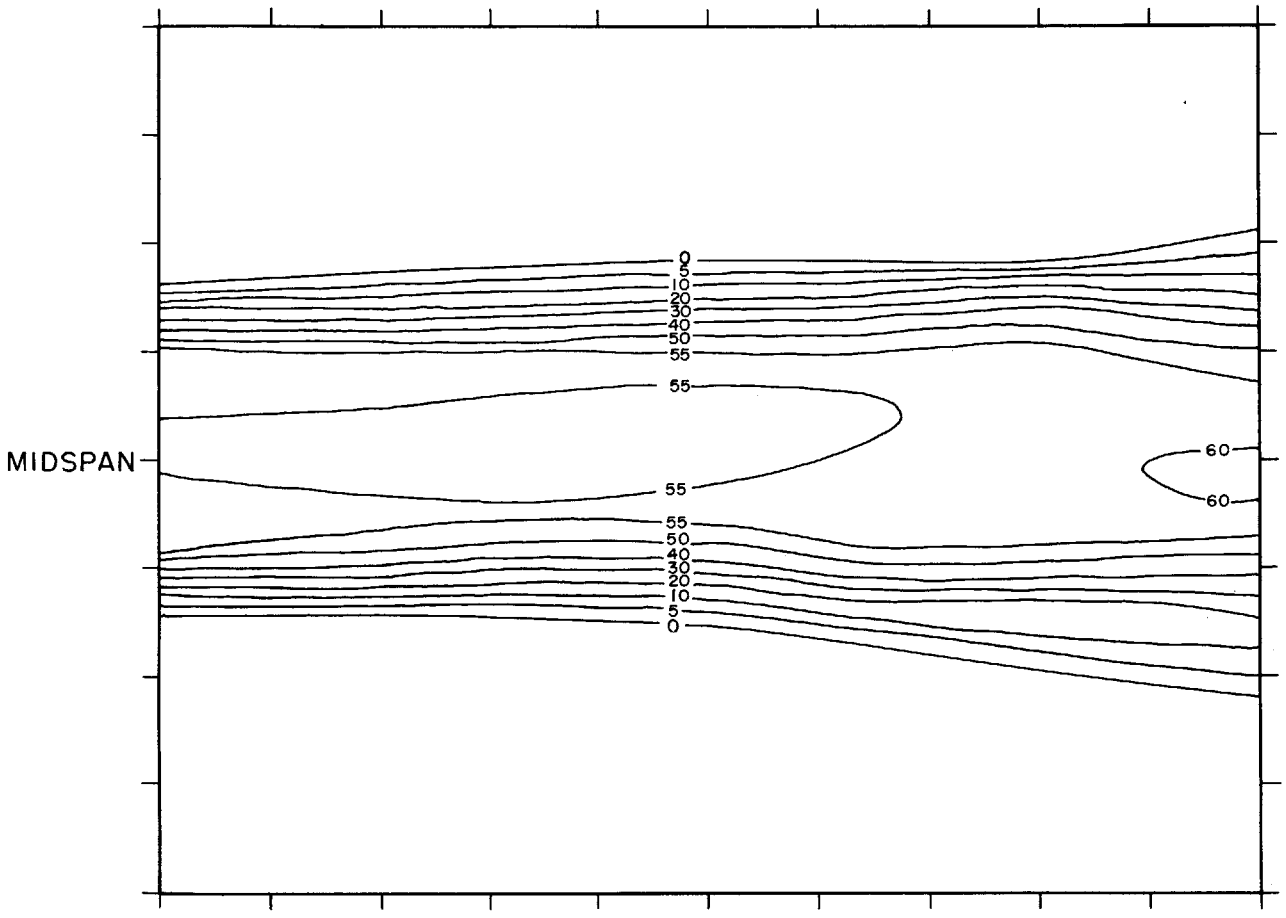

FIG. 57 SKEWED WAKEFLOW $\nabla P_o \neq 0$. CONTOURS OF CONSTANT STAGNATION PRESSURE UPSTREAM OF CASCADE

Numbers on Contours Indicate $\frac{P_{or} - P_{ol}}{q_r}$ in Percentage

Scale Divisions Shown are in Inches

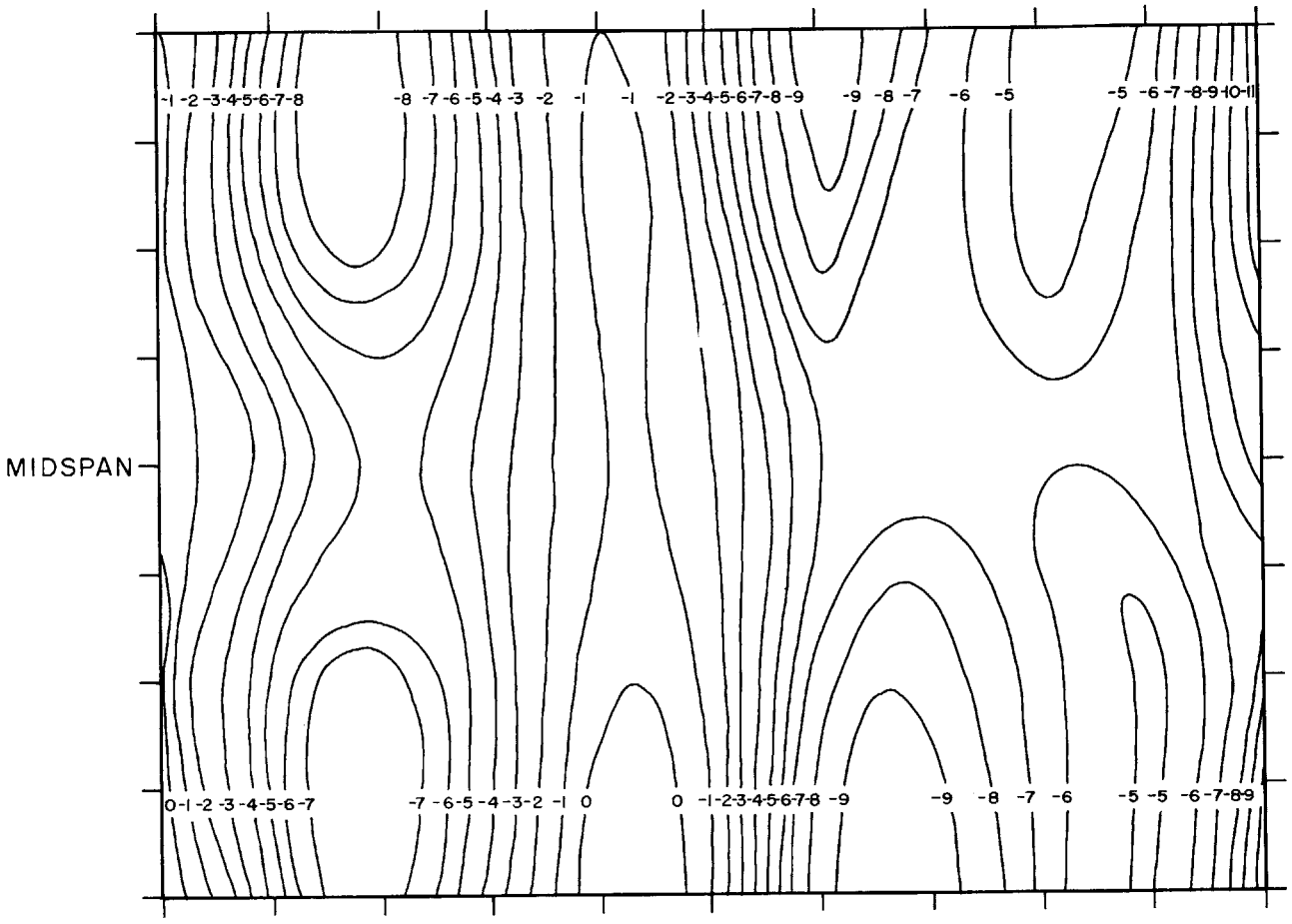

FIG. 58 SKEWED WAKEFLOW $\nabla P_0 \neq 0$. CONTOURS OF CONSTANT STREAM PRESSURE UPSTREAM OF CASCADE

Numbers on Contours Indicate $\frac{P_r - P}{q}$

Scale Divisions Shown are in Inches

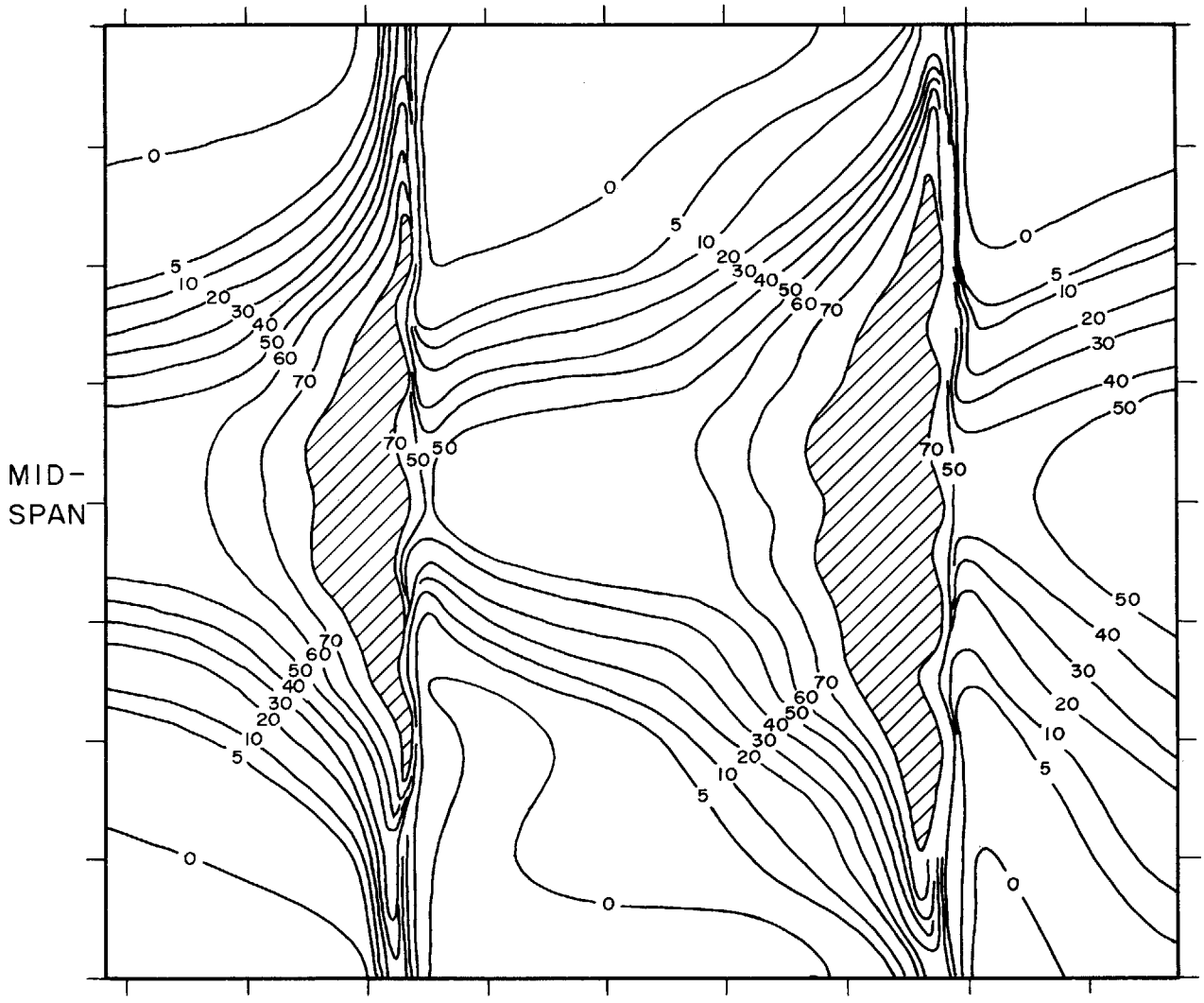

FIG. 59 SKEWED WAKEFLOW $\nabla P_0 \neq 0$. CONTOURS OF CONSTANT STAGNATION PRESSURE

AXIAL POSITION: 0.1" behind the Cascade

Numbers on Contours Indicate Constant $\frac{P_{or}-P_{o2}}{q_r}$ in Percentage

Scale Divisions Shown are in Inches

Shaded Areas are Regions of Backflow

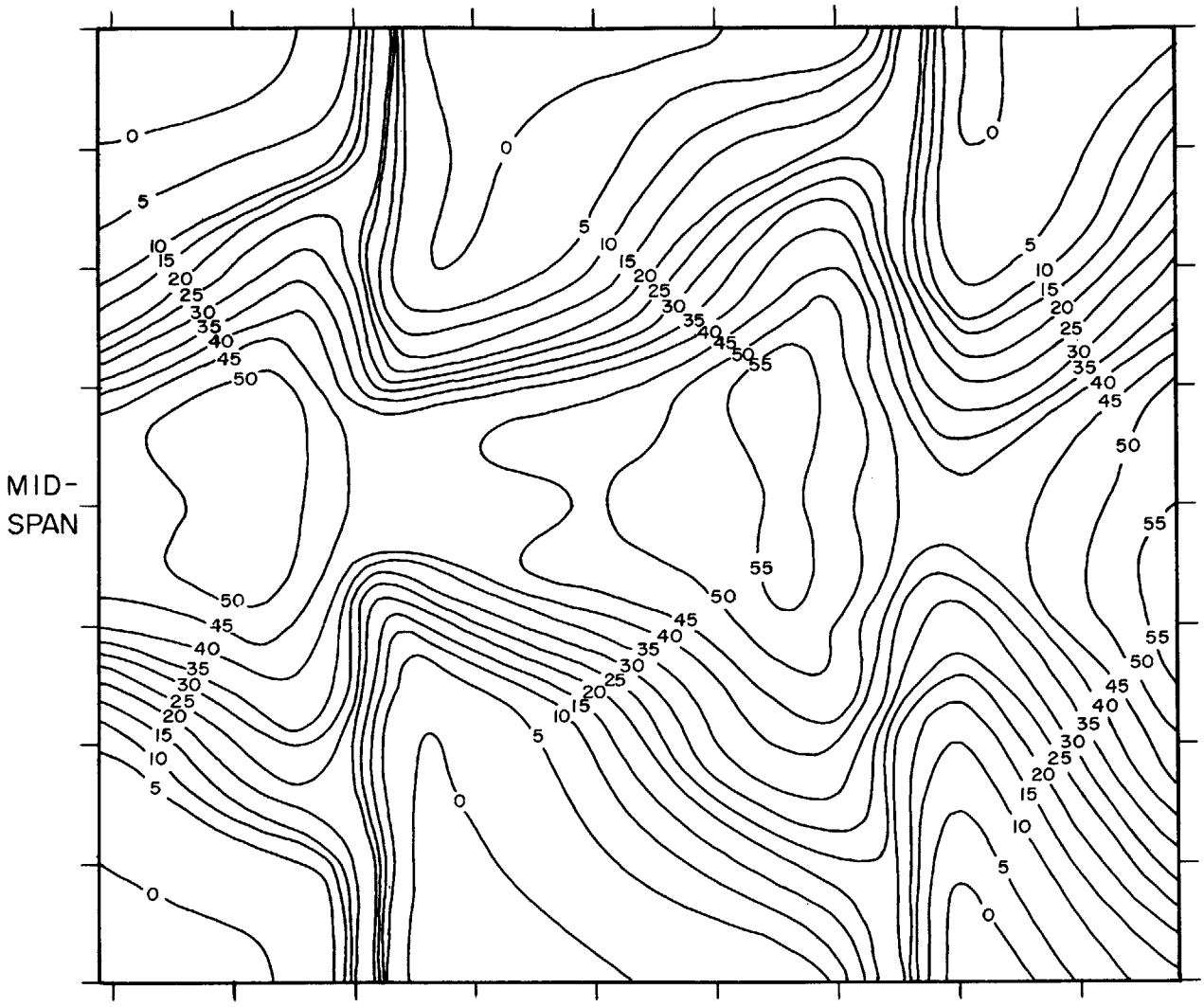

FIG. 60 SKEWED WAKEFLOW $\nabla P_o \neq 0$. CONTOURS OF CONSTANT STAGNATION PRESSURE

AXIAL POSITION: 2.25" behind the Cascade

Numbers on Contours Indicate Constant $\frac{P_{or} - P_{o2}}{q_r}$

Scale Divisions Shown are in Inches

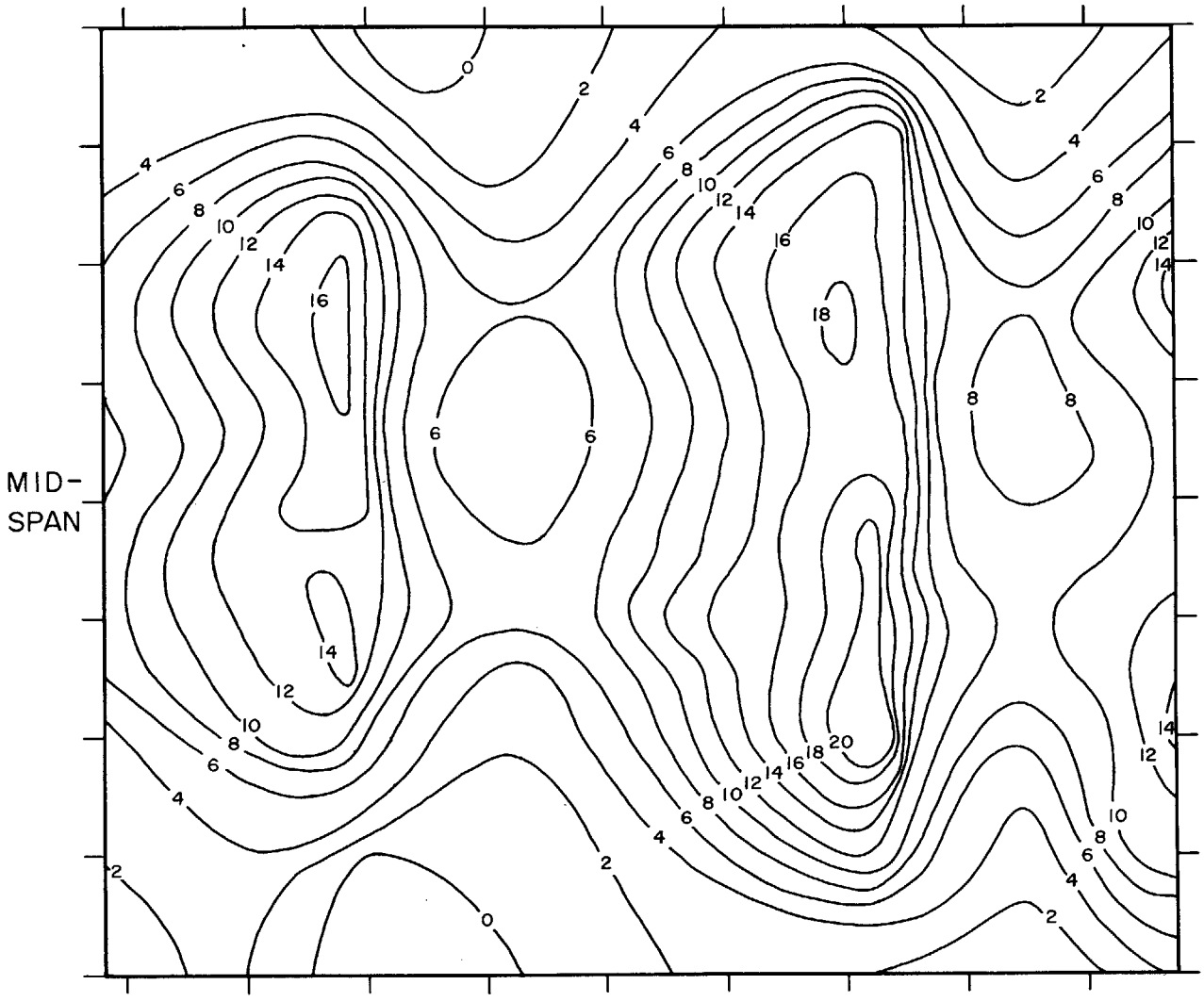

FIG. 61 SKEWED WAKEFLOW $\nabla P_0 \neq 0$. CONTOURS OF CONSTANT STREAM PRESSURE

AXIAL POSITION: 0.35" behind the Cascade

Numbers on Contours Indicate Constant $\frac{P_{atm} - P}{q_r}$

Scale Divisions Shown are in Inches

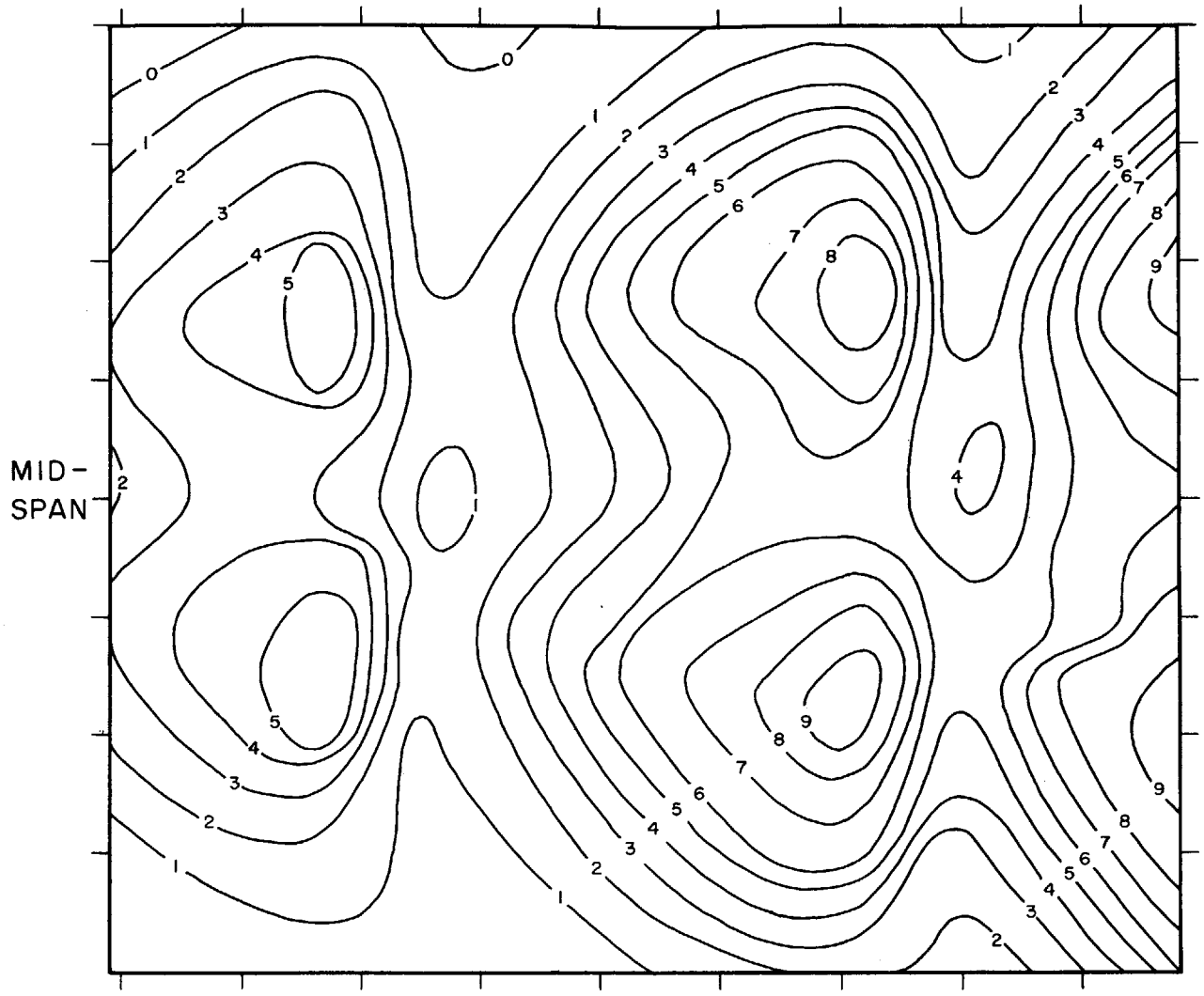

FIG. 62 SKEWED WAKEFLOW $\nabla P_o \neq 0$. CONTOURS OF CONSTANT STREAM PRESSURE

AXIAL POSITION: 2.25" behind the Cascade

Numbers on Contours Indicate Constant $\frac{P_{atm} - P}{q_r}$

Scale Divisions Shown are in Inches

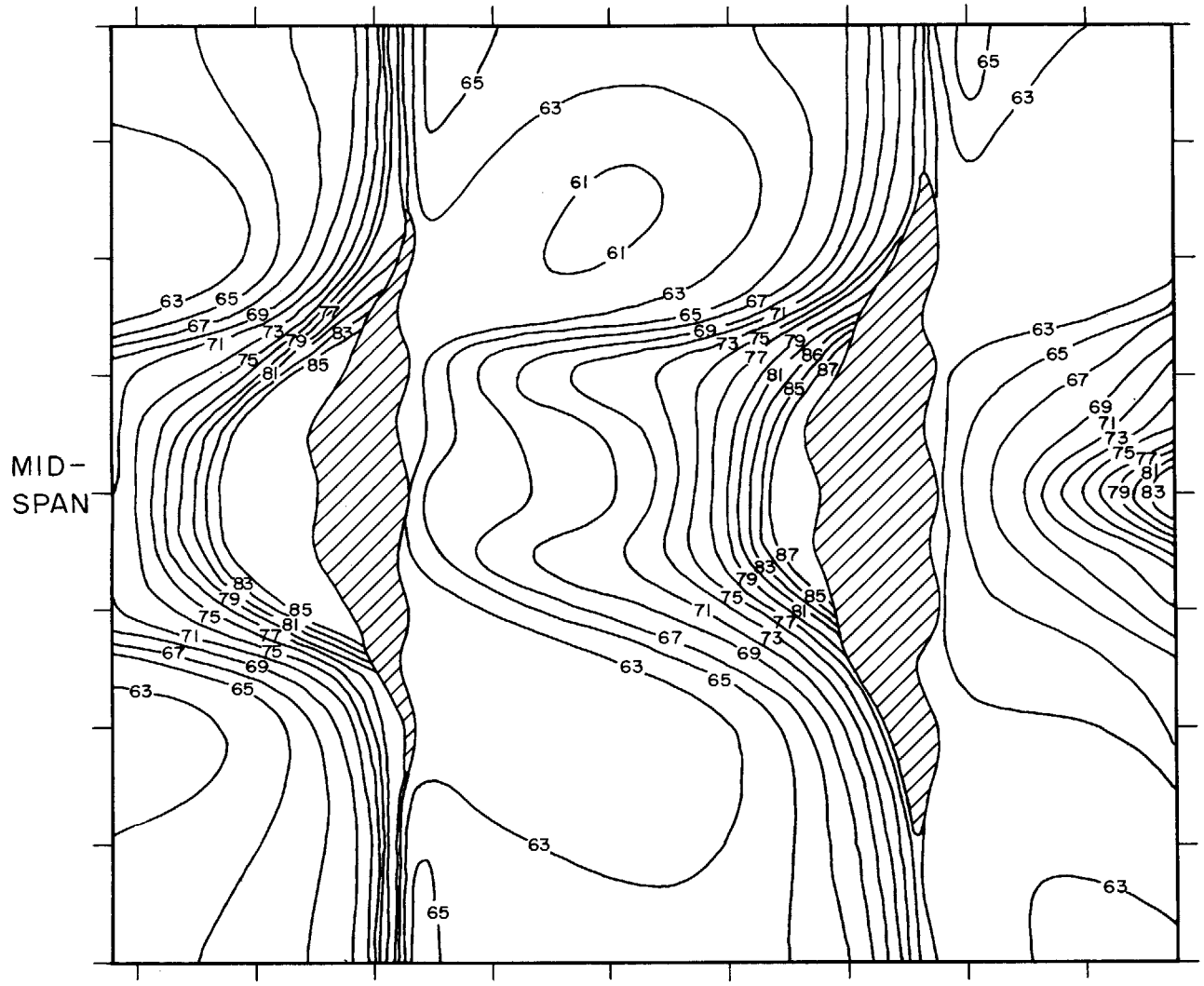

FIG. 63 SKEWED WAKEFLOW $\nabla P_0 \neq 0$. CONTOURS OF CONSTANT TRANSVERSE FLOW ANGLE

AXIAL POSITION: 0.1" behind the Cascade

Numbers on Contours Indicate Constant Transverse Flow Angles Measured from Tangential Direction

Scale Divisions Shown are in Inches

Shaded Areas are Regions of Backflow

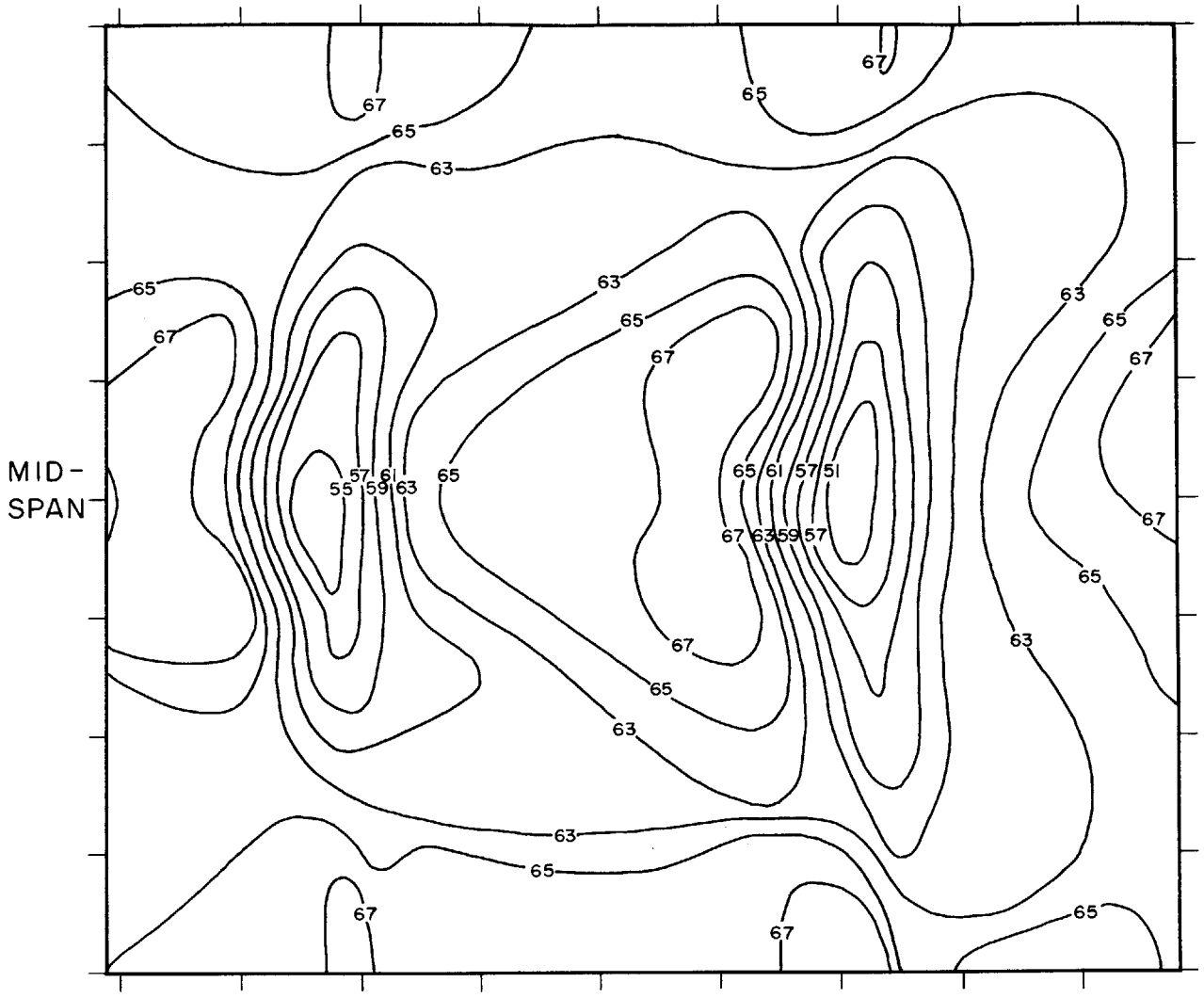

FIG. 64 SKEWED WAKEFLOW $\nabla P_0 \neq 0$. CONTOURS OF CONSTANT TRANSVERSE FLOW ANGLE

AXIAL POSITION: 2.25" behind the Cascade

Numbers on Contours Indicate Constant Transverse Flow Angles Measured from Tangential Direction

Scale Divisions Shown are in Inches

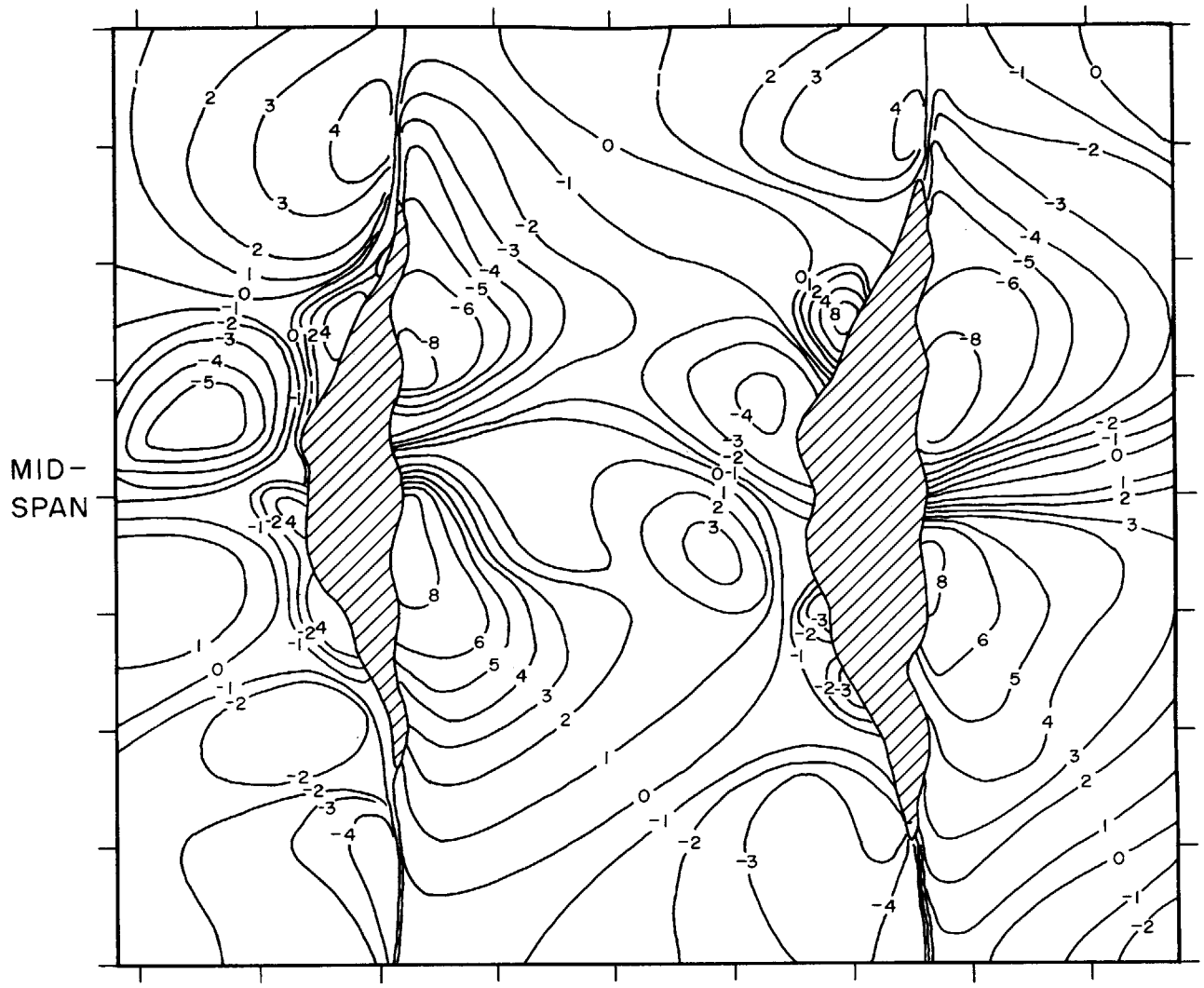

FIG. 65 SKEWED WAKEFLOW $\nabla P_o \neq 0$. CONTOURS OF CONSTANT SPANWISE FLOW DEVIATION ANGLES

AXIAL POSITION: 0.1" behind the Cascade

Numbers on Contours Indicate Constant Spanwise Flow Deviation Angles

Positive Numbers Indicate Flow Towards the Top of the Cascade

Scale Divisions Shown are in Inches

Shaded Areas are Regions of Backflow

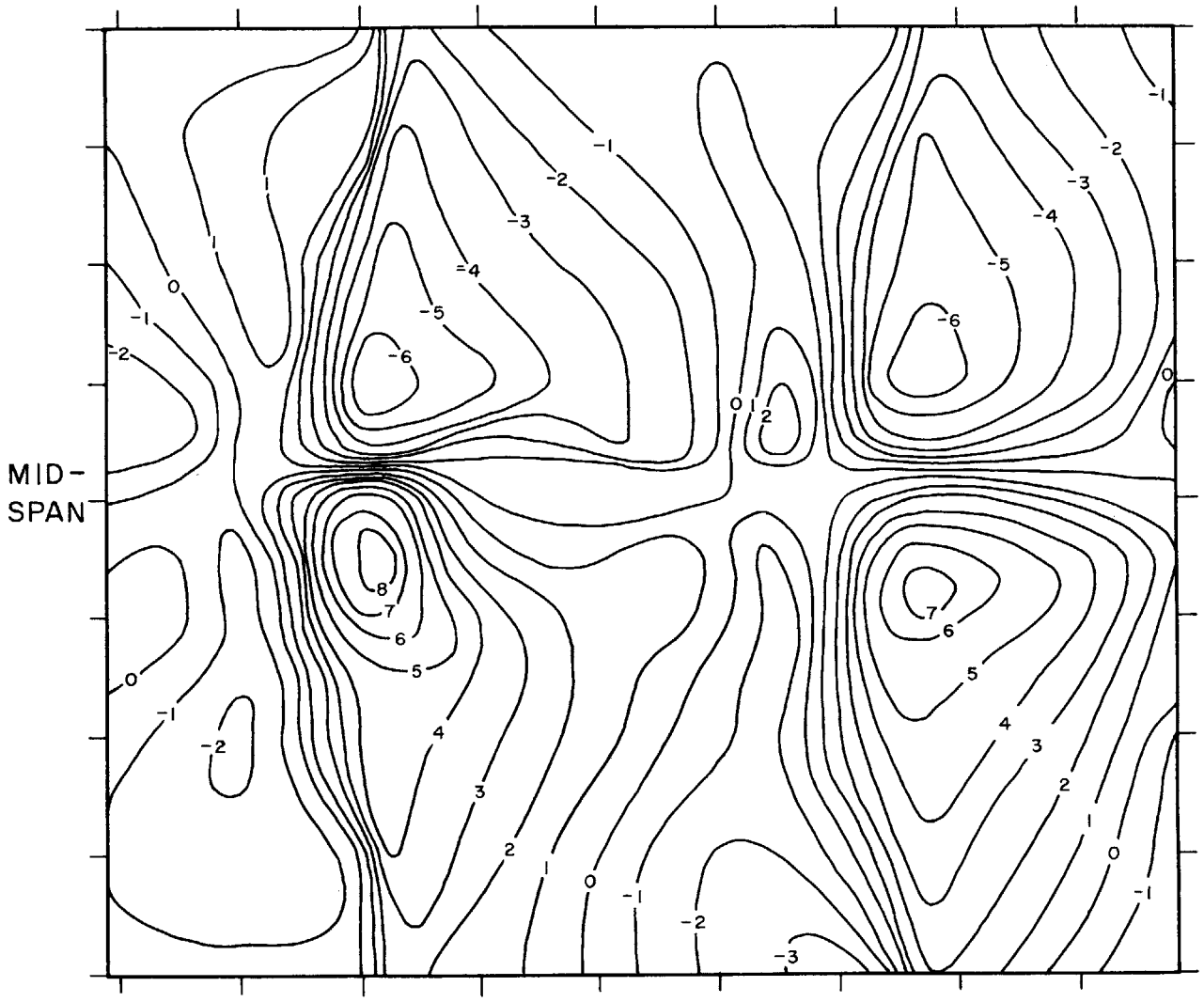

FIG. 66 SKEWED WAKEFLOW $\nabla P_0 \neq 0$. CONTOURS OF CONSTANT SPANWISE FLOW DEVIATION ANGLES

AXIAL POSITION: 2.25" behind the Cascade

Numbers on Contours Indicate Constant Spanwise Flow Deviation Angles

Positive Numbers Indicate Flow Towards The Top of The Cascade

Scale Divisions Shown are in Inches

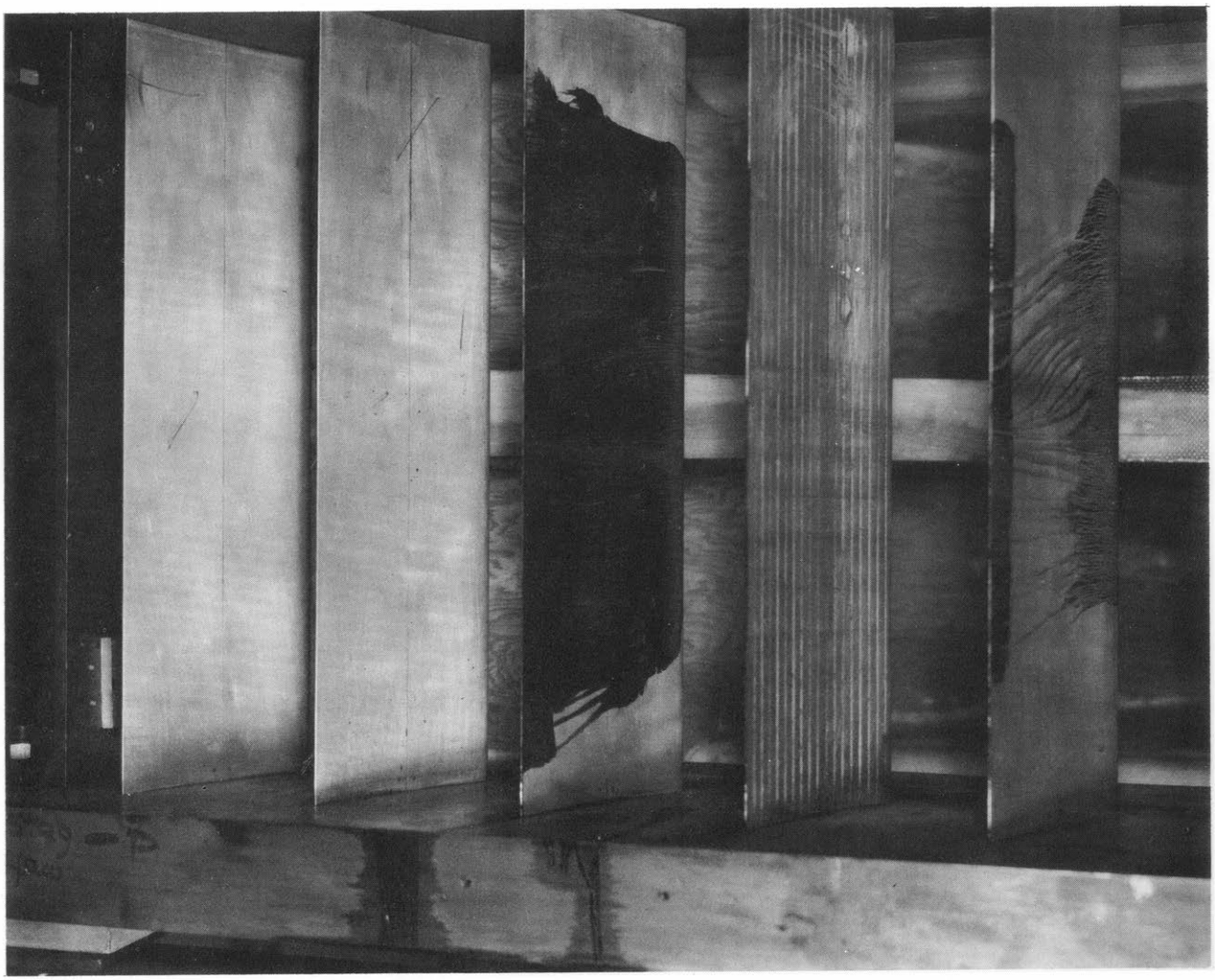

FIGURE 67 SKEWED WAKE FLOW. STREAMLINE TRACES IN CARBON BLACK ON THE BLADE PRESSURE SIDE.

FIGURE 68 SKEWED WAKE FLOW. STREAMLINE TRACES IN CARBON BLACK ON THE BLADE SUCTION SIDE.

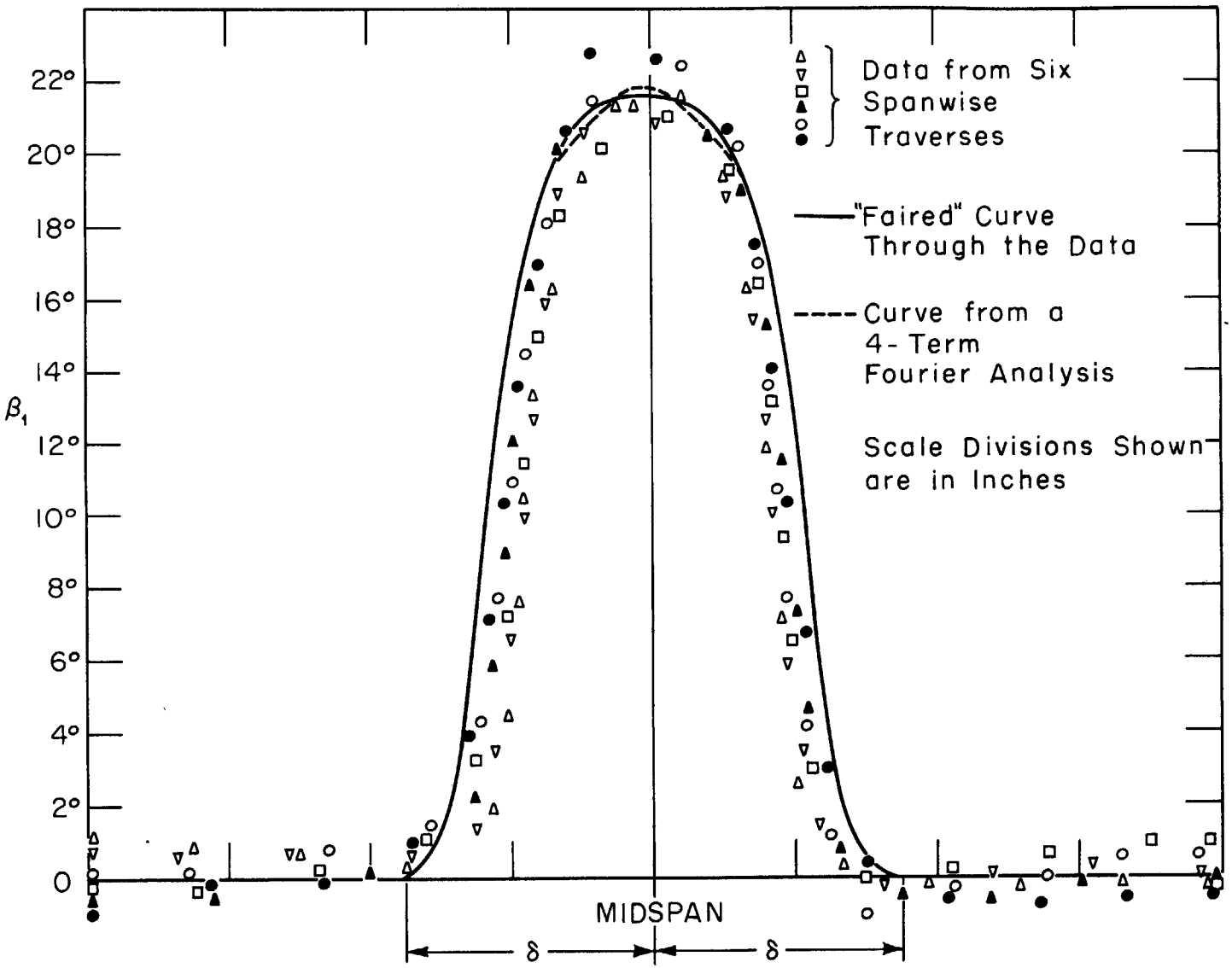

FIG. 69 SKEWED WAKE FLOW TRANSVERSE INLET ANGLE DISTRIBUTION OVER THE SPAN FOR VARIOUS TANGENTIAL POSITIONS

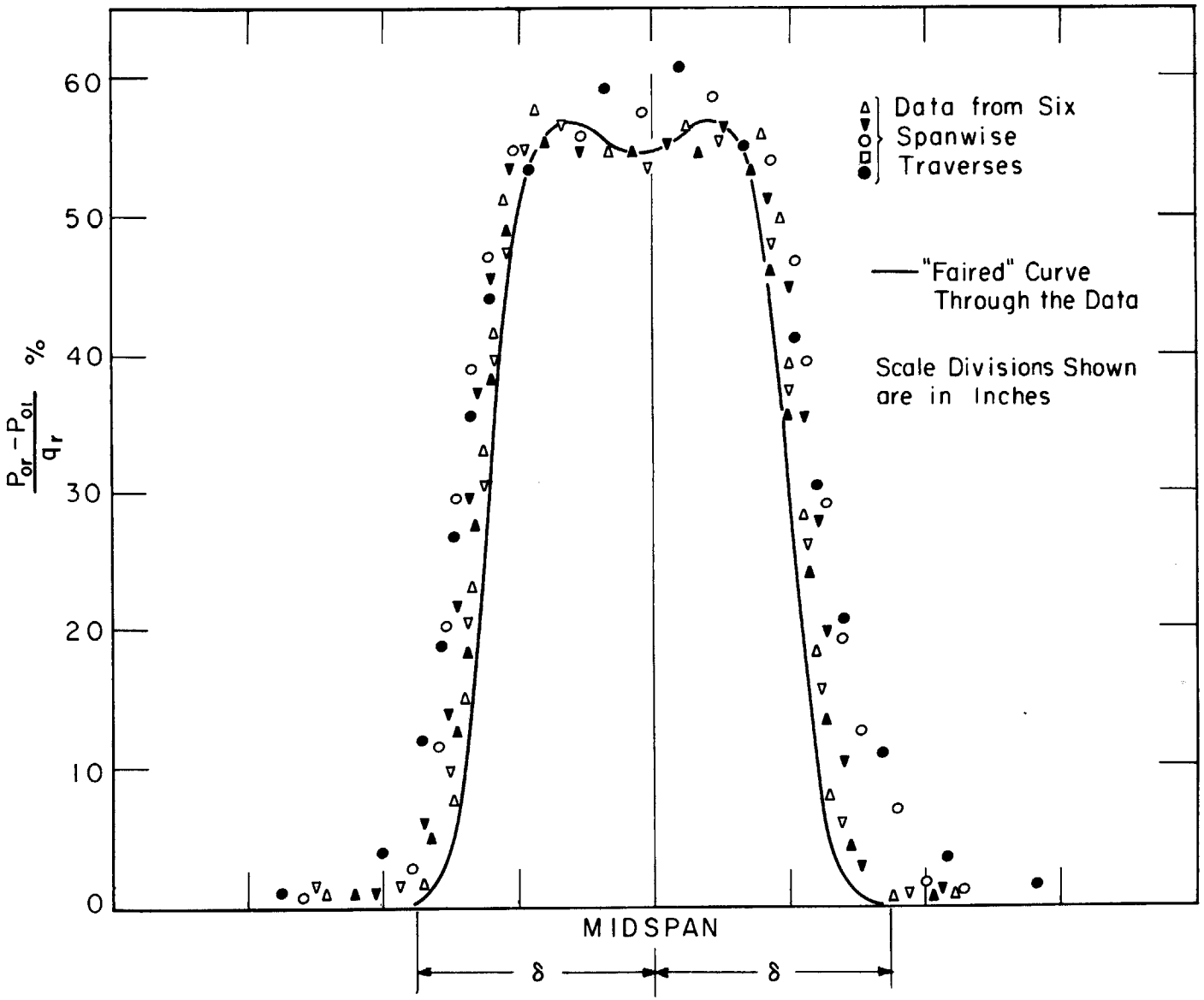

FIG. 70 SKEWED WAKE FLOW INLET STAGNATION PRESSURE DISTRIBUTION OVER THE SPAN FOR VARIOUS TANGENTIAL POSITIONS

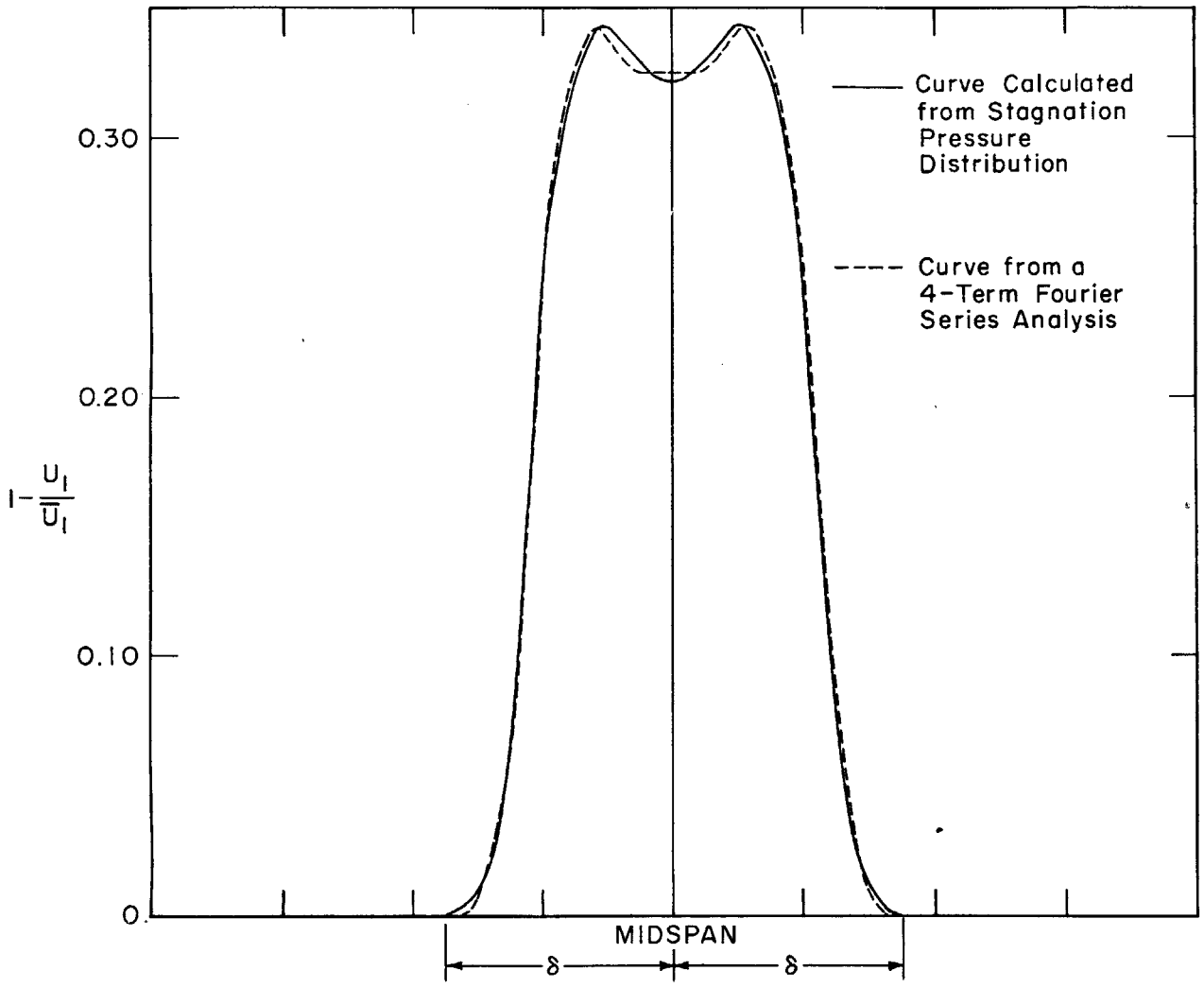

FIG. 71 SKEWED WAKEFLOW INLET VELOCITY DISTRIBUTION OVER THE SPAN

Scale Divisions Shown are in Inches.

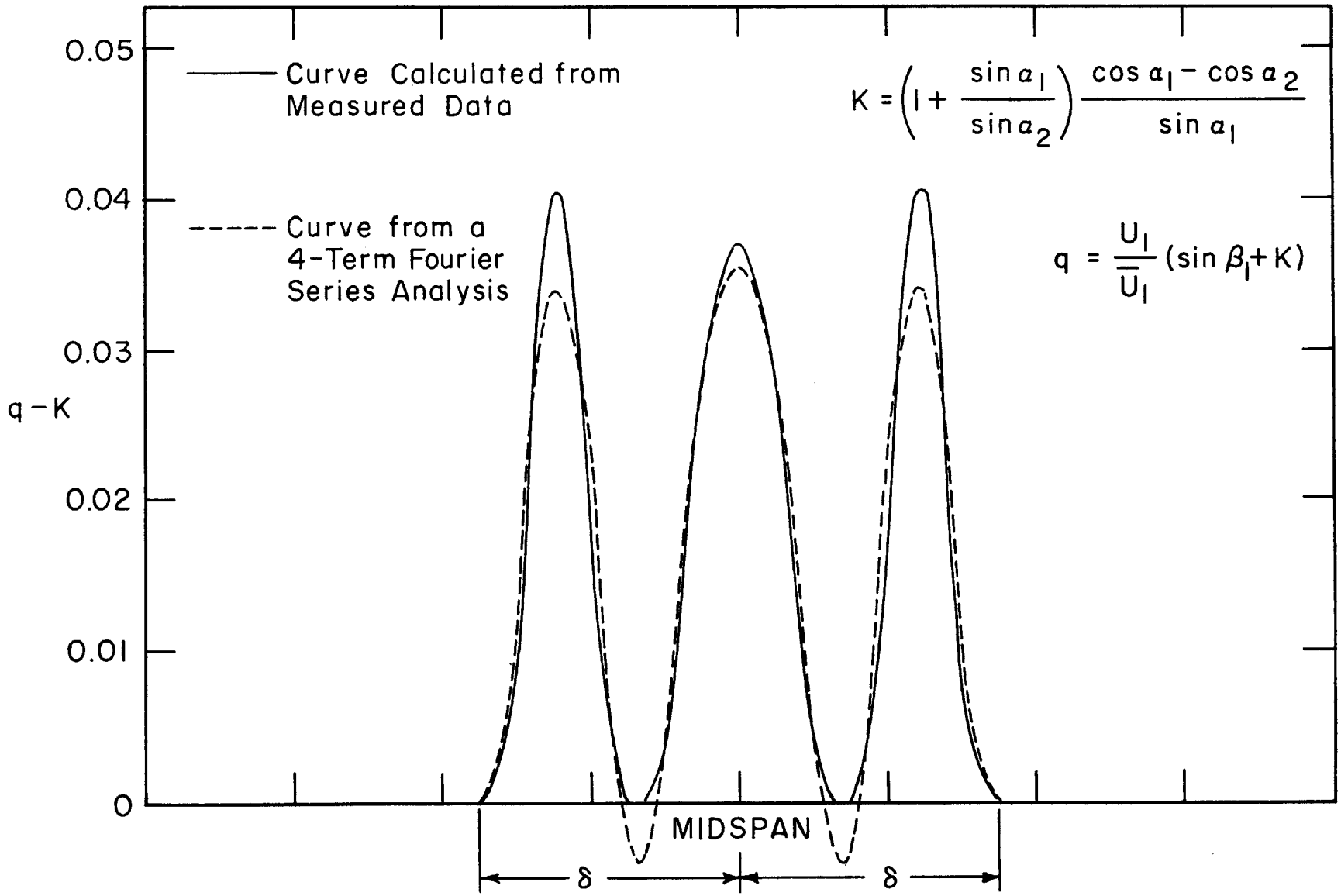

FIG. 72 SKEWED WAKEFLOW INLET CONDITION USED IN CALCULATION FOR SECONDARY FLOW

Scale Divisions Shown are in Inches.

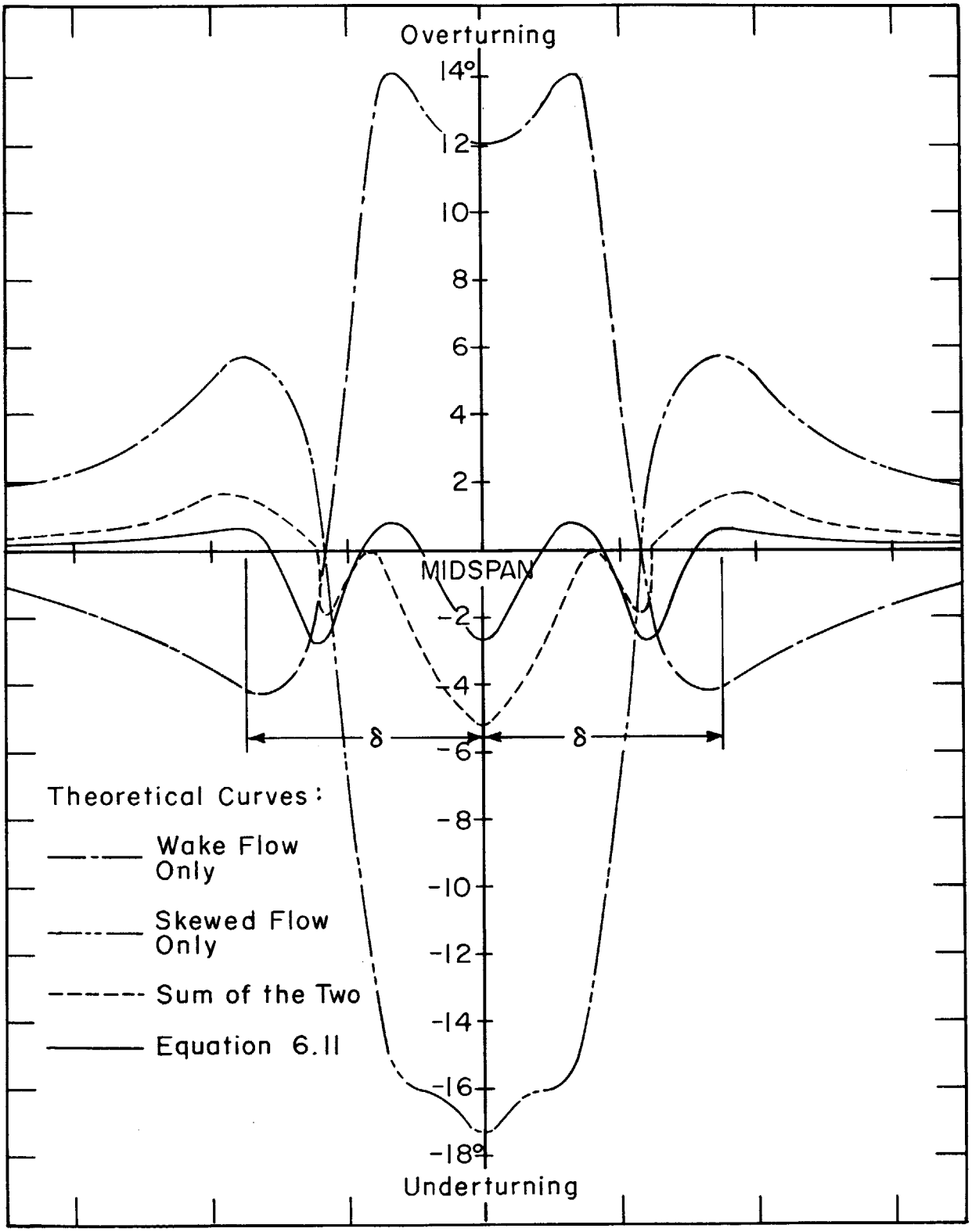

FIG. 73 SKEWED WAKEFLOW MAXIMUM TRANSVERSE FLOW DEVIATION ANGLE

Scale Divisions Shown are in Inches.

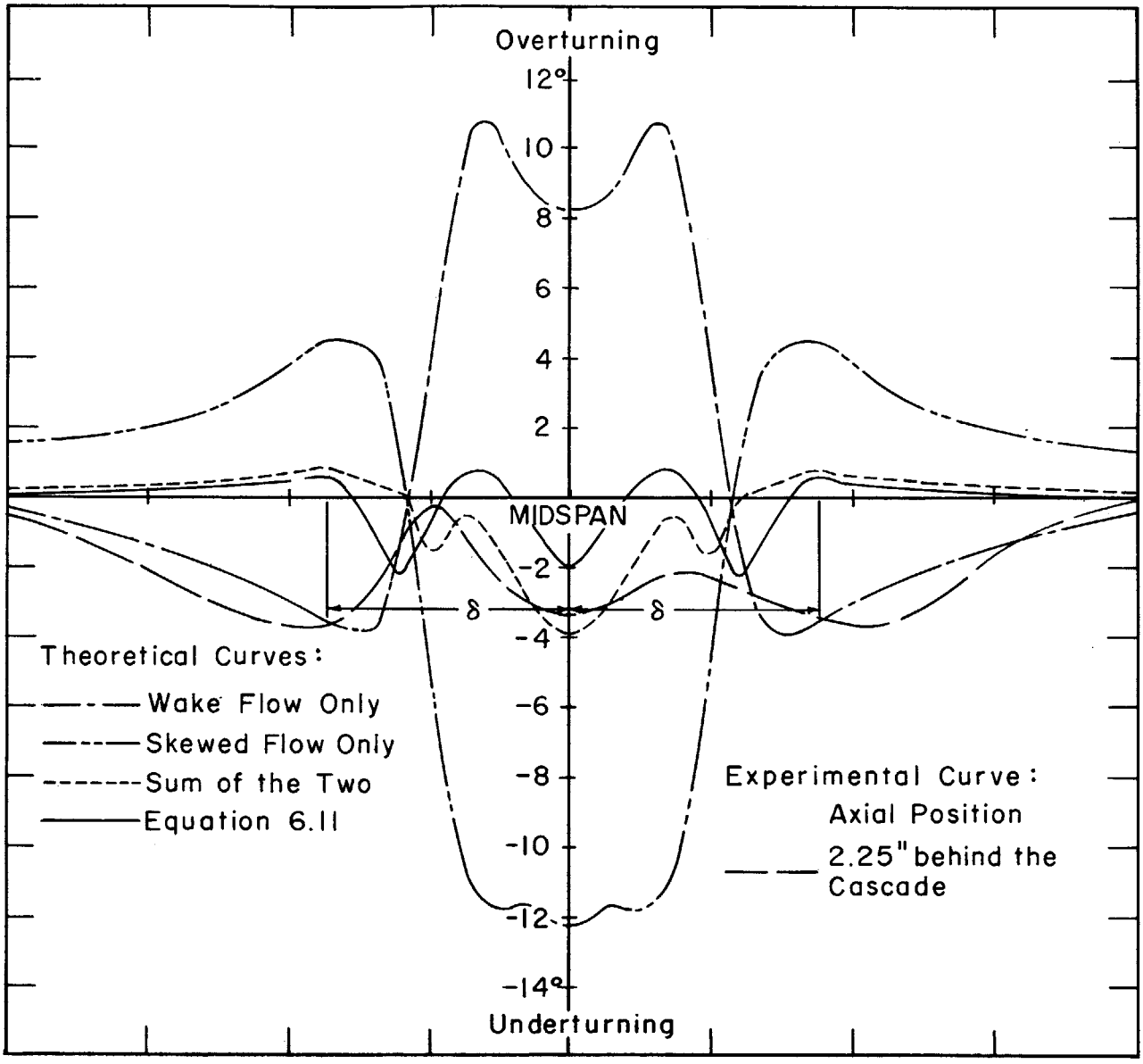

FIG. 74 SKEWED WAKEFLOW AVERAGE TRANSVERSE FLOW DEVIATION ANGLE

Scale Divisions Shown are in Inches.

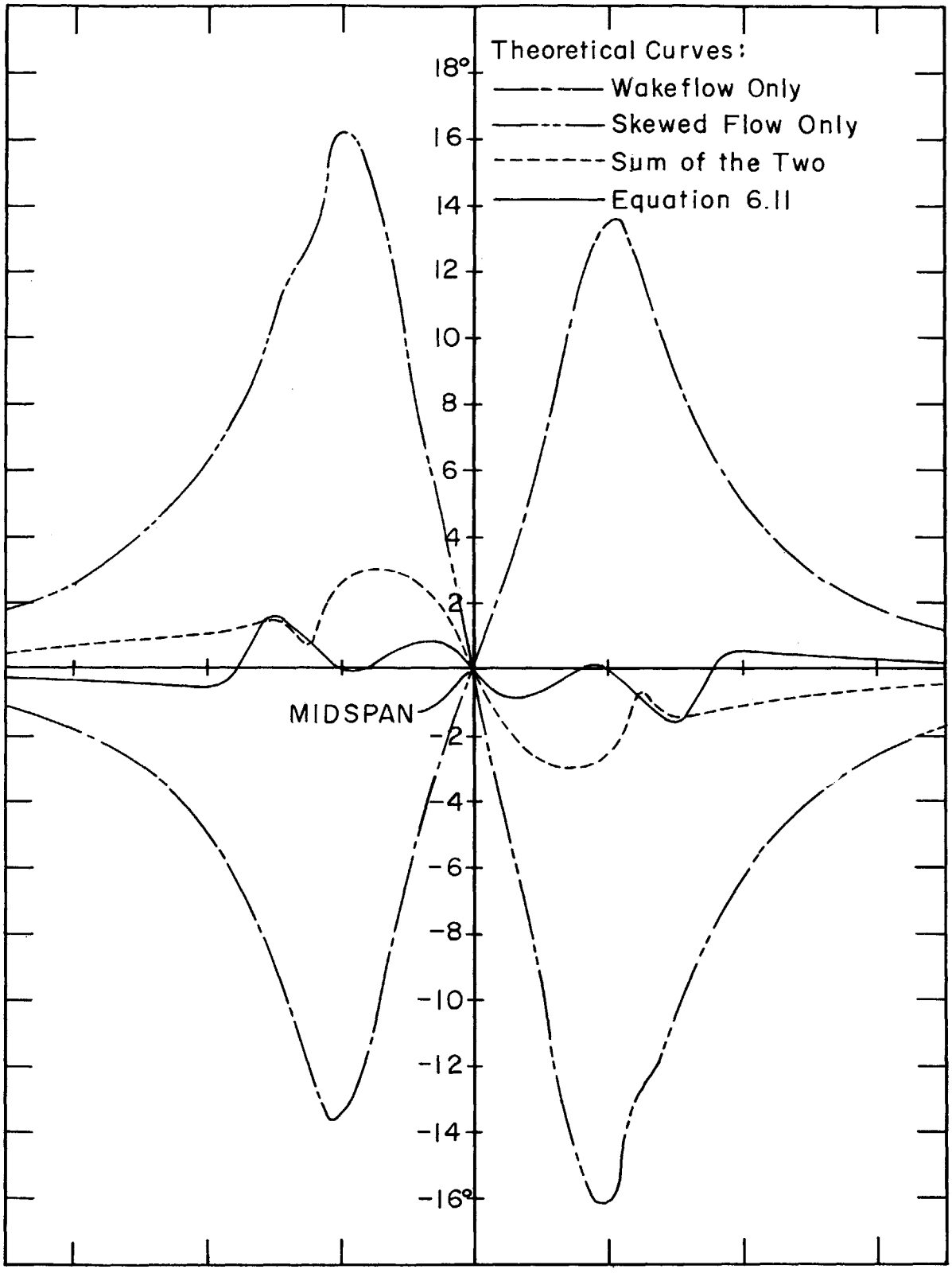

FIG. 75 SKEWED WAKEFLOW SPANWISE FLOW DEVIATION ANGLE

Scale Divisions Shown are in Inches.

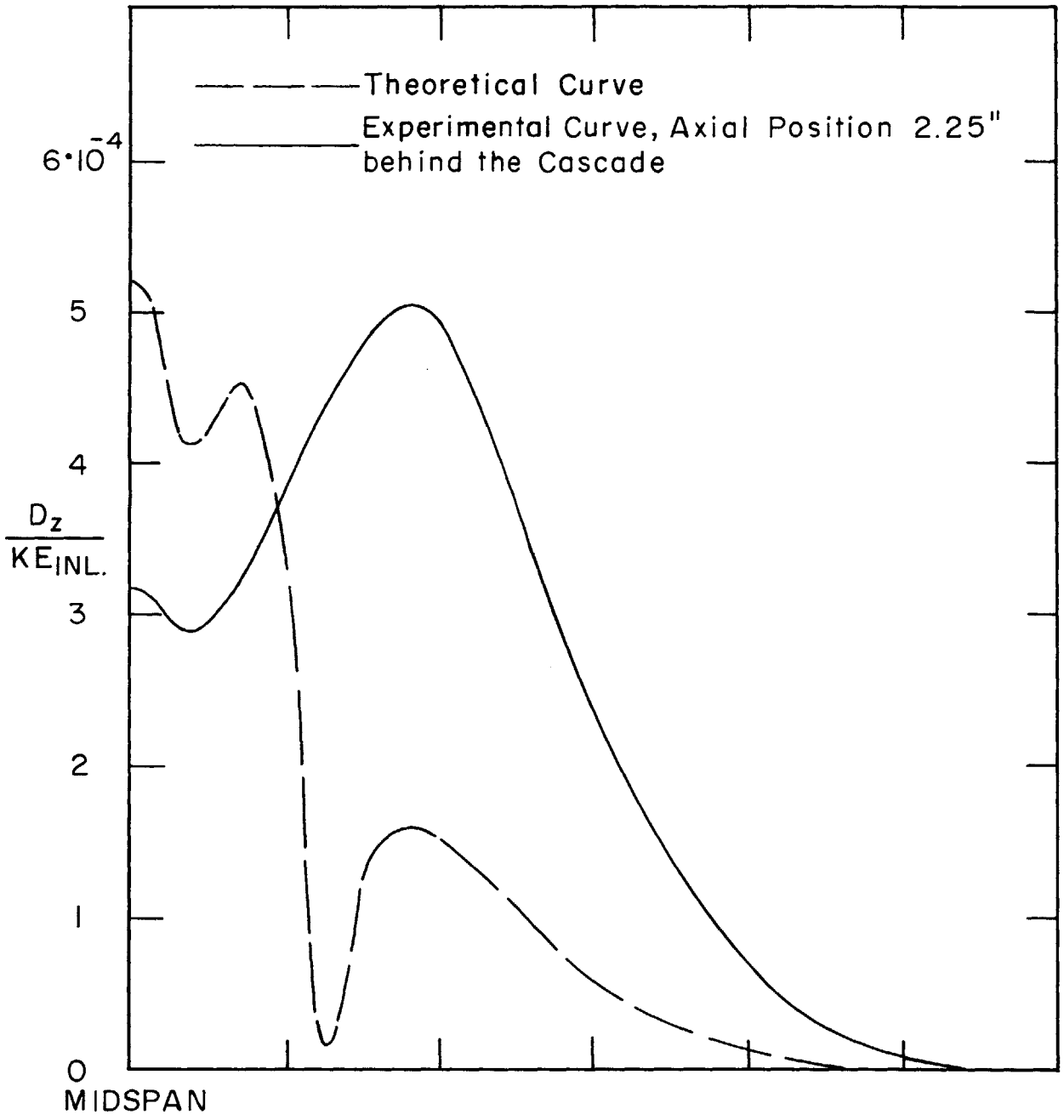

FIG. 76 SKEWED WAKEFLOW SPANWISE DISTRIBUTION OF THE KINETIC ENERGY OF THE SECONDARY FLOW

Scale Divisions Shown are in Inches.

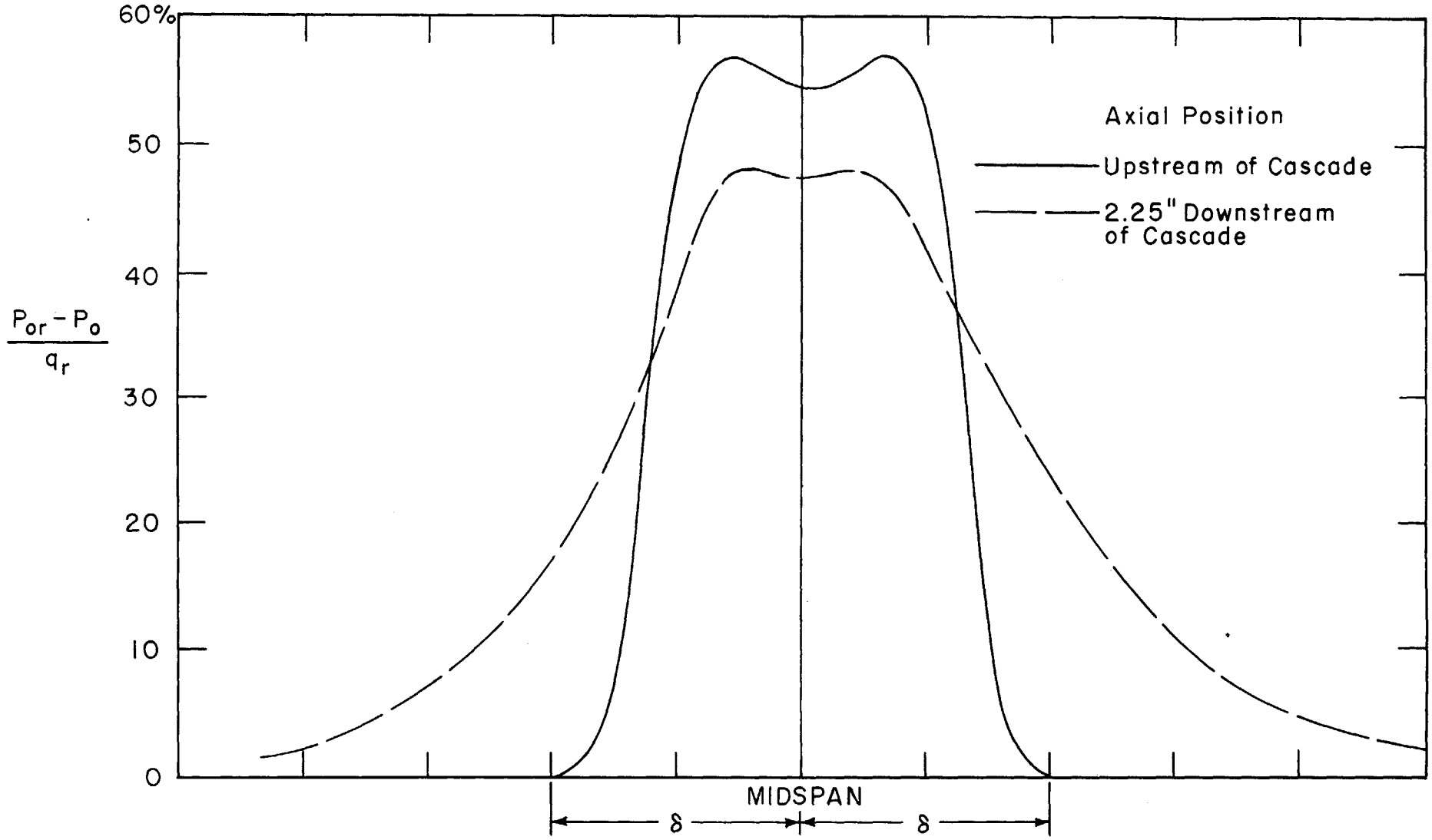

FIG. 77 SKEWED WAKEFLOW SPANWISE DISTRIBUTION OF THE STAGNATION PRESSURE DEFECT (AVERAGED OVER TWO BLADES SPACINGS)
Scale Divisions Shown are in Inches.

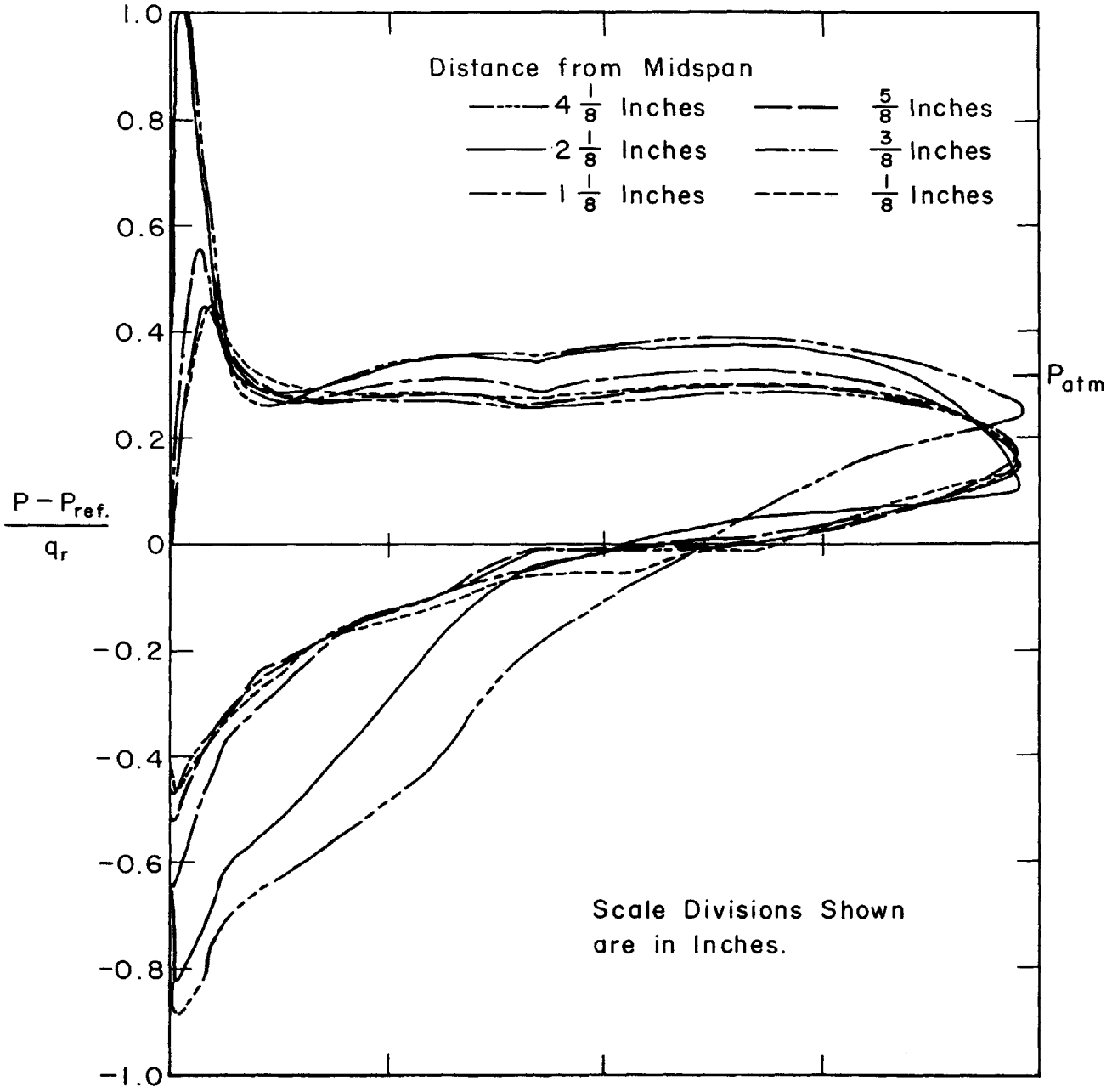

FIG. 78 SKEWED WAKE FLOW. PROJECTED STREAM PRESSURE DISTRIBUTION ON THE BLADE SURFACES

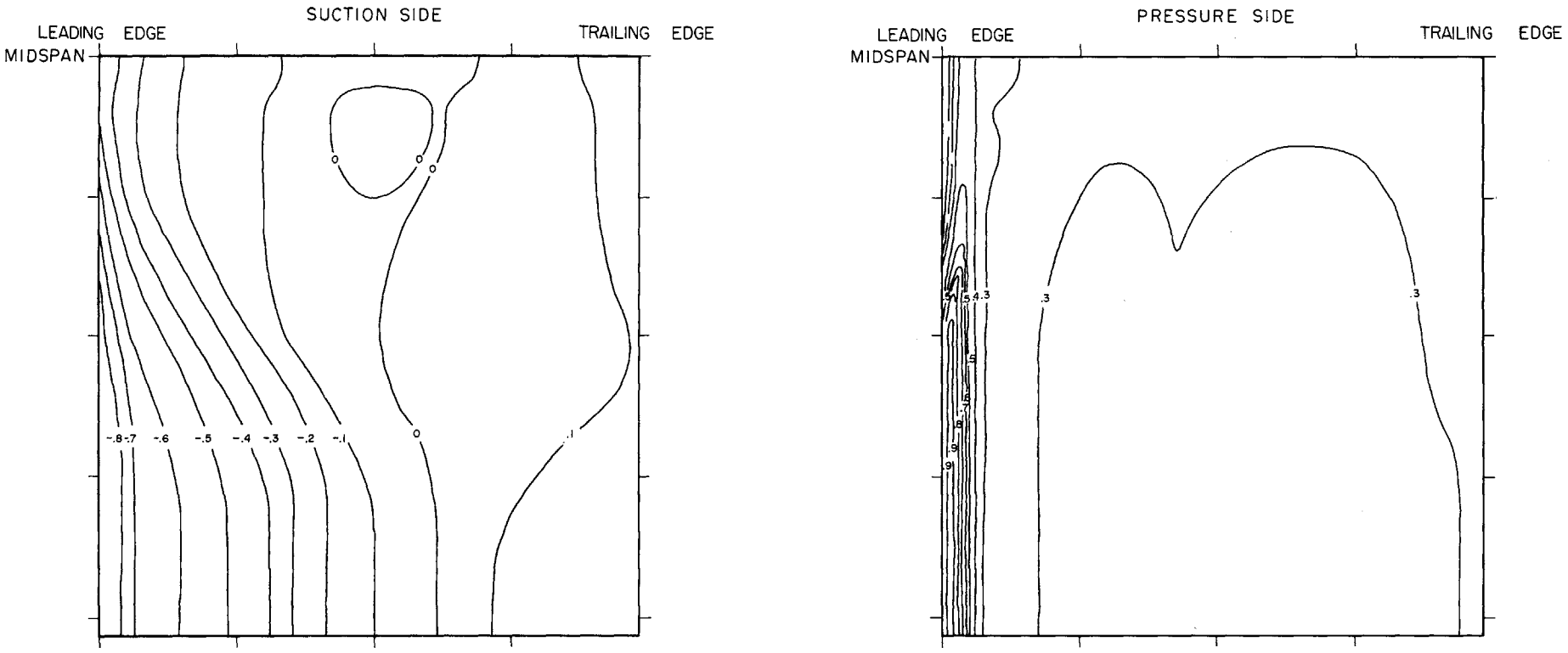

FIG. 79 SKEWED WAKEFLOW $\nabla P_0 \neq 0$. CONTOURS OF CONSTANT STREAM PRESSURE ON THE BLADE SURFACES

Numbers on Contours Indicate $\frac{P - P_r}{q_r}$

Scale Divisions Shown are in Inches.